School of Molecular and Life Science - Chemistry

Tetrazole Functional RAFT Polymers as Macromolecular Ligands for Luminescent Metal Fragments

Elena Dallerba
0000-0001-9259-4106

This thesis is presented for the Degree of
Doctor of Philosophy
of
Curtin University

October 2021

Declaration

To the best of my knowledge and belief this thesis contains no material previously published by any other person except where due acknowledgement has been made.

This thesis contains no material which has been accepted for the award of any other degree or diploma in any university.

Signature:

Date: 29th October 2021

Abstract

In this research, three series of polymeric materials containing tetrazole functionalities were synthesised by reversible addition-fragmentation chain transfer (RAFT) polymerisation and, following post-polymerisation modification, employed as macromolecular ligands for the complexation of luminescent metals. The photophysical properties of the luminescent materials containing Re(I) tricarbonyl diimine metal complexes or cyclometalated Ir(III) complexes were investigated.

A series of novel rhenium-tetrazolato functional copolymers based on a polystyrenic backbone were synthesised. RAFT polymerisation was employed for the synthesis of two statistical and two block copolymers comprised of styrene and 4-cyanostyrene. The parent copolymers were subsequently modified *via* reaction of the cyano appended groups with NaN_3, yielding the corresponding tetrazole functionalised copolymers. The obtained materials were employed as macromolecular ligands for the complexation of a Re(I) tricarbonyl diimine metal complex *via* coordination through the newly introduced tetrazole functional groups. The photophysical properties of the novel copolymer-Re(I) hybrid luminescent materials have been evaluated. Coordination between the tetrazole functionality and the Re(I) complex was confirmed from the absorption and emission profiles of the hybrid materials.

Given the high temperature required for tetrazole formation on the cyano-styrenic polymeric backbone, a subsequent series of well-defined random copolymers containing tetrazole functional groups were prepared by a combination of the RAFT radical homopolymerisation of pentafluorophenyl acrylate (PFPA), end-group modification and post-polymerisation modification of the activated ester side-groups with primary amines. The pendent PFP ester groups were modified in a sequential manner with different molar ratios of *n*-butylamine and 5-aminotetrazole, yielding four

random polymeric amide species. The introduction of the tetrazole functionalities was performed at room temperature, leading to milder reaction conditions compared to the polystyrenic copolymers. Four rhenium-polymer hybrids were obtained by reacting the polymeric materials with a Re(I) tricarbonyl diimine metal complex with attachment *via* the tetrazole functional groups. The photophysical properties of the materials were investigated, confirming that the polymeric backbone does not interfere with the luminescent properties of the luminescent Re(I) complexes. The four luminescent materials were employed as luminescent probes for the staining of rodent brain tissues, with the results suggesting non-specific binding.

Two of the above materials were then reacted with the iridium precursor $[Ir_2(ppy)_4(\mu\text{-}Cl)_2]$, to introduce the luminescent cationic $[Ir(ppy)_2]^+$ fragment *via* coordination to two polymer-bound pendent tetrazole functional groups, yielding negatively charged luminescent materials containing iridium. The photophysical properties of the Ir-functionalised materials were investigated, confirming the attachment of the iridium fragments to the materials and the formation of a negatively charged, polymer-bound iridium luminescent species. Furthermore, one of the iridium functionalised materials was further modified with a second luminescent metal species, $Re(CO)_3(phen)Br$, to yield three hybrid metal Ir/Re copolymers with different compositions. The photophysical properties of the luminescent functionalised materials containing both iridium and rhenium were investigated, confirming the attachment of rhenium fragments. The photophysical results of the materials containing both metal fragments indicated energy transfer phenomena occurring from iridium to rhenium metal centres. The Ir and Ir/Re luminescent materials were employed as luminescent probes for the staining of rodent brain tissues.

To increase the biological compatibility of the luminescent polymeric materials, the synthesis of a new series of seven polymeric materials containing tetrazole-Re(I) metal fragments was performed. Well-defined block copolymers of poly(ethylene glycol (PEG) (meth)acrylate) and PFPA were prepared. PEG acrylate and PEG methacrylate homopolymers were synthesised by RAFT polymerisation and employed as macro chain transfer agents (CTA) for block copolymerisation with PFPA, followed by end-group modification and post-polymerisation modification of the activated ester side-groups with appropriate primary amines. The final rhenium-polymer hybrid materials were obtained by complexation reaction with Re(I) tricarbonyl diimine complexes *via* coordination through the tetrazole functional groups. Detailed photophysical studies were performed showing that the different compositions in the rhenium-polymer hybrid materials did not affect their photophysical properties, as confirmed by lifetime and quantum yield analysis. The PEG acrylate luminescent materials have been employed as luminescent probes for the staining of rodent brain tissues, suggesting non-specific binding into tissues.

Supporting literature:

E. Dallerba, M. Massi and A. B. Lowe "Rhenium(I)-Tetrazolato Functional Luminescent Polymers: Organic-Inorganic Hybrids via RAFT and Post-Polymerization Modification" *European Polymer Journal*, 2020, **126**, 109559.

E. Dallerba, M. Massi and A. B. Lowe "Tetrazole Functional Copolymers: Facile access to Well-defined Rhenium(I)-Polymeric Luminescent Materials". *Polymer*, 2020, **198**, 122522.

Acknowledgement of Country

We acknowledge that Curtin University works across hundreds of traditional lands and custodial groups in Australia, and with First Nations people around the globe. We wish to pay our deepest respects to their ancestors and members of their communities, past, present, and to their emerging leaders. Our passion and commitment to work with all Australians and peoples from across the world, including our First Nations peoples are at the core of the work we do, reflective of our institutions' values and commitment to our role as leaders in the Reconciliation space in Australia.

Dedication

Dedicated to the memory of my grandfather Franco.

Statement of Contribution by Other Authors

All the staining and imaging studies described in Chapters 3, 4 and 5 have been conducted by David Hartnell, under the supervision of Dr Mark Hackett.

Chapter 1, 2 and 3 have been prepared as manuscripts for peer-reviewed publications in scientific literature. These Chapters are adaptations of submitted and published manuscripts, with the exception of formatting consistent with the thesis. Signature of authors approving the candidate's contribution can be found at the end of this section. I have obtained permission from the copyright owners to use any third-party copyright material reproduced (adapted) in this thesis, and to use any of my own published work in which the copyright is held by another party.

The study presented in Chapter 1 was published as a book chapter in "RAFT polymerisation: Methods, Synthesis, and Applications", published in 2021.

RAFT polymerisation: Methods, Synthesis, and Applications, Moad G.; Rizzardo, E. Eds.; John Wiley and Sons, 2021.

Statement of contribution: The manuscripts was written and reviewed by Andrew B. Lowe and Elena Dallerba.

The study presented in Chapter 2 was published in the peer-reviewed journal "European Polymer Journal" in 2020.

E. Dallerba, M. Massi and A. B. Lowe "Rhenium(I)-Tetrazolato Functional Luminescent Polymers: Organic-Inorganic Hybrids via RAFT and Post-Polymerization Modification" *European Polymer Journal*, 2020, **126**, 109559.

Statement of contribution: The manuscripts was written and revised by Andrew B. Lowe, Elena Dallerba and Massimiliano Massi. Experimental data were collected and analysed by Elena Dallerba with the guidance of Andrew B. Lowe and Massimiliano Massi.

The study presented in Chapter 3 was published in the peer-reviewed journal "Polymer" in 2020.

E. Dallerba, M. Massi and A. B. Lowe "Tetrazole Functional Copolymers: Facile access to Well-defined Rhenium(I)-Polymeric Luminescent Materials". *Polymer*, 2020, **198**, 122522.

Statement of contribution: The manuscripts was written by Andrew B. Lowe and Elena Dallerba. The manuscript was revised by all authors. Experimental data were collected and analysed by Elena Dallerba with the guidance of Andrew B. Lowe and Massimiliano Massi.

Author 1

Name: Elena Dallerba

Signature:

Date: 28th October 2021

Author 2

Name: Andrew B. Lowe

Signature:

Date: 28th October 2021

Author 3

Name: Massimiliano Massi

Signature:

Date: 28th October 2021

Table of content

Chapter 1

Introduction

Part of the contents of this Chapter were published in 2021:

RAFT polymerisation: Methods, Synthesis, and Applications, Moad G.; Rizzardo, E. Eds.; John Wiley and Sons, 2021.

1.1 Radical polymerisation

Today, radical polymerisation (RP) processes account for more than 45% of the total production of commercial polymers (nearly 100 million tons in 2008) and 40% of synthetic rubber (nearly 4.6 million tons in 2008) worldwide.[1] The story of polymers starts in 1832, when a Swedish chemist named Berzelius acknowledged the existence of molecules with the same composition but different molecular weights.[1] He named those molecules "polymers", which comes from the Greek word "*πολυμερή"* which means "consisting of many parts".[1] It was only almost 100 years later, between the 1920s and 1930s, that the first polymerisation employing a radical initiator took place.[2,3] Finally, in the 1950s, upon systematic investigation of reactions employing azo compounds as radical initiators, more knowledge on RP processes became available and the fragmentation of peroxides was theorised together with the report of the primary steps of radical polymerisation.[4,5]

Radical polymerisation is a chain growth process that proceeds *via* a radical active centre. The primary radicals can be generated by one of various methods including for example thermally, UV irradiation or redox initiator. RP is described by three elementary reactions: initiation, propagation and termination (**Scheme 1-1**). The active species in a RP is a radical. Under steady-state conditions, the rate of initiation

and the rate of termination are considered to be the same (~1000 times slower than the propagation rate).[6] The inconvenience of the slow initiation rate can be overcome by using a radical initiator with a longer lifetime. Termination rates in RP are very fast and in order to avoid bimodal radical coupling and termination by disproportionation, the termination rate must be slower than the propagation rate. This can be achieved by employing low concentrations of radical sources, in the range of ppm or ppb.[6] Nevertheless, since the average lifetime of propagating chains is very short (~1s), it is virtually impossible to manipulate the polymers by end-functionalisation or addition of a second monomer to form block copolymers.[6] Therefore, it is not possible to control molecular weight (MW), molecular weight distribution (MWD) and the overall architecture of the synthesised polymers. Reversible deactivation radical polymerisation (RDRP) offers a possibility over the control of these factors.

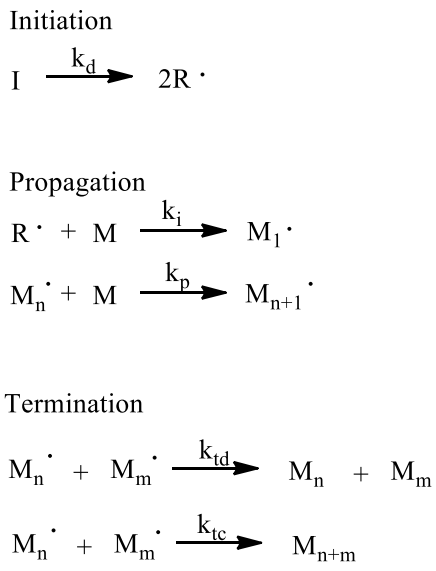

Scheme 1-1 Initiation, propagation, and termination reactions in radical polymerisation.

1.2 Reversible deactivation radical polymerisation (RDRP) techniques

RDRP enables the synthesis of polymers with predetermined molecular weights, narrow molecular weight distributions, low dispersity and tailored architectures such as block, graft, branched and star copolymers. This is possible because RDRP suppresses the occurrence of undesirable chain termination/transfer.

The first example of a living polymerisation was reported by Szwarc, who pioneered living anionic polymerisation and is considered the founder of modern controlled polymer synthesis.[7,8] Since its discovery, RDRP has garnered enormous interest. Currently, there are a number of established RDRP techniques including stable free-radical polymerisation (SFRP), atom transfer radical polymerisation (ATRP), tellurium-mediated radical polymerisation (TERP), and reversible addition-fragmentation chain transfer polymerisation (RAFT). Common features of these techniques will be covered, but only RAFT will be discussed in detail.

Fundamental to RDRP is that the contribution of chain breaking reactions, such as termination and chain transfer reactions, is minimised so that the polymer chains can undergo effectively simultaneous growth with near complete initiation prior to any significant propagation.[6] This results in the apparent simultaneous growth of all polymeric chains and the formation of "monodisperse" polymers. A key and central feature common to all RDRP systems is the establishment of a dynamic equilibrium between active propagating radical species and dormant chains.[6]

To be considered "living" a polymerisation process must obey the following criteria:

- The number average molecular weight (M_n) must be a linear function of monomer conversion;
- The molecular weight can be controlled by the stoichiometry of the reaction;

- The molecular weight distribution of the final polymer is narrow;
- The final polymer is able to further increase in molecular weight upon addition of monomer.

1.3 RAFT polymerisation

Reversible addition-fragmentation chain transfer (RAFT) polymerisation is a type of RDRP process performed in the presence of certain thiocarbonylthio compounds.[9-12] RAFT polymerisation was firstly reported in 1998 by a team of researchers at the Commonwealth Scientific and Industrial Research Organisation (CSIRO) in Melbourne, Australia.[13] Around the same time, a similar process was patented in France, and termed MADIX (macromolecular design *via* interchange of xanthates), which employed xanthates as chain transfer agents and proceeds *via* the same mechanism as the RAFT process.[14] Since its disclosure, RAFT polymerisation has been widely studied and employed because of its advantages compared to other RDRP techniques.

The key features of this technique are: the ability to prepare (co)polymers with predetermined molecular weights and narrow molecular weight distributions, its ease of execution, high tolerance towards a wide range of functional groups and experimental conditions and the ease of polymer end-group modification.[13] The RAFT process is today recognised as one of the most versatile methods to provide radically-prepared (co)polymers with characteristics typical of traditional anionic living polymerisation.[15,16] In practice, RAFT polymerisation can be considered a conventional radical polymerisation performed in the presence of an added thiocarbonylthio compound.

1.3.1 Mechanism of RAFT polymerisation

The generally accepted mechanism of RAFT polymerisation is illustrated in 5 steps, as shown in **Scheme 1-2**, in which the RAFT agent, also known as CTA (chain transfer agent), is shown with the general formula ZC(=S)SR. The mechanism involves the same initiation, propagation and termination steps typical of traditional radical polymerisation, but with the addition of degenerative chain transfer steps involving radicals and the CTA. Multiple reversible addition-fragmentation steps are involved in the RAFT process. Initiation occurs in the same way as in traditional radical polymerisation and typically involves the thermal decomposition of an appropriate initiator generating primary radicals (I·). During the so-called "pre-equilibrium", the radical generated from the decomposition of the initiator adds to a few monomers to form the propagating radical P_m· which reacts with the chain-transfer agent (CTA) **1**, forming the intermediate carbon-centred adduct **2**, as shown in step (II).

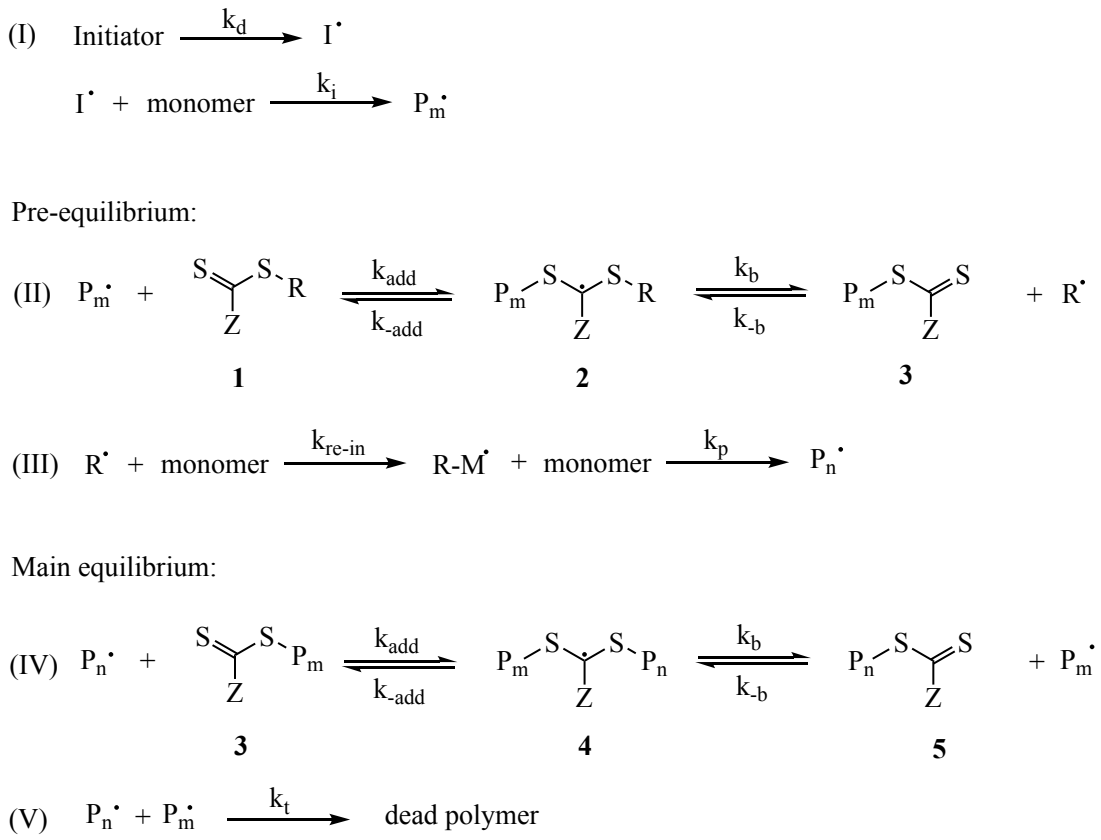

Scheme 1-2 Mechanism of RAFT polymerisation showing the steps of initiation (I), pre-equilibrium (II), re-initiation (III), main equilibrium (IV) and termination (V).

During the pre-equilibrium (or "reversible chain transfer") step (II), radical **2** forms a new radical R· and the polymeric thiocarbonylthio compound **3**. At the "re-initiation" stage (III), the new radical R· is able to re-initiate polymerisation by adding to a monomer molecule, forming P_n·, a new propagating radical. During the "chain equilibrium" step (IV), an equilibrium is established between the two propagating radicals P_m· and P_n· and the dormant polymeric thiocarbonylthio compounds **3** and **5**. This step, involving addition-fragmentation between the aforementioned species, is also known as the "main equilibrium"; it provides to all chains the same probability to grow, thus ensuring narrow molecular weight distributions and low dispersity.[17] An essential feature of the RAFT process is that the product of chain transfer **3** is also a

CTA agent and has a similar or greater activity to re-initiate polymerisation than the precursor **1**, ensuring that the process is "degenerative chain transfer" in nature.[18] It is important to note that the two radical intermediate species **2** and **4** should not be able to re-initiate polymerisation due to steric hindrance. The final step is the "termination" process, which occurs in the same fashion as normal radical polymerisation, *via* combination and/or disproportionation processes.[16]

1.3.2 Kinetics of RAFT polymerisation

Based on the steady-state assumption and as in a conventional radical polymerisation, the rate of a RAFT polymerisation is expressed by **Equation 1-1**:

$$R_p = -\frac{d[\mathrm{M}]}{dt} = k_p[\mathrm{R}\cdot][\mathrm{M}] \qquad \textbf{Equation 1-1}$$

where R_p is the rate of polymerisation; [M] is the concentration of the monomer; k_p is the rate coefficient; [R·] is the radical concentration.

As the concentration of the radical [R·] can be considered constant, k_p [R·] can be replaced by k_{app}, which is defined as the apparent rate constant. **Equation 1-1** can be re-written as **Equation 1-2**:

$$R_p = -\frac{d[\mathrm{M}]}{dt} = k_{app}[\mathrm{M}] \qquad \textbf{Equation 1-2}$$

According to the proposed RAFT mechanism, and the principle of degenerative addition-fragmentation chain transfer, for each radical consumed by addition to the C=S bond, a new radical is generated through fragmentation. Thus, if the addition-fragmentation process is fast enough, the effect of the degenerative chain

transfer process should be negligible on the overall polymerisation rate. In theory, the kinetics of the RAFT process should be the same as in conventional radical polymerisation and not dependent on the concentration of CTA. Nevertheless, predictions are different from what is observed experimentally and the rate of RAFT polymerisation is often slower than the corresponding conventional radical polymerisation for a given monomer. Moreover, an increase in the concentration of CTA causes a decrease in the polymerisation rate.[16]

From the mechanism of RAFT polymerisation, one can observe that all polymer chains are initiated either by the primary radical I· or by R·. The concentration of I· can be considered negligible with respect to the concentration of R·, therefore the theoretical M_n can be expressed by **Equation 1-3**:

$$M_n = [M]_0 \cdot MW_{monomer} \cdot x/[CTA]_0 + MW_{CTA} \qquad \textbf{Equation 1-3}$$

where $MW_{monomer}$ is the molecular weight of the monomer, x is the fractional conversion of monomer, $[CTA]_0$ is the initial concentration of CTA and MW_{CTA} is the molecular weight of the CTA.

1.3.3 RAFT agents

Key to successful RAFT polymerisation is the choice of an appropriate chain-transfer agent. Typically, the thiocarbonylthio species employed belongs to one of the following group of compounds: dithioesters, xanthates, dithiocarbamates or trithiocarbonates. **Figure 1-1** illustrates the general structure of a chain-transfer agent and the most common examples of the RAFT agent families: dithioesters (typically dithiobenzoates), trithiocarbonates, dithiocarbamates and xanthates.

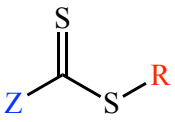

General structure of RAFT CTA

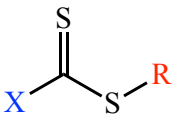

dithioester
X = alkyl or aryl

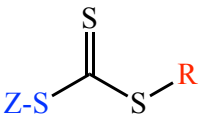

trithiocarbonate

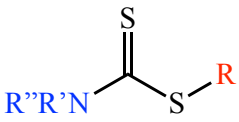

dithiocarbamate

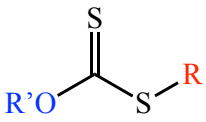

xanthate

Figure 1-1 General chemical structures of the different RAFT agent families.

The relevant features of CTAs are the so-called R and Z groups, **Figure 1-1**, and both play a crucial role in determining the outcome of a polymerisation. These groups control the rate of addition and fragmentation, the efficiency of chain transfer and the possibility of retardation or inhibition.[19]

1.3.4 The Z group

The Z substituent is chosen to control the bulk reactivity of the CTA towards monomers and will also directly impact the stability of the carbon-centred radical intermediates.[19] Generally, the Z group should have a strong stabilising influence towards the formation of the intermediate radicals **2** and **4** to favour the reactivity of the C=S bond to radical addition (high k_{add}). At the same time, the intermediate radicals **2** and **4** need to be able to fragment into species **3** and **5**, therefore the stability needs to be finely tuned to ensure the fragmentation rate is sufficiently fast (k_{β}).[19] It has been observed that the phenyl group is considered to be the most ideal activating group due to its ability to balance the stability and the reactivity towards fragmentation of the

intermediate radical.[19] Benzyl and alkyl Z groups have a lower stabilising effect on the intermediate radical leading to a faster fragmentation rate, but slower addition rates.[19] Moreover, dithioesters and trithiocarbonates, where the atom adjacent to the thiocarbonylthio group is a carbon or a sulfur atom, are the most versatile in respect to the range of suitable monomers.[19] To understand this, we need to consider RAFT agents with a lone pair of electrons on a nitrogen or oxygen adjacent to the thiocarbonyl group, in which the reactivity towards radical addition is dramatically lower.

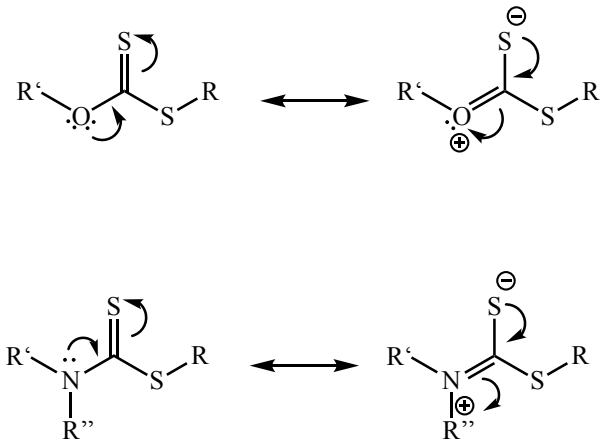

Figure 1-2 Canonical forms of xanthates and dithiocarbamates.

The interaction between a lone pair of electrons on N or O and the C=S bond, reduces its susceptibility to undergo radical addition, hence reducing its reactivity in the addition step in the RAFT process (**Figure 1-2**). This happens, for example, for RAFT agents such as *O*-alkyl xanthates, *N*,*N*-dialkyldithiocarbamates and *N*-alkyl-*N*-aryldithiocarbamates.[20,21] Interestingly, dithiocarbamates where the lone pair is part of an aromatic ring or where a carbonyl group is α to the nitrogen lone pair, show a similar reactivity as dithioesters and trithiocarbonates.[21,22] **Figure 1-3** illustrates the general guidelines for the selection of the Z group of RAFT CTAs.

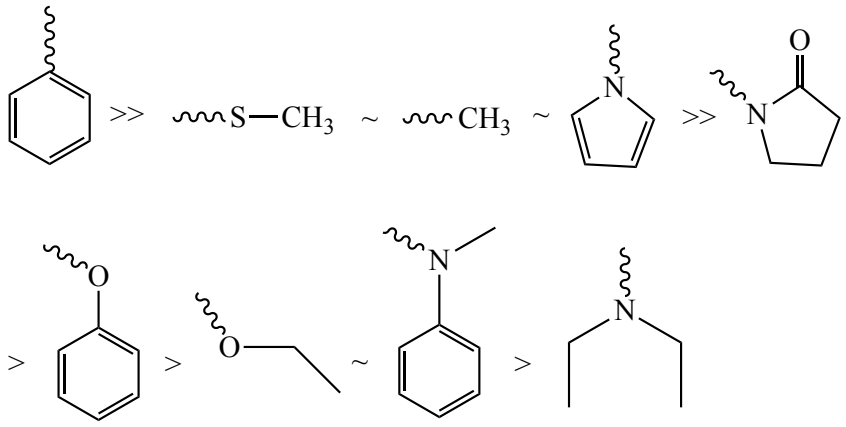

Figure 1-3 Guidelines for the selection of the Z group of RAFT CTAs. From left to right: addition rates decrease and fragmentation rates increase.

The polymerisation of styrene and methacrylates employing CTAs with stabilising groups, such as for example the phenyl group as the Z group, results in more efficient polymerisation, while the polymerisation of vinyl esters is inhibited.[6] Nevertheless, vinyl esters can be polymerised by using CTAs bearing weakly stabilising groups such as -NR_2 in dithiocarbamates or -OR groups in xanthates.[6]

In conclusion, the most versatile and widely employed families of RAFT agents are dithioesters and trithiocarbonates, while the use of xanthates and dithiocarbamates is generally limited to specific classes of monomers such as vinyl esters and vinyl amides.[19]

1.3.5 The R group

On the other hand, the R group needs to be chosen to be a good homolytic leaving group in respect to $P_m^{\cdot}$ to favour the formation of the polymeric thiocarbonylthio compound **3** (**Scheme 1-2**). At the same time, the expelled radical $R^{\cdot}$ needs to be able to reinitiate the polymerisation process during step III, otherwise

retardation will be likely to happen.[23] The leaving ability of the R groups is strongly influenced by both steric and electronic effects (**Figure 1-4**).[23] Generally, a tertiary R group has a better leaving ability than a secondary R group, which is better than a primary. Electron-withdrawing and electron donating substituents on R can also affect the leaving ability of the R group, as electron-donating groups tend to stabilise the newly formed radical.[23]

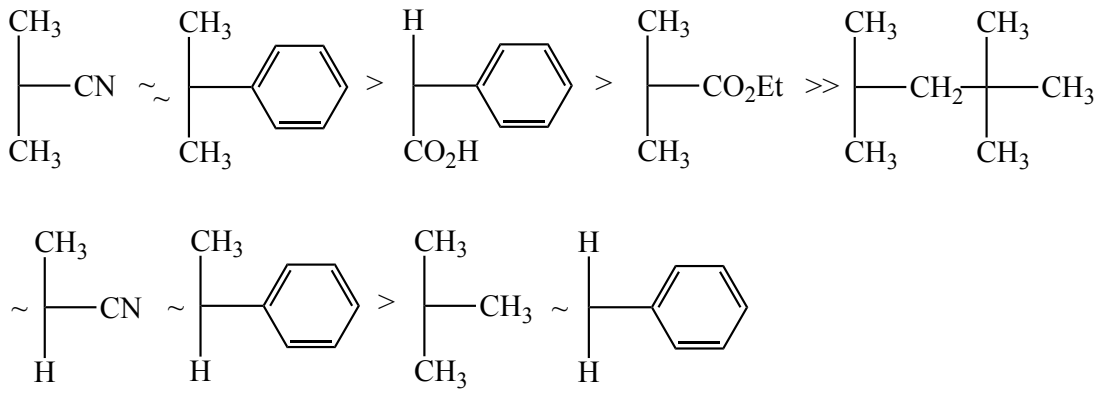

Figure 1-4 Guidelines for the selection of the R group of RAFT CTAs. From left to right: fragmentation rates decrease.

The final (co)polymer products of a RAFT polymerisation will contain specific functionality at the α- and ω-termini, the nature of which will be determined by the choice of RAFT agent employed for the polymerisation process. Typically, and assuming that the R group in the CTA initiates the vast majority of the polymer chains, the final polymer will contain the R functionality at the α-chain end (**Scheme 1-3**). If the primary radicals formed from the initiator possess the same structure as R, for example when azobisisobutyronitrile (AIBN) is used in conjunction with a CTA such as 2-cyano-2-propyl benzodithioate, then all polymer chains will have identical initiating R groups.

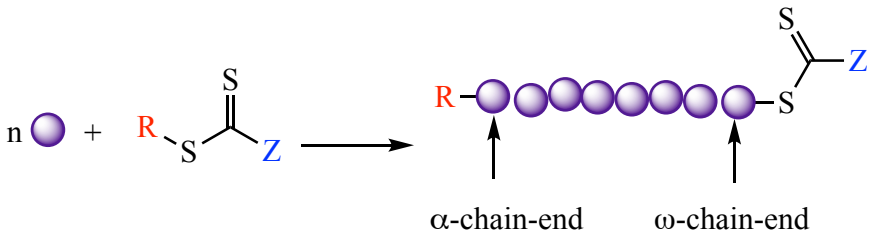

Scheme 1-3 RAFT polymerisation highlighting the presence of functionality at the α- and ω-termini.

If we assume that there are no side reactions, all polymer chains will have a Z thiocarbonylthio functionality at the ω-chain end. In practice, under ideal conditions, at the end of the polymer synthesis, the product can be considered as a macromolecular CTA, with a certain amount of monomers inserted between the C-S bond.

As shown in the previous section, a wide number of species can be chosen as the R and Z groups for RAFT CTAs. By combining them, a large number of CTAs with different structures and functionalities become available. Some examples of CTA agents are shown in **Table 1-1**. Aromatic dithioesters such as 2-cyano-2-propyl benzodithioate (**Table 1-1**, **7**) and cyanobenzyl dithiobenzoate (**Table 1-1**, **8**) are among the most versatile CTAs and are efficient in the RAFT polymerisation of more-activated monomers (MAMs) such as styrene, (meth)acrylates and (meth)acrylamides.[24] The downside is that they are prone to degradation over time and are less efficient for less-activated monomers (LAM) such as vinyl acetates, vinyl chloride and alkenes.[24] Trithiocarbonates can be obtained by simple synthetic procedures and are the most popular CTAs for the polymerisation of MAMs.[24] Commercially available cyanopropyldodecyl trithiocarbonate (**Table 1-1**, **9)** is a very versatile trithiocarbonate CTA and one of the most widely used.[24]

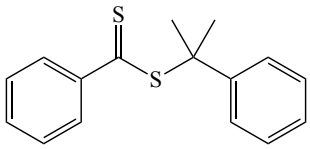

cumyl dithiobenzoate

6

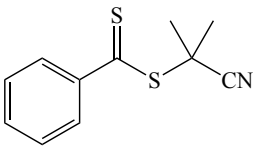

cyanoisopropyl dithiobenzoate

7

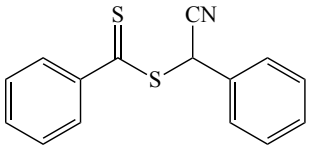

cyanobenzyl dithiobenzoate

8

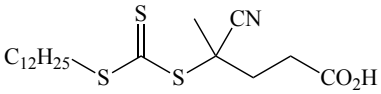

cyanopropyldodecyl trithiocarbonate

9

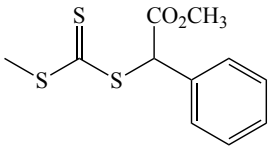

methyl 2-(((methylthio) carbonylthio)thio)-2-phenylacetate

10

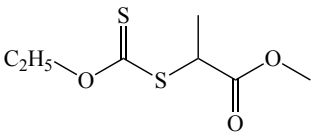

Rhoxidan A1

11

Table 1-1 Examples of CTAs for RAFT polymerisation.

Methyl 2-(((methylthio)carbonylthio)thio)-2-phenylacetate (**Table 1-1**, **10**) is a less known CTA but very versatile trithiocarbonate.[24] Among the family of xanthates, Rhoxidan A1, (**Table 1-1**, **11**) is a very versatile CTA for LAMs such as vinyl esters.[25,26]

1.3.6 Photoinduced electron transfer RAFT process

The photoinduced electron/energy transfer (PET-RAFT) process was first reported in 2014 by Boyer's group as a greener and more sustainable alternative to the RAFT process.[27] In early examples of this new photoinduced radical polymerisation technique, iridium and ruthenium transition-metal complexes were employed as photoredox catalysts.[27]

The mechanism of PET-RAFT exploits the photoredox properties of the catalyst and the ability of the thiocarbonyl compound to accept electrons (**Scheme 1-4**). Upon excitation of the catalyst *fac*-[Ir(ppy)$_3$] under visible light, the excited species Ir(III)* is formed, which can reduce the thiocarbonylthio moiety of the CTA *via*

electron transfer. The result is the production of radicals $P_n\cdot$, which are able to initiate the polymerisation of the monomeric species *via* the RAFT process. The radical species $P_n\cdot$ could also undergo deactivation by reacting with Ir(IV) to generate the initial species Ir(III) and the CTA, resulting in a catalytic cycle. This process has been employed for the controlled polymerisation of a wide variety of monomers such as methacrylates, acrylates, styrene, acrylamides, methacrylamides, vinyl esters, vinyl phosphonate and *N*-vinyl pyrrolidinone.[27] Moreover, this process has been proven to be efficient with various classes of CTA such as trithiocarbonates, dithiocarbamates and xanthates.[27]

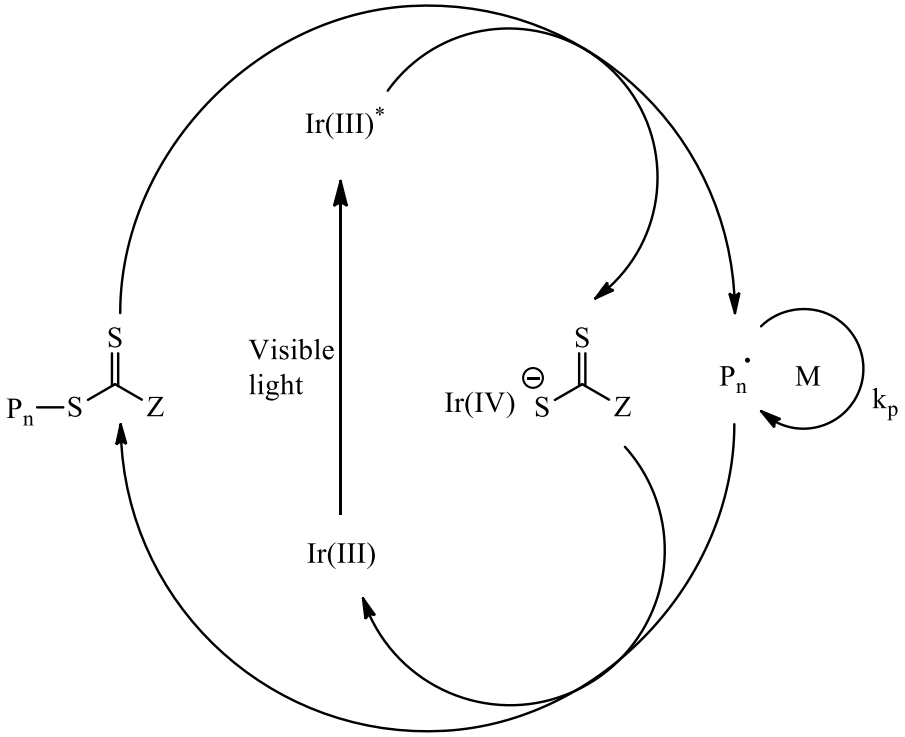

Scheme 1-4 Proposed mechanism of a photoinduced controlled polymerisation using the Ir(III) complex the *fac*-[Ir(ppy)$_3$] as a photoredox catalyst.

It is important to note that the radicals are generated directly from the CTA and thus no external source of radical initiator is necessary. Other advantages of the PET-RAFT process are the fact that polymerisations can be carried out at room temperature, the recyclability of the photocatalysts, its selectivity, and oxygen tolerance. In fact, no prior deoxygenation step is necessary when performing PET-RAFT.[27] Further developments of PET-RAFT led to the investigation of alternatives to transition metal species as catalysts, such as chlorophyll, zinc metalloporhyrin and inorganic semi-conductor metal oxides such as TiO_2 and ZnO.[28]

1.4 Thiocarbonylthio End-Group Removal and Transformation

As mentioned previously, a characteristic of RAFT polymerisation is that the RAFT agent species is retained in the final polymeric structure as the α- and ω-chain end functional groups. This feature is a consequence of the mechanism of the RAFT polymerisation process, and it ensures the suitability of the polymeric product for the synthesis of block copolymers or well-defined end-functional polymers. Nevertheless, in some cases, it is desirable, or even necessary, to remove the thiocarbonylthio end group in RAFT-prepared (co)polymers. In fact, the presence of the thiocarbonylthio end group results in the polymers produced by RAFT being coloured. The colour may range from violet through red/pink to pale yellow, depending on the absorption characteristic of the specific thiocarbonylthio compound.[29] Moreover, the presence of the thiocarbonylthio group, in some cases, can be accompanied by the elimination of possible sulfur-based degradation products which can result in the release of toxic or malodorous sulfur-containing compounds. The presence of such compounds and the inherent high reactivity of thiocarbonylthio groups can be considered disadvantageous for some applications.

Several different approaches are available for the removal or chemical modification of thiocarbonylthio end-groups in RAFT polymers (**Figure 1-5**). Since the chemistry of thiocarbonylthio species is well known from small molecule chemistry, this knowledge has been applied to the modification of thiocarbonylthio compounds associated with RAFT synthesised polymers. Two general approaches for modification of RAFT thiocarbonylthio end-groups are:

1. Complete desulfurisation. This approach facilitates complete removal of the thiocarbonylthio group *via* one of several available pathways, and typically involves radical-based modification;
2. Chemical modification of the thiocarbonylthio group. This approach involves the end-group being chemically converted into a macromolecular thiol or other S-based species. The versatility of this approach is highlighted by the possibility of yielding different types of newly functionalised end-functional materials.

For the scope of this thesis, only reactions leading to the complete desulfurisation of the CTA will be discussed in the next section.

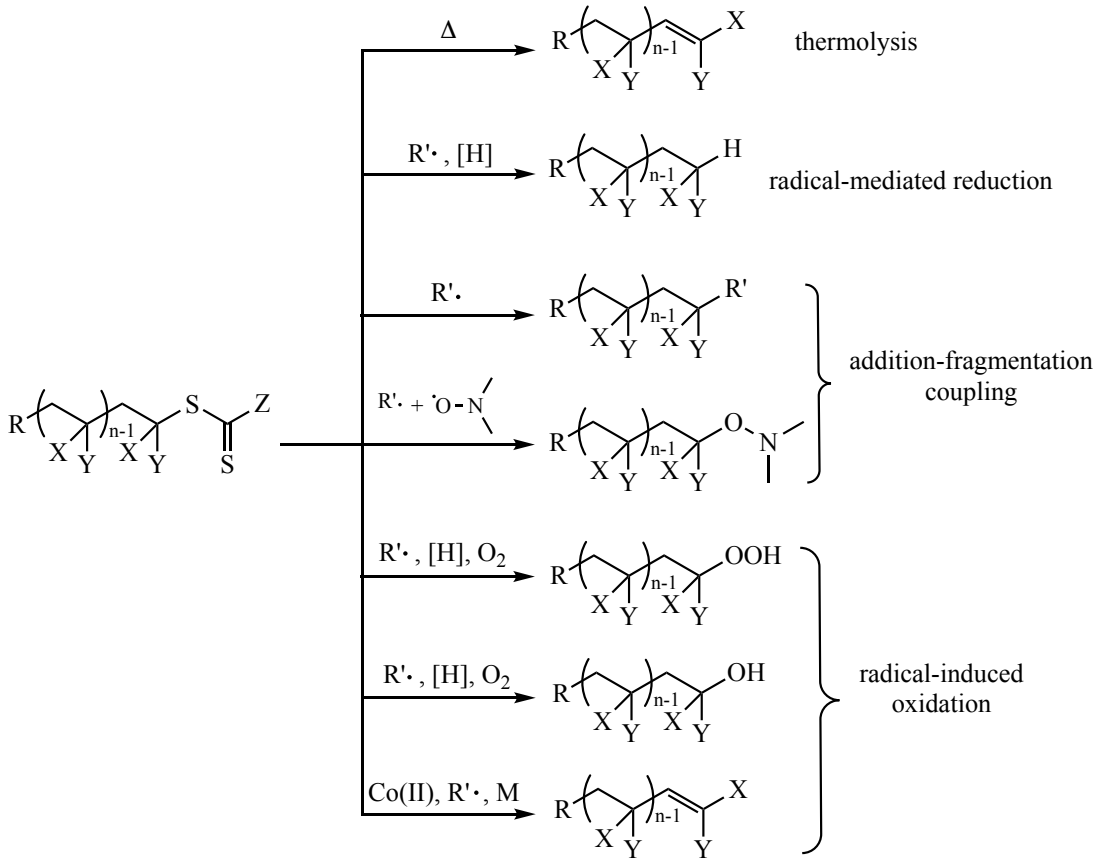

Figure 1-5 Overview of general reactions for the complete desulfurisation of RAFT thiocarbonylthio end-groups.

1.4.1 Desulfurisation of RAFT (Co)Polymers

1.4.1.1 Thermolysis

The total removal of S-containing species from RAFT polymers can be accomplished by several radical-based routes, **Figure 1-5**. From a practical point of view, thermolysis is the easiest method because it simply involves heating the (co)polymer.[30] However, the extent, purity of the product, and mechanism by which end-group removal occurs under such conditions are dependent on the monomer and the nature of the thiocarbonylthio species. This was evident even in the earliest reports from Postma *et al*. in their studies on trithiocarbonate and xanthate end-group removal in polymers prepared with phthalimidomethyl R-group functional CTAs.[31,32]

Researchers from the same group have studied the thermolysis of RAFT-prepared poly(methyl methacrylate) (PMMA), observing that the products obtained were highly dependent on the RAFT agent employed in polymer synthesis.[33] For PMMA prepared with a trithiocarbonate CTA (2-cyanoprop-2-yl methyl trithiocarbonate), end group removal was proposed to occur *via* homolytic cleavage of the PMMA-S bond followed by depolymerisation; a process that continued until radical annihilation, **Scheme 1-5**.

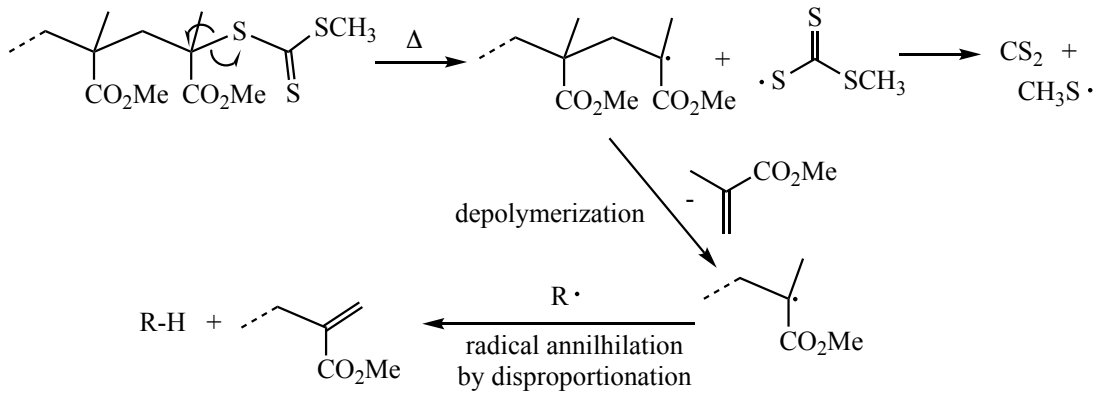

Scheme 1-5 Desulfurisation pathways in poly(methyl methacrylate) prepared with a trithiocarbonate CTA.

For PMMA prepared with a dithiobenzoate CTA, elimination was proposed to proceed by a concerted intramolecular process analogous to the Chugaev reaction, **Scheme 1-6**.[34]

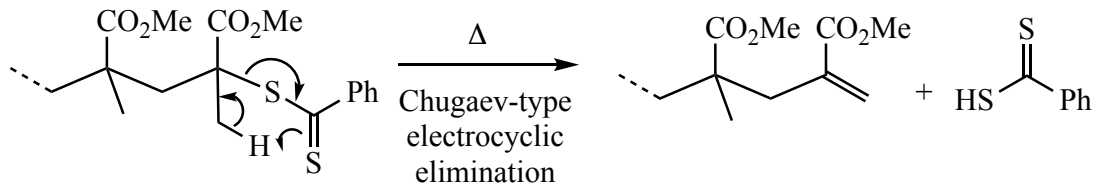

Scheme 1-6 Desulfurisation pathways in poly(methyl methacrylate) prepared with a dithioester CTA.

In general, thermolysis on dithiobenzoate-prepared (co)polymers is cleaner and yields macromonomer products whose molecular weight and molecular weight distribution are comparable to the parent polymer whereas degradation products are also observed with PMMA prepared with a trithiocarbonate.

1.4.1.2 Radical-Mediated Reduction

Complete desulfurisation of RAFT terminated polymers can be achieved by radical-mediated reduction. Inspired by the Barton-McCombie reaction for the deoxygenation of secondary alcohols, such radical-mediated reduction has been applied to other thiocarbonylthio species including RAFT agents.[35,36] Not surprisingly, the general approach has also been successfully applied to the complete removal of thiocarbonylthio end-groups in RAFT-prepared (co)polymers.[37,38]

The general process is based on the fundamental RAFT addition-fragmentation mechanism, **Scheme 1-7**. The reaction involves the addition of a radical (X·) to the thiocarbonyl group of the RAFT-prepared (co)polymer (**5**) generating an intermediate (**12**) which fragments to provide a new thiocarbonylthio compound (**13**) and the propagating radical (**14**). The reaction of the propagating radical (**14**) with an H atom donor gives the final product, P_n-H, in which the thiocarbonylthio group is replaced with hydrogen.

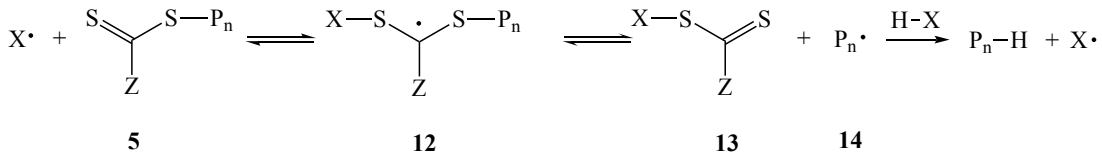

5 **12** **13** **14**

Scheme 1-7 General mechanism for the radical-mediated reduction of a RAFT thiocarbonylthio end-group.

However, various side reactions can occur, including "normal" termination reactions. For example, the intermediate (**12**) and the propagating radical (**14**) can react with other radical species such as initiator-derived radicals, transfer agent-derived radicals and propagating radicals.

Tributylstannane, Bu_3SnH, has been employed extensively as the H-donor source in radical-mediated reductions on RAFT-prepared (co)polymers.[39,40] However, due to the toxicity of stannanes and stannane-derived byproducts, alternative H-donors have also been investigated. Silanes are one alternative as H-donors in radical-mediated reduction reactions.[41] Chong *et al*. evaluated a range of potential H-donors for the radical-mediated reduction of well-defined polystyrene terminated with dodecyltrithiocarbonate chain ends.[38] They reported, for example, that a bimodal molecular weight distribution was observed when tris(trimethylsilyl)silane was employed as an H-donor.[38] They concluded that for RAFT end-groups, radical-mediated reduction is more effective with more active hydrogen-donor species, with the most effective being tributylstannane, followed by *N*-ethylpiperidine hypophosphite (EPHP) and tris(trimethylsilyl)silanes, followed by 2-propanol, with the least effective being toluene.[38]

While not as effective as Bu_3SnH, hypophosphite salts, such as EPHP, do serve as convenient alternatives to both stannanes and silanes given their reduced toxicity and aqueous solubility that can aid significantly in work-up. In fact, EPHP has been shown to be effective for the removal of dithioester, trithiocarbonate and dithiocarbamate end-groups on different RAFT-prepared (co)polymers.[42-45] A further indication of the advantages of using EPHP is the fact that it is commonly employed to reduce end-groups in polymers specifically targeted for bioapplications.[46-48]

More recently, there has been interest in photo-induced RAFT end-group reduction.[49,50] For example, Carmean and co-workers described the efficient, catalyst-free, UV-mediated removal of thiocarbonylthio groups of all four major RAFT agent families from a range of polymers including poly(*N,N*-dimethylacrylamide), poly(methyl methacrylate), poly(*N*-vinylpyrrolidone), polystyrene, and poly(methyl acrylate).[51] The general approach, with poly(*N,N*-dimethylacrylamide) highlighted, is shown in **Scheme 1-8**. Simple UV irradiation of the parent RAFT polymer results in homolytic cleavage of the terminal C-S bond liberating what is in essence a propagating poly(*N,N*-dimethylacrylamide) radical. This immediately abstracts H from the donor source, EPHP in this instance, yielding the H-terminated polymer. The use of EPHP was efficient for all the above noted polymers with the exception of polystyrene. In this instance incomplete end-group conversion was observed with EPHP; however, switching the H-donor source to Bu_3SnH did yield full H-terminated polystyrene without any evidence of undesirable coupled products.

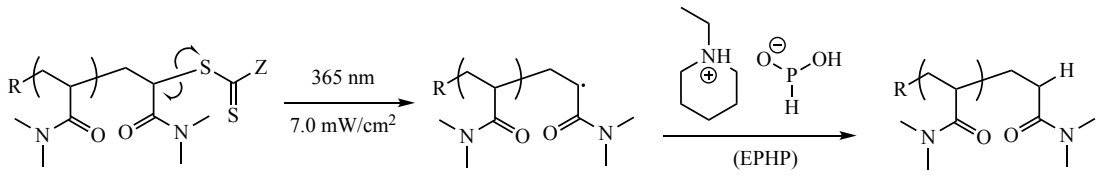

Scheme 1-8 UV-initiated photolysis followed by H abstraction from EPHP as a facile route to H-terminated poly(*N,N*-dimethylacrylamide).

1.4.1.3 Addition-Fragmentation Coupling

In a related process, the reaction of thiocarbonylthio end-terminated (co)polymers with an excess (typically > 20:1 molar ratio of azo compound to end groups) of an added azo species can be employed to substitute RAFT end-groups with radical fragments originating from the thermal decomposition of the added azo compound.[52] The general process, highlighting the use of AIBN is shown in **Scheme**

1-9.

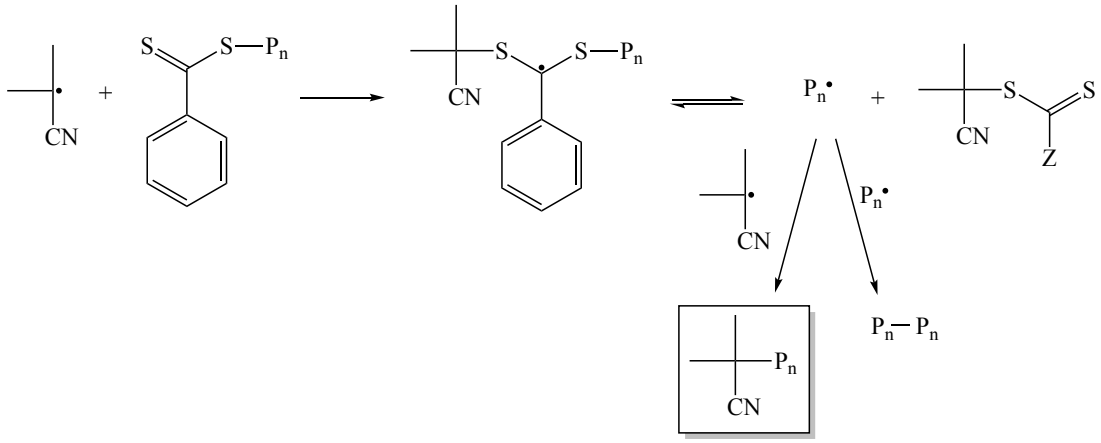

Scheme 1-9 Desulfurisation of RAFT-prepared polymer *via* the reaction with an excess of AIBN.

AIBN decomposes under thermal conditions to form two cyanoisopropyl radicals, which react at the C=S bond of the thiocarbonylthio group, forming the intermediate carbon-centred radical, just as expected in a typical RAFT reaction. This intermediate can either fragment back into the original attacking radical or fragment the polymeric leaving group. Assuming fragmentation occurs in the direction liberating the polymeric radical, $P_n\cdot$, then this species is formed in the absence of monomer but in the presence of a potentially high concentration of cyanoisopropyl radicals. This species can, of course, self-terminate, but under the right conditions, $P_n\cdot$ will react with a cyanoisopropyl radical yielding the target end-capped polymer. Perrier *et al*. were the first to describe such addition-fragmentation coupling reactions, highlighting not just the ability to use this chemistry as a means for end-group modification, but also as a potential route for recovering chain transfer agent.[53] The authors have successfully applied this approach to a variety of dithiobenzoate/thiocarbonylthio end-group methacrylic, acrylic, acrylamido and styrenic polymers with various azo initiators.[53] Chen *et al*. also examined the removal

of thiocarbonylthio end-groups in RAFT-prepared polymers with AIBN.[54] These authors found that while end-group transformation was successful with methacrylic polymers it was less effective with acrylic and styrenic polymers.[54] In contrast, the use of lauryl peroxide did result in the complete removal of end-groups in acrylic and styrenic polymers, but it was not a clean process and yielded a significant amount of polymer-polymer coupled products.[54] Interestingly, the amount of polymer-polymer coupled species could be minimised if a combination of lauryl peroxide (2 equivalents) with AIBN (20 equivalents) was employed.

1.4.1.4 Radical-Induced Oxidation

End-group modification of RAFT-synthesised (co)polymers can occur upon reaction with oxidising species. Cleavage of the thiocarbonylthio end-group and substitution with a hydroxide group can be achieved through radical-induced oxidation. It has, for example, been observed that the storage of RAFT CTAs and RAFT-prepared polymers in cyclic ethers such as tetrahydrofuran (THF) and 1,4-dioxane, can lead to the formation of hydroperoxide end-groups through a radical autoxidation process with molecular oxygen.[55] It is possible to control the reaction by heating a RAFT-synthesised (co)polymer at 60°C with an azo initiator (typically AIBN) in ambient air. The first step produces hydroperoxide end-terminated (co)polymers, and subsequent reduction to hydroxyl functional (co)polymers is achieved by using triphenylphosphine, **Scheme 1-10**.[56,57]

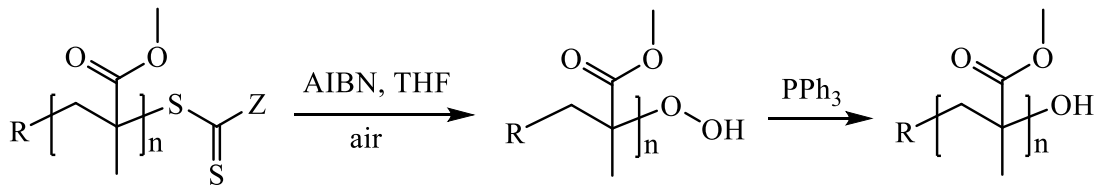

Scheme 1-10 Formation of hydroxy-terminated poly(methyl methacrylate).

The mechanism involves a radical oxidation cycle with an intermediate chain transfer step, analogous to the radical autoxidation of ethers.[58]

Li and co-workers studied the kinetics of radical-induced oxidation of RAFT agents with respect to the effect of molecular structure.[59] They found that, according to chain-transfer ability, the stability of thiocarbonylthio compounds towards oxidation depends on both Z and R groups: electron deficient Z-groups or bulky R-substituents lead to decreased stability, while electron-donating groups in the Z-substituents increase stability. As such, trithiocarbonates and xanthates were found to have higher stability than dithioesters towards oxidation.

1.5 Post-polymerisation modification

The history of post-polymerisation modification reactions is as old as polymer science. During the middle of the 19th century some processes, that we now classify as post-polymerisation reactions, were discovered: the transformation of natural rubber into a more solid material through sulfurisation, the formation of nitrocellulose by reacting cellulose with nitric acid and lastly, the preparation of cellulose acetate by heating cellulose with acetic anhydride.[60-62] Those processes have been widely used during the past two centuries, but non-quantitative reactions of functional groups, poor reaction efficiency and the necessity of harsh reaction conditions caused potential defects in the polymeric structure of the final product and greatly increased polymer heterogeneity. During the 1950s, after the concept of “macromolecules” was widely accepted by the scientific community, post-polymerisation chemistry saw further developments. During those years, processes such as functionalisation of butadiene polymers with aliphatic thiols, chlorination of polystyrene and divinylbenzene, the development of solid-state peptide synthesis, just to name a few, were discovered and

studied.[63-65] It was only in the early 1990s, with the discovery of RDRP techniques such as atom-transfer radical polymerisation (ATRP), reversible addition-fragmentation chain transfer (RAFT) and nitroxide-mediated polymerisation (NMP), and the concomitant emergence of coupling reactions known as "click chemistry", that a wider range of chemical reactions became available and accessible for post-polymerisation modifications.[13,66,67]

RDRP techniques brought improved functional group tolerance compared to traditional "living" polymerisation techniques, enabling the synthesis of well-defined polymers bearing a plethora of functional groups, many of which could be quantitatively and selectively modified under mild conditions and without side reactions.[68] This, fortuitously coincided with the report of several chemoselective coupling reactions known as "click chemistry", such as the copper(I)-catalysed alkyne-azide cycloaddition (CuAAC) and 1,3-dipolar cycloaddition reaction.[69,70]

The advantages of functionalisation of a reactive polymer, over direct polymerisation, are numerous: the possibility to synthesise a library of functional polymers from the same parent precursor, ensuring that all polymeric derivatives will have the same degree of polymerisation, tacticity and molecular weight distribution.[71] Moreover, the direct polymerisation of functionalised monomers can have the disadvantage of limited functional group tolerance under the polymerisation conditions. For example, the functional group attached to the monomer could undergo side reactions which could lead to uncontrolled polymerisation or suppression of the polymerisation process by reacting with the initiator/catalyst or the monomer. Functional groups could also be incompatible with the reaction solvent or reaction conditions, which can lead to retardation in chain growth.[72] Post-polymerisation modification allows chemical modifications to be routinely conducted under mild

conditions avoiding the occurrence of all the aforementioned potential issues. Among the many different chemical reactions available to modify a polymer for functionalisation, activated ester amine exchange has some advantages over other synthetic approaches, which will be examined in the next section.

1.5.1 Activated esters

In the 1970s Ringsdorf and Ferruti demonstrated the reactivity and utilisation of active ester functionalities, pioneering the synthesis and post-polymerisation modification of active ester polymers.[73,74] Since these reports, scientists have developed a wide variety of active ester polymers utilising the entire spectrum of available polymerisation techniques. Among the many different chemical approaches to undertake post-polymerisation functionalisation, the advantages of activated ester-amine exchange over other reactions, have led to the growth in the field and the development of a variety of monomers bearing active esters. This type of reaction provides ready access to polyacrylamide and polymethacrylamide derivatives which cannot necessarily be prepared *via* traditional polymerisation of the corresponding functionalised monomer (**Scheme 1-11**).

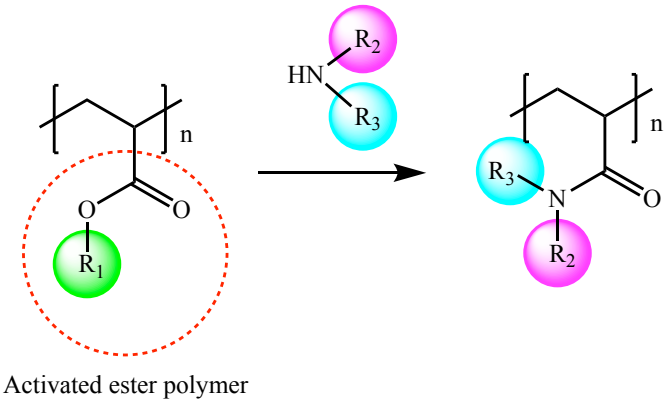

Scheme 1-11 Post polymerisation modification using activated ester-amine chemistry.

Activated esters are a useful tool for the covalent binding of functional amines through the formation of a stable amide bond, which is the basis of many biological systems. In fact, activated esters have been studied and utilised in synthetic peptide chemistry.[75] From the synthetic viewpoint, activated ester chemistry is convenient owing to the abundant availability of many functional amines from natural or commercial sources, compared to other chemicals which could be employed in post-polymerisation modification reactions.

1.5.2 Selection of activated ester-containing monomers

The growth in the field has led to the development of a variety of monomers bearing active esters. A selection of the various types of monomers featuring different activated ester moieties that have been utilised as the reactive site for post-polymerisation modifications is shown in **Table 1-2**.

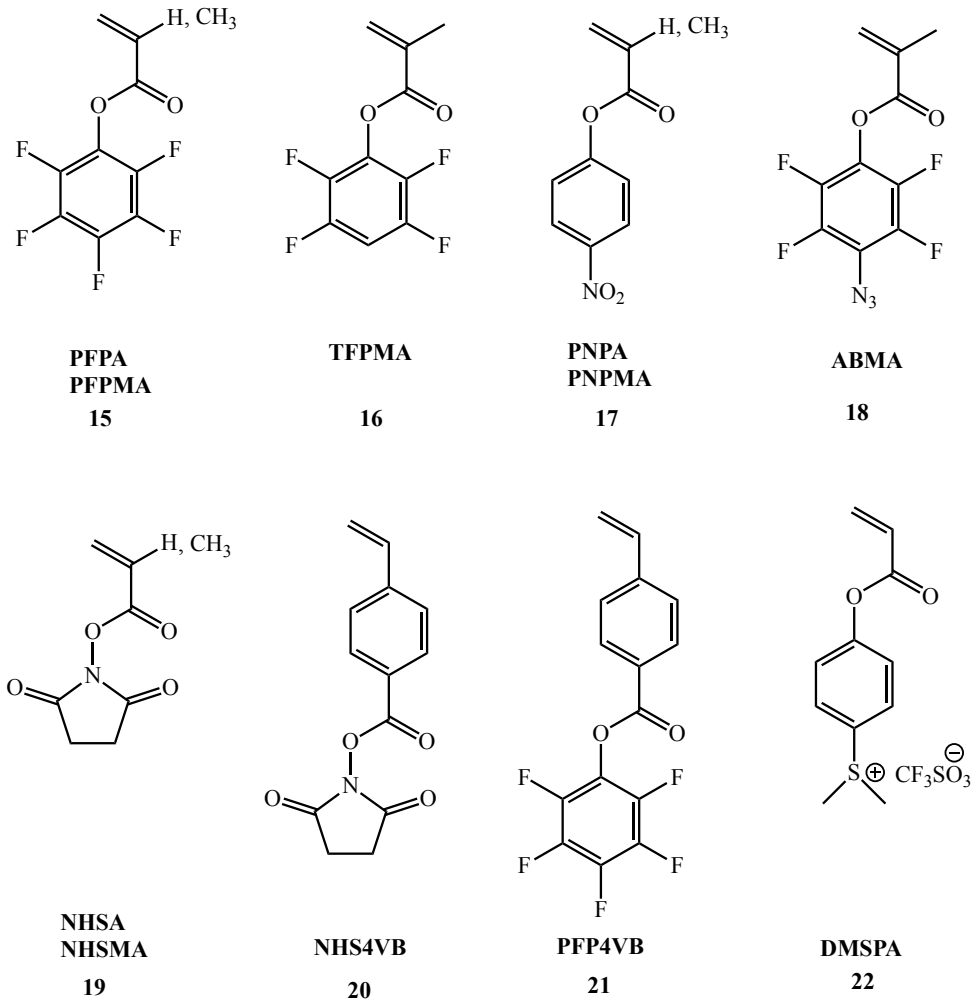

Table 1-2 Structures of selected activated ester-containing monomers.[72]

The most utilised activated esters monomers are *N*-hydroxysuccinimide (NHS) ester-containing monomers (**Table 1-2**, **19**). *N*-Hydroxysuccinimide (NHS) and *N*-hydroxysuccinimide acrylate (NHSA)/methacrylate (NHSMA) were used for the first time in radical polymerisation reactions with AIBN in the 1970s (**Scheme 1-12**).[73,74]

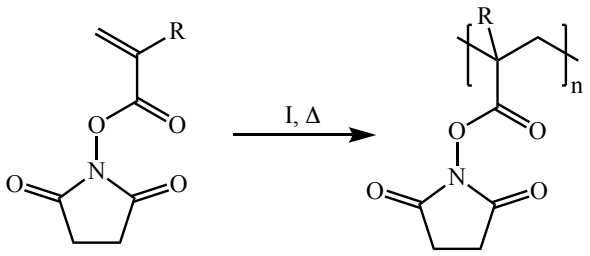

R = H, Me
NHSA
NHSMA
19

R = H, Me
poly(NHSA)
poly(NHSMA)

Scheme 1-12 Radical homopolymerisation of NHSA/NHSMA.

Polymers containing NHS-ester reactive moieties are fairly resistant to hydrolysis, but readily undergo nucleophilic acyl substitution with primary and secondary amines under mild conditions generating functionalised polyacrylamide derivatives.[76] It was reported that under the exact same conditions, polyNHSA was more reactive than polyNHSMA and this was attributed to a steric effect.[73] Nevertheless, the major drawback of polyNHSA and polyNHSMA is the fact that, while they are soluble in dimethylformamide (DMF) and dimethyl sulfoxide (DMSO), they are poorly soluble in most other organic solvents. Therefore, NHSA and NHSMA are commonly copolymerised with other monomers to increase the overall copolymer solubility in a wider range of organic solvents.[72,77] Limitations in the use of NHS-ester based monomers are possible side reactions, as described below.

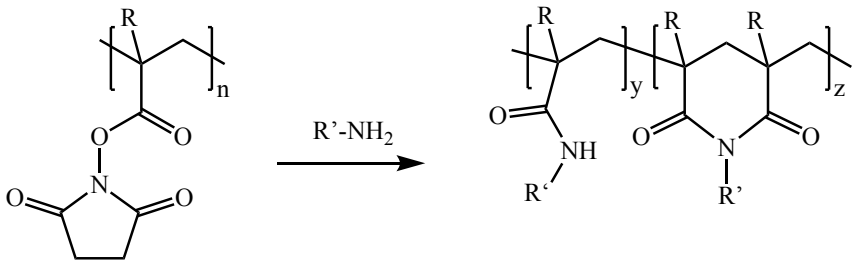

R = H, Me

poly(NHSA)
poly(NHSMA)

R = H, Me

Scheme 1-13 Possible side reactions during aminolysis of polyNHSA/polyNHSMA.

During the acyl substitution step, *N*-substituted glutarimides can be formed by the attack of adjacent activated esters *via* the formation of an imide bond (**Scheme 1-13**). This issue can be mitigated by performing the reaction at a high temperature or by employing an excess of amine or other proton scavenging agents such as triethylamine.[78]

Given the possible drawbacks in the use of this type of functional monomer and its poor solubility in common organic solvents, other monomer-containing active-ester functionalities have been explored by synthetic chemists. Very common and versatile are pentafluorophenyl (PFP) ester-based monomers (**Table 1-2**, **15**, **16**, **18**, **21**). After NHS-esters, pentafluorophenyl (PFP) ester-based acrylates (PFPA) methacrylates (PFPMA, **Table 1-2**, **15**) and vinylbenzoates (PFP4VP, **Table 1-2**, **21**) are the second most examined species of active-esters for post-polymerisation modification reactions.[79] One example of a monomer containing a sulfonium triflate functionality is shown, 4-acryloxyphenyl-dimethylsulfonium triflate (DMSPA, **Table 1-2**, **22**).[68] The synthesis and use of PFPA as a monomer was first reported by Blazejewski and co-workers.[80]

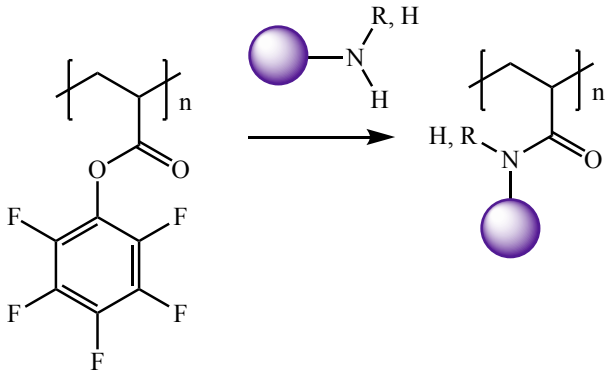

Scheme 1-14 Pendant amide formation using polyPFPA activated ester chemistry.

In contrast to NHS-ester based polymers, polyPFPA and polyPFPMA are soluble in most organic solvents and are considered easier to handle in a laboratory setting. Comparative reactivity studies between NHS-ester based polymers and PFP-based polymers have been carried out with various primary, secondary and aromatic amines and alcohols (**Scheme 1-14**). It was reported that PFP-ester polymers were in general more reactive than NHS-ester based polymers, with pentafluorophenyl acrylates showing higher reactivity than the methacylates.[79] Moreover, the reactivity of PFP-ester polymers towards primary and secondary amines was much higher than aromatic amines and alcohols.[79] The PFP moiety as an active ester has been incorporated in different types of monomers. As an example, 4-vinyl benzoate monomers containing PFP active esters have been studied and functionalised with various amines by Nilles and Theato.[81] The most reactive was pentafluorophenyl 4-vinyl benzoate (PFP4VB) monomer (**Table 1-2**, **21**), whose reactivity was even higher than the polymethacrylic and polyacrylic analogues, resulting in the successful substitution by traditionally less reactive amines such as aniline.[81] Interestingly, the reaction of polyPFP4VB with aliphatic amines occurred at 0°C in only 5 minutes.[81] A more recent example of functionalised active ester monomer bearing PFP modified structure is the 4-azido PFPA monomer (ABMA), (**Table 1-2**, **18**) which has been

synthesised and studied by Roth's group.[82] This novel monomer has been employed in RAFT homopolymerisation and modified post-polymerisation with phosphines to give iminophosphoranes (**Scheme 1-15**, **A**) with near quantitative conversions and with phenylacetaldehyde, morpholine and piperidine to give the corresponding amidine derivatives (**Scheme 1-15**, **B**).[82]

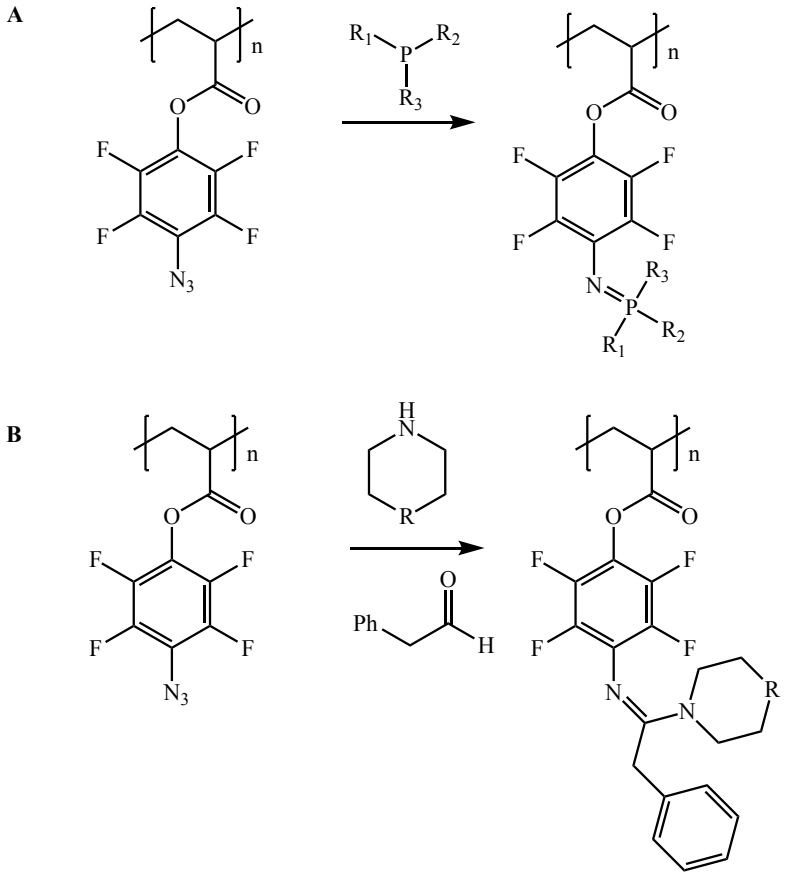

Scheme 1-15 Reaction scheme of phosphines to give iminophosphoranes (A) and azide-aldehyde-amine reaction involving phenylacetaldehyde and piperidine (B).

There are fewer examples of polymers containing other activated ester functionalities. One alternative example is *p*-nitro phenyl methacrylate (PNPMA), **Table 1-2**, **17**. This monomer has been copolymerised with *N*-(2-hydroxypropyl)-methacrylate *via* radical polymerisation.[83,84]

Another interesting functionalised monomer that has attracted attention from synthetic chemists is 2-vinyl-4,4-dimethyl-5-azlactone (VDMA).[85] Azlactone containing polymers have been utilised for post-polymerisation modification due to the ability of the azlactone ring to undergo ring-opening upon reaction with a wide selection of nucleophiles, including amines and thiols (**Scheme 1-16**).[86] PolyVDMA has shown its ability to react quantitatively with amines to form amide bonds producing novel bis-amine functionalised polymers.[87,88]

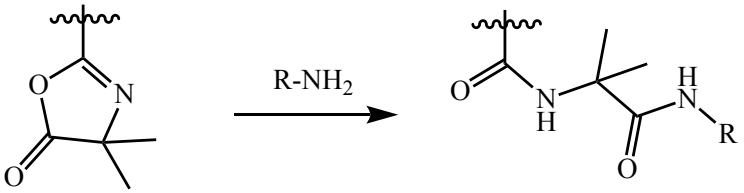

Scheme 1-16 Reaction of the azlactone group with primary amines.

Interestingly, this reaction can successfully proceed in aqueous solutions, with minimum hydrolysis.[89] For instance, polyVDMA-protein conjugates have been synthesised using this chemistry for applications in drug delivery.[90]

1.6 RAFT-metal hybrids

The idea of including metals into (co)polymers prepared by RAFT polymerisation has been explored in the past two decades. Three general approaches for the synthesis of RAFT polymer-metal hybrids are as follows:

- Click chemistry: RAFT polymers and metal complexes are grafted together through azide-alkyne reactions;

- Functionalised monomer: the monomer is functionalised with either a ligand or a metal complex prior to polymerisation;
- Functionalised CTA: the RAFT agent is functionalised with either a ligand or a metal complex prior to polymerisation.

Click chemistry has been employed for the synthesis of polypyridine ruthenium(II) chromophores on polystyrenic polymers, employed as light-harvesting antenna.[91] In this case, poly(4-vinylbenzyl chloride) was made by RAFT and subsequently functionalised with azide, followed by a "click" reaction with a Ru(II) polypyridine complex (**Figure 1-6**) with an alkyne functionality on one of the ligands.[91] Both photophysical and electrochemical properties of the materials were investigated.

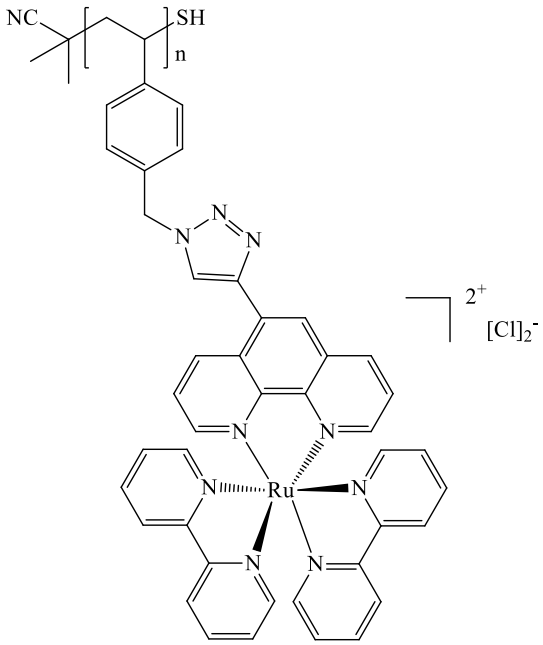

Figure 1-6 Polypyridine ruthenium(II) complex on a polystyrenic polymer. Adapted from ref. 91.

The functionalisation of monomers has also been explored as a method to make RAFT-metal hybrids. Schubert *et al.* reported the synthesis of a PMMA Ru(II) polypyridine complex made by RAFT.[92] Firstly, a methacrylate monomer containing a Ru(II) heteroleptic complex was made, followed by its RAFT copolymerisation with methyl methacrylate. The authors employed a similar approach for the incorporation of Os(II) bis-terpyridine complex into a RAFT PMMA polymer, by synthesising an Os(II) bis-terpyridine functionalised monomer, followed by RAFT polymerisation with MMA (**Figure 1-7**).[93]

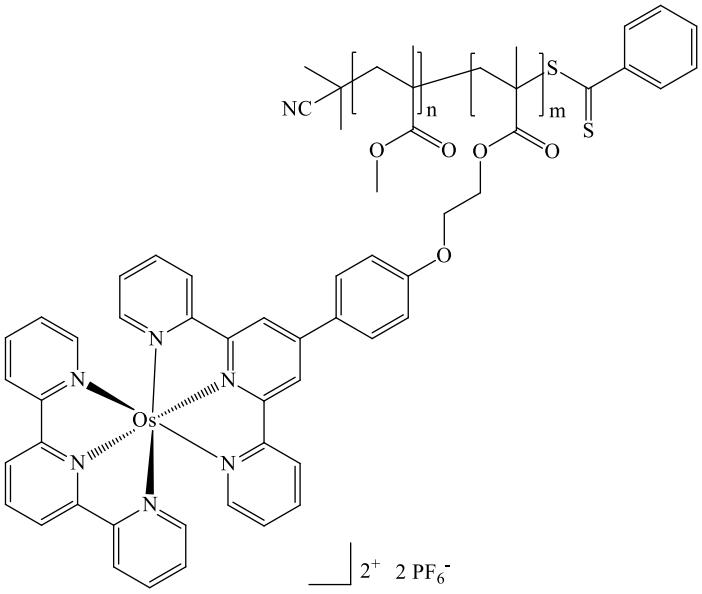

Figure 1-7 Os(II) bis-terpyridine complex into a RAFT PMMA polymer. Adapted from ref. 93.

Moreover, the same research group synthesised a methacrylate-based copolymer bearing ligands sites for the coordination of iridium complexes and investigated its photophysical properties.[94]

The idea of incorporating either a ligand or a metal complex into the RAFT agent itself has also been explored. Zhou *et al*. reported the synthesis of a terpyridine-functionalised dithioester CTA used for the polymerisation of styrene, followed by a complexation reaction with Ru(II) complexes.[95] Interestingly, the ruthenium complex coordinates to two terpyridine-functionalised polystyrenic polymers, giving rise to a metal complex containing two polymeric chains. The same research group synthesised a ruthenium tris-pyridine complex by following the same methodology.[96] In this case, a bipyridine-functionalised dithioester was made and employed for polymerisation of styrene, followed by a complexation reaction with a Ru precursor.[96] Interestingly, each metal centre was coordinated to three bipyridine ligands, forming tri-functionalised star copolymers.

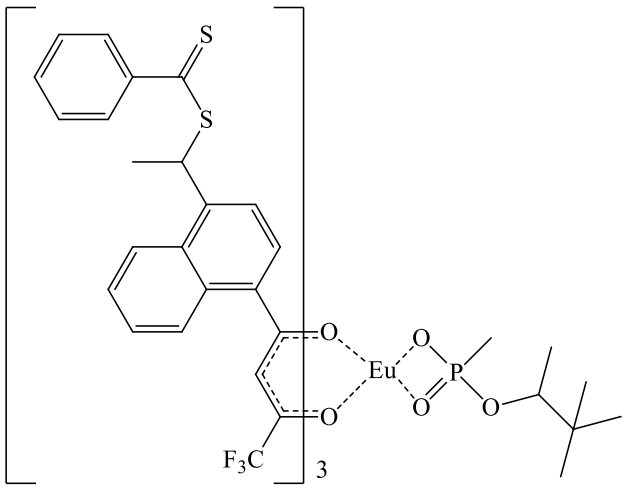

Figure 1-8 Dithiobenzoate CTA containing tris(β-diketonate) europium(III) complex. Adapted from ref. 97.

Other than incorporating a ligand into the CTA prior to RAFT polymerisation, it is possible to synthesise a CTA containing a metal complex. This approach has been reported with the synthesis of a dithiobenzoate CTA containing tris(β-diketonate)

europium(III) complex (**Figure 1-8**).[97] The lanthanide-containing CTA has then been employed in the polymerisation of MMA.

1.7 Photophysical properties of metal complexes

1.7.1 Fundamental concepts

Light can interact with matter: upon irradiation with electromagnetic radiation, materials can emit light and luminesce.[98] The Beer-Lambert law describes the absorption of light in a dilute solution (**Equation 1-4**):

$$I_0 = I\,10^{\varepsilon bc} \qquad \textbf{Equation 1-4}$$

where I is the radiation transmitted intensity and I_0 is the incident radiation at a given wavelength, b is the path length of the radiation, c is the concentration and ε is the molar absorptivity coefficient which is a constant proportional to the ability of the molecule to absorb light at given wavelengths.

When a molecule absorbs a photon, electrons can be excited to a higher energy level, producing electronically-excited states. This happens because ions and molecules have quantised electronic levels, which have a separation that is of the same order as the energy of visible and ultraviolet light.[98] Thus, absorption and emission of light are phenomena that occur due to the excitation of electrons, which have dual wavelike and particle-like properties. S_0 is the lowest vibrational state of the electronic ground state and, according to the Boltzmann distribution, at room temperature, almost all molecules will be in this state.[98] Therefore, when absorption occurs, it always takes place from this electric ground state (S_0) to an excited state S_n (where $n > 0$). The Franck-Condon principle states that electronic transitions are fast enough for the nuclei

movement to be considered negligible.[99] As a consequence, electronic transitions between states S_n are referred to as vertical transitions and can be represented as vertical arrows in potential energy diagrams. The Jablonski diagram in **Figure 1-9** illustrates what can happen after the excitation of a molecule.[98]

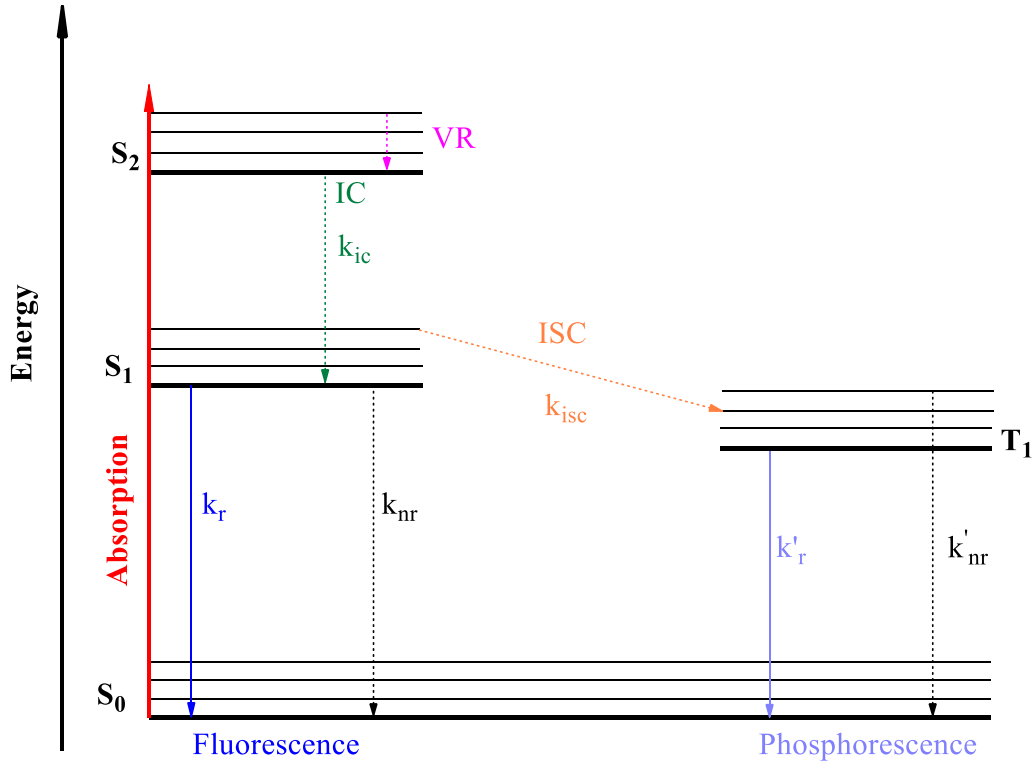

Figure 1-9 Simplified representation of a Jablonski diagram illustrating fluorescence and phosphorescence.

Once a molecule is in the so-called "electronically-excited state" (S_n), vibrational relaxation (VR) and internal conversion (IC) processes can occur. Each S_n level is divided into vibrational sublevels and during vibrational relaxation, energy is dissipated between vibrational levels of the same excited state. Internal conversion is the transition between excited energy levels with the same spin multiplicity and it occurs between the excited levels to S_1 as a result of the strong overlap between many

states of nearly equal energy.[99] According to Kasha's rule, photon emission can only occur from the lowest electronically excited state, therefore, as a consequence of this rule, the emission wavelength is independent of the excitation wavelength. Both VR and IC are very rapid processes that occur in the order of $10^{-13}/10^{-14}$ seconds.[99]

Intersystem crossing (ISC) is the transition between excited states of different multiplicity and, despite violating the selection rules which will be discussed below, it can occur in the presence of heavy atoms which favour spin-orbit coupling making the transition partially allowed. The coupling between the electron spin angular momentum and the orbital angular momentum, is responsible for the occurrence of intersystem crossing, despite being formally forbidden. ISC is characterised by k_{isc}, a rate constant that is usually in the order of $10^{-8}/10^{-9}$ s^{-1} and is correlated to the dimension of the nucleus, which explains why heavier atoms can partially allow this transition.[99]

Decay to the ground state can happen *via* radiative and non-radiative processes. Non-radiative decays are governed by the energy gap law (**Equation 1-5**), which describes the relationship between the dissipation of energy throughout overlap of vibrational levels and the non-radiative decay constant k_{nr}:

$$k_{nr} = Ae^{-\alpha \Delta E} \qquad \textbf{Equation 1-5}$$

where k_{nr} is the non-radiative decay constant, A is the pre-exponential coefficient, α is a proportionality constant and ΔE is the energy gap between the excited and the ground state. From **Equation 1-5** it is possible to observe how low rates of non-radiative decay are a consequence of high energy gaps between the excited and the ground state.[100]

Aside from non-radiative decays, dissipation of energy can occur through radiative processes, i.e. *via* the emission of light. Radiative emissions consist of the spontaneous emission of light ($h\nu$) during a transition to the ground state. This phenomenon is known as luminescence. Two types of luminescence phenomena exist, depending on the nature of the excited state. Fluorescence is the spin-allowed transition that occurs when the excited state and the ground state have the same multiplicity ($S_1 \rightarrow S_0 + h\nu$). Phosphorescence, on the other hand, is formally spin-forbidden and occurs between states of different multiplicity ($T_1 \rightarrow S_0 + h\nu$). The timeframe of fluorescence is between 10^{-9} and 10^{-7} seconds, while for phosphorescence it is between $10^{-4}/10^{-1}$ seconds. Phosphorescence is associated with slower decay rates, as a consequence of the change in spin multiplicity required for the decay from the triplet excited state T_1 to the ground state S_0.[99]

The probability that a given transition will occur is governed by the so-called "selection rules" which are related to the symmetry and the multiplicity of the ground and excited states. According to the spin conservation rule, only transitions between states of the same multiplicity (or same spin quantum number) will be allowed. For instance, singlet to singlet transitions are allowed, whereas singlet to triplet transitions are forbidden. The Laporte selection rule is related to centrosymmetric systems, and it states that for a transition to occur, the change in the orbital angular momentum quantum number for the individual electron must be $\Delta l \pm 1$, and for the entire multi-electronic system $\Delta L = 0 \pm 1$, thus allowed transitions must involve a change in parity: $g \rightarrow u$ or $u \rightarrow g$ are allowed, where *g* states for *gerade* and *u* for *ungerade*. The Laporte rule can be relaxed when phenomena called "vibronic coupling" occur, which are processes arising from the interaction between a vibrational transition and an electronic transition, during which the asymmetric vibration of the latter temporarily

removes the inversion centre of the molecule.[99] In this case, the overall symmetry of the system decreases, making forbidden transitions possible, such as d → d transitions in metal complexes. Due to the loss of absorbed energy throughout non-radiative processes after excitation, emission spectra are typically red-shifted to lower energies compared to absorption spectra; this phenomenon was observed for the first time in 1852 by Sir G. G. Stokes and today is known as the "Stokes shift".[99,101]

In order to investigate luminescence phenomena and evaluate the competition between radiative and non-radiative decay pathways, it is essential to define some essential parameters. Luminescence lifetime (τ) is defined as the time after which the population of an excited state has decayed by 1/e or 36.8%. Lifetime is expressed as a function of a radiative and non-radiative rate constant (**Equation 1-6**).[99]

$$\tau = \frac{1}{k_r + \Sigma k_{nr}} \qquad \textbf{Equation 1-6}$$

The quantum yield is expressed as the ratio between the number of emitted photons and the number of absorbed photons and is defined by **Equation 1-7**:

$$\Phi_r = \frac{k_r}{k_r + \Sigma k_{nr}} \qquad \textbf{Equation 1-7}$$

1.7.2 Molecular oxygen

The emission arising from the triplet state of a metal complex can be quenched by molecular oxygen. Molecular oxygen has a very small size and can diffuse quickly into solutions. Since molecular oxygen has a triplet ground configuration, it can quench the excited states of metal complexes through intermolecular collisions. This

can happen because, as previously mentioned, the emission from the triplet state of metal complexes is spin forbidden and therefore long lived.[102-104]

The process is illustrated in **Figure 1-10**: molecular oxygen in its ground triplet state can collide with metal complex excited states through triplet-triplet energy transfer (ET). Exchange of electrons occurs causing both states to become singlet states: oxygen in its excited state $^1O_2$ and the metal complex in its ground state S_0.

The emission arising from the lowest excited state of oxygen ($^1\Delta_g$) occurs at a characteristic band at 1270 nm and can be easily detected with a NIR detector.[105]

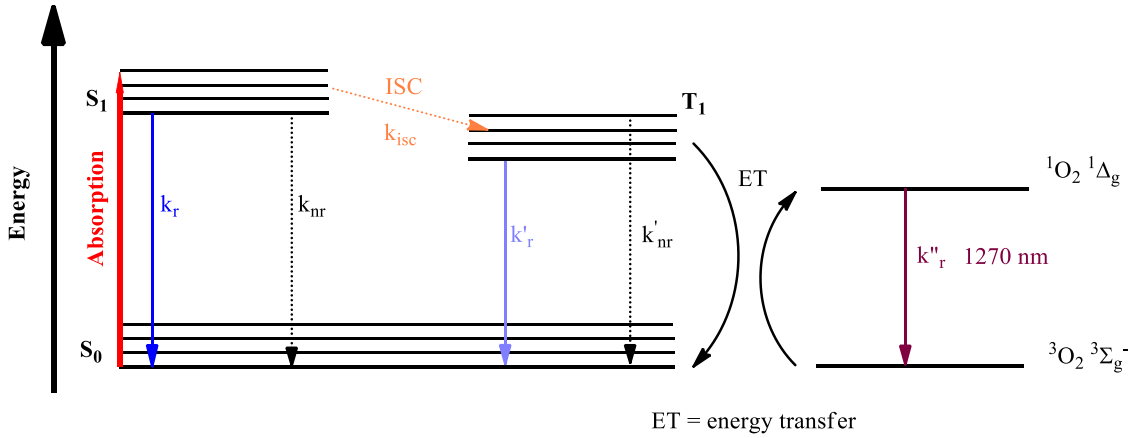

Figure 1-10 Simplified Jablonski diagram showing how molecular oxygen can quench the triplet state emission of metal complexes.

When studying and designing probes for biological imaging, it is essential to be aware of this phenomenon, because the production of singlet oxygen can lead to cytotoxicity in biological systems. Singlet oxygen can react with proteins, DNA and lipids *via* redox processes. For this reason, when designing biological probes, the generation of singlet oxygen should be kept very low if not completely avoided, to ensure no damage is caused to cells or biological tissues. Nevertheless, molecular

oxygen toxicity and its ability to undergo apoptosis and programmed cell death can be exploited for pathology treatments, for example, cancer, employing photodynamic therapy.[106,107]

1.7.3 Drawbacks of fluorescent probes

An organic molecule that possesses high molar extinction coefficients and high quantum yields can absorb and emit sufficient light to be used as a fluorophore.[108] Nevertheless, organic fluorophores can suffer from some issues which will reduce the quality of the images and the resolution, limiting the fluorophores from being employed. Usually, fluorescent organic molecules possess relatively short Stokes shifts, which cause the absorption and emission profiles to overlap, causing self-quenching of adjacent molecules due to the re-absorption of emitted photons.[99] Self-quenching can drastically reduce the intensity of the signal arising from the probe used. Moreover, organic fluorophores can emit signals which overlap with background autofluorescence in biological systems, therefore the signal arising from organic fluorophores may be difficult to distinguish from autofluorescence. Autofluorescence is a phenomenon that originates from endogenous fluorophores present in biological systems such as aromatic amino acids able to absorb light (tryptophan, tyrosine and phenylalanine) or some enzymes cofactors (nicotinamide adenine dinucleotide, NADH or flavin adenine nucleotide, FAD).[109] Usually, those endogenous molecules exhibit small Stokes shifts and short luminescence lifetimes (< 10 ns), which can cause an overlap between autofluorescence and the signal arising from organic fluorophores. Given the intrinsic issues of organic fluorophores, extensive research efforts have been focused on the synthesis of probes with advanced features. Because of the forbidden nature of the triplet emission of transition metal complexes, they exhibit longer

lifetimes and higher Stokes shifts when compared to organic fluorophores and can therefore be excellent alternatives in optical imaging.[110] In the next section, the photophysical properties of d^6 transition metal complexes will be highlighted.

1.8 Photophysics of d^6 Metal Complexes

1.8.1 Molecular Orbital of model d^6 metal complexes

In the molecular orbital model, covalent interactions between the metal centre and the ligands are considered.[111] According to molecular orbital theory (MOT), the orbitals of the coordinating ligands are linearly combined to form a set of composite orbitals called "ligand group orbitals" (LGO). Successively, the molecular orbital (MO) diagram can be constructed by combining the LGOs with the metal orbitals, according to symmetry rules. By combining the metal and ligand orbitals of σ symmetry (a_{1g}, e_g, t_{1u}), six bonding molecular orbitals are obtained (**Figure 1-11**). Furthermore, by combining ligand orbitals of symmetry t_{2g}, corresponding with the empty π^* system, and residual t_{2g} of *d* orbitals, a system of bonding and anti-bonding molecular orbitals is generated. This is valid for systems with octahedral symmetry.

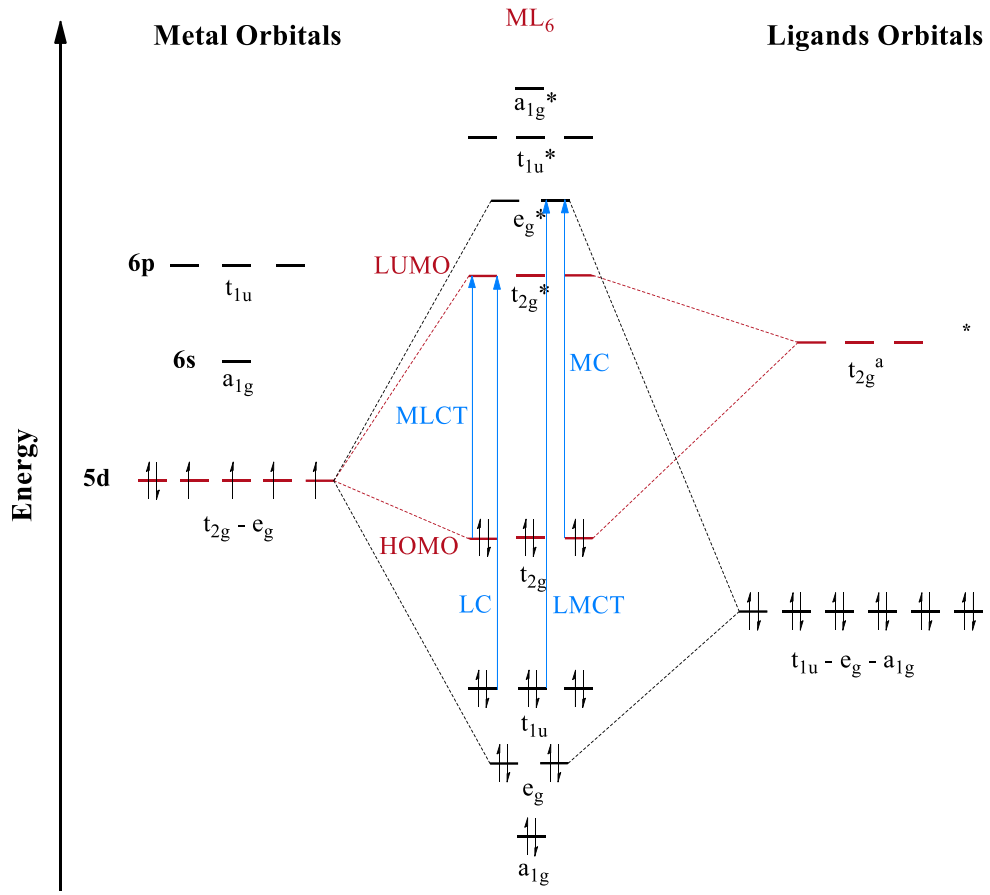

Figure 1-11 Simplified MO diagram for a low spin d^6 third-row transition metal complex, coordinated to six equivalent π accepting ligands. Dashed lines indicate the formation of the relevant molecular orbitals. The HOMO and LUMO orbitals are highlighted in red, whereas MC, LC, LMCT, and MLCT transitions are highlighted in blue.

Moreover, the molecular orbital (MO) diagram in **Figure 1-11** shows the electronic structure and the possible electronic transitions which can occur in a d^6 transition metal complex. In this section, only d^6 transition metal complexes will be considered as they are the focus of this research.

When constructing molecular orbital diagrams, each ligand surrounding the metal centre is considered equivalent and only the π^* ligand orbitals of t_{2g} symmetry forming molecular orbitals with the metal are shown. Moreover, in **Figure 1-11** a

stable, low spin third-row d^6 metal complex molecular orbital in shown; this can be noted by the fact that the molecular orbital has completely filled bonding orbitals and empty anti-bonding orbitals. If the symmetry of the complex is approximated to octahedral symmetry, the orbitals of a third-row metal centre contributing to the bond are *5d*, *6d* and *6p* orbitals, which are classified according to their point group symmetry. t_{2g} and e_g represent the *5d* orbital (with t_{2g} corresponding to d_{xy}, d_{xz}, d_{yz} while e_g corresponds to $d_{x^2-y^2}$ and d_{z^2}), a_{1g} represents the *6s* orbitals while t_{1u} represents the *6p* orbitals. The e_g and a_{1g} orbitals are involved exclusively in σ bonding interaction, t_{2g} orbitals are involved exclusively in π bonding interaction; whereas t_{1u} orbitals can give rise to both σ and π bonding interactions. The presence of π accepting ligands usually stabilises the t_{2g} orbitals, while the diffuse nature of the five *d* orbitals for third-row metals, usually destabilises the e_g* molecular orbitals, causing the MLCT excited state to be lower in energy than MC, which is a condition of luminescence.

The highest occupied molecular orbital (HOMO) is represented by the t_{2g} whereas the lowest unoccupied molecular orbital (LUMO) is represented by the t_{2g}* orbitals. The HOMO-LUMO gap is the separation between those two levels and strictly depends on the π donating/accepting ability of the ligands coordinated to the metal.[112] Upon absorption of photons, different types of transitions can occur, according to the main character of the orbitals involved in the process. The most common transitions are highlighted in the Jablonski diagram of an octahedral metal complex shown in **Figure 1-12**.

Metal centred transitions (MC) occur from the t_{2g} orbitals and the e_g* anti-bonding orbitals; because of the formally spin-forbidden nature of those transitions, they are generally associated with small absorptivity. Ligand centred (LC) transitions take place between the ligand orbitals that are not involved in the coordination to the

metal. LC transitions occur from the π bonding to the π^* anti-bonding system of the ligands. Charge transfer (CT) transitions can be of different types: ligand to metal charge transfer (LMCT) for transitions from the π system of the ligands to the σ^* (e_g) anti-bonding orbital of the metal; metal to ligand charge transfer (MLCT) when starting either from σ (t_{2g}) non-bonding or σ^* (e_g) orbital of the metal to the π^* system of the ligands and finally ligand to ligand charge transfer (LLCT), when CT transitions happen between inequivalent ligands.

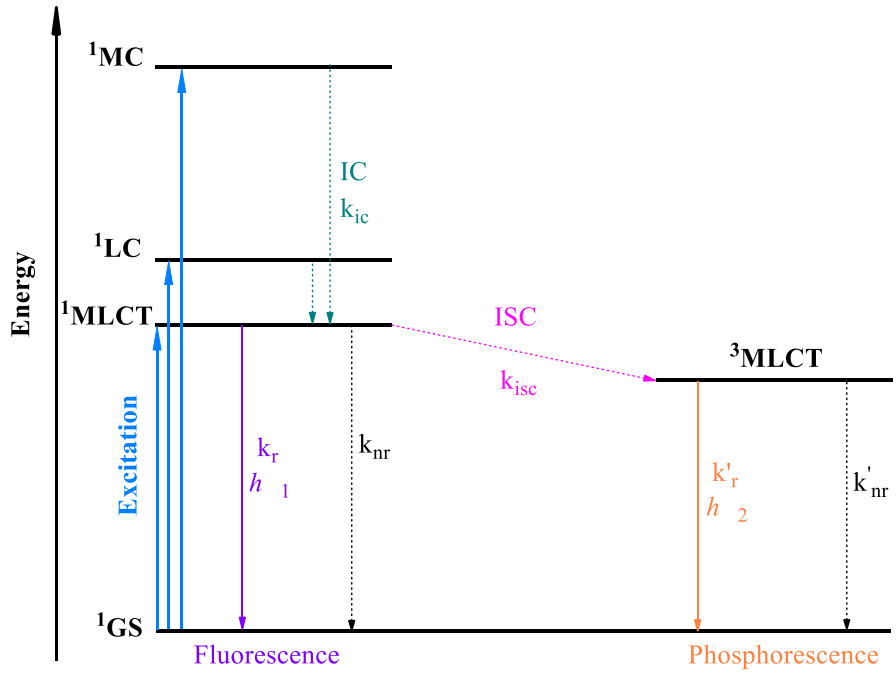

Figure 1-12 Simplified Jablonski diagram for octahedral d^6 transition metal complexes with lowest MLCT excited state. VR and LLCT transitions are not included for simplicity. In this diagram, we consider third-row transition metals, where the MC state is above the MLCT state.

The simplified Jablonski diagram for octahedral d^6 transition metal complexes is shown in **Figure 1-12**. It is important to note that because of the forbidden nature of

the phosphorescent ^{3}MLCT relaxation to the ground state, this type of transition is associated with longer lifetimes compared to fluorescent organic fluorophores.

1.9 Tetrazoles

Tetrazoles are heterocyclic compounds consisting of four nitrogen atoms and one carbon atom. Tetrazoles are considered isosteres of carboxylic acids because they have a pK_a ($pK_a \sim 5$) which is very similar to the pK_a of carboxylic acids.[113,114] This feature, combined with their low toxicity, greater metabolic stability and lipophilicity when compared to the carboxylic acid analogues, prompted their use in medicinal chemistry as carboxylic acid alternatives for the synthesis of biologically active compounds. In fact, tetrazoles and their derivatives have been used in various applications including as antibacterial and anticancer agents.[115,116]

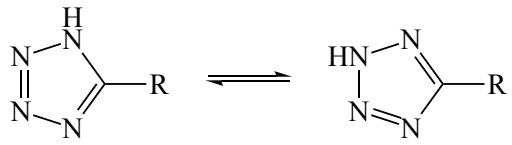

N1 **N2**

Scheme 1-17 The N1 and N2 tautomers of a 5-substituted tetrazole.

Protonated tetrazoles can exist in two tautomeric forms since the tetrazolic proton can be either on N1 or N2, as shown in **Scheme 1-17**. Besides application in medicinal chemistry, tetrazoles can be employed in coordination chemistry as ligands, because of the ability of the diimine-type nitrogens to coordinate transition metals and lanthanides. In the past decade, tetrazoles have been employed as ligands for metal complexation of transition metals such as Fe(II), Ru(II), Ir(III), and Re(I).[117-120]

Rhenium(I) and iridium (III) tetrazoalto complexes will be discussed in the following sections.

1.10 Rhenium tricarbonyl complexes and rhenium tetrazolato complexes

Re(I)-tricarbonyl diimine complexes (shown in **Figure 1-13**) have been extensively studied since the early '70s when the luminescent properties of the rhenium complex *fac*-[Re(phen)$(CO)_3$Cl] (**Figure 1-13**, **23**) and its ability to display phosphorescent emission upon the population of an emissive ^{3}MLCT excited state were discovered.[121] The facile synthesis of Re(I)-tricarbonyl diimine complexes, together with the possibility to finely tune the photophysical properties of the complex by changing the ligands, are the reason why this type of complexes have been used for a variety of applications. Rhenium tricarbonyl complexes have been employed in material science for the synthesis of organic light emitting diodes (OLED) (**Figure 1-13**, **24**), in life sciences as chemical and biological sensors (**Figure 1-13**, **25**) and as luminescent probes in biological imaging (**Figure 1-13**, **26**).[122-125]

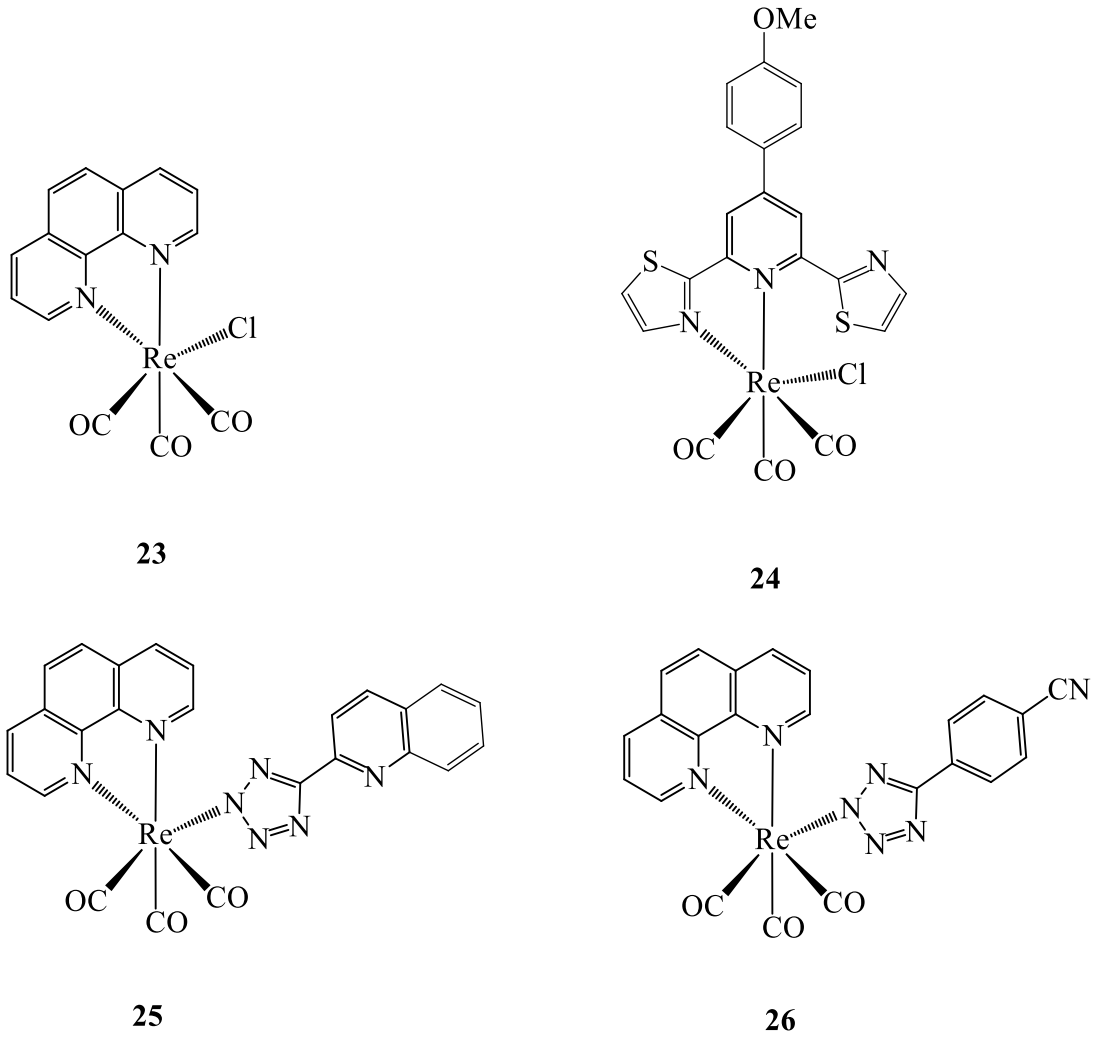

23 **24** **25** **26**

Figure 1-13 Examples of Re(I)-tricarbonyl complexes.

Rhenium (I) complexes **25** and **26** in **Figure 1-13** containing tetrazole ligands have been synthesised and studied by Massi and collaborators.[124] The emission properties of these Re-tetrazolate complexes appeared to be strongly influenced by the nature of the tetrazolate ligand, which showed a major contribution in the determination of the HOMO level.[120] It has been reported that the coordination of Re(I) to a tetrazolate ring leads to a blue shift of the emission profile of the Re(I) complex and a concomitant improvement of the emission performances, as evidenced by the substantial increase of the quantum yield values and the elongation of the phosphorescence lifetimes.[126]

Along with reactivity studies, Re(I) tetrazole complexes were also investigated in a biological context. For instance, the neutral Re(I) tetrazolate complex **26** (**Figure 1-13**) displayed an affinity for lipid droplets.[127] Most recently, Re(I) complexes with different tetrazolato ligands found application in the targeting of metal cations, in the luminescent staining of proteins and for studies of interaction with bovine serum albumin (BSA).[124,128,129]

1.11 Iridium cyclometalated complexes and iridium tetrazolato complexes

In the past 15 years, bis-cyclometalated Ir(III) complexes have gained increasing popularity in the field of luminescent materials because of their outstanding photophysical properties. In particular, Ir(III) complexes of the form $[Ir(C^N)(L^L)]^{0/+}$ (where C^N represents a cyclometalating ligand and L^L a chelating ligand), have been widely investigated because of the characteristic intense phosphorescent emissions deriving from MLCT or LLCT (or both) excited states.

The photophysical properties of Ir(III) cyclometalated complexes can be modulated by chemical modification of the coordinated ligands. In fact, by coordinating to the appropriate ligands, the emission properties of Ir(III) cyclometalated complexes can be significantly tuned to obtain emissions across the entire range of the visible spectrum. Moreover, Ir(III) cyclometalated complexes offer the possibility to obtain neutral, cationic or anionic complexes, making them great candidates for applications in lightning devices such as organic light-emitting diodes (**Figure 1-14**, **27**).[130]

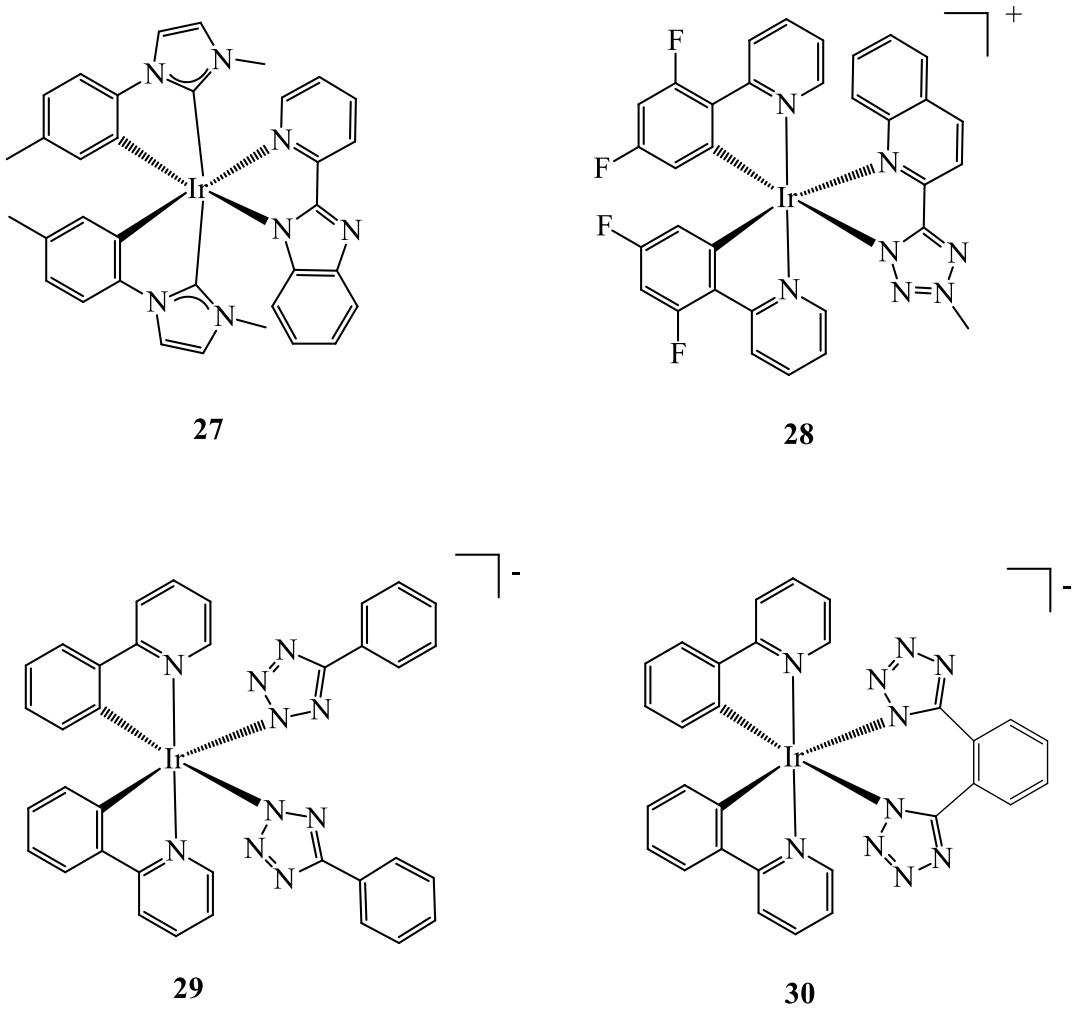

Figure 1-14 Examples of Ir(III) cyclometalated complexes.

It has been demonstrated that functionalisation of the coordinated ligands can confer upon these complexes' selectivity features to achieve localisation towards specific organelles. Therefore, upon appropriate design and choice of the coordinated ligands, luminescent Ir(III) metal complexes can be excellent candidates as versatile probes for the luminescent bioimaging of live cells.[131] For example, Ir(III) complexes possessing selectivity towards lysosome have been reported in the literature.[132]

Recently, Ir(III) tetrazolate complexes have been investigated leading to interesting results in the fields of material and life sciences. By changing the ligands

coordinating the iridium centre, it is possible to obtain charged luminescent complexes. For instance, a cationic Ir(III) tetrazolate complex has shown antimicrobial activity in *Deinococcus radiodurans* (**Figure 1-14**, **28**).[133] More recently, the non-methylated neutral form of the aforementioned Ir(III) complex has found application in the luminescent bio-imaging of living bacteria.[134] Examples of luminescent anionic Ir(III)-tetrazolate complexes have been reported (**Figure 1-14, 29** and **30**).[135,136]

1.12 Research Objectives

In the Introductory Chapter, we have highlighted the advantages of adopting RAFT polymerisation for the design and synthesis of new materials, including its broad versatility and impressive functional group (FG) tolerance. Today, there are only a few FGs that have not been incorporated into RAFT-prepared (co)polymers. However, one particularly important FG that has received little attention, especially in chain growth polymerisation processes, is the tetrazole species.

We have also highlighted the application of tetrazoles as ligands in the synthesis of interesting luminescent transition metal complexes. Tetrazolato-metal luminescent complexes have been prepared and employed in many applications including as cellular labels. This has been motivated primarily due to their outstanding photophysical properties. In this thesis, the synthesis and evaluation of photophysical properties of a range of new tetrazole functional (co)polymers that are able to serve as macromolecular ligands for the attachment of luminescent metal complexes, will be illustrated. The objectives of this research may be summarised as follows:

- To utilise RAFT radical polymerisation to prepare reactive, well-defined, parent (co)polymers that are amenable to facile post-polymerisation modification;
- To synthesise, isolate and characterise well-defined (co)polymers containing tetrazole functional groups employing post-polymerisation modification protocols;

- To examine the ability to employ tetrazole functional (co)polymers as macromolecular ligands for the covalent attachment of luminescent metal species based on Re(I) and/or Ir(III);
- To study the photophysical properties of the novel polymer-hybrid luminescent materials;
- To evaluate the ability of the materials to act as probes in the staining of rodent brain tissues.

1.13 List of references

1. D. Braun, *International Journal of Polymer Science*, 2009, **2009**, 893234.
2. H. Staudinger, *Berichte der deutschen chemischen Gesellschaft (A and B Series)*, 1926, **59**, 3019-3043.
3. P. J. Flory, *Journal of the American Chemical Society*, 1937, **59**, 241-253.
4. J. C. Bevington, H. W. Melville and R. P. Taylor, *Journal of Polymer Science*, 1954, **14**, 463-476.
5. V. W. Kern, *Die Makromolekulare Chemie*, 1948, **1**, 229-248.
6. W. A. Braunecker and K. Matyjaszewski, *Progress in Polymer Science*, 2007, **32**, 93-146.
7. M. Szwarc, *Nature*, 1956, **178**, 1168.
8. M. Szwarc, M. Levy and R. Milkovich, *Journal of the American Chemical Society*, 1956, **78**, 2656-2657.
9. G. Moad, E. Rizzardo and S. H. Thang, *Australian Journal of Chemistry*, 2005, **58**, 379-410.
10. G. Moad, E. Rizzardo and S. H. Thang, *Australian Journal of Chemistry*, 2006, **59**, 669-692.
11. G. Moad, E. Rizzardo and S. H. Thang, *Australian Journal of Chemistry*, 2009, **62**, 1402-1472.
12. G. Moad, E. Rizzardo and S. H. Thang, *Australian Journal of Chemistry*, 2012, **65**, 985-1076.
13. J. Chiefari, Y. K. Chong, F. Ercole, J. Krstina, J. Jeffery, T. P. T. Le, R. T. A. Mayadunne, G. F. Meijs, C. L. Moad, G. Moad, E. Rizzardo and S. H. Thang, *Macromolecules*, 1998, **31**, 5559-5562.

14. P. Corpart, D. Charmot, T. Biadatti, S. Zard and D. Michelet, *Patent Number WO*, 1998, **98**, 9858974.

15. S. Perrier, P. Takolpuckdee, *Journal of Polymer Science, Part A*: *Polymer Chemistry*, 2005, **42**, 5347-5393.

16. G. Moad, E. Rizzardo and S. H. Thang, *Polymer*, 2008, **49**, 1079-1131.

17. K. Matyjaszewski Ed., C*ontrolled/living radical polymerization: progress in ATRP, NMP, and RAFT*, American Chemical Society, Washington, DC, USA, 2000.

18. G. Moad and C. Barner-Kowollik, in *Handbook of RAFT Polymerization*, C. Barner-Kowollik Ed., Wiley-VCH, Weinheim, Germany, 2008, pp. 51-104.

19. D. J. Keddie, G. Moad, E. Rizzardo and S. H. Thang, *Macromolecules*, 2012, **45**, 5321-5342.

20. G. Moad, J. Chiefari, Y. K. Chong, J. Krstina, R. T. A. Mayadunne, A. Postma, E. Rizzardo and S. H. Thang, *Polymer International*, 2000, **49**, 993-1001.

21. J. Chiefari, R. T. A. Mayadunne, C. L. Moad, G. Moad, E. Rizzardo, A. Postma and S. H. Thang, *Macromolecules*, 2003, **36**, 2273-2283.

22. R. T. A. Mayadunne, E. Rizzardo, J. Chiefari, Y. K. Chong, G. Moad and S. H. Thang, *Macromolecules*, 1999, **32**, 6977-6980.

23. M. Benaglia, M. Chen, Y. K. Chong, G. Moad, E. Rizzardo and S. H. Thang, *Macromolecules*, 2009, **42**, 9384-9386.

24. S. Perrier, *Macromolecules*, 2017, **50**, 7433-7447.

25. E. Girard, J.-D. Marty, B. Ameduri and M. Destarac, *ACS Macro Letters*, 2012, **1**, 270-274.

26. E. Girard, T. Tassaing, J.-D. Marty and M. Destarac, *Polymer Chemistry*, 2011, **2**, 2222-2230.

27. J. Xu, K. Jung, A. Atme, S. Shanmugam and C. Boyer, *Journal of the American Chemical Society*, 2014, **136**, 5508-5519.

28. J. Phommalysack-Lovan, Y. Chu, C. Boyer and J. Xu, *Chemical Communications*, 2018, **54**, 6591-6606.

29. T. G. McKenzie, L. P. d. M. Costa, Q. Fu, D. E. Dunstan and G. G. Qiao, *Polymer Chemistry*, 2016, **7**, 4246-4253.

30. C. H. Hornung, A. Postma, S. Saubern and J. Chiefari, *Polymer*, 2014, **55**, 1427-1435.

31. A. Postma, T. P. Davis, G. Moad and M. S. O'Shea, *Macromolecules*, 2005, **38**, 5371-5374.

32. A. Postma, T. P. Davis, G. Li, G. Moad and M. S. O'Shea, *Macromolecules*, 2006, **39**, 5307-5318.

33. B. Chong, G. Moad, E. Rizzardo, M. Skidmore and S. H. Thang, *Australian Journal of Chemistry*, 2006, **59**, 755-762.

34. C. H. DePuy and R. W. King, *Chemical Reviews*, 1960, **60**, 431-457.

35. D. H. R. Barton and S. W. McCombie, *Journal of the Chemical Society, Perkin Transactions 1*, 1975, 1574-1585.

36. D. Crich and L. Quintero, *Chemical Reviews*, 1989, **89**, 1413-1432.

37. G. Moad, Y. K. Chong, A. Postma, E. Rizzardo and S. H. Thang, *Polymer*, 2005, **46**, 8458-8468.

38. Y. K. Chong, G. Moad, E. Rizzardo and S. H. Thang, *Macromolecules*, 2007, **40**, 4446-4455.

39. A. J. Tilley, M. Chen, S. M. Danczak, K. P. Ghiggino and J. M. White, *Polymer Chemistry*, 2012, **3**, 892-899.

40. M. Chen, K. P. Ghiggino, E. Rizzardo, S. H. Thang and G. J. Wilson, *Chemical Communications*, 2008, 1112-1114.

41. A. Postma, T. P. Davis, R. A. Evans, G. Li, G. Moad and M. S. O'Shea, *Macromolecules*, 2006, **39**, 5293-5306.

42. A. O. Moughton, K. Stubenrauch and R. K. O'Reilly, *Soft Matter*, 2009, **5**, 2361-2370.

43. U. Hasegawa, A. J. van der Vlies, E. Simeoni, C. Wandrey and J. A. Hubbell, *Journal of the American Chemical Society*, 2010, **132**, 18273-18280.

44. C. H. Hornung, A. Postma, S. Saubern and J. Chiefari, *Macrmolecular Reaction Engineering*, 2012, **6**, 246-251.

45. K. J. Sykes, S. Harrisson and D. J. Keddie, *Macromolecular Chemistry and Physics*, 2016, **217**, 2310-2320.

46. Y. Xia, S. Tang and B. D. Olsen, *Chemical Communications*, 2013, **49**, 2566-2568.

47. T. D. Michl, K. E. S. Locock, N. E. Stevens, J. D. Hayball, K. Vasilev, A. Postma, Y. Qu, A. Traven, M. Haeussler, L. Meagher and H. J. Griesser, *Polymer Chemistry*, 2014, **5**, 5813-5822.

48. J. Y. T. Chong, D. J. Keddie, A. Postma, X. Mulet, B. J. Boyd and C. J. Drummond, *Colloids and Surfaces A: Physiochem. Eng. Aspects*, 2015, **470**, 60-69.

49. E. H. Discekici, S. L. Shankel, A. Anastasaki, B. Oschmann, I.-H. Lee, J. Niu, A. J. McGrath, P. G. Clark, D. S. Laitar, J. R. de Alaniz, C. J. Hawker and D. J. Lunn, *Chemical Communications*, 2017, **53**, 1888-1891.

50. K. M. Mattson, C. W. Pester, W. R. Gutekunst, A. T. Hsueh, E. H. Discekici, Y. Luo, B. V. K. J. Schmidt, A. J. McGrath, P. G. Clark and C. J. Hawker, *Macromolecules*, 2016, **49**, 8162-8166.

51. R. N. Carmean, C. A. Figg, G. M. Scheutz, T. Kubo and B. S. Sumerlin, *ACS Macro Letters*, 2017, **6**, 185-189.

52. M. A. Harvison, P. J. Roth, T. P. Davis and A. B. Lowe, *Australian Journal of Chemistry*, 2011, **64**, 992-1006.

53. S. Perrier, P. Takolpuckdee and C. A. Mars, *Macromolecules*, 2005, **38**, 2033-2036.

54. M. Chen, G. Moad and E. Rizzardo, *Journal of Polymer Science Part A: Polymer Chemistry*, 2009, **47**, 6704-6714.

55. T. Gruendling, R. Pickford, M. Guilhaus and C. Barner-Kowollik, *Journal of Polymer Science, Part A: Polymer Chemistry*, 2008, **46**, 7447-7461.

56. M. Dietrich, M. Glassner, T. Gruendling, C. Schmid, J. Falkenhagen and C. Barner-Kowollik, *Polymer Chemistry*, 2010, **1**, 634-644.

57. T. Gruendling, M. Dietrich and C. Barner-Kowollik, *Australian Journal of Chemistry*, 2009, **62**, 806-812.

58. J. A. Howard and K. U. Ingold, *Canadian Journal of Chemistry*, 1969, **47**, 3809-3815.

59. C. Li, J. He, Y. Zhou, Y. Gu and Y. Yang, *Journal of Polymer Science, Part A: Polymer Chemistry*, 2011, **49**, 1351-1360.

60. W. A. Cunningham, *Journal of Chemical Education*, 1935, **12**, 120.

61. R. E. Oesper, *Journal of Chemical Education*, 1929, **6**, 677.

62. P. Rustemeyer, *Macromolecular Symposia*, 2004, **208**, 1-6.

63. K. W. Pepper, H. M. Paisley and M. A. Young, *Journal of the Chemical Society*, 1953, 4097-4105.

64. R. B. Merrifield, *Journal of the American Chemical Society*, 1963, **85**, 2149-2154.

65. G. E. Serniuk, F. W. Banes and M. W. Swaney, *Journal of the American Chemical Society*, 1948, **70**, 1804-1808.

66. J.-S. Wang and K. Matyjaszewski, *Journal of the American Chemical Society*, 1995, **117**, 5614-5615.

67. C. J. Hawker, A. W. Bosman and E. Harth, *Chemical Reviews*, 2001, **101**, 3661-3688.

68. P. Theato and H.-A. Klok Eds., *Functional Polymers by Post-Polymerization Modification*, Wiley-VHC, Weinheim, Germany, 2013.

69. H. C. Kolb, M. G. Finn and K. B. Sharpless, *Angewandte Chemie International Edition*, 2001, **40**, 2004-2021.

70. J. F. Lutz, *Angewandte Chemie International Edition*, 2007, **46**, 1018-1025.

71. E. Blasco, M. B. Sims, A. S. Goldmann, B. S. Sumerlin and C. Barner-Kowollik, *Macromolecules*, 2017, **50**, 5215-5252.

72. A. Das and P. Theato, *Chemical Reviews*, 2016, **116**, 1434-1495.

73. H. G. Batz, G. Franzmann and H. Ringsdorf, *Die Makromolekulare Chemie*, 1973, **172**, 27-47.

74. P. Ferruti, A. Bettelli and A. Feré, *Polymer*, 1972, **13**, 462-464.

75. J. A. Farringrton, P. J. Hextall, G. W. Kenner and J. M. Turner, *Journal of the Chemical Society*, 1957, 1407-1413.

76. E. Pedone, X. Li, N. Koseva, O. Alpar and S. Brocchini, *Journal of Materials Chemistry*, 2003, **13**, 2825-2837.

77. A. M. Alb, P. Enohnyaket, M. F. Drenski, R. Shunmugam, G. N. Tew and W. F. Reed, *Macromolecules*, 2006, **39**, 8283-8292.

78. S. Y. Wong and D. Putnam, *Bioconjugate Chemistry*, 2007, **18**, 970-982.

79. M. Eberhardt, R. Mruk, R. Zentel and P. Théato, *European Polymer Journal*, 2005, **41**, 1569-1575.

80. J.-C. Blazejewski, J. W. Hofstraat, C. Lequesne, C. Wakselman and U. E. Wiersum, *Journal of Fluorine Chemistry*, 1999, **97**, 191-199.

81. K. Nilles and P. Theato, *Polymer Chemistry*, 2011, **2**, 376-384.

82. Y. Li, N. Busatto and P. J. Roth, *Macromolecules*, 2021, **54**, 3101-3111.

83. S. Thamizharasi, P. Gnanasundaram and S. Balasubramanian, *Journal of Applied Polymer Science*, 2003, **88**, 1817-1824.

84. M. V. Solovskij, E. F. Panarin, O. P. Gorbunova, E. V. Korneeva, N. A. Petuhkova, N. A. Michajlova and G. M. Pavlov, *European Polymer Journal*, 2000, **36**, 1127-1135.

85. L. D. Taylor, C. K. Chiklis and T. E. Platt, *Journal of Polymer Science Part B: Polymer Letters*, 1971, **9**, 187-190.

86. S. M. Heilmann, J. K. Rasmussen and L. R. Krepski, *Journal of Polymer Science Part A: Polymer Chemistry*, 2001, **39**, 3655-3677.

87. D. C. Tully, M. J. Roberts, B. H. Geierstanger and R. B. Grubbs, *Macromolecules*, 2003, **36**, 4302-4308.

88. Y. Zhu, J. Y. Quek, A. B. Lowe and P. J. Roth, *Macromolecules*, 2013, **46**, 6475-6484.

89. L. Fontaine, T. Lemele, J.-C. Brosse, G. Sennyey, J.-P. Senet and D. Wattiez, *Macromolecular Chemistry and Physics*, 2002, **203**, 1377-1384.

90. J. S. Kim, A. R. Sirois, A. J. Vazquez Cegla, E. Jumai'an, N. Murata, M. E. Buck and S. J. Moore, *Bioconjugate Chemistry*, 2019, **30**, 1220-1231.

91. Y. Sun, Z. Chen, E. Puodziukynaite, D. M. Jenkins, J. R. Reynolds and K. S. Schanze, *Macromolecules*, 2012, **45**, 2632-2642.

92. B. Happ, C. Friebe, A. Winter, M. D. Hager and U. S. Schubert, *European Polymer Journal*, 2009, **45**, 3433-3441.

93. A. M. Breul, J. Schäfer, E. Altuntas, M. D. Hager, A. Winter, B. Dietzek, J. Popp and U. S. Schubert, *Journal of Inorganic and Organometallic Polymers and Materials*, 2013, **23**, 74-80.

94. C. Ulbricht, C. R. Becer, A. Winter and U. S. Schubert, *Macromolecular Rapid Communications*, 2010, **31**, 827-833.

95. G. Zhou and I. I. Harruna, *Macromolecules*, 2005, **38**, 4114-4123.

96. G. Zhou and I. I. Harruna, *Macromolecules*, 2004, **37**, 7132-7139.

97. G. E. Southard, K. A. Van Houten, E. W. Ott and G. M. Murray, *Analytica Chimica Acta*, 2007, **581**, 202-207.

98. B. Wardle, *Principles and Applications of Photochemistry*, Wiley, Manchester, UK, 2009.

99. J. R. Lakowicz, *Principles of Fluorescence Spectroscopy*, Springer, Baltimore, USA, 2006.

100. J. V. Caspar and T. J. Meyer, *The Journal of Physical Chemistry*, 1983, **87**, 952-957.

101. G. G. Stokes, *Philosophical Transactions of the Royal Society of London*, 1852, **142**, 463-562.

102. A. A. Abdel-Shafi and D. R. Worrall, *Journal of Photochemistry and Photobiology A: Chemistry*, 2005, **172**, 170-179.

103. A. A. Abdel-Shafi, P. D. Beer, R. J. Mortimer and F. Wilkinson, *The Journal of Physical Chemistry A*, 2000, **104**, 192-202.

104. C. Schweitzer and R. Schmidt, *Chemical Reviews*, 2003, **103**, 1685-1758.

105. A. Leonidova, V. Pierroz, R. Rubbiani, J. Heier, S. Ferrari and G. Gasser, *Dalton Transactions*, 2014, **43**, 4287-4294.

106. L. He, Z.-Y. Pan, W.-W. Qin, Y. Li, C.-P. Tan and Z.-W. Mao, *Dalton Transactions*, 2019, **48**, 4398-4404.

107. J.-C. G. Bünzli, *Chemical Reviews*, 2010, **110**, 2729-2755.

108. M. Y. Berezin, W. J. Akers, K. Guo, G. M. Fischer, E. Daltrozzo, A. Zumbusch and S. Achilefu, *Biophysical Journal*, 2009, **97**, L22-24.

109. N. Billinton and A. Knight, *Analytical Biochemistry*, 2001, **291**, 175-197.

110. J. R. Lakowicz, E. Terpetschnig, Z. Murtaza and H. Szmacinski, *Journal of Fluorescence*, 1997, **7**, 17-25.

111. C. E. Housecroft and A. G. Sharpe, *Inorganic Chemistry*, Pearson Education Limited, Harlow, UK, 2012.

112. L. Flamigni, A. Barbieri, C. Sabatini, B. Ventura and F. Barigelletti, in *Photochemistry and Photophysics of Coordination Compounds II*, Balzani and S. Campagna Eds., Springer Berlin Heidelberg, Berlin, Germany, 2007, pp. 143-203.

113. H. Singh, A. S. Chawla, V. K. Kapoor, D. Paul and R. K. Malhotra, *Progress in Medicinal Chemistry*, 1980, **17**, 151-183.

114. H. Sharghi, S. Ebrahimpourmoghaddam and M. M. Doroodmand, *Journal of Organometallic Chemistry*, 2013, **738**, 41-48.

115. M. A. Malik, M. Y. Wani, S. A. Al-Thabaiti and R. A. Shiekh, *Journal of Inclusion Phenomena and Macrocyclic Chemistry*, 2014, **78**, 15-37.

116. C. N. S. S. P. Kumar, D. K. Parida, A. Santhoshi, A. K. Kota, B. Sridhar and V. J. Rao, *MedChemComm*, 2011, **2**, 486-492.

117. A. Palazzi, S. Stagni, S. Bordoni and M. Monari, S. Selva, *Organometallics*, 2002, **21**, 3774-3781.

118. Stagni, A. Palazzi, S. Zacchini, B. Ballarin, C. Bruno, M. Marcaccio, F. Paolucci, M. Carano and M. Monari, A. J, Bard, *Inorganic Chem*istry, 2006, **45**, 695-709.

119. V. Fiorini, E. Marchini, M. Averardi, L. Giorgini, S. Muzzioli, A. Dellai, R. Argazzi, A. Sanson, N. Sangiorgi, S. Caramori and S.Stagni, *Dalton Transactions*, 2020, **49**, 14543.

120. M. V. Werrett, D. Chartrand, J. D. Gale, G. S. Hanan, J. G. MacLellan, M. Massi, S. Muzzioli, P. Raiteri, B. W. Skelton, M. Silberstein and S. Stagni, *Inorganic Chemistry*, 2011, **50**, 1229-1241.

121. M. Wrighton and D. L. Morse, *Journal of the American Chemical Society*, 1974, **96**, 998-1003.

122. T. Klemens, A. Świtlicka, B. Machura, S. Kula, S. Krompiec, K. Łaba, M. Korzec, M. Siwy, H. Janeczek, E. Schab-Balcerzak, M. Szalkowski, J. Grzelak and S. Maćkowski, *Dyes and Pigments*, 2019, **163**, 86-101.

123. G.-W. Zhao, J.-H. Zhao, Y.-X. Hu, D.-Y. Zhang and X. Li, *Synthetic Metals*, 2016, **212**, 131-141.

124. V. Fiorini, A. M. Ranieri, S. Muzzioli, K. D. M. Magee, S. Zacchini, N. Akabar, A. Stefan, M. I. Ogden, M. Massi and S. Stagni, *Dalton Transactions*, 2015, **44**, 20597-20608.

125. C. A. Bader, A. Sorvina, P. V. Simpson, P. J. Wright, S. Stagni, S. E. Plush, M. Massi and D. A. Brooks, *FEBS Letters*, 2016, **590**, 3051-3060.

126. M. V. Werrett, G. S. Huff, S. Muzzioli, V. Fiorini, S. Zacchini, B. W. Skelton, A. Maggiore, J. M. Malicka, M. Cocchi, K. C. Gordon, S. Stagni and M. Massi, *Dalton Transactions*, 2015, **44**, 8379-8393.

127. C. A. Bader, R. D. Brooks, Y. S. Ng, A. Sorvina, M. V. Werrett, P. J. Wright, A. G. Anwer, D. A. Brooks, S. Stagni, S. Muzzioli, M. Silberstein, B. W. Skelton, E. M. Goldys, S. E. Plush, T. Shandala and M. Massi, *RSC Advances*, 2014, **4**, 16345-16351.

128. V. Fiorini, L. Bergamini, N. Monti, S. Zacchini, S. E. Plush, M. Massi, A. Hochkoeppler, A. Stefan and S. Stagni, *Dalton Transactions*, 2018, **47**, 9400-9410.

129. N. Monti, V. Longo, S. Zacchini, G. Vigarani, L. Giorgini, E. Bonora, M. Massi, V. Fiorini and S. Stagni, *Inorganica Chimica Acta*, 2021, **518**, 120244.

130. T.-Y. Li, J. Wu, Z.-G. Wu, Y.-X. Zheng, J.-L. Zuo and Y. Pan, *Coordination Chemistry Reviews*, 2018, **374**, 55-92.

131. C. Caporale and M. Massi, *Coordination Chemistry Reviews*, 2018, **363**, 71-91.

132. L. He, Y. Li, C.-P. Tan, R.-R. Ye, M.-H. Chen, J.-J. Cao, L.-N. Ji and Z.-W. Mao, *Chemical Science*, 2015, **6**, 5409-5418.

133. V. Fiorini, I. Zanoni, S. Zacchini, A. L. Costa, A. Hochkoeppler, V. Zanotti, A. M. Ranieri, M. Massi, A. Stefan and S. Stagni, *Dalton Transactions*, 2017, **46**, 12328-12338.

134. A. M. Ranieri, C. Caporale, V. Fiorini, A. Hubbard, P. Rigby, S. Stagni, E. Watkin, M. I. Ogden, M. J. Hackett and M. Massi, *Chemistry – A European Journal*, 2019, **25**, 10566-10570.

135. V. Fiorini, S. Zacchini, P. Raiteri, R. Mazzoni, V. Zanotti, M. Massi and S. Stagni, *Dalton Transactions*, 2016, **45**, 12884-12896.

136. V. Fiorini, A. D'Ignazio, K. D. M. Magee, M. I. Ogden, M. Massi and S. Stagni, *Dalton Transactions*, 2016, **45**, 3256-3259.

Chapter 2

Synthesis and photophysical investigation of styrenic-based rhenium(I)-tetrazolato functional luminescent polymers

The contents of this Chapter were published in 2020:

E. Dallerba, M. Massi and A. B. Lowe "Rhenium(I)-Tetrazolato Functional Luminescent Polymers: Organic-Inorganic Hybrids via RAFT and Post-Polymerization Modification" *European Polymer Journal*, 2020, **126**, 109559.

2.1 Abstract

A series of novel rhenium-tetrazolato functional (co)polymers based on a polystyrenic backbone are presented. The polymerisation, structural and photophysical investigations are reported. The copolymers containing tetrazole functionality are able to serve as macromolecular ligands for the coordination of a luminescent Re(I) complex. Reversible addition-fragmentation chain transfer (RAFT) polymerisation has been employed for the synthesis of two statistical and two block copolymers of styrene and 4-cyanostyrene as monomers. The parent copolymers have been modified *via* post polymerisation modification of the cyano appended groups in a reaction with NaN_3 to yield the corresponding tetrazole functionalised copolymers. The tetrazole modified copolymers have shown the ability to serve as macromolecular ligands for the coordination of a metal complex. In this Chapter, a precursor complex has been attached to the polymeric scaffold by coordination through the tetrazole functional groups. The formation of the tetrazole functional group and subsequent metal

coordination have been confirmed by inverse-gated proton decoupled ^{13}C NMR and infrared spectroscopies. The photophysical properties of the novel copolymer-Re(I) hybrid luminescent materials have been studied. Coordination between the tetrazole functionality and the Re(I) complex was confirmed from the absorption and emission profiles of the hybrid materials. Lifetime measurements and quantum yields confirmed that the luminescent properties of the Re(I) complex were not affected by the coordination to the polymeric scaffolds.

2.2 Introduction

Reversible addition-fragmentation chain transfer (RAFT) radical polymerisation is an example of a reversible deactivation radical polymerisation (RDRP) technique mediated by certain thiocarbonylthio compounds and operates on the principle of degenerative chain transfer.[1-3] Particularly salient features of RAFT include its ease of execution, broad applicability under a range of experimental conditions and its high functional group tolerance. Indeed, there are few "common" functional groups that have not been incorporated into (co)polymers by the direct (co)polymerisation of an appropriate functional monomer or introduced by one of the many available post-polymerisation modification approaches and especially utilising "click" chemistries.

One functional group, however, that has attracted comparatively little attention in synthetic polymer chemistry, and especially with respect to chain-growth polymerisation processes, is the tetrazole species. Such aromatic heterocycles, containing four nitrogen atoms (3 pyridine-like and 1 pyrrole-like) and one carbon atom, are well-known (although are not naturally occurring) and have been previously investigated as highly energetic materials, biologically active species (as antivirals,

anticancer, antibacterials and antifungals) and as a key functionality in some medicines (specific hypotensive and antihistamines).[4] The latter feature is particularly important with tetrazoles serving as carboxylic acid bioisosteres, a feature with potential beyond biomedical applications.

5-(Methacrylamido)tetrazole (co)polymers have been prepared under conventional radical polymerisation conditions while poly(5-vinyltetrazole)-based materials are accessible *via* the reaction of polyacrylonitrile (co)polymers with NaN_3 including in well-defined (co)polymers prepared by atom transfer radical polymerisation (ATRP).[5-10] Indeed, the reaction of nitriles, -C≡N, with NaN_3, or other suitable co-reagent, is one of the more common routes for preparing tetrazoles.[11-15] Poly(3-((1*H*-tetrazol-5-yl)amino)-2-hydroxypropyl methacrylate) (**Figure 2-1**, **A**) has been reported and its proton conductivity properties evaluated. In this instance, poly(glycidyl methacrylate) was homopolymerised under radical conditions and the pendent epoxy rings subsequently ring-opened with 5-aminotetrazole.[16] There are reports in which tetrazole-containing monomers have been polymerised directly by RAFT, although they are few in number. For example, Xue *et al*. reported the multi-step synthesis of (*E*)-2-((4-((4-(5-chlorotetrazol-1-yl)phenyl)diazenyl)phenyl) (methyl)amino) ethyl methacrylate (**Figure 2-1**, **B**) and its subsequent RAFT homopolymerisation and block copolymerisation (with a poly(methyl methacrylate) macro-CTA) to yield well-defined (co)polymers; the photoiosomerisation behaviour, associated with the pendent azo functional groups, of these materials was examined.[17]

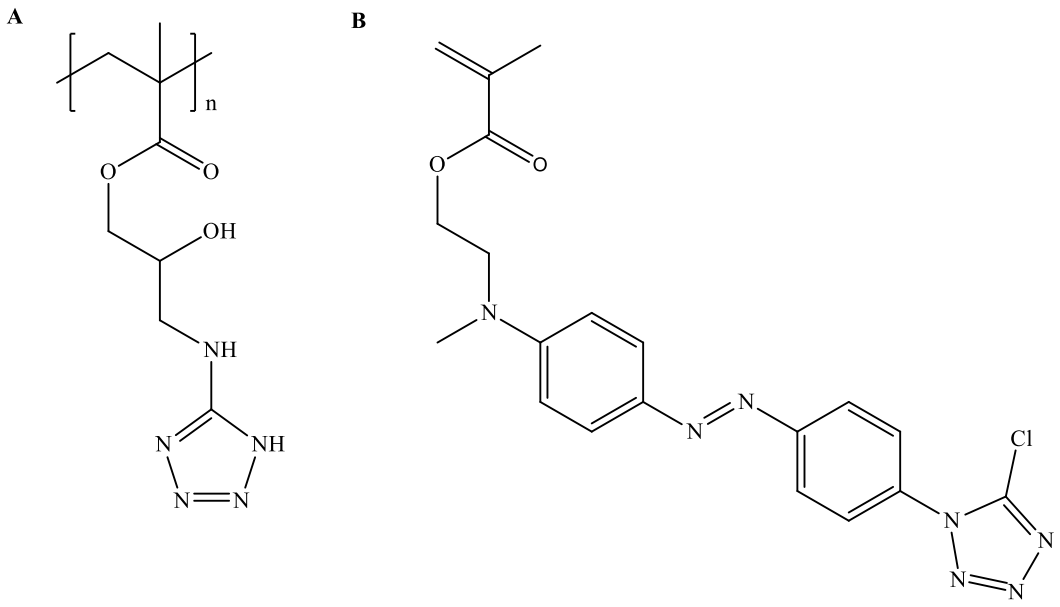

Figure 2-1 Poly(3-((1*H*-tetrazol-5-yl)amino)-2-hydroxypropyl methacrylate) (**A**) and (*E*)-2-((4-((4-(5-chlorotetrazol-1-yl)phenyl)diazenyl)phenyl)(methyl)amino) ethyl methacrylate (**B**).

Luminescent transition metal complexes such as those of rhenium(I), ruthenium(II), iridium(III) and platinum(II) have drawn significant attention due to the potential use of their photophysical properties in a variety of fields. In recent years, the investigation of rhenium complexes as alternatives to commonly used organic fluorophores has expanded. High photostability, long emission lifetimes, large Stokes shifts and fine tunability of the emission profiles have enabled such complexes to be employed in a range of applications including biomolecular luminescent probes, light emitting devices and photocatalysis.[18-20] In particular, rhenium(I) tricarbonyl diimine complexes, *fac*-$[Re(CO)_3(diim)(L)]^{0/+}$, where diim represents a diimine-type chelating ligand such as 1,10-phenantroline (phen) or 2,2'-bipyridine (bipy) and L represents a monodentate ancillary ligand, have been widely studied for their photophysical properties.[21] These complexes show intense and long-lived phosphorescent emission

arising from a metal-to-ligand charge transfer excited state, ^{3}MLCT, which confers upon them the unique photophysical properties.[22] It has been widely demonstrated, that upon chemical modification of the diimine-type ligand and L ligands it is possible to tune the photophysical properties of the metal complexes. For example, Massi's group has shown how tetrazolato ligands can be exploited to prepare luminescent Re(I) complexes whose emission can be tuned by direct reaction with electrophilic reagents.[23] These properties have been beneficial for cell and tissue staining; they have, in fact, demonstrated that these probes have low cytotoxicity and often display specificity for organelles and/or classes of biomolecules.[24,25] However, desirable improvements of these complexes, and their subsequent use in imaging could be obtained by appropriately tuning their solubility and biocompatibility and preventing the generation of singlet oxygen from excited states of triplet multiplicity. The biocompatibility and bioavailability of small molecules can often be enhanced by conjugation to polymeric chains, most commonly with poly(ethylene oxide) (so-called PEGylation), and metal-containing polymers are widely studied for their potential in applications such as polymeric metallodrugs, drug delivery and as bioimaging agents.[26-28]

Inspired by the use of tetrazoles as a coordinating ligand for metal fragments, and the significant dearth of tetrazole-functional (co)polymers, the work described in this Chapter, will detail the synthesis of a series of four model styrenic-based (co)polymers (two statistical and two block copolymers) containing pendent tetrazole functional groups *via* a combination of RAFT polymerisation and post-polymerisation modification. The tetrazole-functional copolymers are able to serve as macromolecular ligands capable of complexing $[Re(CO)_3(phen)]^+$ as evidenced by the absorption/emission profiles of the modified copolymers. These modified materials

are the first examples of such polymer-tetrazole-metal hybrids. Model targeted materials are shown in **Figure 2-2**.

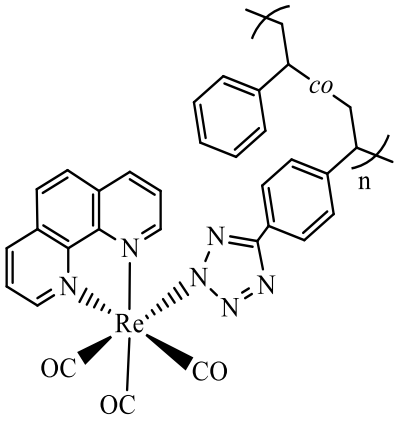

Figure 2-2 Structure of model targeted rhenium-tetrazolato functional polymers described in this Chapter.

2.3 Experimental

2.3.1 Materials

All reagents were purchased from the Sigma-Aldrich Chemical Company, or Alfa Aesar, at the highest available purity and used as received unless noted otherwise. $Re(CO)_3(phen)Br$ and $[Re(CO)_3(phen)(NCCH_3)][BF_4]$ were synthesised accordingly to published procedures.[29,30] 2,2'-Azobis(2-methylpropionitrile) (AIBN) was purchased as a 12 wt% solution in acetone. The solvent was removed on a rotary evaporator and the remaining solid dissolved in methanol from which AIBN recrystallised.

2.3.2 Size Exclusion Chromatography (SEC)

SEC was performed on a Shimadzu modular system consisting of a 4.0 mm × 3.0 mm Phenomenex Security Guard™ Cartridge guard column and two linear

phenogel columns (10^3 and 10^4 Å pore size) in tetrahydrofuran (THF) operating at a flow rate of 1.0 mL/min and 40 °C using a RID-20A refractive index detector, a SPD-M20A prominence diode array detector and a miniDAWN TREOS multiangle static light scattering (MALLS) detector. The system was calibrated with a series of narrow molecular weight distribution polystyrene standards with molecular weights ranging from 0.27 to 66 kg mol^{-1}. Chromatograms were analysed by Lab Solutions SEC software.

2.3.3 NMR Measurements

^{1}H NMR and ^{13}C NMR spectra were recorded at 298 K on a Bruker Avance 400 spectrometer. The data were processed with Bruker's TopSpin 3.1 Software. ^{13}C NMR spectra were recorded at 298 K with inverse-gated proton decoupling using 30° pulse angle, relaxation delay of 2.0 s and 25,700 scans.

2.3.4 FTIR Analysis

Infrared spectra (IR) were recorded on solid-state samples using an attenuated total reflectance Perkin Elmer Spectrum Two and Spectrum 100 FT-IR. The spectra were recorded from 4000 to 650 cm^{-1}.

2.3.5 Photophysical Measurements

Absorption spectra were recorded at room temperature using a Perkin Elmer Lambda 35 UV/Vis spectrometer. Uncorrected steady-state emission spectra were recorded using an Edinburgh FLSP980-stm spectrometer equipped with a 450 W xenon arc lamp and emission monochromators, a Peltier cooled Hamamatsu R928P photomultiplier (185-850 nm) and a Hamamatsu R5509-42 photomultiplier for

detection of NIR radiation (800-1400 nm). Emission and excitation spectra were corrected for source intensity (lamp and grating) and emission spectral response (detector and grating) by a calibration curve supplied with the instrument. Luminescent quantum yields were measured according to the procedure described by Demas and Crosby in optically dilute solutions (O.D < 0.1 at excitation wavelength) obtained from absorption spectra on a wavelength scale (nm) and compared to the reference emitter by **Equation 2-1**:

$$\Phi_x = \Phi_r \left[\frac{A_r(\lambda_r)}{A_x(\lambda_x)}\right]\left[\frac{I_r(\lambda_r)}{I_x(\lambda_x)}\right]\left[\frac{n_x^2}{n_r^2}\right]\left[\frac{D_x}{D_r}\right] \qquad \textbf{Equation 2-1}$$

where A is the absorbance at the excitation wavelength λ, I is the intensity of the excitation light at the excitation wavelength, n is the refractive index of the solvent, D is the integrated intensity of the luminescence and Φ is the quantum yield. The subscripts r and x refer to the reference and the sample. The quantum yields of complexes were measured against quinine sulphate solution in 0.5 M H_2SO_4 (Φ_r = 0.55).[31] Excited-state decays (τ) were recorded on the same Edinburgh FLSP980-stm spectrometer using pulsed picosecond LEDs (EPLED/EPL 375nm, FHWM < 800 ps). The goodness of fit was assessed by minimising the reduced χ^2 function and by visual inspection of the weighted residuals. All solvent used in the preparation of the solutions for the photophysical investigations were of spectrometric grade.

2.4 Synthesis

2.4.1 Synthesis of Random 1

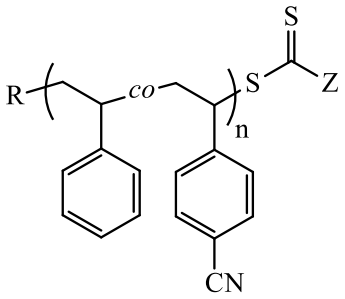

polystyrene:4-cyanopolystyrene 95:5

Figure 2-3 Structure of random copolymer **Random 1**.

Styrene (10.00 g, 96.00 mmol), 4-cyanostyrene (0.65 g, 5.05 mmol), 4-cyano-4-[(dodecylsulfanylthiocarbonyl)sulfanyl]pentanoic acid (0.21 g, 0.53 mmol) and AIBN (0.02 g, 0.13 mmol) were combined in a round-bottomed flask equipped with a magnetic stir bar. The flask was sealed with a rubber septum and the solution was purged with nitrogen for 30 min before being placed in a preheated oil bath set at 75°C. The copolymerisation was allowed to proceed for 5 h. and was halted by exposure to air and immersion in an ice bath. The reaction mixture was diluted with THF and the product precipitated into a large excess of *n*-hexane. The product copolymer **Random 1** (3.63 g) was isolated as a yellow powder by re-precipitation in *n*-hexane followed by drying *in vacuo* overnight at 50°C.

2.4.2 Synthesis of Random 2

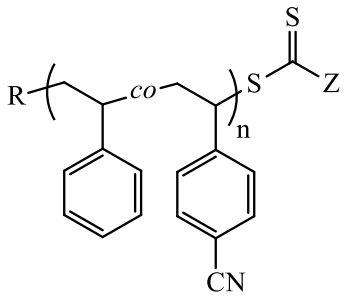

polystyrene:4-cyanopolystyrene 90:10

Figure 2-4 Structure of random copolymer **Random 2**.

Random 2 was prepared as **Random 1** with styrene (5.00 g, 48.00 mmol), 4-cyanostyrene (0.65 g, 5.05 mmol), 4-cyano-4-[(dodecylsulfanylthiocarbonyl) sulfanyl]pentanoic acid (0.11 g, 0.28 mmol), and AIBN (0.01 g, 0.07 mmol). The product **Random 2** (2.22 g) was isolated as a yellow solid.

2.4.3 Synthesis of PS homo

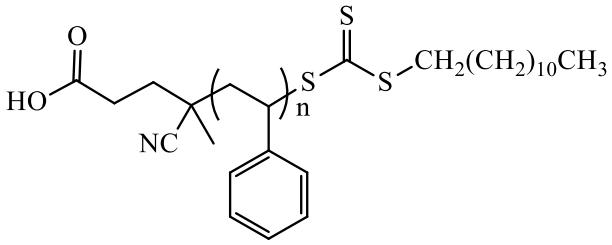

Figure 2-5 Structure of homo-polymer **PS homo**.

Styrene (5.00 g, 48.00 mmol, 4-cyano-4-[(dodecylsulfanylthiocarbonyl) sulfanyl] pentanoic acid (0.10 g, 0.25 mmol) and AIBN (0.01 g, 0.06 mmol) were combined in a round-bottomed flask equipped with a magnetic stir bar. The flask was sealed with a rubber septum and the solution was purged with nitrogen for 30 min

before being placed in a preheated oil bath set at 75°C. The copolymerisation was allowed to proceed for 7 h. and was halted by exposure to air and immersion in an ice bath. The reaction mixture was diluted with THF and the product precipitated into a large excess of *n*-hexane. The product polymer **PS homo** (1.73 g) was isolated as a yellow powder and dried *in vacuo* overnight at 50°C.

2.4.4 Synthesis of Block 1

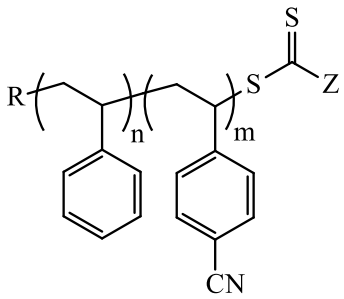

polystyrene:4-cyanopolystyrene 85:15

Figure 2-6 Structure of block copolymer **Block 1**.

PS homo (0.50 g), 4-cyanostyrene (0.09 g, 0.72 mmol) and traces of AIBN were dissolved in 2 mL of toluene and combined in a round-bottomed flask equipped with a magnetic stir bar. The flask was sealed with a rubber septum and the solution was purged with nitrogen for 30 min before being placed in a preheated oil bath set at 65°C. The copolymerisation was allowed to proceed for 6 h. and was halted by exposure to air and immersion in an ice bath. The reaction mixture was diluted with THF and the product precipitated into a large excess of *n*-hexane. The product copolymer **Block 1** (0.47 g) was isolated as a yellow powder and dried *in vacuo* overnight at 50°C.

2.4.5 Synthesis of Block 2

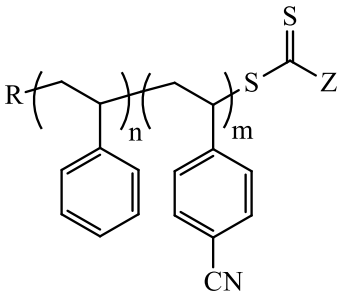

polystyrene:4-cyanopolystyrene 70:30

Figure 2-7 Structure of block copolymer **Block 2**.

PS homo (0.20 g), 4-cyanostyrene (0.07 g, 0.54 mmol) and traces of AIBN were dissolved in 1 mL of toluene and combined in a round-bottomed flask equipped with a magnetic stir bar. The flask was sealed with a rubber septum and the solution was purged with nitrogen for 30 min before being placed in a preheated oil bath set at 65°C. The copolymerisation was allowed to proceed for 6 h. and was halted by exposure to air and immersion in an ice bath. The reaction mixture was diluted with THF and the product precipitated into a large excess of *n*-hexane. The product copolymer **Block 2** (0.13 g) was isolated as a yellow powder and dried *in vacuo* overnight at 50°C.

2.4.6 Synthesis of Random 1-tz

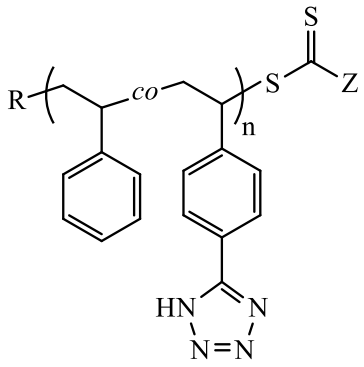

polystyrene:4-tetrazolepolystyrene 95:5

Figure 2-8 Structure of tetrazole functionalised copolymer **Random 1-tz**.

Triethylamine (2.50 mL, 18.00 mmol) and HCl (1.50 mL 37% v/v, 18.0 mmol) were dissolved in 10.00 mL of toluene at 0 °C, resulting in the formation of triethylammonium chloride. The mixture was subsequently allowed to warm to room temperature. The 95:5 styrene/4-cyanostyrene copolymer (**Random 1**) (3.50 g) was dissolved in 10.00 mL of toluene and then added to the solution. Sodium azide (1.00 g, 15.40 mmol) was then added and the mixture was stirred under reflux for 24 h. Subsequently, the solvent was removed under reduced pressure and the crude product was washed with distilled water to remove excess sodium azide and triethylammonium chloride. The product **Random 1-tz** (3.50 g) was obtained after drying *in vacuo* overnight at 50 °C.

2.4.7 Synthesis of Random 2-tz

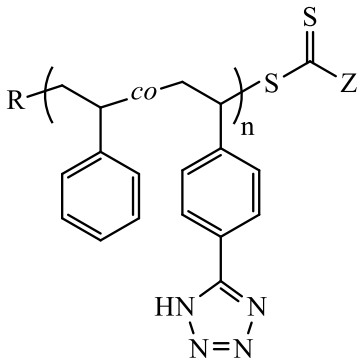

polystyrene:4-tetrazolepolystyrene 90:10

Figure 2-9 Structure of tetrazole functionalised copolymer **Random 2-tz**.

Triethylamine (2.50 mL, 18.00 mmol) and HCl (1.50 mL 37% v/v, 18.00 mmol) were dissolved in 10.00 mL of toluene at 0 °C, resulting in the formation of triethylammonium chloride. The mixture was subsequently allowed to warm to room temperature. The 90:10 styrene/4-cyanostyrene copolymer (**Random 2**) (2.00 g, 0.21 mmol) was dissolved in 10.00 mL of toluene and then added to the solution. Sodium azide (1.00 g, 15.40 mmol) was then added and the mixture was stirred under reflux for 24 h. Subsequently, the solvent was removed under reduced pressure and the crude product was washed with distilled water to remove excess sodium azide and triethylammonium chloride. The product **Random 2-tz** (2.00 g) was obtained after drying *in vacuo* overnight at 50 °C.

2.4.8 Synthesis of Block 1-tz

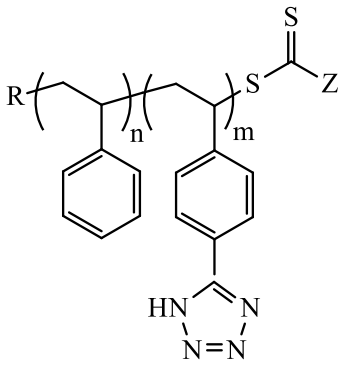

polystyrene:4-tetrazolepolystyrene 85:15

Figure 2-10 Structure of tetrazole functionalised copolymer **Block 1-tz**.

Triethylamine (1.70 mL, 13.00 mmol) and HCl (1.10 mL 37% v/v, 13.00 mmol) were dissolved in 10.00 mL of toluene at 0 °C, resulting in the formation of triethylammonium chloride. The mixture was subsequently allowed to warm to room temperature. The 85:15 styrene/4-cyanostyrene block copolymer (**Block 1**) (0.40 g, 0.05 mmol) was dissolved in 10 mL of toluene and then added to the solution. Sodium azide (0.40 g, 6.20 mmol) was then added and the mixture was stirred under reflux for 24 h. Subsequently, the solvent was removed under reduced pressure and the crude product was washed with distilled water to remove excess sodium azide and triethylammonium chloride. The product **Block 1-tz** (0.30 g) was obtained after drying *in vacuo* overnight at 50 °C.

2.4.9 Synthesis of Block 2-tz

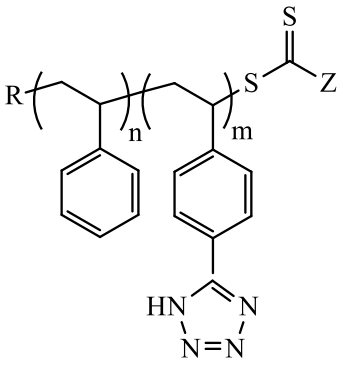

polystyrene:4-tetrazolepolystyrene 70:30

Figure 2-11 Structure of tetrazole functionalised copolymer **Block 2-tz**.

Triethylamine (1.00 mL, 7.60 mmol) and HCl (0.60 mL 37% v/v, 7.90 mmol) were dissolved in 10.00 mL of toluene at 0 °C, resulting in the formation of triethylammonium chloride. The mixture was subsequently allowed to warm to room temperature. The 85:15 styrene/4-cyanostyrene block copolymer (**Block 2**) (0.10 g, 0.01 mmol) was dissolved in 10 mL of toluene and then added to the solution. Sodium azide (0.20 g, 3.10 mmol) was then added and the mixture was stirred under reflux for 24 h. Subsequently, the solvent was removed under reduced pressure and the crude product was washed with distilled water to remove excess sodium azide and triethylammonium chloride. The product **Block 2-tz** (0.07 g) was obtained after drying *in vacuo* overnight at 50 °C.

2.4.10 Synthesis of Random 1-tz-[Re]

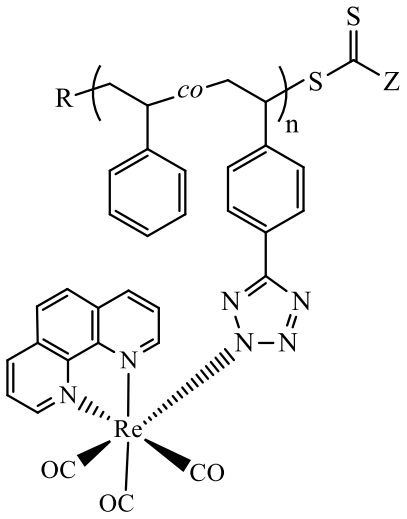

Random copolymer:Rhenium(I) complex 95:5

Figure 2-12 Structure of rhenium functionalised copolymer **Random 1-tz-[Re]**.

To a round-bottomed flask equipped with a magnetic stir bar was added $Re(CO)_3(phen)Br$ (0.05 g, 0.09 mmol) and ethanol (7.50 mL). To a separate flask was added **Random 1-tz** (0.20 g, 0.02 mmol), water (2.50 mL) and triethylamine (1.00 mL). The solution containing $Re(CO)_3(phen)Br$ was then added dropwise to the polymer solution and subsequently heated under refluxing conditions for 24 h. Solvents were removed under reduced pressure and the crude product was washed with deionised water. The crude product was subsequently dissolved in dichloromethane and precipitated in cold *n*-pentane. The product **Random 1-tz-[Re]** (0.10 g) was obtained after drying *in vacuo* overnight at 50 °C.

2.4.11 Synthesis of Random 2-tz-[Re]

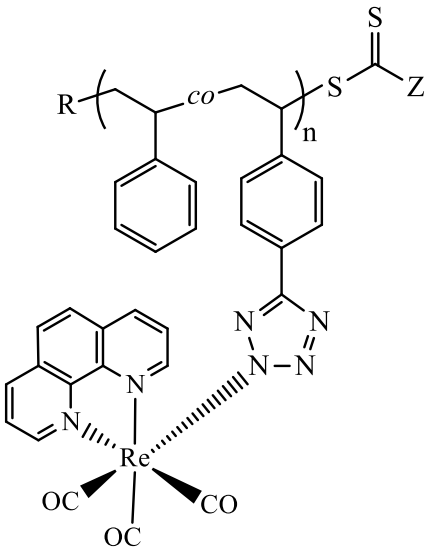

Random copolymer:Rhenium(I) complex 90:10

Figure 2-13 Structure of rhenium functionalised copolymer **Random 2-tz-[Re]**.

To a round-bottomed flask equipped with a magnetic stir bar was added $Re(CO)_3(phen)Br$ (0.05 g, 0.09 mmol) and ethanol (7.50 mL). To a separate flask was added **Random 2-tz** (0.10 g, 0.01 mmol), water (2.50 mL) and triethylamine (1.0 mL). The solution containing $Re(CO)_3(phen)Br$ was then added dropwise to the polymer solution and subsequently heated under refluxing conditions for 24 h. Solvents were removed under reduced pressure and the crude product was washed with deionised water. The crude product was subsequently dissolved in dichloromethane and precipitated in cold *n*-pentane. The product **Random 2-tz-[Re]** (0.09 g) was obtained after drying *in vacuo* overnight at 50 °C.

2.4.12 Synthesis of Block 1-tz-[Re]

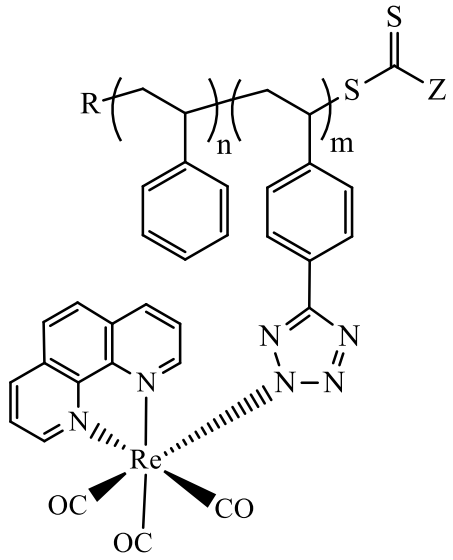

Block copolymer:Rhenium(I) complex 85:15

Figure 2-14 Structure of rhenium functionalised copolymer **Block 1-tz-[Re]**.

To a round-bottomed flask equipped with a magnetic stir bar was added $Re(CO)_3(phen)Br$ (0.02 g, 0.05 mmol) and ethanol (3.50 mL). To a separate flask was added **Block 1-tz** (0.03 g, 0.01 mmol), water (1.50 mL) and triethylamine (0.50 mL). The solution containing $Re(CO)_3(phen)Br$ was then added dropwise to the polymer solution and subsequently heated under refluxing conditions for 24 h. Solvents were removed under reduced pressure and the crude product was washed with deionised water. The crude product was subsequently dissolved in dichloromethane and precipitated in cold *n*-pentane. The product **Block 1-tz-[Re]** (0.03 g) was obtained after drying *in vacuo* overnight at 50 °C.

2.4.13 Synthesis of Block 2-tz-[Re]

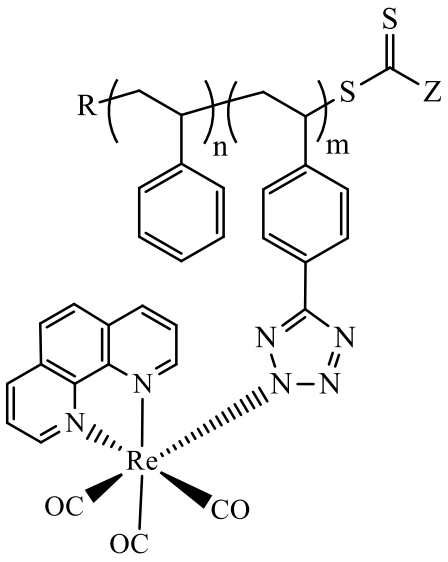

Block copolymer:Rhenium(I) complex 70:30

Figure 2-15 Structure of rhenium functionalised copolymer **Block 2-tz-[Re]**.

To a round-bottomed flask equipped with a magnetic stir bar was added $Re(CO)_3(phen)Br$ (0.02 g, 0.04 mmol) and ethanol (3.50 mL). To a separate flask was added **Block 2-tz** (0.01 g, 0.01 mmol), water (1.50 mL) and triethylamine (0.50 mL). The solution containing $Re(CO)_3(phen)Br$ was then added dropwise to the polymer solution and subsequently heated under refluxing conditions for 24 h. Solvents were removed under reduced pressure and the crude product was washed with deionised water. The crude product was subsequently dissolved in dichloromethane and precipitated in cold *n*-pentane. The product **Block 2-tz-[Re]** (0.01 g) was obtained after drying *in vacuo* overnight at 50 °C.

2.4.14 Synthesis of $Re(CO)_3(phen)(L)$

$Re(CO)_3(phen)(L)$ L=5-phenyltetrazolate was prepared according to previously published procedure.[32]

2.5 Results and Discussion

2.5.1 Statistical RAFT copolymerisation of styrene with 4-cyanostyrene

Two statistical copolymeric precursors of styrene (STY) with 4-cyanostyrene (CNSTY) were prepared by RAFT copolymerisation employing the trithiocarbonate 4-cyano-4-[(dodecylsulfanylthiocarbonyl)sulfanyl] pentanoic acid (**Figure 2-16**) as the CTA and AIBN as the source of primary radicals. This trithiocarbonate CTA was chosen for the polymerisation of the styrenic monomers based on previously reported synthesis.[33]

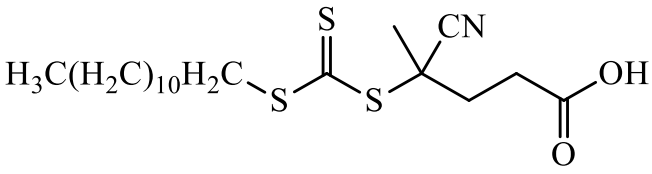

Figure 2-16 RAFT trithiocarbonate chain transfer agent 4-cyano-4-[(dodecylsulfanylthiocarbonyl) sulfanyl] pentanoic acid employed in copolymer synthesis.

The two STY-CNSTY statistical copolymers were synthesised with two different molar ratios of CNSTY and STY (**Scheme 2-1**). The first precursor, **Random 1,** contains 5 mol % CNSTY repeating units and 95 mol % STY, while for the polymerisation of **Random 2** 10 mol % CNSTY monomer and 90 mol % STY were used. Both polymerisations were performed under the same conditions: bulk polymerisation at 75 °C for 5 hours, as shown in **Scheme 2-1**.

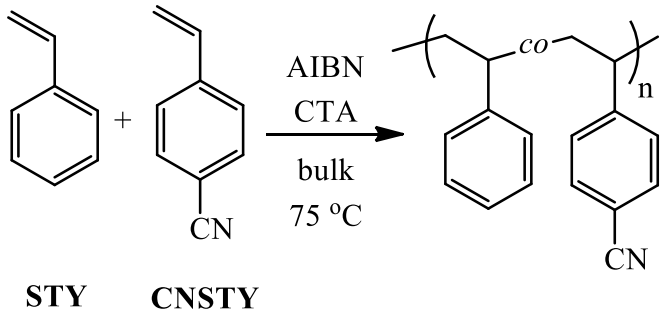

Scheme 2-1 Outline for the synthesis of precursor statistical copolymers **Random 1** and **Random 2** *via* RAFT copolymerisation.

SEC traces of **Random 1** and **Random 2** are shown in **Figure 2-16** and **Figure 2-17**. In both cases the theoretical M_n of the target copolymers was 20,000. SEC analysis (**Figure 2-17** and **Figure 2-18**) of **Random 1** and **Random 2** indicate a conversion of about 50% with a measured M_n of 10,200 for **Random 1** and 9,500 for **Random 2**, relative to narrow molecular weight distribution polySTY standards. The monomer conversion was intentionally kept low (about 50%) to avoid the occurrence of side reactions, including bimodal radical coupling.

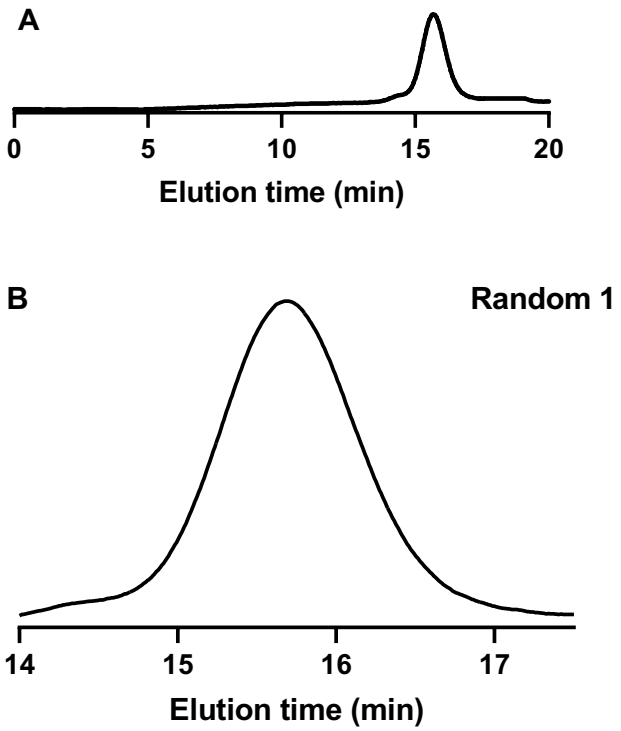

Figure 2-17 A: full SEC trace of **Random 1** from 0 to 20 min; B: SEC trace of **Random 1** from 14 to 17.5 min.

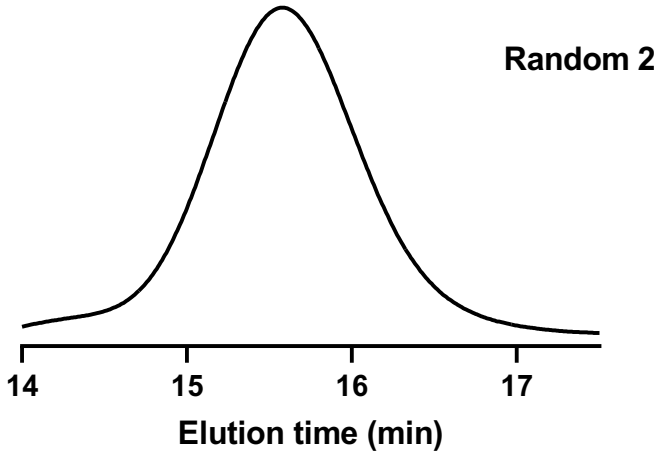

Figure 2-18 SEC trace of **Random 2**.

A summary of the polymerisation conditions and SEC-measured of the number average molecular weight, M_n, the weight average molecular weight, M_w, and the dispersity, $Đ$ (ratio M_w/M_n) values of the product parent (co)polymers are given in **Table 2-1**.

Table 2-1 Summary of the RAFT-prepared (co)polymers, polymerisation conditions and molecular weights and dispersity as measured by size exclusion chromatography, for **Random 1** and **Random 2**.

Polymer[a]	STY: CNSTY	^{13}C NMR comp.	Polym. Temp. [°C]	Polym. Time [h]	Solvent	M_n[b]	M_w[b]	$Đ$[b]
Random 1	95:5	94:6	75	5	Bulk	10,200	11,200	1.10
Random 2	90:10	88:12	75	5	Bulk	9,500	10,400	1.09

[a] Theoretical M_n at 100% conversion was 20,000; [b] As determined by size exclusion chromatography in THF by using RI detector.

FTIR analysis of the two random copolymers was performed after copolymerisation. FTIR spectroscopy showed the presence of cyano groups in the parent copolymers (**Figure 2-19**) with the characteristic -C≡N stretch visible at ca. 2229 cm^{-1}.

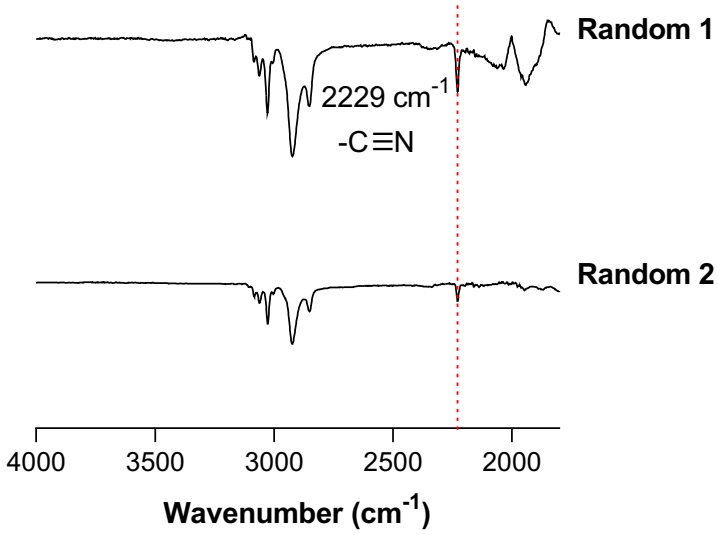

Figure 2-19 FTIR spectra, plotted between 4000 and 1800 cm^{-1}, for **Random 1** (top) and **Random 2** (bottom).

2.5.2 RAFT block copolymerisation of styrene with 4-cyanostyrene

Two poly(styrene-*b*-4-cyanostyrene) copolymers were prepared by RAFT copolymerisation employing the trithiocarbonate 4-cyano-4-[(dodecylsulfanylthiocarbonyl)sulfanyl] pentanoic acid (**Figure 2-16**) as the CTA and AIBN as the source of primary radicals, consistent with the synthesis of the analogue statistical copolymers.

Block copolymerisation was performed as follows. A polystyrene homopolymer (target M_n = 20,000) was synthesised under bulk conditions for 7 hours with the RAFT CTA noted above. Following purification, the polystyrene homopolymer was employed as macro RAFT agent for the subsequent block copolymerisation of CNSTY, **Scheme 2-2**. Two STY-CNSTY block copolymers were synthesised with two different molar ratios of CNSTY and STY. The first precursor, **Block 1**, contained 15 mol % CNSTY and 85 mol % STY, while the second

copolymer, **Block 2**, was comprised of 30 mol % CNSTY monomer and 70 mol % STY. Both reactions were carried out under the same conditions in bulk at 65°C for 6 hours, as illustrated in **Scheme 2-2**.

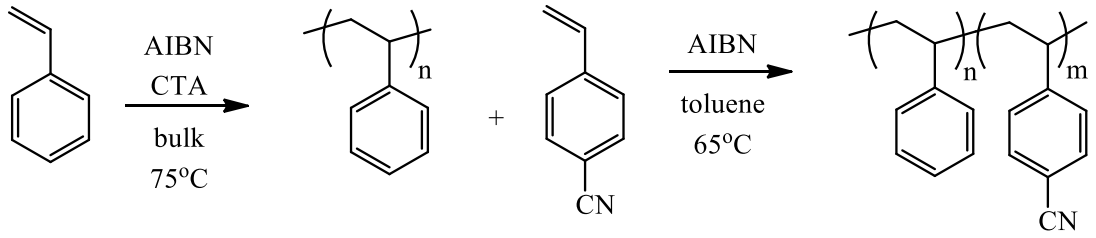

Scheme 2-2 Outline for the synthesis of precursor STY-CNSTY block copolymers **Block 1** and **Block 2**.

SEC traces of both block copolymers (**Figure 2-20** and **Figure 2-21**) show a shift in the molecular weight distribution to shorter elution time after the addition of 4-cyanostyrene, confirming successful copolymerisation.

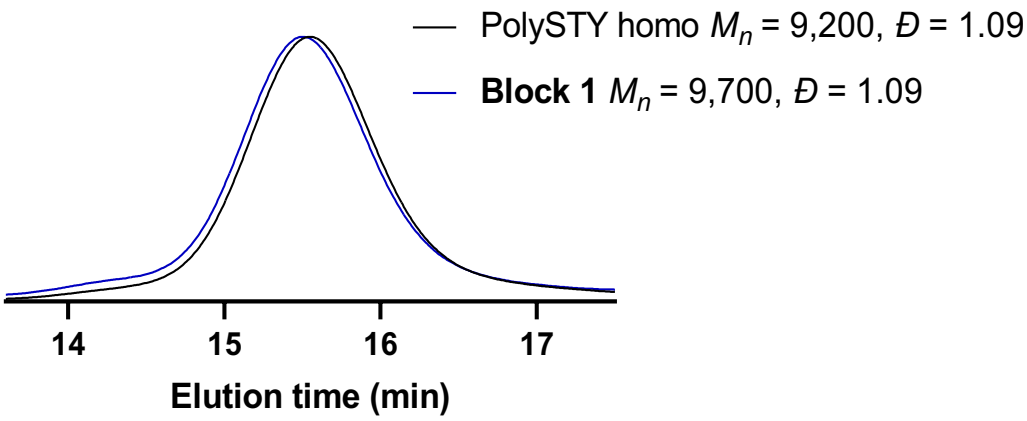

Figure 2-20 SEC traces of the PolySTY and the corresponding poly(styrene-*b*-4-cyanostyrene) copolymer **Block 1.**

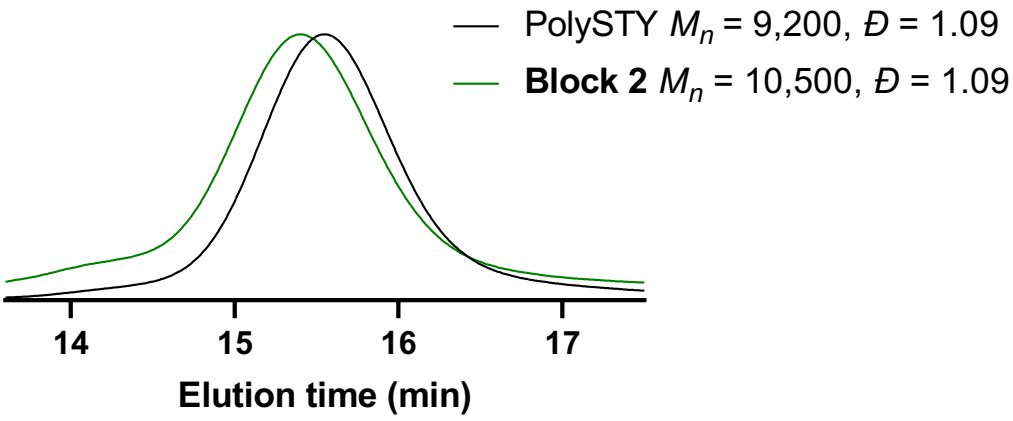

Figure 2-21 SEC traces of the PolySTY and the corresponding poly(styrene-*b*-4-cyanostyrene) copolymer **Block 2**.

A summary of the polymerisation conditions and SEC-measured M_n, M_w and dispersity (Đ = M_w/ M_n) values of the polystyrene homopolymer and the STY-CNSTY block (co)polymers are given in **Table 2-2**.

Table 2-2 Summary of the RAFT-prepared (co)polymers, polymerisation conditions and molecular weights and dispersity as measured by size exclusion chromatography.

Polymer[a]	STY:CNSTY	Polym. temperature [°C]	Polym. time [hr]	Solvent	M_n[b]	M_w[b]	Đ[b]
PS homo	100	75	7	Bulk	9,200	10,700	1.09
Block 1	85:15	65	12	Toluene	9,700	10,500	1.09
Block 2	70:30	65	12	Toluene	10,500	11,400	1.09

[a] Theoretical M_n at 100% conversion was 20,000; [b] As determined by size exclusion chromatography in THF.

The presence of cyano groups in the block copolymers was confirmed by FTIR spectroscopy (**Figure 2-22**), with the characteristic -C≡N stretch visible at ca. 2229 cm^{-1}.

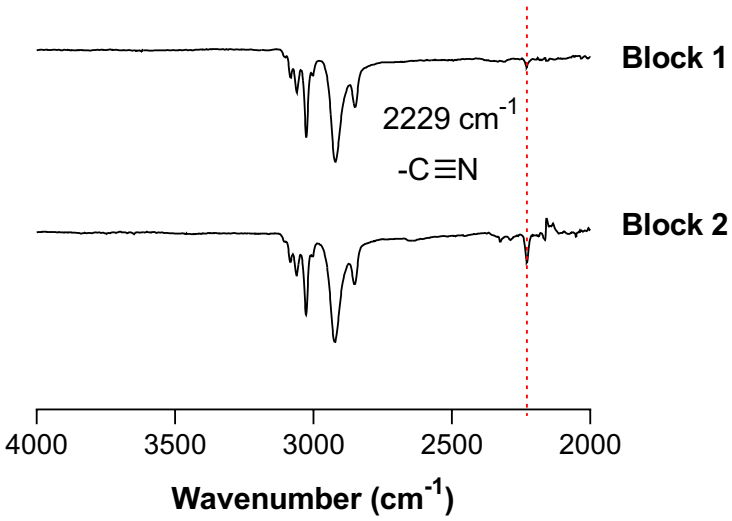

Figure 2-22 FTIR spectra, plotted between 4000 and 2000 cm^{-1}, for **Block 1** (top) and **Block 2** (bottom).

2.5.3 Conversion of cyano functional groups to the corresponding tetrazole species

With the cyano-functional (co)polymers in hand, the pendent nitrile groups were then converted to the corresponding 1*H*-tetrazole species *via* reaction of the precursor copolymers with NaN_3/NEt_4Cl in refluxing toluene, based on the method of Koguro *et al*.[34]

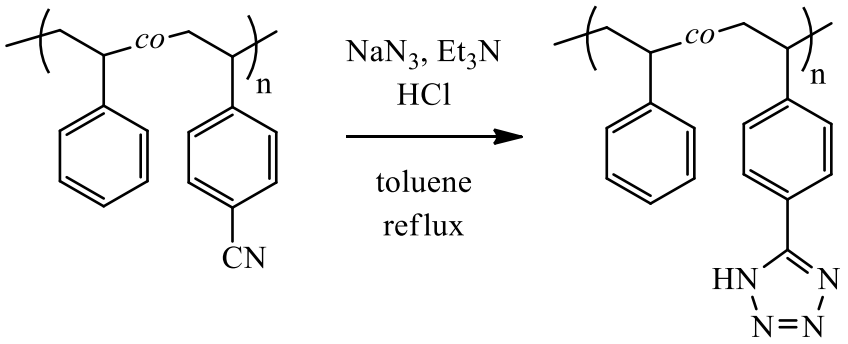

Scheme 2-3 Synthesis of 1*H*-tetrazole functionalised styrenic copolymers from cyano functional precursor.

Following the reaction, the excess NaN_3 was removed by washing with water and the final polymeric materials containing tetrazole were obtained. The conversion of the nitrile functionalities to tetrazole rings was confirmed by FTIR and ^{13}C NMR spectroscopies. As noted above, in the precursor copolymers there is a clear band in the FTIR spectra at 2229 cm^{-1} associated with the -C≡N stretch; this band is absent in all copolymers after reaction with NaN_3, **Figure 2-23**, indicating (near) quantitative conversion of the cyano groups to the corresponding tetrazole species. Additionally, we observe the appearance of a weak, broad signal centred around 3387 cm^{-1} which is typical of the N-H stretch in the newly formed tetrazole ring (**Figure 2-23**, blue dotted line). [35,36]

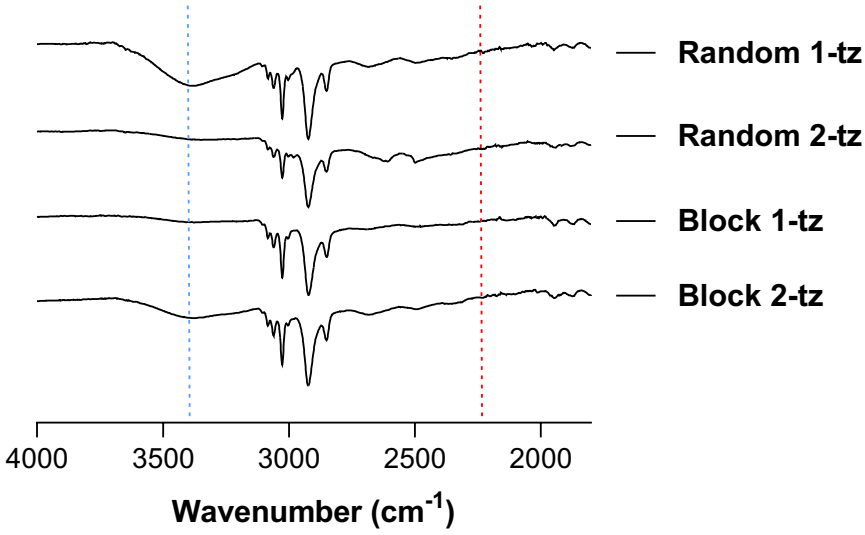

Figure 2-23 FTIR spectra of tetrazole functionalised copolymers **Random 1-tz**, **Random 2-tz**, **Block 1-tz** and **Block 2-tz**.

Attempted SEC analysis on the modified copolymers proved unsuccessful with no signal being observed. This is likely due to absorption of the tetrazole functional copolymer on the guard column packing material and (or) removal of the copolymer during pre-filtration due to limited solubility; this is a common feature of tetrazoles in non- and low polarity solvents.[37] One potential drawback in using NaN_3 to affect tetrazole formation with RAFT-prepared copolymers is nucleophilic cleavage of the thiocarbonylthio end-groups to give the corresponding macromolecular thiols; a reaction that has been reported to proceed rapidly.[38] This can, in principle, be negated by modification of the thiocarbonylthio end-group prior to tetrazole formation, although we did not adopt this route in this report since the presence of any resulting disulfide coupled material was not anticipated to impact the photophysical properties of the final hybrid materials.[39] UV-Vis spectroscopic analysis of **Random 1**, **Random 2**, **Block 1** and **Block 2** before and after reaction with NaN_3 suggests that (quantitative) cleavage of the thiocarbonylthio end-groups had occurred based on the significant

reduction/absence of the broad band spanning the range ~ 280-350 nm associated with the π-π* transition of the C=S bond, **Figure 2-24** to **Figure 2-27**.[40]

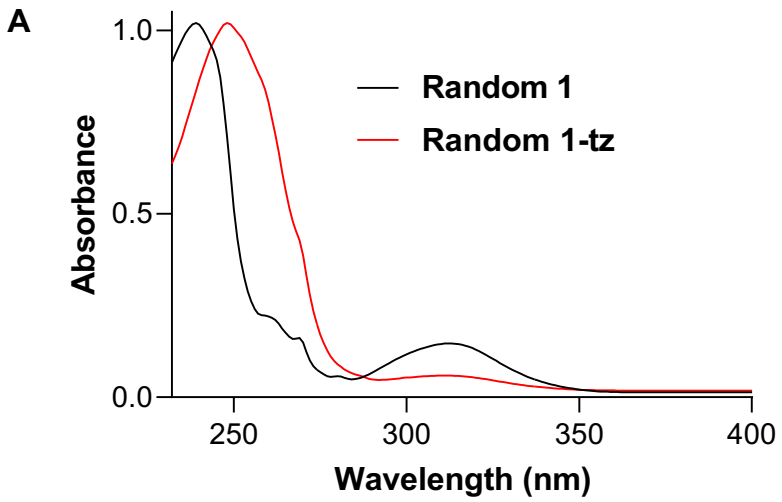

Figure 2-24 UV-Vis spectra of **Random 1** before and after reaction with NaN_3.

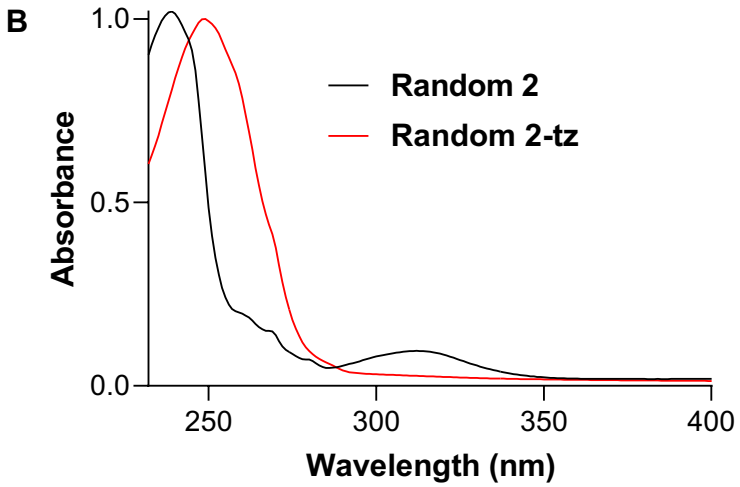

Figure 2-25 UV-Vis spectra of **Random 2** before and after reaction with NaN_3.

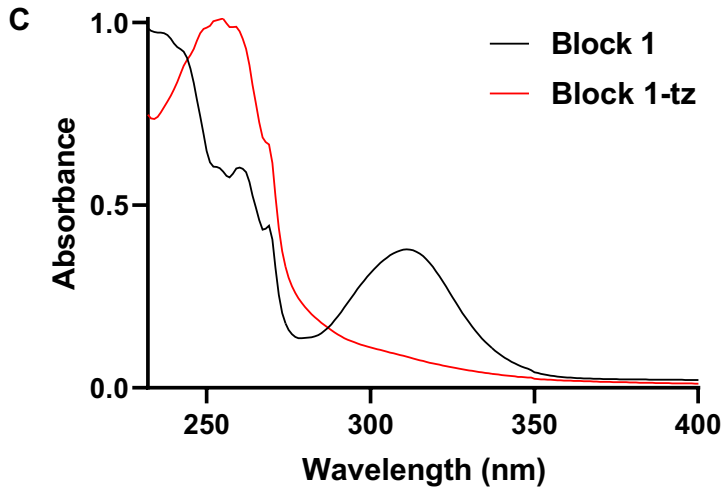

Figure 2-26 UV-Vis spectra of **Block 1** before and after reaction with NaN_3.

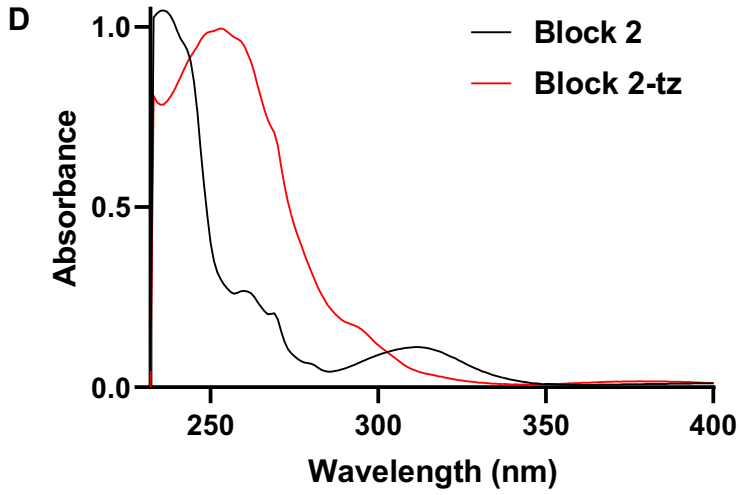

Figure 2-27 UV-Vis spectra of **Block 2** before and after reaction with NaN_3.

The tetrazole functional (co)polymers were utilised to determine the copolymer compositions *via* inverse-gated proton decoupled ^{13}C NMR spectroscopy.[41] **Figure 2-28** and **Figure 2-29** show the ^{13}C NMR spectrum of **Random 1-tz** and **Random 2-tz**, recorded in $CDCl_3$, with the key signals highlighted.

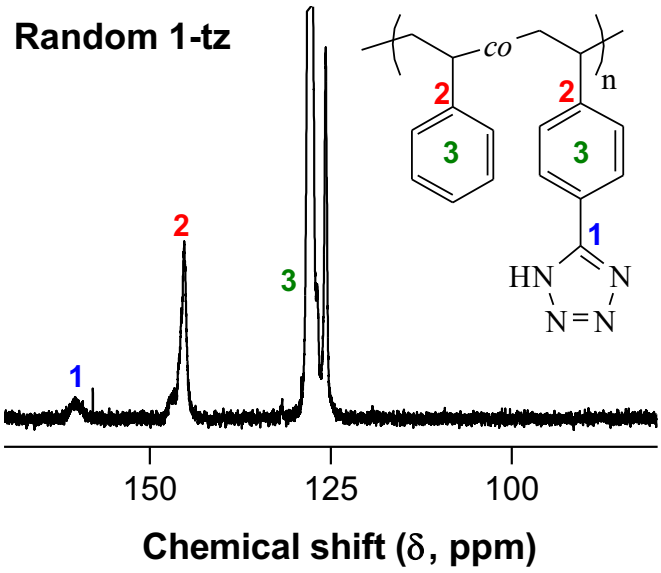

Figure 2-28 Inverse-gated proton decoupled ^{13}C NMR spectra of **Random 1-tz**, recorded in $CDCl_3$, highlighting the polymer aromatic region and the tetrazole ring carbon.

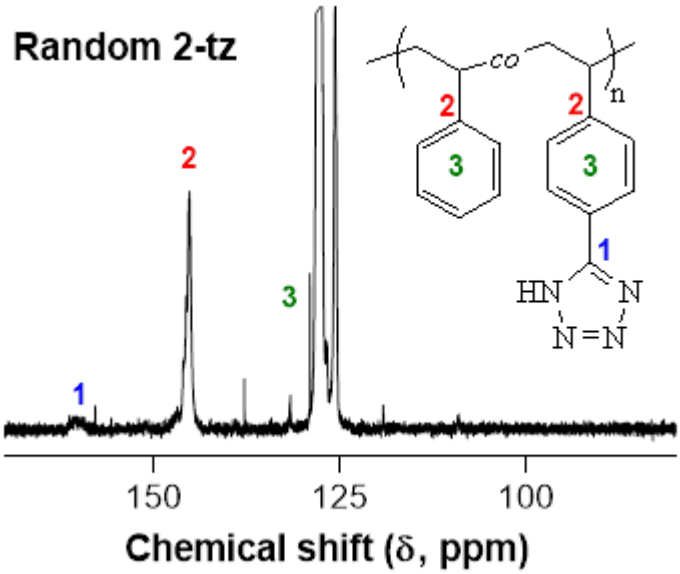

Figure 2-29 Inverse-gated proton decoupled ^{13}C NMR spectra of **Random 2-tz** recorded in $CDCl_3$, highlighting the polymer aromatic region and the tetrazole ring carbon.

Inverse-gated proton decoupled ^{13}C NMR spectroscopy is a technique that allows quantitative analysis of ^{13}C NMR spectra, through proton decoupling between the relaxation delay and acquisition period. With inverse-gated proton decoupled ^{13}C NMR spectroscopy, it is possible to obtain spectra consisting of singlets whose intensities correspond to the number of ^{13}C nuclei they represent.[41]

The signal corresponding to the C in the tetrazole ring has been previously reported.[42] The signal centred around δ = 160 ppm, labelled **1**, is attributed to the quaternary tetrazolic carbon. This chemical shift value is consistent with values reported for small molecule complexes such as the *N*-methylated Re(I) tetrazole species reported by Werrett *et al*.[23] The signal labelled **2** at $\delta \sim 146$ ppm is assigned to the *ipso* quaternary C atom of the aromatic rings of the polystyrene main chain while the remaining aromatic carbons, **3**, appear over the range δ = 124-131 ppm. These chemical shifts are consistent with literature values such as those reported by Ziaee and Khoshkhoo in their ^{13}C NMR spectroscopic study of the effect of temperature on tacticity in the thermal polymerisation of *para*-methylstyrene.[43] Copolymer compositions were determined by calculating the ratio of C1 and C2 integrated signals. The calculated compositions agree extremely well with the target values with, for example, the targeted 90:10 STY-CNSTY random copolymer having a calculated composition of 88:12. Analysis of the tetrazole functionalised block copolymers proved inconclusive with no tetrazole-associated resonances detected. This is most likely due to self-assembly (or very minimal solvation) in $CDCl_3$ and is consistent with the limited solubility of tetrazoles in organic media, *vide supra*.

2.5.4 Synthesis of hybrid polymeric-rhenium(I) luminescent complexes

The synthesis of the hybrid polymer-rhenium species was achieved by adapting a previously reported method.[44] Commercially available $[Re(CO)_5(Br)]$ was heated at reflux with 1,10-phenantroline (phen) in toluene to give *fac*-$[Re(CO)_3(phen)(Br)]$, **Scheme 2-4**.

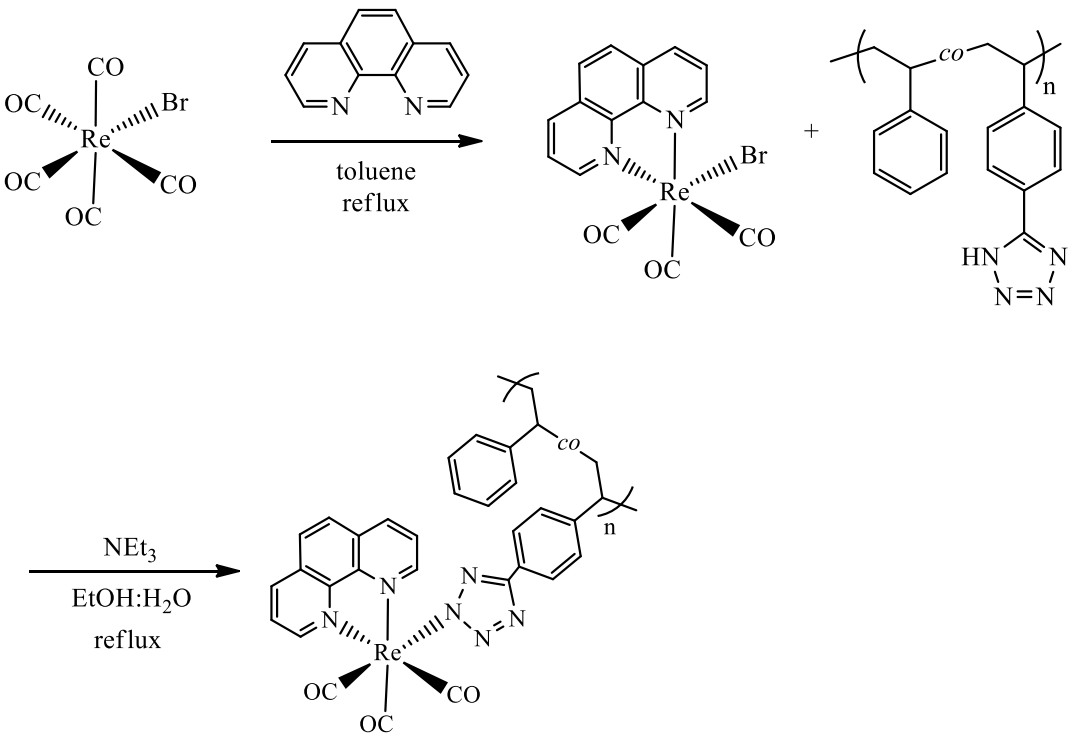

Scheme 2-4 General approach for the preparation of polymer-rhenium hybrid materials.

The coordination of the polymer-bound tetrazole groups to the rhenium species was subsequently achieved by reaction of *fac*-$[Re(CO)_3(phen)(Br)]$ in ethanol/water 3:1 (v/v) with the tetrazole functional statistical and block copolymers dissolved in triethylamine. After heating at reflux overnight, the desired polymer-metal hybrid material was obtained by precipitation in cold *n*-pentane. The success of the reaction was confirmed by FTIR spectroscopy and by photophysical investigations. **Figure 2-**

30 to **Figure 2-33** show FTIR spectra, plotted between 4000 and 1800 cm^{-1}, for parent copolymers containing cyano functionalities (top), the same block copolymer after treatment with NaN_3 (middle) highlighting the presence, and absence, of the -C≡N stretching band before and after modification and the final target Re-complexed products (bottom), with the disappearance of the N-H stretch and appearance of two bands associated with the -C≡O ligands on [Re] ([Re]: $Re(CO)_3(phen)$, phen = 1,10-phenanthroline) highlighted in light blue.

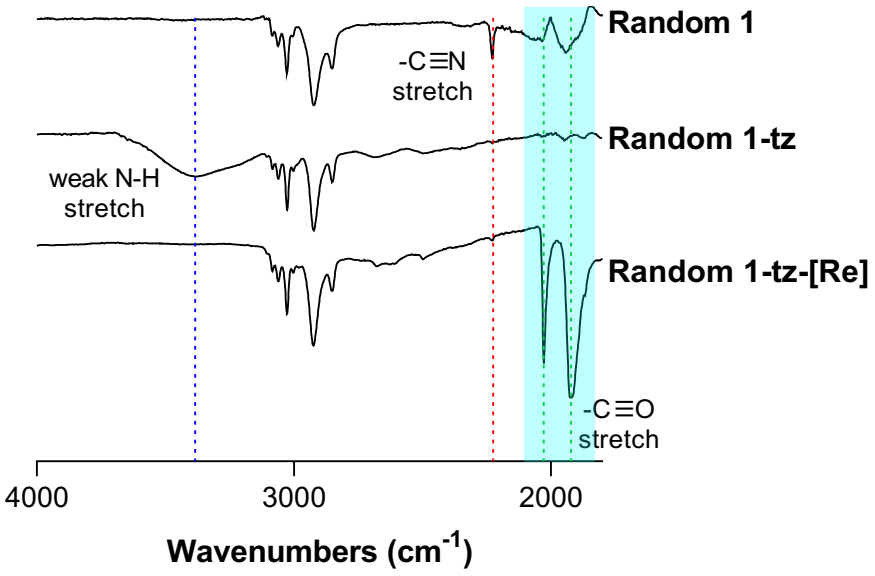

Figure 2-30 FTIR spectra of **Block 2**, **Block 2-tz** and **Block 2-tz-[Re]**.

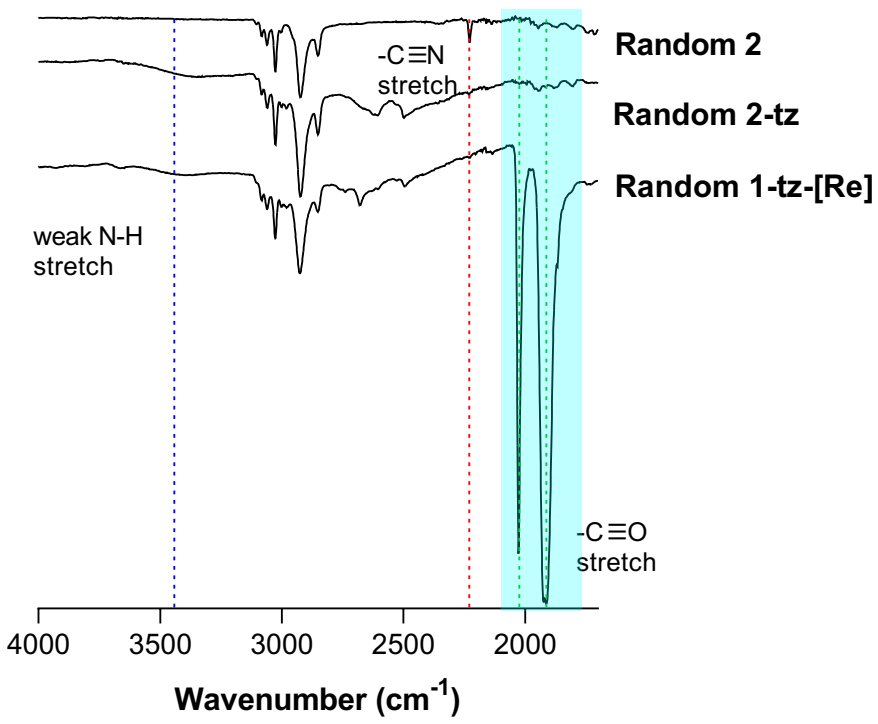

Figure 2-31 FTIR spectra of **Random 2**, **Random 2-tz** and **Random 2-tz-[Re]**.

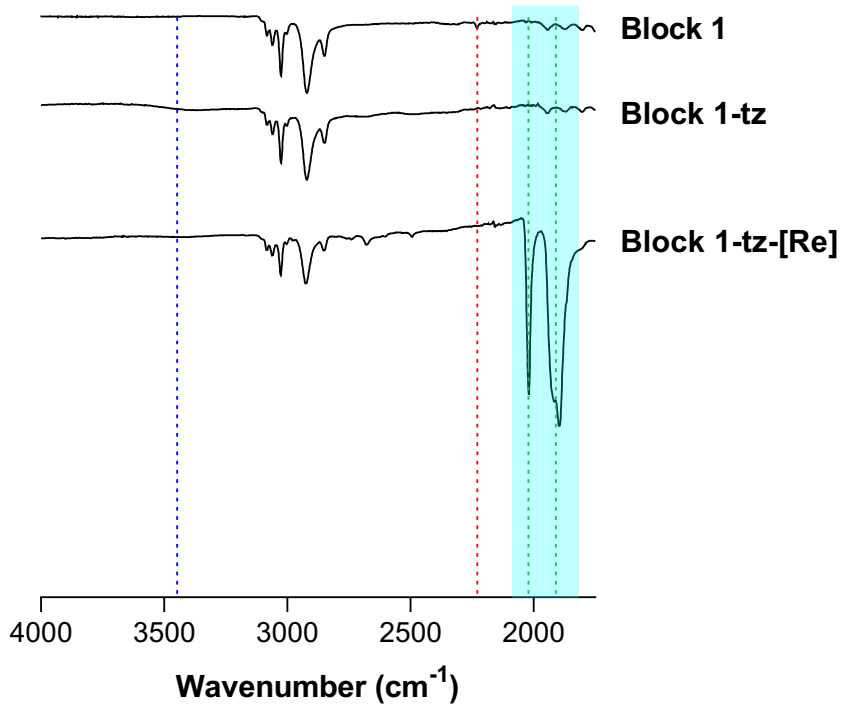

Figure 2-32 FTIR spectra of **Block 1**, **Block 1-tz** and **Block 1-tz-[Re]**.

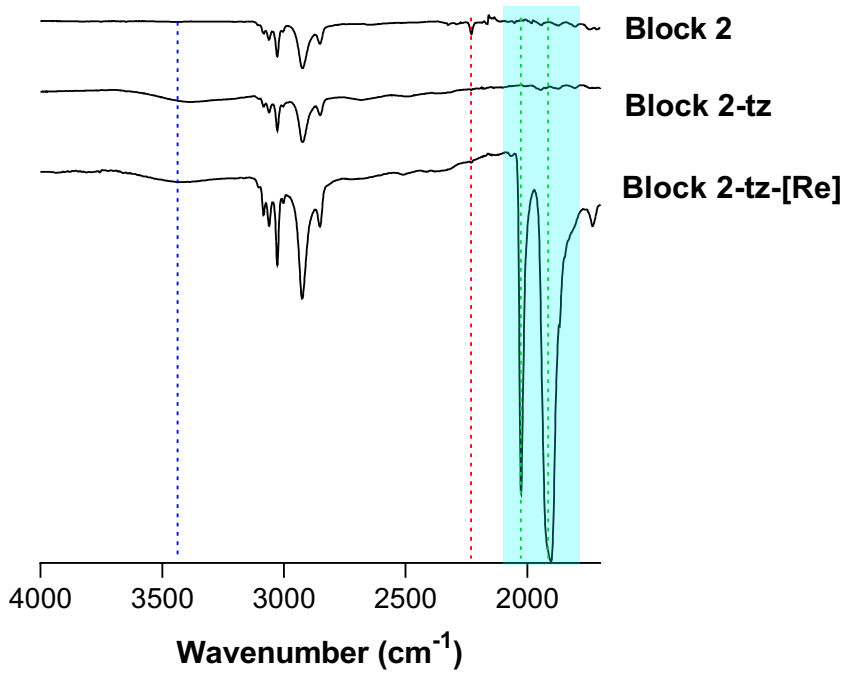

Figure 2-33 FTIR spectra of **Block 2**, **Block 2-tz** and **Block 2-tz-[Re]**.

2.5.5 Photophysical studies of polystyrenic-rhenium complexes hybrid materials

Photophysical studies of the final Re-copolymer hybrid materials were performed in dilute dichloromethane. The polymer-metal hybrid solutions were prepared by dissolving 1 mg of material in 10 mL of dichloromethane.

A summary of the absorption and emission properties of the rhenium-polymer hybrid materials in dichloromethane, is given in **Table 2-3**.

Table 2-3 Summary of the photophysical data for all polymer-Re hybrid materials in dichloromethane.

Polymer	λ_{abs} [nm]	λ_{em} [nm]	τ^a [ns]	τ^b [ns]	Φ^a [%]	Φ^b [%]	$k_r{}^b$ [10^6 s^{-1}]	$k_{nr}{}^b$ [10^6 s^{-1}]
Random 1-tz-[Re]	259 293 375	602	205	602	0.017	0.040	0.066	1.60
Random 2-tz-[Re]	259 293 375	600	232	648	0.029	0.054	0.083	1.46
Block 1-tz-[Re]	266 293 375	602	192	532	0.022	0.052	0.098	1.86
Block 2-tz-[Re]	266 293 375	600	215	540	0.020	0.034	0.063	1.80

[a] Measured from air-equilibrated solutions. [b] Measured from degassed solutions. Where τ = lifetime; Φ = luminescent quantum yield; k_r = radiative constant; k_{nr} = non-radiative constant.

The absorption spectra of the air-equilibrated solutions were measured in dichloromethane at a concentration of 0.10 mg/mL. All four copolymeric hybrid materials exhibited similar absorption profiles (**Figure 2-34**). All profiles displayed intense broad bands in the UV region at wavelengths shorter than 300 nm and broad bands of lower intensity at wavelengths longer than 375 nm. The high energy bands can be attributed to π-π* transitions occurring on the polymer backbone overlaid on π-π* ligand centred (LC) transitions occurring on the diimine systems bound to the Re centres, in agreement with similar previously reported rhenium complexes.[32] The broad bands of lower intensity are visible at wavelengths longer than 350 nm, and are associated with metal-to-ligand charge transfer (MLCT) transitions that are typical of Re diimine tetrazolato complexes.[23]

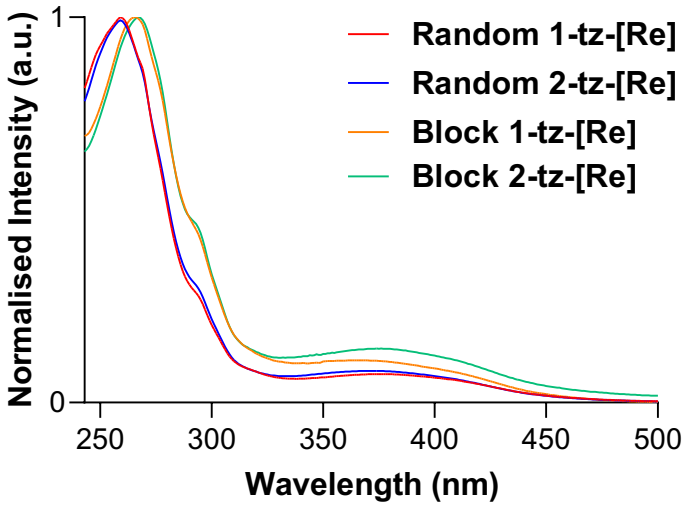

Figure 2-34 Normalised absorption profiles of **Random 1-tz-[Re]** (red trace), **Random 2-tz-[Re]** (blue trace), **Block 1-tz-[Re]** (orange trace) and **Block 2-tz-[Re]** (green trace) in dilute dichloromethane, air-equilibrated samples.

Upon excitation to the MLCT state, all polymer-Re hybrid materials exhibit very similar broad emission bands centred around 600 nm (**Figure 2-35**) in air-equilibrated dichloromethane solutions.[32,45] Based on previously reported structurally similar complexes, these broad bands are associated with emission from ^{3}MCLT excited states. The triplet spin multiplicity is in agreement with the relatively long excited-state lifetime decays which were measured to be within the range 192-232 ns. These values are increased to 532-648 ns upon degassing due to the sensitivity of the ^{3}MLCT excited states to the presence of $^3O_2$. To confirm that the emission profiles were originating from Re diimine tetrazolato complexes formed by attachment of the precursor Re(phen)(CO)$_3$Br to the tetrazole functional copolymers, the emission profiles were directly compared with the emission bands of Re(phen)(CO)$_3$Br, Re(phen)(CO)$_3$L (L = 5-phenyltetrazolate), and the cationic acetonitrile solvated complex [Re(phen)(CO)$_3$(NCCH$_3$)]$^+$ (**Figure 2-36**). In agreement with previously

published analogous complexes, the emission bands of the polymeric materials overlapped nicely with the mononuclear complex $Re(phen)(CO)_3L$. Their maxima appear blue shifted with respect to $Re(phen)(CO)_3Br$ due to the more π acidic nature of the tetrazolato ligand compared to the bromo ligand. The neutral charge of the Re complexes appended to the polymeric backbone is further confirmed by the fact that their emission bands are red-shifted when compared to the emission of the cationic complex $[Re(phen)(CO)_3(NCCH_3)]^+$, a feature that is explained by the increase in electron density for the Re centre with consequent destabilisation of the 5*d* orbitals of the Re and lowering of the energy gap between the ground and MLCT states. The similarities between the emission profiles of the polymeric materials and $Re(phen)(CO)_3L$ (L = 5-phenyltetrazolate), in **Figure 2-36** confirm that the polymeric styrenic backbone does not affect the emission features of the Re(I) complexes. Similar observations have been made by Ulbricht *et al.* in RAFT-prepared methacrylic copolymers containing a pendent Ir(III) species.[45]

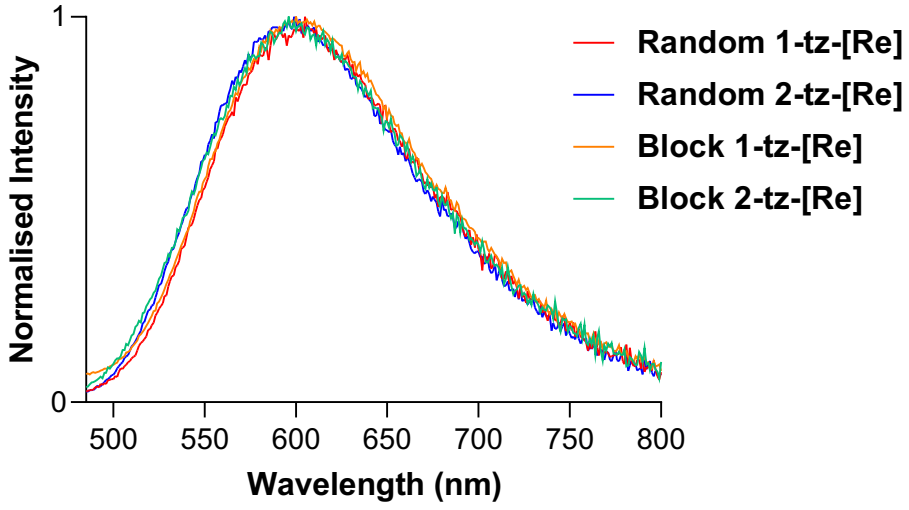

Figure 2-35 Normalised emission profiles of final rhenium-polymeric hybrid materials in dichloromethane, air-equilibrated solutions.

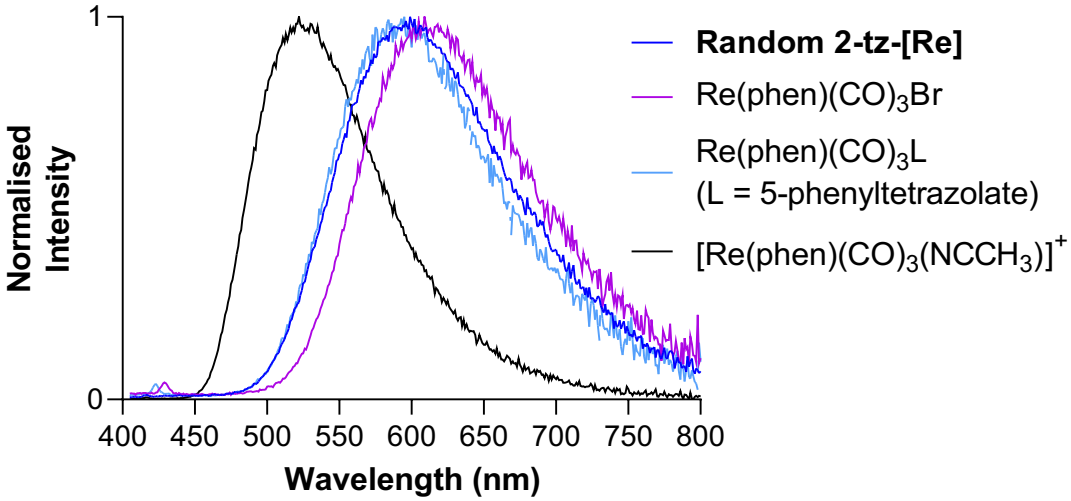

Figure 2-36 Normalised emission profiles of **Random 2-tz-[Re]** (blue trace), $Re(phen)(CO)_3Br$ (purple trace), $Re(phen)(CO)_3L$ (light blue trace), $[Re(phen)(CO)_3(NCCH_3)]^+$ (black trace) in dilute dichloromethane, air-equilibrated samples.

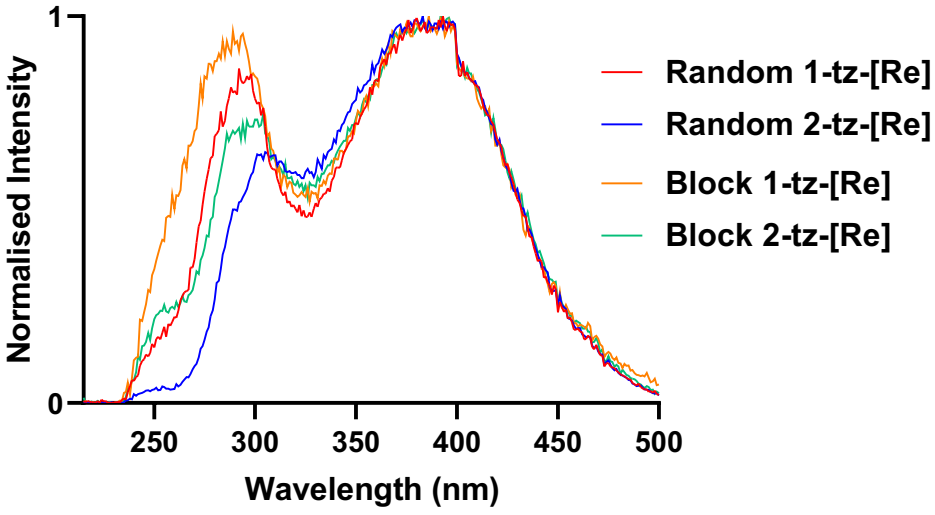

Figure 2-37 Normalised excitation profiles of **Random 1-tz-[Re]** (red trace), **Random 2-tz-[Re]** (blue trace), **Block 1-tz-[Re]** (orange trace) and **Block 2-tz-[Re]** (green trace) in dilute dichloromethane, air-equilibrated samples.

From the normalised excitation profiles shown in **Figure 2-37**, of all hybrid polymer-rhenium final materials it can be seen that the range of excitation profiles match absorption profiles, as expected.

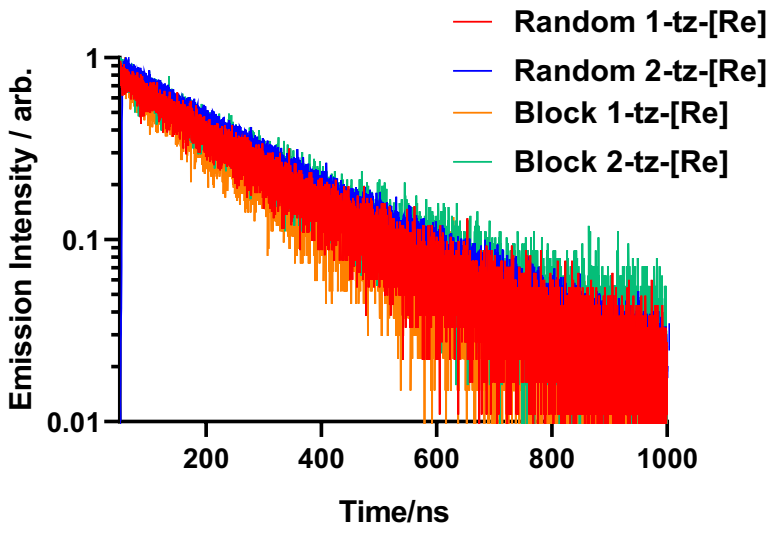

Figure 2-38 Normalised TCSPC decay of ^{3}MLCT emission of air equilibrated solutions under excitation at 375 nm.

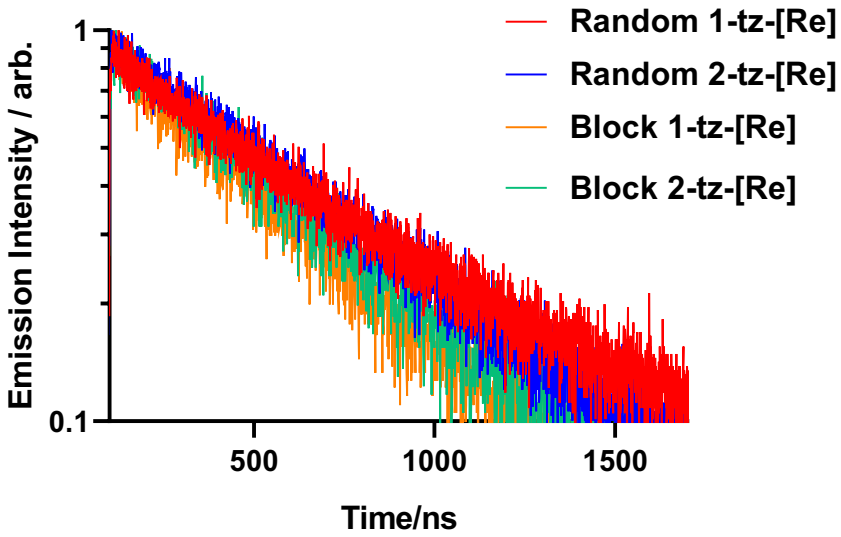

Figure 2-39 Normalised TCSPC decay of ^{3}MLCT emission of degassed solutions under excitation at 375 nm.

Lifetime values were found to be within the typical range for this type of rhenium-tetrazolato luminescent complexes. Lifetime plots shown in **Figure 2-38** and **Figure 2-39** confirm monoexponential decay of all Re-polymer hybrid species. The lifetime value range is between 192 ns and 232 ns for air-equilibrated samples and between 532 ns and 648 ns for degassed solutions. From the obtained values of quantum yields and lifetime, the radiative [$k_r = \Phi \cdot \tau^{-1}$] and non-radiative decay constant [$k_{nr} = (1-\Phi) \cdot \tau^{-1}$] were determined (**Table 2-4**). The values of k_r and k_{nr} are consistent for all samples suggesting that the distribution, and amount, of coordinated Re(I) species, has no effect on the photophysical properties of the luminescent metal complex. [22,32,46,47]

2.6 Conclusions

In this Chapter, we have described the first examples of well-defined, styrenic-based copolymers containing pendent tetrazole functional groups and demonstrated the ability of such materials to serve as macromolecular ligands capable of complexing a Re(I) tricarbonyl diimine precursor *via* tetrazole coordination to the metal centre. A series of four new materials containing various percentages of tetrazole moieties were synthesised and modified: two statistical and two block copolymers. The novel tetrazole appended materials were further reacted with a rhenium(I) luminescent precursor to yield four new polymeric luminescent materials. The new hybrid polymeric-inorganic materials exhibit photophysical properties demonstrating that the polymeric moiety does not interfere with the luminescent properties of the final luminescent material. Coordination between tetrazole appended groups and Re(I) complex has been confirmed by absorption and emission measurements. Lifetime measurements and quantum yields confirmed that the polymeric backbone does not

modify the luminescent properties of the attached Re(I) tricarbonyl diimine complex. Significantly, these studies open the route to the development of a new class of transition metal tetrazolato functional luminescent polymers.

2.7 References

1. G. Moad, E. Rizzardo and S. H. Thang, *Australian Journal of Chemistry*, 2005, **58**, 379-410.
2. G. Moad, E. Rizzardo and S. H. Thang, *Australian Journal of Chemistry*, 2006, **59**, 669-692.
3. G. Moad, E. Rizzardo and S. H. Thang, *Australian Journal of Chemistry*, 2012, **65**, 985-1076.
4. R. Varala and B. H. Babu, in: D.P. Vlachakis (Ed.), *Molecular Docking*, IntechOpen, 2018.
5. A. Taden, A. H. Tait and A. Kraft, *Journal of Polymer Science Part A: Polymer Chemistry*, 2002, **40**, 4333-4343.
6. D. Sinirliroglu, S. U. Celik, A. E. Muftuoglu and A. Bozkurt, *Macromolecular Chemistry and Physics*, 2014, **215**, 269-279.
7. H.-T. Pu and S. Ye, *Reactive and Functional Polymers*, 2006, **66**, 856-862.
8. N. V. Tsarevsky, K. V. Bernaerts, B. Dufour, F. E. Du Prez and K. Matyjaszewski, *Macromolecules*, 2004, **37**, 9308-9313.
9. A. D. Kshirsagar, D. G. Hundiwale, V. V. Gite and P. P. Mahulikar, *Chemistry of Heterocylic Compounds*, 2017, **53**, 1090-1093.
10. L. Bai, X. Jiang, B. Liu, W. Wang, H. Chen, Z. Xue, Y. Niu, H. Yang and D. Wei, *RSC Advances*, 2018, **8**, 28660-28667.
11. T. Jin, F. Kitahara, S. Kamijo and Y. Yamamoto, *Tetrahedron Letters*, 2008, **49**, 2824-2827.
12. P. B. Palde and T. F. Jamison, *Angewandte Chemie International Edition*, 2011, **50**, 3525-3528.

13. G. Venkateshwarlu, A. Premalatha, K. C. TRajanna and P. K. Saiprakash, *Synthetic Communications*, 2009, **39**, 4479-4485.

14. L. Lang, B. Li, W. Liu, L. Jiang, Z. Xu and G. Yin, *Chemical Communications*, 2010, **46**, 448-450.

15. A. N. Chermahini, A. Teimouri, F. Momenbeik, A. Zarei, Z. Dalirnasab, A. Ghaedi and M. Roosta, *Journal of Heterocyclic Chemistry*, 2010, **47**, 913-922.

16. S. Ü. Çelik and A. Bozkurt, *European Polymer Journal*, 2008, **44**, 213-218.

17. X. Xue, J. Yang, W. Huang, H. Yang and B. Jiang, *Reactive and Functional Polymers*, 2015, **96**, 61-70.

18. H. Yersin, A. F. Rausch, R. Czerwieniec, T. Hofbeck and T. Fischer, *Coordination Chemistry Reviews*, 2011, **255**, 2622-2652.

19. V. Fernández-Moreira, F. L. Thorp-Greenwood and M. P. Coogan, *Chemical Communications*, 2010, **46**, 186-202.

20. D. C. Grills and E. Fujita, *The Journal of Physical Chemistry Letters*, 2010, **1**, 2709-2718.

21. M. Wrighton and D. L. Morse, *Journal of the American Chemical Society*, 1974, **96**, 998-1003.

22. V. Fiorini, L. Bergamini, N. Monti, S. Zacchini, S. E. Plush, M. Massi, A. Hochkoeppler, A. Stefan and S. Stagni, *Dalton Transactions*, 2018, **47**, 9400-9410.

23. M. V. Werrett, G. S. Huff, S. Muzzioli, V. Fiorini, S. Zacchini, B. W. Skelton, A. Maggiore, J. M. Malicka, M. Cocchi, K. C. Gordon, S. Stagni and M. Massi, *Dalton Transactions*, 2015, **44**, 8379-8393.

24. A. Sorvina, C. A. Bader, C. Caporale, E. A. Carter, I. R. D. Johnson, E. J. Parkonson-Lawrence, P. V. Simpson, P. J. Wright, S. Stagni, P. A. Lay, M. Massi, D. A. Brooks and S. E. Plush, *Oncotarget*, 2018, **9**, 35541.

25. C. A. Bader, A. Sorvina, P. V. Simpson, P. J. Wright, S. Stagni, S. E. Plush, M. Massi and D. A. Brooks, *FEBS Letters*, 2016, **590**, 3051.

26. M. J. Webber, E. A. Appel, B. Vinciguerra, A. B. Cortinas, L. S. Thapa, S. Jhunjhunwala, L. Isaacs, R. Langer and D. G. Anderson, *Proceedings of the National Academy of Sciences of the United States of America*, 2016, **113**, 14189-14194.

27. H. Zhou, M. Chen, Y. Liu and S. Wu, *Macromolecular Rapid Communications*, 2018, **39**, 1800372.

28. A. M.-H. Yip and K. K.-W. Lo, *Coordination Chemistry Review*, 2018, **361**, 138-163.

29. A. J. Amoroso, M. P. Coogan, J. E. Dunne, V. Fernández-Moreira, J. B. Hess, A. J. Hayes, D. Lloyd, C. Millet, S. J. A. Pope and C. Williams, *Chemical Communications*, 2007, 3066-3068.

30. Z. Si, X. Li, X. Li and H. Zhang, *Journal of Organometallic Chemistry*, 2009, **694**, 3742-3748.

31. G. A. Crosby and J. N. Demas, *The Journal of Physical Chemistry*, 1971, **75**, 991-1024.

32. M. V. Werrett, D. Chartrand, J. D. Gale, G. S. Hanan, J. G. MacLellan, M. Massi, S. Muzzioli, P. Raiteri, B. W. Skelton, M. Silberstein and S. Stagni, *Inorganic Chemistry*, 2011, **50**, 1229-1241.

33. K. Matyjaszewski Ed., C*ontrolled/living radical polymerization: progress in ATRP, NMP, and RAFT*, American Chemical Society, Washington, DC, USA, 2000.

34. K. Koguro, T. Oga, S. Mitsui and R. Orita, *Synthesis*, 1998, **1998**, 910-914.

35. A. F. Mironov, L. D. Miroshnichenko, R. P. Evstigneeva and N. A. Preobrazhenskii, *Chemistry of Heterocylic Compounds*, 1965, **1**, 49-53.

36. D. Hadži, J. Jan and A. Ocvirk, *Spectrochimica Acta Part A: Molecular and Biomolecular*, 1969, **25**, 97-102.

37. G. Chen, J. Chen, C. Cheng, Y. Cong, P. Jian and H. Zhao, *The Journal of Chemical Thermodynamics*, 2017, **112**, 114-121.

38. Y. Wu, Y. Zhou, J. Zhu, W. Zhang, X. Pan, Z. Zhang and X. Zhu, *Polymer Chemistry*, 2014, **5**, 5546-5550.

39. M. A. Harvison, P. J. Roth, T. P. Davis and A. B. Lowe, *Australian Journal of Chemistry*, 2011, **64**, 992-1006.

40. K. Skrabania, A. Miasnikova, A. M. Bivigou-Koumba, D. Zehm and A. Laschewsky, *Polymer Chemistry*, 2011, **2**, 2074-2083.

41. R. M. Silverstein, F. X. Webster, D. J. Kiemle, Spectrometric identification of organic compounds, Seventh Edition, Wiley, USA, 2005.

42. D. A. L. Otte, D. E. Borchmann, C. Lin, M. Weck and K. A. Woerpel, *Organic Letters*, 2014, **16**, 1566-1569.

43. F. Ziaee and S. Khoshkhoo, *Iranian Polymer Journal*, 2012, **21**, 21-29.

44. K. Kalyanasundaram, *Journal of the Chemical Society, Faraday Transactions 2: Molecular and Chemical Physics*, 1986, **82**, 2401-2415.

45. C. Ulbricht, C. R. Becer, A. Winter and U. S. Schubert, *Macromolecular Rapid Communications*, 2010, **31**, 827-833.

46. V. Fiorini, A. M. Ranieri, S. Muzzioli, K. D. M. Magee, S. Zacchini, N. Akabar, A. Stefan, M. I. Ogden, M. Massi and S. Stagni, *Dalton Transactions*, 2015, **44**, 20597-20608.

47. C. A. Bader, R. D. Brooks, Y. S. Ng, A. Sorvina, M. V. Werrett, P. J. Wright, A. G. Anwer, D. A. Brooks, S. Stagni, S. Muzzioli, M. Silberstein, B. W. Skelton, E. M. Goldys, S. E. Plush, T. Shandala and M. Massi, *RSC Advances*, 2014, **4**, 16345-16351.

Chapter 3

Synthesis and photophysical investigation of poly(pentafluorophenyl acrylate) based rhenium(I)-tetrazolato functional luminescent polymers

The content of this Chapter has been published in:

E. Dallerba, M. Massi and A. B. Lowe "Tetrazole Functional Copolymers: Facile access to Well-defined Rhenium(I)-Polymeric Luminescent Materials". *Polymer*, 2020, **198**, 122522.

3.1 Abstract

Well-defined random copolymers containing tetrazole functional groups were prepared by a combination of reversible addition-fragmentation chain transfer (RAFT) radical homopolymerisation of pentafluorophenyl acrylate (PFPA), end-group modification and post-polymerisation modification of the activated ester side-groups with primary amines. PolyPFPA with a size exclusion chromatography (SEC) measured M_n of 10,800 and dispersity, $Đ$, of 1.05 was prepared with 2-cyano-2-propyl benzodithioate as the RAFT chain transfer agent (CTA) and azobisisobutyronitrile (AIBN) as the source of primary radicals in 1,4-dioxane. Prior to modification of the pentafluorophenyl (PFP) ester side-groups the thiocarbonylthio end-group was removed *via* radical-mediated desulfurisation employing two equivalents of AIBN. Complete removal of the end-group was successful as judged by UV-vis spectroscopy with no effect on the molecular weight distribution of the parent homopolymer based

on SEC analysis. The pendent PFP ester groups were subsequently modified in a sequential manner with *n*-butylamine and 5-aminotetrazole yielding the corresponding random amide species quantitatively, as judged by ^{19}F NMR and FTIR spectroscopies, and of varying molar composition as determined by ^{1}H NMR spectroscopy. The reaction of the tetrazole functional copolymers with $Re(CO)_3(phen)Br$ (phen = 1,10-phenanthroline) yielded the corresponding rhenium-polymer hybrids *via* coordination through the pendent tetrazole functional groups. Successful, and quantitative, coordination was confirmed by FTIR spectroscopy and detailed photophysical studies in dimethyl sulfoxide (DMSO). In the case of the latter, the absorption profiles of all hybrid materials possessed broad bands centred around ca. 370 nm associated with metal-to-ligand charge transfer (MLCT) transitions; excitation as this wavelength resulted in a broad emission centred at 606 nm for all hybrid species and is due to emission from the triplet MLCT excited states. Lifetime and quantum yield analysis confirmed that the different compositions in the rhenium-polymer hybrid materials did not affect their photophysical properties.

3.2 Introduction

Reversible addition-fragmentation chain transfer (RAFT) radical polymerisation is an example of a reversible deactivation radical polymerisation (RDRP) process that operates on the principle of degenerative chain transfer.[1-4] Key to RAFT is the use of certain thiocarbonylthio compounds (most commonly dithioesters or trithiocarbonates) that act as the mediating chain transfer agents (CTAs).[5-16] Since its literature disclosure in late 1998, RAFT has evolved into, arguably, the most widely applicable and versatile of the common RDRP processes.[17] One particularly important characteristic of RAFT is its impressive

functional group (FG) tolerance; today there are few FGs that cannot be incorporated into RAFT-prepared (co)polymers directly (by polymerisation of the corresponding functional monomer) or by chemical modification of an appropriate reactive precursor. However, one FG that has garnered comparatively little attention, especially in chain growth processes, is tetrazole.

Tetrazoles are five-membered heterocycles containing three pyridine-like and one pyrrole-like nitrogen atom. Although the structure is not found in naturally occurring compounds, tetrazoles have been widely studied in organic chemistry, and examples are known to have broad biological activity including antifungals, anti-cancer agents, antidiabetics, antibacterials and antioxidants.[18-20] Tetrazole functional (co)polymers are known although there are comparatively few examples of such materials. The synthesis and conventional radical polymerisation of 5-(methacrylamido) tetrazole, an acidic water-soluble material, was reported by Taden, Tait and Kraft while Sinirlioglu, Muftuoglu and Bozkurt reported the synthesis of copolymers of 5-(methacrylamido)tetrazole with vinyl tetrazole and evaluated their effectiveness as proton conducting membranes.[21,22] The same team has also prepared copolymers of 5-(methacrylamido)tetrazole with 2-acrylamido-2-methyl-1-propanesulfonic acid and vinyl phosphonic acid and evaluated the resulting membrane materials in the same application.[23,24] Çelik and Bozkurt reported the synthesis and proton-conducting properties of poly(3-((1*H*-tetrazol-5-yl)amino)-2-hydroxypropyl methacrylate) (**Figure 2-1**, **A**) prepared from poly(glycidyl methacrylate) *via* reaction of the pendant epoxy groups with 5-aminotetrazole.[25] There are reports in which tetrazole-containing monomers have been polymerised directly in a controlled fashion by RAFT. For example, Xue *et al*. reported the preparation of (*E*)-2-((4-((4-(5-chlorotetrazol-1-

yl)phenyl)diazenyl)phenyl)(methyl)amino)ethyl methacrylate (**Figure 2-1**, **B**) and its RAFT homopolymerisation and block copolymerisation with a poly(methyl methacrylate) macro-CTA to yield well-defined (co)polymers; the photoisomerisation behaviour associated with the pendant azo functional groups of these materials was examined.[26]

During the preceding two decades there have been significant efforts dedicated to the preparation and study of luminescent transition metal complexes including those based on Re(I), Ru(II) and Ir(III); the interest in such species has been driven primarily by their impressive photophysical properties.[27,28] This class of metal complex exhibits properties which are conferred by the emitting triplet metal-to-ligand charge transfer states (^{3}MLCT), making them excellent alternatives to organic fluorophores. In particular, Re(I) tricarbonyl diimine complexes, *fac*-[Re(CO)$_3$(diim)(L)]$^{0/+}$ (diim is a diimine-type chelating ligand and L is a monodentate ancillary ligand) exhibit high photostability, long luminescent lifetimes, large Stokes shifts and high quantum yields and have been examined extensively.[29,30] One important feature of these complexes is that the phosphorescence emission is promoted by spin-orbit coupling at the metal centre which favours intersystem crossing between singlet (^{1}MLCT) and triplet (^{3}MLCT) excited states. Indeed, it has been shown that it is possible to tune the photophysical properties of such complexes by modifying the diimine or the monodentate ligands.[31,32] For example, the use of tetrazolato ligands has been exploited for tailoring the luminescent properties of Re(I) complexes with fine tunability.[33]

Massi and co-workers have previously examined Re(I) tetrazolato complexes as potential bioimaging agents and have demonstrated that they can serve as cellular labels, exhibit low cytotoxicity and specificity for organelles

and can be employed as luminescent protein staining agents.[30,34-36] Nevertheless, while effective, further improvements to enhance biocompatibility, biodistribution, solubility and reduce/prevent singlet oxygen formation from excited states of triplet multiplicity are key for the future evaluation and application of such luminescent complexes in bioapplications. One approach to help address the above features involves the covalent attachment of the active Re species to a polymeric scaffold. Indeed, this is a common approach with ca. 30 metal elements, many of them transition metals, having been coordinated to polymeric scaffolds for bioapplications including drug delivery, metal-containing drugs including antivirals, antimicrobials, anticancer drugs and radiotherapy agents, as biosensors and as bioimaging agents.[18,19,37]

In the previous Chapter, we detailed the RAFT synthesis of new styrenic copolymers based on styrene and 4-cyanostyrene in which the pendent cyano groups were converted to tetrazole functional groups by reaction with sodium azide. Subsequently, we demonstrated that these tetrazole functional copolymers were able to efficiently coordinate a luminescent Re(I) species as confirmed by spectroscopic characterisation and detailed photophysical studies. While a valid approach to novel rhenium-polymer hybrid materials, this particular route suffers from two disadvantages – the high cost of the 4-cyanostyrene monomer and the comparatively harsh conditions required for tetrazole formation.

In this Chapter, we report an improved synthetic route to well-defined luminescent Re(I)-polymer hybrid materials *via* RAFT polymerisation of pentafluorophenyl acrylate followed by end-group modification and reaction of the pendent activated esters, sequentially, with *n*-butylamine and 5-aminotetrazole. This approach circumvents the above-noted drawbacks

associated with the styrenic-based copolymers and facilitates ready access to tetrazole functional copolymers of tuneable composition that can serve as macromolecular ligands for a rhenium(I) complex with luminescent properties.

3.3 Experimental

3.3.1 Materials

All reagents were purchased from the Sigma-Aldrich Chemical Company, or Alfa Aesar, at the highest available purity and used as received unless noted otherwise. $Re(CO)_3(phen)Br$, and pentafluorophenyl acrylate (PFPA) were prepared according to previously published procedures.[38,39] 2,2'-azobis(2-methylpropionitrile) (AIBN) was purchased as a 12 wt% solution in acetone. The solvent was removed on a rotary evaporator and the remaining solid dissolved in methanol from which AIBN recrystallised.

3.3.2 Size exclusion chromatography (SEC)

SEC was performed on a Shimadzu modular system consisting of a 4.0 mm × 3.0 mm Phenomenex Security Guard^{TM} cartridge guard column and two linear phenogel columns (10^3 and 10^4 Å pore size) in tetrahydrofuran (THF) operating at a flow rate of 1.0 mL/min. The system was equipped with a RID-20A refractive index and SPD-M20A prominence diode array detector. The system was calibrated with a series of narrow molecular weight distribution polystyrene standards with molecular weights ranging from 0.27 to 66 kg mol^{-1}. Data were analysed with Lab Solutions SEC software.

3.3.3 NMR Measurements

^{1}H (400 MHz) and ^{19}F (376 MHz) NMR spectra were recorded at 298 K on a Bruker Avance 400 spectrometer. Chemical shifts were referenced against residual non-deuterated solvent. Data were processed with Bruker's TopSpin 3.1 software.

3.3.4 FTIR Analysis

Infrared spectra (4000-650 cm^{-1}) were recorded on solid-state samples using attenuated total reflectance on a Perkin Elmer Spectrum Two and Spectrum 100 FT-IR.

3.3.5 Photophysical Measurements

Absorption spectra were recorded at room temperature using a Perkin Elmer Lambda 35 UV/Vis spectrometer. Uncorrected steady-state emission spectra were recorded using an Edinburgh FLSP980-stm spectrometer equipped with a 450 W xenon arc lamp and emission monochromators, a Peltier cooled Hamamatsu R928P photomultiplier (180-850 nm) and a Hamamatsu R5509-42 photomultiplier for detection of NIR radiation (800-1400 nm). Emission and excitation spectra were corrected for source intensity (amp and grating) and emission spectral response (detector and grating) by a calibration curve supplied with the instrument. Luminescent quantum yields were measured from absorption spectra on a wavelength scale (nm) and compared to the reference emitter by **Equation 3-1**:

$$\Phi_x = \Phi_r \left[\frac{A_r(\lambda_r)}{A_x(\lambda_x)}\right]\left[\frac{I_r(\lambda_r)}{I_x(\lambda_x)}\right]\left[\frac{n_x^2}{n_r^2}\right]\left[\frac{D_x}{D_r}\right] \quad \textbf{Equation 3-1}$$

where A is the absorbance at the excitation wavelength λ, I is the intensity of the excitation light at the excitation wavelength, n is the refractive index of the solvent, D is the integrated intensity of the luminescence and Φ is the quantum yield. The subscripts r and x refer to the reference and the sample. The quantum yields of complexes were measured against quinine sulphate solution in 0.5 M H_2SO_4.[40] Excited-state decays (τ) were recorded on the same Edinburgh FLSP980-stm spectrometer using pulsed picosecond light emitting diodes (LEDs) (EPLED/EPL 375 nm, FHWM < 800 ps). The goodness of fit was assessed by minimising the reduced χ^2 function and by visual inspection of the weighted residuals. The solvent used (dimethyl sulfoxide) in the preparation of the solutions for the photophysical investigations was of spectrometric grade.

3.3.6 Tissue Preparation and Staining

Tissue preparation and tissue staining was conducted by David Hartnell. Rodent brain tissue was generated from excess sham operated (10 - 12 weeks old) male Sprague Dawley rats from previously published traumatic brain injury study.[41] Animal tissue was generated with approval from Monash University Standing Committee on Ethics in Animal Experimentation. Coronal brain tissue sections (10 μm thick) containing cerebellum, were cut on a cryo-microtome (-18 °C) and transferred to glass slides, allowed to air dry and then stored at room temperature.

Tissue sections were then fixed in paraformaldehyde (4% in phosphate buffered saline (PBS)) for 10 minutes. The slides were then washed for 10 minutes with PBS. Slides were then stained with the polymeric probe containing solution (100 μg/mL in DMSO, 200 μL per tissue section) and incubated for 30 minutes at room temperature. The probe containing solution was then washed

off the slides with deionised water and then washed in PBS for 10 minutes. Slides were then further rinsed with deionised water and allowed to dry at room temperature and imaged.

3.3.7 Imaging

Fluorescence microscopy was conducted on a Nikon Ti2-U inverted microscope with a DS-Qi2 camera, pE-300^{white} LED fluorescence lamp and NIS Elements standard software. Images were gathered at an exposure time of 500 ms and an analog gain of 7.6%. Images were processed in ImageJ.

3.4 Synthesis

3.4.1 Synthesis of pentafluophenyl acrylate (PFPA)

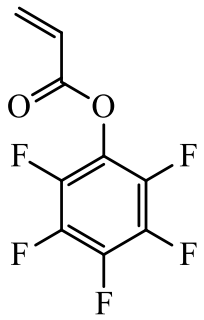

PFPA

Figure 3-1 Chemical structure of pentafluorophenyl acrylate (PFPA).

Pentafluorophenyl acrylate (PFPA) was prepared according to a previously published procedure.[38]

Pentafluorophenol (18.40 g, 100.00 mmol), triethylamine (14.6 mL, 105 mmol), and dichloromethane (500.00 mL) were mixed and cooled at 0 °C. Acryloyl chloride (8.94 mL, 110.00 mmol) was added dropwise, and the mixture was stirred and left to warm to room temperature overnight. 18.90 g of the product was obtained after washing the organic phase with water (5 x 400.00 mL), followed by silica chromatography column in petroleum spirit and drying under *vacuum*. ^{19}F NMR ($CDCl_3$) δ/ppm = -152.7 (m, F, *ortho*), -158.1 (t, 1 F, *para*), -162.5 (m, 2 F, *meta*).

3.4.2 RAFT polymerisation of PFPA (P1)

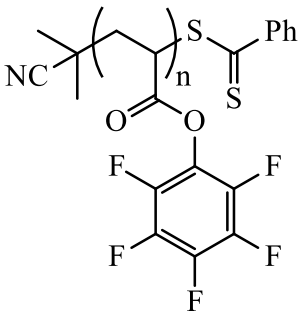

P1

Figure 3-2 Poly(pentafluorophenyl acrylate) homopolymer (polyPFPA) made by RAFT polymerisation (**P1**).

PFPA (20.00 g, 84.00 mmol), 2-cyano-2-propyl benzodithioate (CPBD, 0.22 g, 1.00 mmol) and AIBN (0.03 g, 0.20 mmol) were added to anhydrous 1,4-dioxane (20.00 mL) in a round-bottomed flask equipped with a magnetic stir bar. The flask was sealed with a rubber septum and the solution was purged with nitrogen for 30 min before being placed in a preheated oil bath set at 70°C. The homopolymerisation was allowed to proceed for 7 h and was halted by exposure to air and immersion of the reaction vessel in an ice bath. An aliquot was withdrawn, diluted with $CDCl_3$ and analysed by ^{19}F NMR spectroscopy; monomer conversion was determined to be 50% based on a comparison of the signal at δ = -157.1 ppm with the signal at δ = -158.1 ppm, associated with the signal arising from the F in *para* position of the homopolymer and the monomer, respectively. PolyPFPA was isolated as a pink powder by precipitation into a large excess of methanol and a second re-precipitation from a THF solution into an excess of methanol. The product (5.00 g) was dried under *vacuum* overnight

at 50 °C. ^{19}F NMR ($CDCl_3$) δ/ppm = -153.2 (m, F, *ortho*), -157.1 (t, 1 F, *para*), -162.4 (m, 2 F, *meta*).

3.4.3 End-group modification of polyPFPA (P2)

Radical-induced removal of the thiocarbonylthio end-group was accomplished following a previously published procedure.[42]

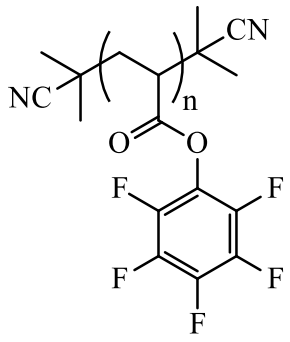

P2

Figure 3-3 Structure of end-group modified polyPFPA (**P2**).

P1 (1.00 g, 0.09 mmol) and AIBN (0.03 g, 0.18 mmol) were dissolved in anhydrous 1,4-dioxane (1.00 mL) in a round-bottomed flask equipped with a magnetic stir bar. The flask was sealed with a rubber septum and the solution was purged with nitrogen for 30 min before being placed in a preheated oil bath set at 80 °C. After 6 h the clear solution was allowed to cool to room temperature and the solvent was removed by rotary evaporation. The crude product was dissolved in 1.0 mL of dichloromethane and the product was isolated by precipitation into cold *n*-pentane. 0.85 g of product **P2** was obtained.

3.4.4 Procedure for the sequential modification of polyPFPA with primary amines (P2-12%)

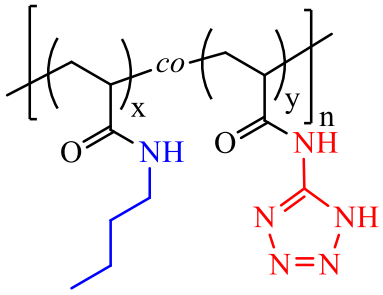

88 mol % 12 mol %

P2-12%

Figure 3-4 Post-functionalised structure of polyPFPA with primary amines (**P2-12%**).

To a round-bottomed flask equipped with a magnetic stir bar was added **P2** (0.88 g, 0.08 mmol), *n*-butylamine (0.24 g, 3.33 mmol) and dimethylformamide (DMF) (15.0 mL). The reaction mixture was left stirring overnight at room temperature. Subsequently, an excess of 5-aminotetrazole (0.11 g, 1.08 mmol) was added to the reaction mixture and the solution was left stirring overnight at room temperature. The solution was subsequently dialysed against methanol for 36 h. Methanol from the polymer solution was removed using a rotary evaporator and the product **P2-12%** was obtained as a powder (0.36 g) after drying under vacuum overnight at 50 °C. The other functionalised polymers **P2-24%**, **P2-35%** and **P2-45%** were synthesised by following the same procedure, with different ratios of amines. In the case of **P2-24%**, **P2** (1.00 g, 0.09 mmol), *n*-butylamine (0.24 g, 3.33 mmol) and 5-aminotetrazole (0.17 g, 1.66 mmol) were employed and 0.30 g of product **P2-24%** was obtained. In the

case of **P2-35%**, **P2** (1.00 g, 0.09 mmol), *n*-butylamine (0.21 g, 2.92 mmol) and 5-aminotetrazole (0.27 g, 2.20 mmol) were employed and 0.25 g of product **P2-35%** was obtained. In the case of **P2-45%**, **P2** (0.90 g, 0.08 mmol) and *n*-butylamine (0.16 g, 2.21 mmol) and 5-aminotetrazole (0.38 g, 3.70 mmol) were employed and 0.35 g of product **P2-45%** was obtained.

3.4.5 Complexation of $Re(CO)_3(phen)Br$ to a tetrazole functional copolymer

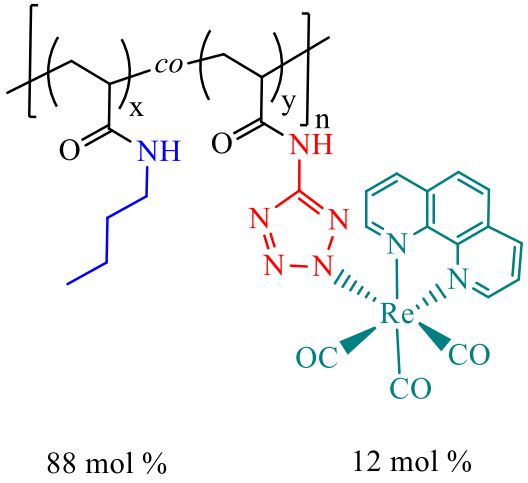

88 mol % 12 mol %

Figure 3-5 Structure of **P2-12%** reacted with rhenium precursor $Re(CO)_3(phen)Br$ to synthesise (**P2-12%-[Re]**).

To a round-bottomed flask equipped with a magnetic stir bar was added $Re(CO)_3(phen)Br$ (0.05 g, 0.09 mmol) and ethanol (10.00 mL). To a separate flask was added **P2-12%** (0.12 g, 0.02 mmol), water (3.50 mL) and triethylamine (2.00 mL). The solution containing $Re(CO)_3(phen)Br$ was then added dropwise to the polymer solution and subsequently heated under refluxing conditions for 24 h. Solvents were removed under reduced pressure and the crude product was washed with deionised water. The crude product was subsequently dissolved in dichloromethane and

precipitated in cold *n*-pentane. The product **P2-12%-[Re]** was obtained (0.10 g) as a yellow solid and dried under *vacuum* overnight at 50 °C.

The other rhenium-functionalised polymers **P2-24%-[Re]**, **P2-35%-[Re]** and **P2-45%-[Re]** were synthesised following the same procedure, with different amounts of polymer and Re precursor. In the case of **P2-24%-[Re]** $Re(CO)_3(phen)Br$ (0.03 g, 0.06 mmol) and **P2-24%** (0.03 g, 5.66 μmol) were employed and 0.02 g of product was obtained. For the synthesis of **P2-35%-[Re]** $Re(CO)_3(phen)Br$ (0.05 g, 0.09 mmol) and **P2-35%** (0.04 g, 6.93 μmol) were employed and 0.04 g of product was obtained. For the synthesis of **P2-45%-[Re]** $Re(CO)_3(phen)Br$ (0.05 g, 0.09 mmol) and **P2-45%** (0.03 g, 5.66 μmol) were employed and 0.02 g of product was obtained.

3.5 Results and Discussion

3.5.1 Polymerisation of pentafluorophenyl acrylate

The parent PFPA homopolymer (polyPFPA, target M_n of 20,000) was prepared by RAFT polymerisation employing 2-cyano-2-propyl benzodithioate (CPBD) as the RAFT CTA (**Figure 3-6**).

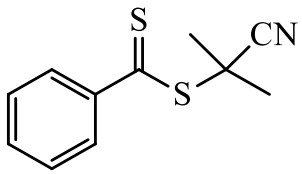

Figure 3-6 RAFT dithioester chain transfer agent 2-cyano-2-propyl benzodithioate (CPBD).

AIBN was employed as the source of primary radicals, with the homopolymerisation performed in 1,4-dioxane. The dithioester CTA was chosen for the polymerisation of pentafluorophenyl acrylate based on a previously reported synthesis.[42]

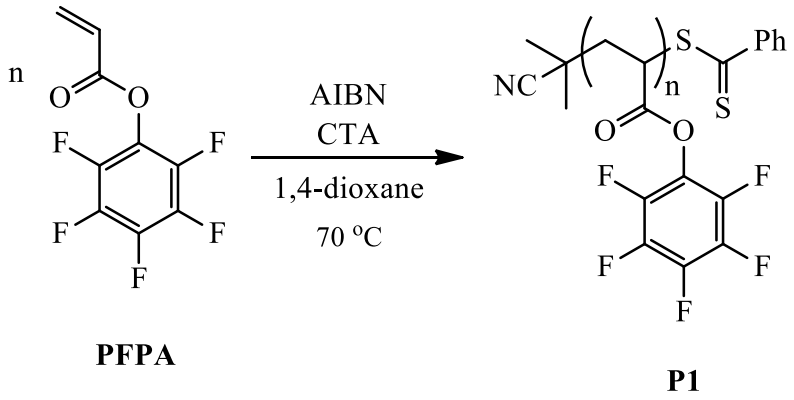

PFPA **P1**

Scheme 3-1 Homopolymerisation of pentafluorophenyl acrylate.

After polymerisation for 7 h at 70 °C, PFPA homopolymer **P1** was isolated with 50 % monomer conversion as determined by ^{19}F NMR spectroscopy with the isolated polymer having a SEC-measured M_n of 10,800 and dispersity ($Đ = M_w/ M_n$) of 1.05.

3.5.2 Dithioester end-group removal of polyPFPA (P1)

Before chemical modification of the pendent pentafluorophenyl (PFP) ester groups with primary amines, and to avoid any potential complicating side reactions associated with RAFT end-groups, the dithioester end-group of the **P1** polyPFPA homopolymer was removed *via* a radical-mediated desulfurisation reaction employing two equivalents of AIBN (**Scheme 3-2**).[43]

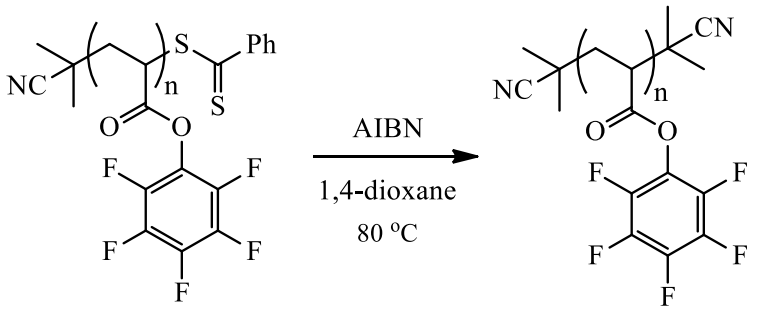

P1 **P2**

Scheme 3-2 End-group cleavage by addition-fragmentation coupling of polyPFPA to achieve complete desulfurisation, yielding **P2**.

This reaction was monitored by UV-Vis spectroscopy. **Figure 3-7** shows the UV absorption spectra of the polyPFPA homopolymer before (**P1**) and after (**P2**) treatment with AIBN. The UV absorption spectrum of **P1** is typical of RAFT-prepared (co)polymers with intact end-groups. The key feature is the broad absorption band associated with the π-π* transition of the C=S bond seen covering ca. 280-340 nm.[44]

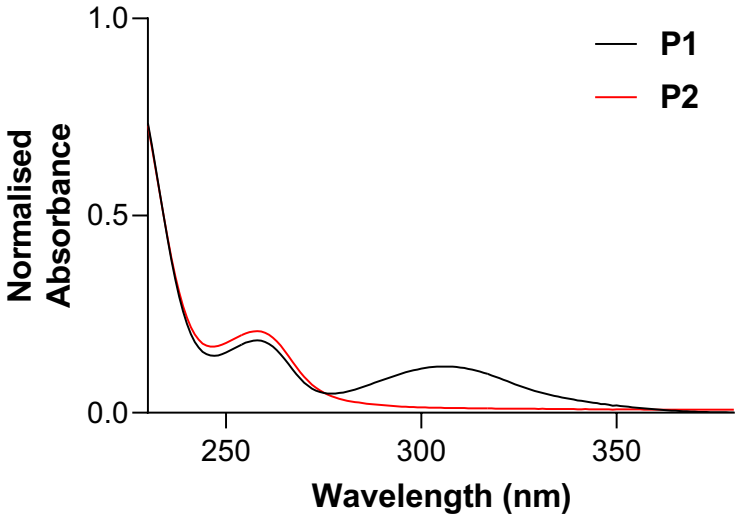

Figure 3-7 UV-Vis spectra of polyPFPA homopolymer **P1** (black) before end-group modification and the same homopolymer, **P2** after reaction with two equivalents of AIBN (red).

Following reaction with AIBN this key absorption is absent, indicating the successful end-group modification. The SEC traces of both homopolymers were also evaluated. Importantly, no effect was observed of the radical modification reaction on the molecular weight distribution, **Figure 3-8**. The SEC trace of the end-group modified polyPFPA homopolymer, **P2**, has a slightly higher elution time, as expected, with SEC measured M_n of 9,200 and $Đ$ of 1.08.

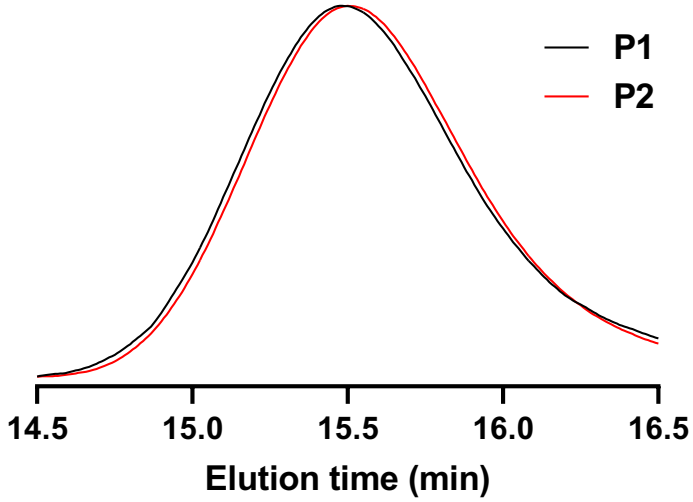

Figure 3-8 SEC traces of **P1** (black) before end-group modification and the same homopolymer, **P2** after reaction and end-group removal with AIBN (red).

3.5.3 Post-functionalisation procedure for the modification of polyPFPA with primary amines

Following end-group removal, **P2** was modified by the sequential addition of two primary amines (**Scheme 3-3**) and specifically with *n*-butyl amine ($BuNH_2$) followed by 5-aminotetrazole ($TetNH_2$) for a final target of four different copolymers with compositions of 10:90, 20:80, 30:70 and 40:60 $TetNH_2$:$BuNH_2$.

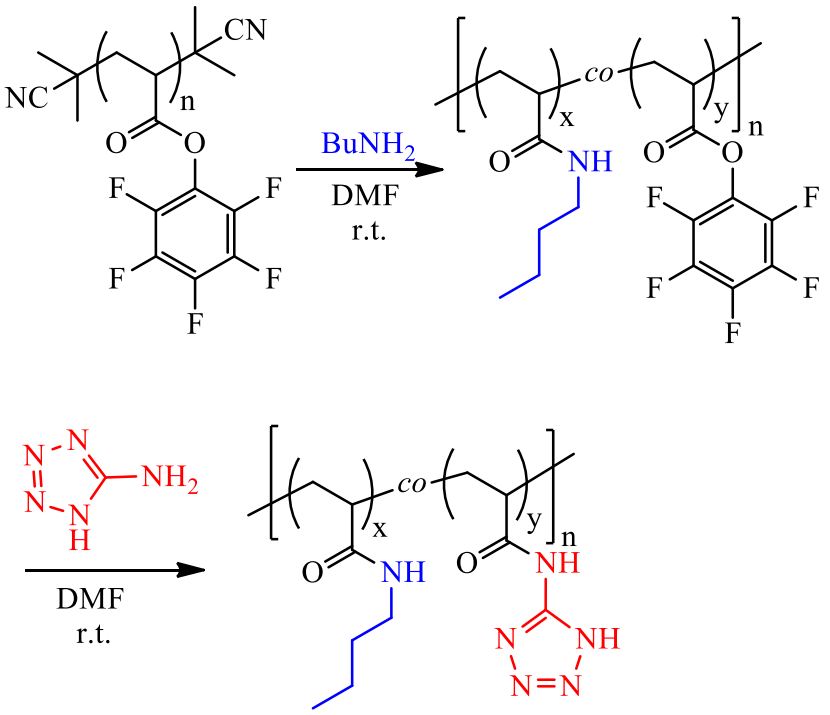

Scheme 3-3 Post-functionalisation procedure for the sequential modification of polyPFPA, **P2** with primary amines.

One advantage of employing polyPFPA as a reactive scaffold is that the key nucleophilic acyl substitution reaction of primary amines with the PFP ester groups is readily monitored by ^{19}F NMR spectroscopy. As a representative example, **Figure 3-9** shows a series of ^{19}F NMR spectra obtained before, during and after reaction with $BuNH_2$ and $TetNH_2$ for a final target composition of 40:60.

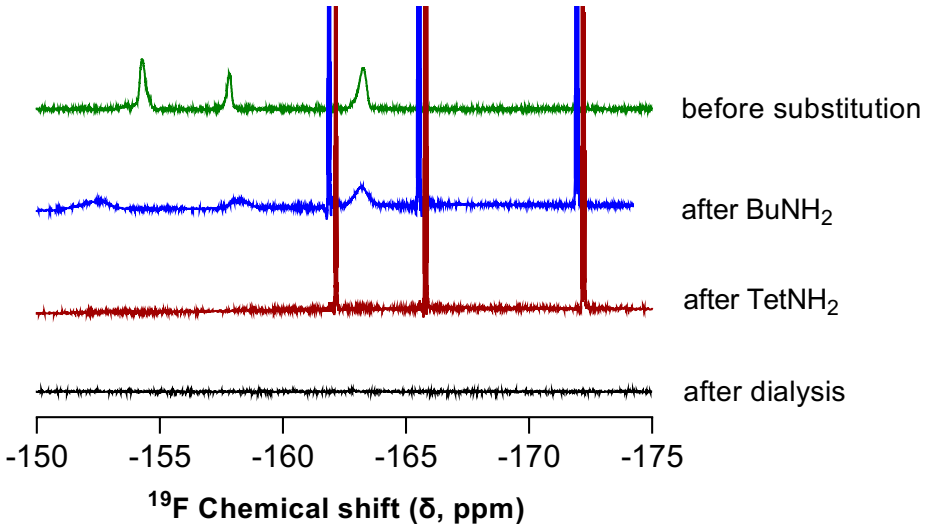

Figure 3-9 ^{19}F NMR spectra, recorded in d_6-DMSO, of the sequential, post-polymerisation modification of **P2** to **P2-45%** *via* reaction with *n*-butylamine and 5-aminotetrazole.

Prior to chemical modification, **P2** (green spectrum) shows the three characteristic signals at δ (ppm) = -152.7 (2 F, *ortho*), -158.1 (1 F, *para*) and -162.5 (2 F, *meta*) consistent with previously reported ^{19}F chemical shifts for polyPFPA.[38] Following treatment with $BuNH_2$ (blue spectrum) these signals decrease in intensity with the concomitant appearance of three sharp resonances associated with pentafluorophenol – the small molecule by-product. The three characteristic signals of pentafluorophenol at δ (ppm) = -162.1 (2 F, *ortho*), -165.5 (2 F, *meta*) and -172.0 (1 F, *para*) can be seen in Figure 3-9, blue and red spectra. After subsequent reaction with $TetNH_2$ (red spectrum), we observed the total disappearance of the signals attributed to polymer associated pendent PFP functional groups with only those of pentafluorophenol being detected; this confirms successful and quantitative conversion of the pendent PFP groups to the corresponding amide species. Finally, after purification by dialysis (black

spectrum), we observed no detectable signals indicating the successful removal of pentafluorophenol from the modified polymer.

Successful modification of **P2** can also be qualitatively monitored by FTIR spectroscopy. **Figures 3-10**, **3-11**, **3-12** and **3-13** show the FTIR spectra of the polyPFPA precursor **P2** (top), the modified polymers **P2-x%** at the bottom of the figures. The FTIR results are consistent for all the materials with different compositions. The spectrum of the parent **P2** polyPFPA homopolymer shows the characteristic C=O stretch associated with an activated ester at 1780 cm^{-1} (red dotted line), confirming the presence of the PFP moieties in the parent homopolymer. Following sequential modification with $BuNH_2$ and $TetNH_2$ (**P2-x%**) the distinguishing ester band completely disappears while simultaneously we observed the appearance of a new C=O stretch at 1640 cm^{-1} (green line) associated with the carbonyl of an amide species as well as a broad peak at 3300 cm^{-1} associated with N-H stretching, collectively confirming successful, and quantitative, side-chain modification.

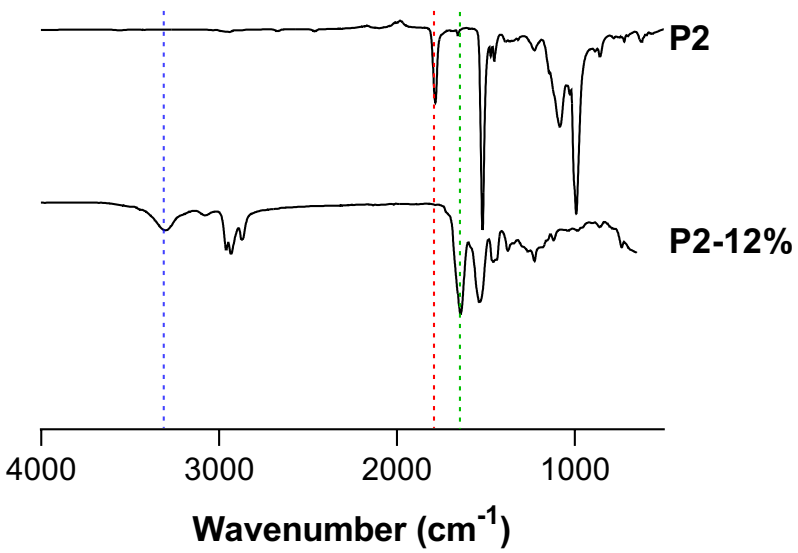

Figure 3-10 FTIR spectra of the polyPFPA precursor **P2** (top), the modified polymer, **P2-12%** (middle), containing 86 mol% butyl acrylamide and 12 mol% *N*-(1*H*-tetrazol-5-yl)acrylamide repeat units.

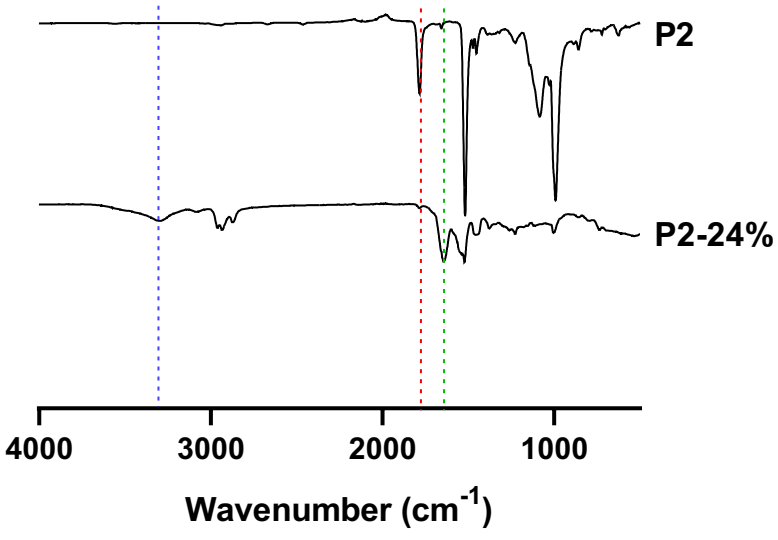

Figure 3-11 FTIR spectra of the polyPFPA precursor **P2** (top), the modified polymer, **P2-24%** (middle), containing 24 mol% butyl acrylamide and 76 mol% *N*-(1*H*-tetrazol-5-yl)acrylamide repeat units.

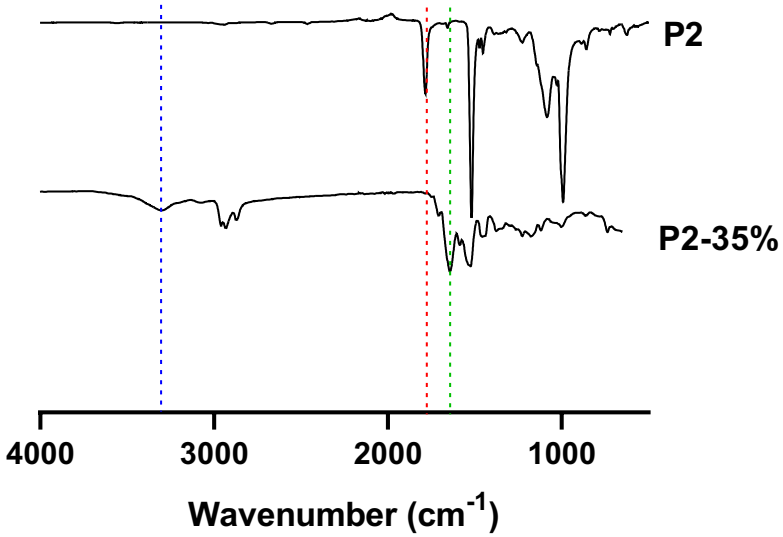

Figure 3-12 FTIR spectra of the polyPFPA precursor **P2** (top), the modified polymer, **P2-35%** (middle), containing 65 mol% butyl acrylamide and 35 mol% *N*-(1*H*-tetrazol-5-yl)acrylamide repeat units.

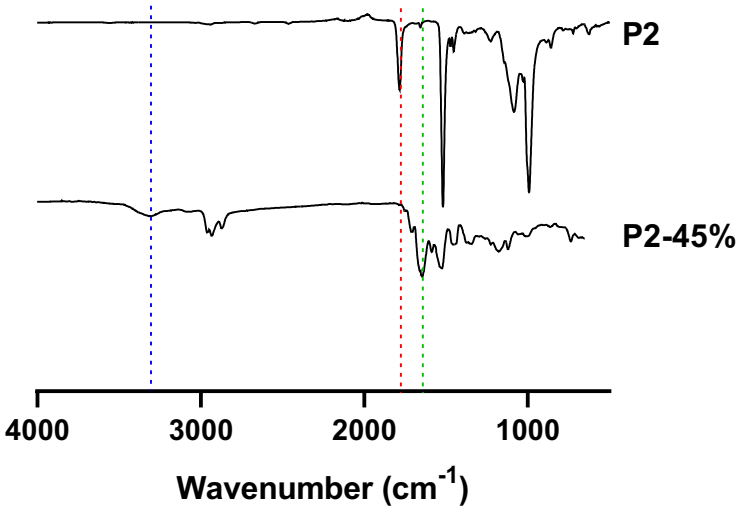

Figure 3-13 FTIR spectra of the polyPFPA precursor **P2** (top), the modified polymer, **P2-45%** (middle), containing 55 mol% butyl acrylamide and 45 mol% *N*-(1*H*-tetrazol-5-yl)acrylamide repeat units.

Further confirmation of successful side-group modification, and copolymer composition, was achieved by ^{1}H NMR spectroscopy (**Figure 3-14)**. The final copolymer compositions of the four random copolymers were determined by a comparison of the integrals of signal *c* originating from the methyl group of the butylamide side chains and signal *b*+*b'* associated with the methine backbone species. In all instances, the calculated copolymer compositions were consistent with the targeted values; theory ($BuNH_2$:$TetNH_2$): 10:90, 20:80, 30:70, 40:60 and found: 12:88 (**P2-12%**), 24:76 (**P2-24%**), 35:65 (**P2-35%**) and 45:55 (**P2-45%**).

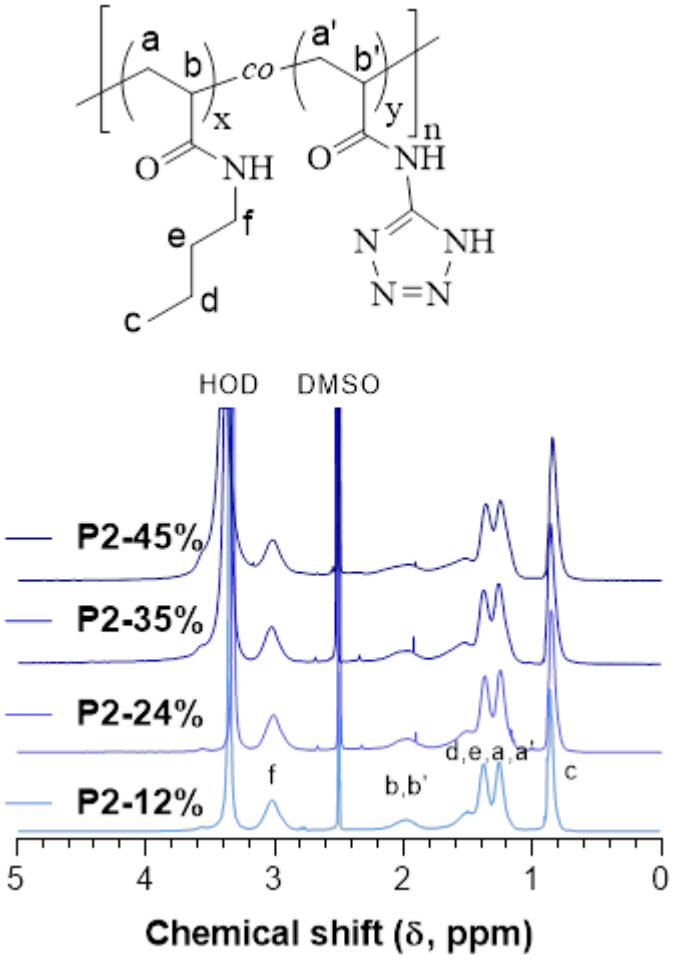

Figure 3-14 ^{1}H NMR spectra, recorded in d_6-DMSO, of the **P2-x%** copolymers (x = 12, 24, 35, 45) with peak assignments.

3.5.4 Synthesis of hybrid polymeric-rhenium(I) luminescent materials

Following successful modification of the parent **P2** homopolymer to give a series of four amide-based random copolymers containing butyl and tetrazole functional side groups, each copolymer was further modified by reaction with $Re(CO)_3(phen)Br$ (**Scheme 3-4**); such reactions yielded the target polymer-Re(I) hybrids *via* coordination through the tetrazole functional groups. The complexation reaction was conducted in ethanol/water 3:1 (v/v). After heating at reflux overnight, the desired polymer-metal hybrid material was obtained by precipitation in cold *n*-pentane, yielding a yellow powder.

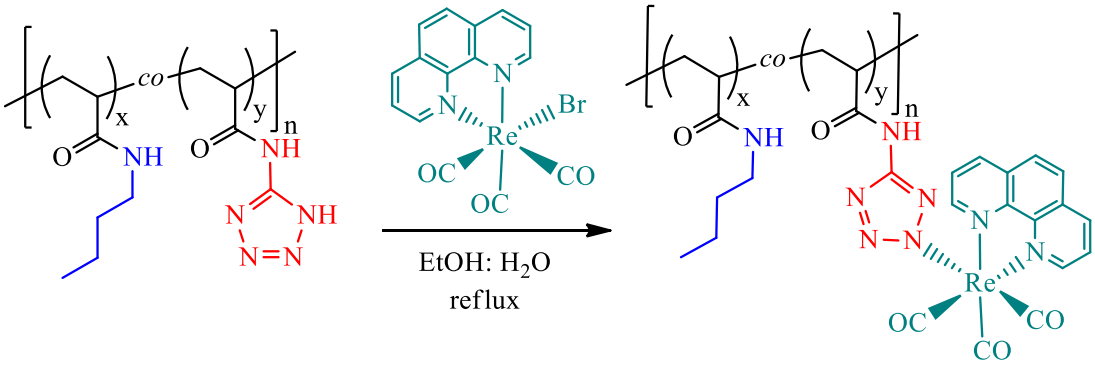

Scheme 3-4 Complexation reaction of **P2-x%** with rhenium precursor $Re(CO)_3(phen)Br$ to synthesise **P2-x%-[Re]**. Coordination to nitrogen atom N2 on the tetrazole is shown for convenience.

Successful coordination was confirmed by FTIR spectroscopy (**Figure 3-15**). For all modified materials **P2-x%-[Re]** we observed the appearance of two new bands at around 2025 and 1915 cm^{-1} associated with the stretch of the carbonyl ligands on the coordinated Re complex (light blue area). Compared to the $Re(CO)_3(phen)Br$ precursor (**Figure 3-16**) these bands are shifted as a result of the decrease in the electron density at the Re(I) metal centre upon exchange

between the bromo and tetrazolato ancillary ligand.[33] This observation further confirms the successful coordination of the luminescent Re species to the polymeric scaffold.

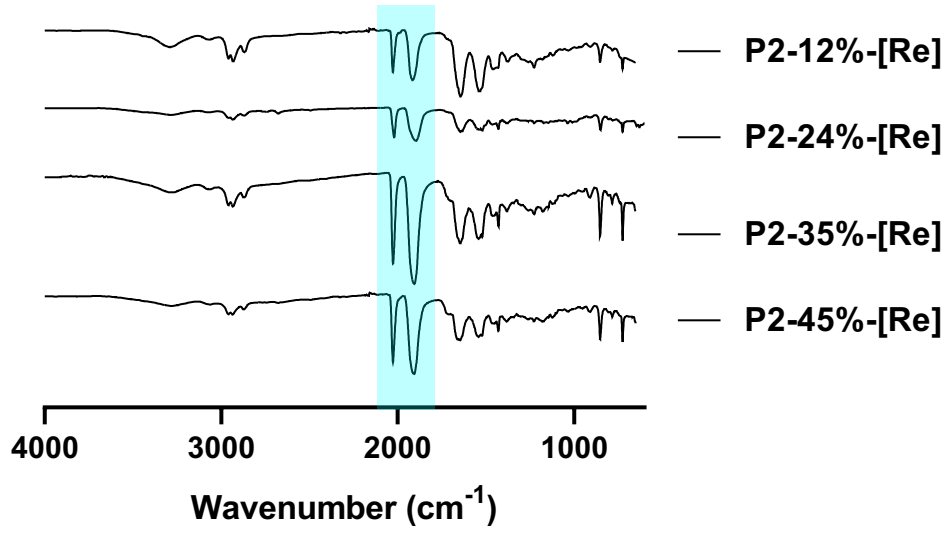

Figure 3-15 FTIR spectra of four polymeric-Re(I) species.

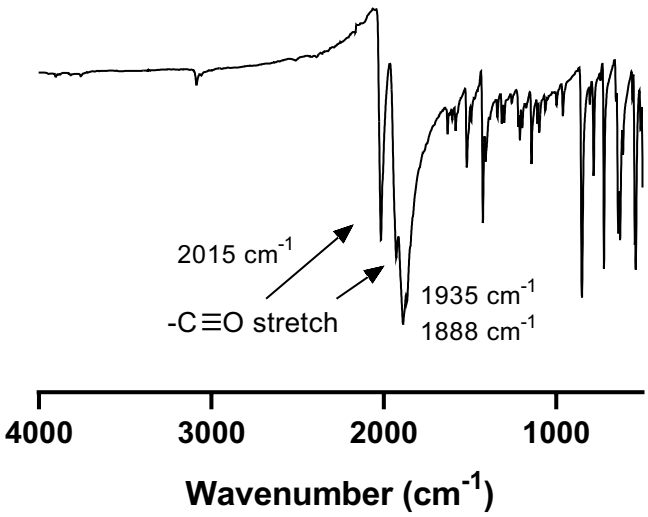

Figure 3-16 FTIR spectrum of precursor $Re(CO)_3(phen)Br$.

3.5.5 Photophysical studies of hybrid polymeric-rhenium(I) luminescent materials

Having synthesised the target Re(I)-copolymer hybrid materials, we subsequently performed detailed photophysical studies, **Table 3-1**. The samples for photophysical studies were prepared by dissolving 1 mg of polymeric-rhenium material in 10 mL of spectroscopic grade dimethyl sulfoxide (DMSO). The absorption profiles of all four Re(I)-polymer hybrid materials were essentially identical, exhibiting a UV region dominated by intense broad bands at $\lambda_{abs} < 300$ nm arising from π–π^* transitions associated with the main polymer scaffold and overlapping with π–π* ligand-centred (LC) transitions of the phenanthroline ligands bound to the Re metal centres, **Figure 3-17**.

Table 3-1 Summary of photophysical data for polymer-rhenium materials, **P2-x%-[Re]** in dilute DMSO.

Polymer	λ_{abs} [nm]	λ_{em} [nm]	τ^a [ns]	τ^b [ns]	Φ^a [%]	Φ^b [%]	k_r^b [10^6 s^{-1}]	k_{nr}^b [10^6 s^{-1}]
P2-12%-[Re]	268 370	606	167	266	0.017	0.026	0.10	3.66
P2-24%-[Re]	268 370	606	165	289	0.016	0.020	0.08	3.38
P2-35%-[Re]	268 370	606	167	270	0.022	0.032	0.12	3.58
P2-45%-[Re]	268 370	606	160	259	0.019	0.031	0.12	3.74

[a] Measured from air-equilibrated solutions. [b] Measured from degassed solutions. Where τ = lifetime; Φ = luminescent quantum yield; k_r = radiative constant; k_{nr} = non-radiative constant.

The UV region at wavelengths longer than 350 nm is dominated by broad bands of lower intensity attributed to metal-to-ligand charge transfer transitions typical of Re diimine tetrazolato complexes.

Upon excitation at 370 nm, near-identical broad emission bands centred at ca. 606 nm were observed for all four hybrid materials, **Figure 3-18**. These bands arise from emission from ^{3}MLCT excited states and are consistent with previously reported tetrazolato-Re(I) complexes.[33]

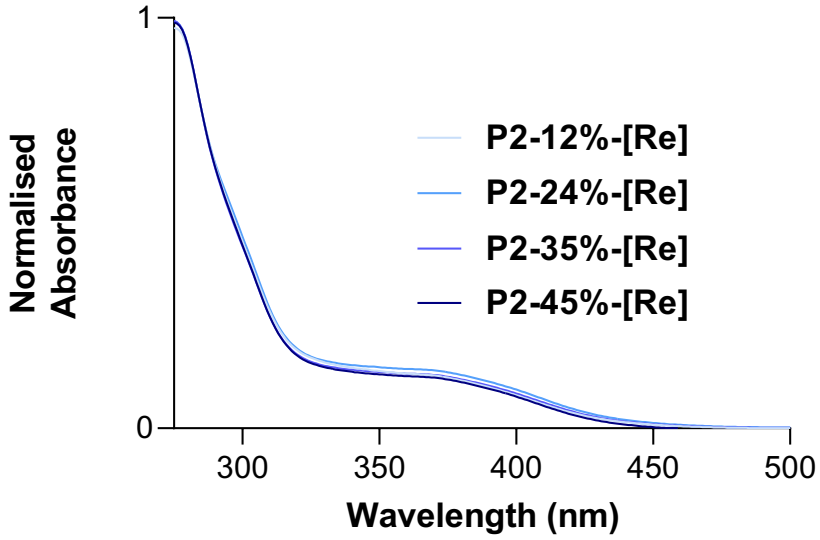

Figure 3-17 Normalised absorption profiles of the **P2-x%** copolymers (x = 12, 24, 35, 45) measured in DMSO by dissolving 1 mg of Re-hybrid material in 10 ml of the solvent.

The triplet spin multiplicity is in agreement with the relatively long excited-state lifetime decays measured to be within the range 160-167 ns. These values increased to 259-289 ns upon degassing. For all four Re(I)-hybrid species the excited state lifetime (τ) and quantum yield (Φ) increased from air-equilibrated to degassed

solutions. This behaviour is due to the phosphorescent nature of the emission from the ^{3}MLCT state and its sensitivity to quenching due to the presence of $^3O_2$.[45]

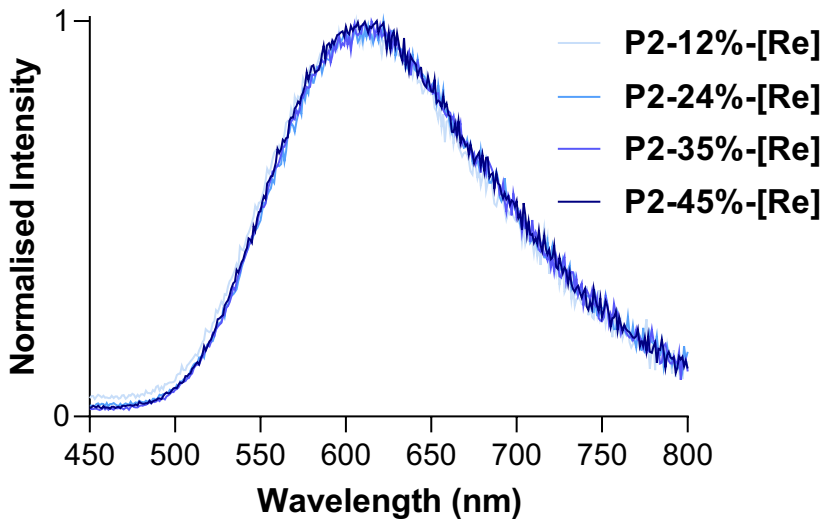

Figure 3-18 Normalised emission profiles of the four polymeric-Re(I) hybrid materials in air-equilibrated, dilute DMSO.

From the values of Φ (which are within the range typical of this kind of neutral Re complex) the radiative [$k_r = \Phi \cdot \tau^{-1}$] and non-radiative [$k_{nr} = (1-\Phi) \cdot \tau^{-1}$] decay constants were determined, **Table 3-1**. The values of k_r and k_{nr} are consistent for all samples. Significantly, the consistency of k_r and k_{nr}, combined with the identical emission profiles of all four species, suggest that the distribution and quantity of coordinated Re(I) species has no effect on the photophysical properties of the luminescent metal complex. From the excitation spectra (**Figure 3-19**) we observed that the range of excitation profiles matches the absorption profiles, as expected.

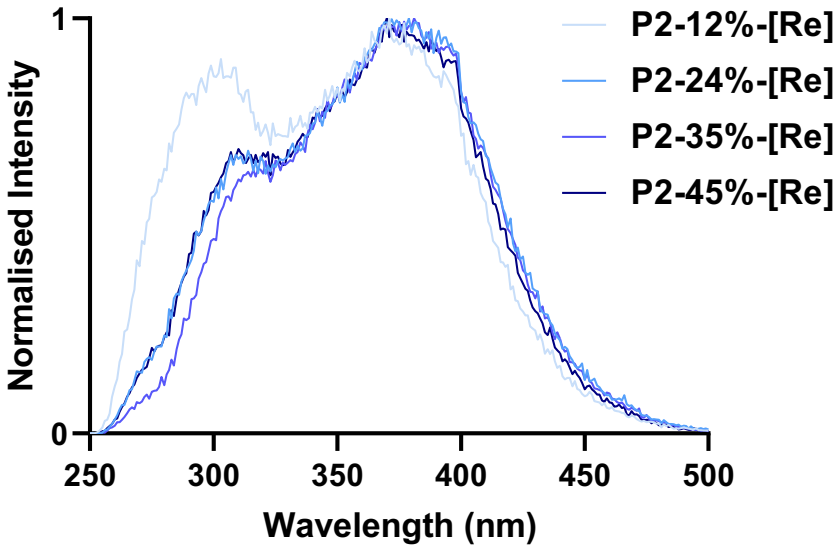

Figure 3-19 Normalised excitation profiles of **P2-12%-[Re]**, **P2-24%-[Re]**, **P2-35%-[Re]** and **P2-45%-[Re]** in dilute DMSO, air-equilibrated samples.

The emission profiles of the polymeric Re(I) hybrid materials were directly compared with the emission bands of the small molecule Re(phen)$(CO)_3$Br precursor species, **Figure 3-20**.

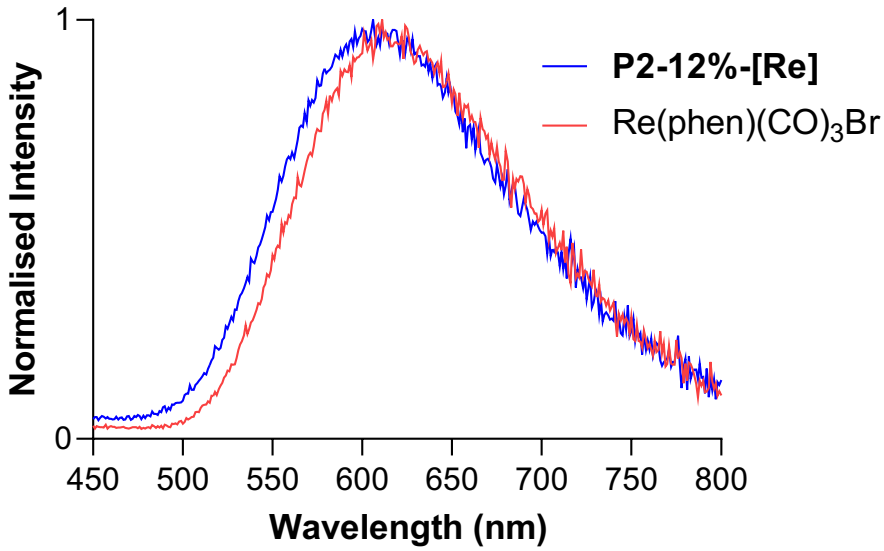

Figure 3-20 Normalised emission profiles of **P2-12%-[Re]** (blue) and $Re(phen)(CO)_3Br$ (red) in dilute DMSO, air-equilibrated solutions.

In the case of **P2-12%-[Re]** (shown as a representative example in **Figure 3-20**) the emission profile confirms that it originates from a rhenium diimine tetrazolato species and also confirms the successful coordination of the Re(I) species to the polymer. The more π acidic nature of the tetrazolato ligand versus Br manifests as a slight blue shift of the emission maximum compared to the precursor bromo complex.[30, 34, 46] Lifetime plots are shown in **Figure 3-21** and **Figure 3-21** to confirm monoexponential decay of all Re-polymer hybrid species.

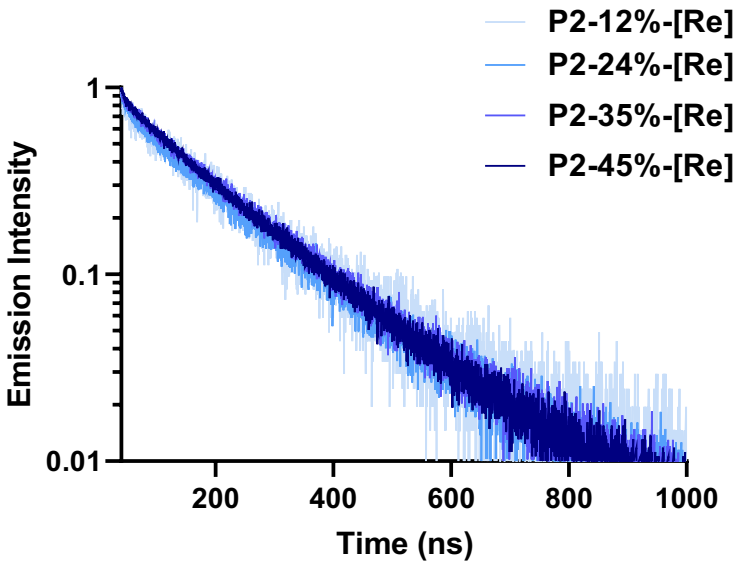

Figure 3-21 Normalised TCSPS decay of ^{3}MLCT emission of air equilibrated solutions of **P2-12%-[Re]**, **P2-24%-[Re]**, **P2-35%-[Re]** and **P2-45%-[Re]** in dilute DMSO under excitation at 375 nm.

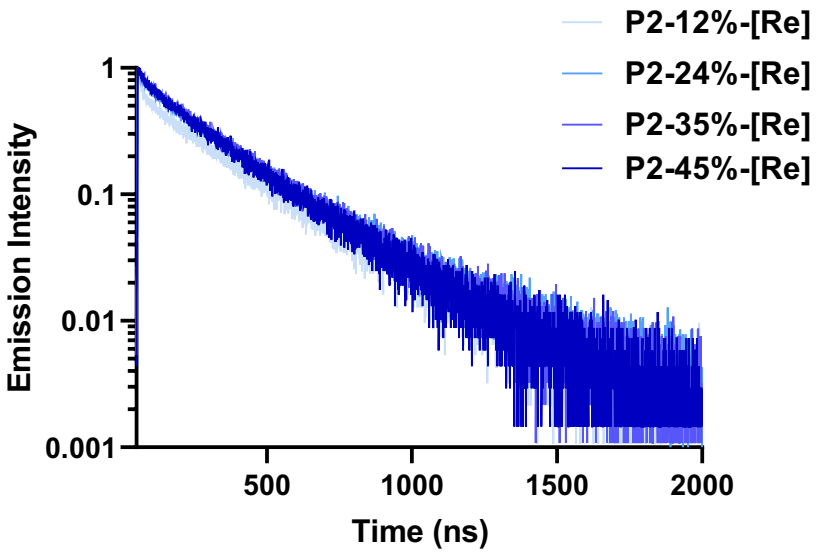

Figure 3-22 Normalised TCSPS decay of ^{3}MLCT emission of solutions of **P2-12%-[Re]**, **P2-24%-[Re]**, **P2-35%-[Re]** and **P2-45%-[Re]** in dilute DMSO (top) and degassed solutions under excitation at 375 nm.

3.5.6 Rodent brain tissues staining

Finally, we wanted to evaluate the ability of the materials to act as probes in the staining of biological tissues. The desired goal was to assess whether the materials described in this Chapter would be suitable probes for the staining of tissues, in particular of lipidic rich tissues. Lipids play an essential role in a wide range of biological functions, such as modulating cell membranes structure and regulating inflammatory signalling roles.[47,48] An organ that is known to be lipidic rich is the brain.[49] The limited understanding of the role of lipids and their metabolism and functions is the driving force for the development of new probes, which has resulted in a research effort from Massi's and Hackett's groups. While polymeric materials with metal complexes have been employed in biological applications, for example polymers containing Gd^{3+} used in Magnetic Resonance Imaging (MRI) or poly(ethylene glycol) (PEG) appended transition metals used as cellular reagents for imaging and sensing, the novelty of our approach is in the use of luminescent polymers containing metal complexes for the targeting of brain lipids, which, to the best of our knowledge, has never been investigated before.[50,51]

In collaboration with Hackett's group, we herein report the preliminary assessment of the luminescent rhenium materials described in this Chapter in lipidic rich tissues. In particular, the four final Re-hybrid materials were utilised as probes for the staining of rodent brain tissues (**Figure 3-23** and **Figure 3-24**). The images suggested uptake of the probes into brain tissues and non-specific binding of the Re(I) polymeric luminescent probes in the staining of the tissues was observed. From the preliminary results, it was demonstrated that the polymeric luminescent materials are capable to act as probes for imaging biological tissues and their ability to stain brain tissues.

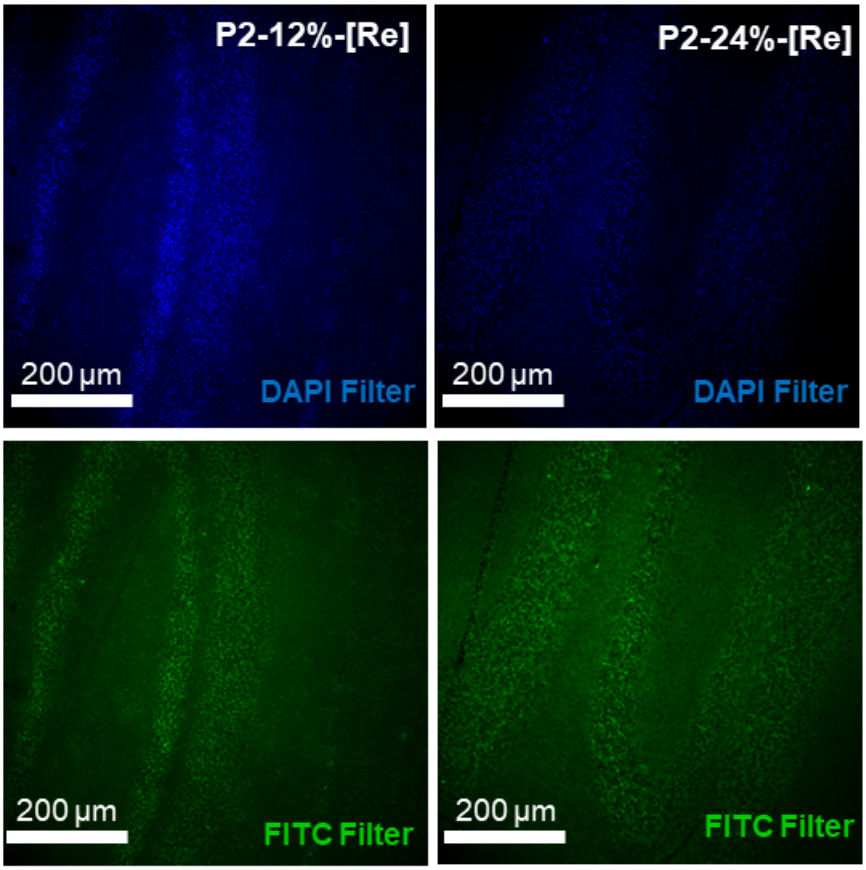

Figure 3-23 Images of rodent brain tissues by employing the **P2-12%-[Re]** and **P2-24%-[Re]** materials containing Re(I) as luminescent probes.

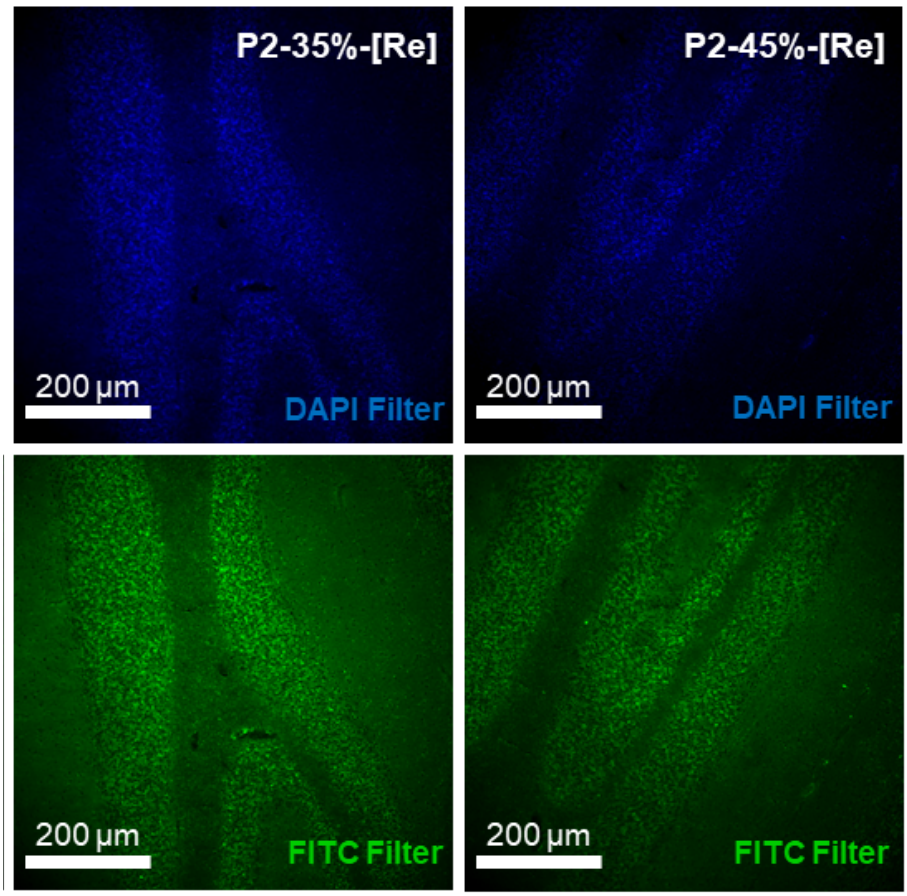

Figure 3-24 Images of rodent brain tissues by employing the materials **P2-35%-[Re]** and **P2-45%-[Re]** containing Re(I) as luminescent probes.

3.6 Conclusions

In this Chapter, the RAFT synthesis of well-defined, acrylamido-based copolymers containing tetrazolato functional groups was detailed. It was demonstrated that such materials can serve as efficient macromolecular ligands for rhenium(I) tricarbonyl diimine luminescent complexes *via* direct coordination to the pendent tetrazolato species. The synthetic approach to such materials, exploiting the facile reaction between pentafluorophenyl esters and primary amines, is significantly more facile than the conventional approach for introducing tetrazole functionality involving the 1,3-dipolar cycloaddition

reaction between nitrile functional groups and an azide source, as detailed in Chapter 2. Coordination of the four materials with a luminescent rhenium(I) species was successfully accomplished by the reaction of the tetrazole-functional copolymers with $Re(CO)_3(phen)Br$, and confirmed by FTIR spectroscopy. The absorption and emission profiles of the rhenium-polymer hybrid materials supported successful metal coordination and the luminescent properties of the rhenium species were not affected by direct coordination to a polymeric scaffold. The final Re-hybrid materials have been employed as probes for the staining of rodent brain tissues. The results suggest probe uptake into tissues with non-specific binding of the polymeric probes in the staining of tissues.

3.7 References

1. G. Moad, E. Rizzardo and S. H. Thang, *Australian Journal of Chemistry*, 2005, **58**, 379-410.
2. G. Moad, E. Rizzardo and S. H. Thang, *Australian Journal of Chemistry*, 2006, **59**, 669-692.
3. G. Moad, E. Rizzardo and S. H. Thang, *Australian Journal of Chemistry*, 2009, **62**, 1402-1472.
4. G. Moad, E. Rizzardo and S. H. Thang, *Australian Journal of Chemistry*, 2012, **65**, 985-1076.
5. R. T. A. Mayadunne, E. Rizzardo, J. Chiefari, Y. K. Chong, G. Moad and S. H. Thang, *Macromolecules*, 1999, **32**, 6977-6980.
6. S. Perrier, P. Takolpuckdee, J. Westwood and D. M. Lewis, *Macromolecules*, 2004, **37**, 2709-2717.
7. C. Schilli, M. G. Lanzendörfer and A. H. E. Müller, *Macromolecules*, 2002, **35**, 6819-6827.
8. M. S. Donovan, A. B. Lowe, B. S. Sumerlin and C. L. McCormick, *Macromolecules*, 2002, **35**, 4123-4132.
9. R. T. A. Mayadunne, E. Rizzardo, J. Chiefari, J. Krstina, G. Moad, A. Postma and S. H. Thang, *Macromolecules*, 2000, **33**, 243-245.
10. Y. K. Chong, J. Krstina, T. P. T. Le, G. Moad, A. Postma, E. Rizzardo and S. H. Thang, *Macromolecules*, 2003, **36**, 2256-2272.
11. G. Moad, E. Rizzardo and S. H. Thang, *Polymer International*, 2011, **60**, 9-25.
12. J. Liu, C.-Y. Hong and C.-Y. Pan, *Polymer*, 2004, **45**, 4413-4421.
13. J. Chiefari, R. T. A. Mayadunne, C. L. Moad, G. Moad, E. Rizzardo, A. Postma and S. H. Thang, *Macromolecules*, 2003, **36**, 2273-2283.

14. M. Destarac, D. Charmot, X. Franck and S. Z. Zard, *Macromolecular Rapid Communications*, 2000, **21**, 1035-1039.

15. R. Wang, C. L. McCormick and A. B. Lowe, *Macromolecules*, 2005, **38**, 9518-9525.

16. Y. A. Vasilieva, C. W. Scales, D. B. Thomas, R. G. Ezell, A. B. Lowe, N. Ayres and C. L. McCormick, *Journal of Polymer Science Part A: Polymer Chemistry*, 2005, **43**, 3141-3152.

17. J. Chiefari, Y. K. Chong, F. Ercole, J. Krstina, T. P. T. Le, R. T. A. Mayadunne, G. F. Meijs, C. L. Moad, G. Moad, E. Rizzardo and S. H. Thang, *Macromolecules*, 1998, **31**, 5559-5562.

18. Y. Yan, J. Zhang, L. Ren and C. Tang, *Chemical Society Reviews*, 2016, **45**, 5232-5263.

19. Y. Wang, D. Astruc and A. S. Abd-El-Aziz, *Chemical Society Reviews*, 2019, **48**, 558-636.

20. A. M.-H. Yip and K. K.-W. Lo, *Coordination Chemistry Reviews*, 2018, **361**, 138-163.

21. A. Taden, A. H. Tait and A. Kraft, *Journal of Polymer Science Part A: Polymer Chemistry*, 2002, **40**, 4333-4343.

22. D. Sinirlioglu, A. E. Muftuoglu and A. Bozkurt, *Journal of Polymer Research*, 2013, **20**, 242.

23. D. Sinirlioglu, A. E. Muftuoglu and A. Bozkurt, *Journal of Macromolecular Science*, 2014, **51**, 420-434.

24. D. Sinirlioglu, S. Ü. Çelik, A. E. Muftuoglu and A. Bozkurt, *Polymer Engineering and Science*, 2015, **55**, 260-269.

25. S. Ü. Çelik and A. Bozkurt, *European Polymer Journal*, 2008, **44**, 213-218.

26. X. Xue, J. Yang, W. Huang, H. Yang and B. Jiang, *Reactive and Functional Polymer*, 2015, **96**, 61-70.

27. V. Fernández-Moreira, F. L. Thorp-Greenwood and M. P. Coogan, *Chemical Communications*, 2010, **46**, 186-202.

28. K. K.-W. Lo, T. K.-M. Lee, J. S.-Y. Lau, W.-L. Poon and S.-H. Cheng, *Inorganic Chemistry*, 2008, **47**, 200-208.

29. R. G. Balasingham, F. L. Thorp-Greenwood, C. F. Williams, M. P. Coogan and S. J. A. Pope, *Inorganic Chemistry*, 2012, **51**, 1419-1426.

30. C. A. Bader, R. D. Brooks, Y. S. Ng, A. Sorvina, M. V. Werrett, P. J. Wright, A. G. Anwer, D. A. Brooks, S. Stagni, S. Muzzioli, M. Silberstein, B. W. Skelton, E. M. Goldys, S. E. Plush, T. Shandala and M. Massi, *RSC Advances*, 2014, **4**, 16345-16351.

31. M. V. Werrett, G. S. Huff, S. Muzzioli, V. Fiorini, S. Zacchini, B. W. Skelton, A. Maggiore, J. M. Malicka, M. Cocchi, K. C. Gordon, S. Stagni and M. Massi, *Dalton Transactions*, 2015, **44**, 8379-8393.

32. S. Stagni, S. Colella, A. Palazzi, G. Valenti, S. Zacchini, F. Paolucci, M. Marcaccio, R. Q. Albuquerque and L. De Cola, *Inorganic Chemistry*, 2008, **47**, 10509-10521.

33. M. V. Werrett, D. Chartrand, J. D. Gale, G. S. Hanan, J. G. MacLellan, M. Massi, S. Muzzioli, P. Raiteri, B. W. Skelton, M. Silberstein and S. Stagni, *Inorganic Chemistry*, 2011, **50**, 1229-1241.

34. V. Fiorini, L. Bergamini, N. Monti, S. Zacchini, S. E. Plush, M. Massi, A. Hochkoeppler, A. Stefan and S. Stagni, *Dalton Transactions*, 2018, **47**, 9400-9410.

35. A. Sorvina, C. A. Bader, C. Caporale, E. A. Carter, I. R. D. Johnson, E. J. Parkinson-Lawrence, P. V. Simpson, P. J. Wright, S. Stagni, P. A. Lay, M. Massi, D. A. Brooks and S. E. Plush, *Oncotarget*, 2018, **9**, 35541-35552.

36. C. A. Bader, A. Sorvina, P. V. Simpson, P. J. Wright, S. Stagni, S. E. Plush, M. Massi and D. A. Brooks, *FEBS Letts.*, 2016, **590**, 3051-3060.

37. A. M.-H. Yip and K. K.-W. Lo, *Coordination Chemistry Review*, 2018, **361**, 138-163.

38. P. A. Woodfield, Y. Zhu, Y. Pei and P. J. Roth, *Macromolecules*, 2014, **47**, 750-762.

39. Z. Si, X. Li, X. Li and H. Zhang, *Journal of Organometallic Chemistry*, 2009, **694**, 3742-3748.

40. G. A. Crosby and J. N. Demas, *Journal of Physical Chemistry*, 1971, **75**, 991-1024.

41. D. Hartnell, K. Gillespie-Jones, C. Ciornei, A. Hollings, A. Thomas, E. Harrild, J. Reinhardt, D. J. Paterson, D. Alwis, R. Rajan and M. J. Hackett, *ACS Chemical Neuroscience*, 2020, **11**, 248-257.

42. G. M. ter Huurne, L. N. J. de Windt, Y. Liu, E. W. Meijer, I. K. Voets and A. R. A. Palmans, *Macromolecules*, 2017, **50**, 8562-8569.

43. H. Willcock and R. K. O'Reilly, *Polymer Chemistry*, 2010, **1**, 149-157.

44. T. G. McKenzie, L. P. d. M. Costa, Q. Fu, D. E. Dunstan and G. G. Qiao, *Polymer Chemistry*, 2016, **7**, 4246-4253.

45. L. A. Casson, S. Muzzioli, P. Raiteri, B. W. Skelton, S. Stagni, M. Massi and D. H. Brown, *Dalton Transactions*, 2011, **40**, 11960-11967.

46. V. Fiorini, A. M. Ranieri, S. Muzzioli, K. D. M. Magee, S. Zacchini, N. Akabar, A. Stefan, M. I. Ogden, M. Massi and S. Stagni, *Dalton Transactions*, 2015, **44**, 20597-20608.

47. R. M. Adibhatla and J. F. Hatcher, *Antioxidants & Redox Signaling*, 2010, **12**, 125-169.

48. J. M. Dietschy and S. D. Turley, *Journal of Lipid Research*, 2004, **45**, 1375-1397.

49. J. S. O'Brien & E. L. Sampson, *Journal of Lipid Research*, 1965, **6**, 537-544.

50. D. L. Ladd, R. Hollister, X. Peng, D. Wei, C. Wu, D. Delecki, R. A. Snow, J. L. Toner, K. Kellar, J. Eck, V. C. Desai, G. Raymond, L. B. Kinter, T. S. Desser M. D. and D. L. Rubin M. D., *Bioconjugate Chemistry*, 1999, **10**, 361-370.

51. A. M-H. Yip & K. K-W. Lo, *Coordination Chemistry Reviews*, 2018, **361**, 138-163.

Chapter 4

Synthesis and photophysical investigation of PEG-PFP block copolymers functionalised with luminescent rhenium(I) species

4.1 Abstract

Well-defined block copolymers of poly(ethylene glycol (PEG) methyl ether (meth)acrylate) and pentafluorophenyl acrylate (PFPA) were prepared by reversible addition-fragmentation chain transfer (RAFT) polymerisation. The target materials were synthesised by homopolymerisation of the PEG (meth)acrylate followed by block copolymerisation with PFPA, end-group modification and post-polymerisation modification of the activated ester side-groups with appropriate primary amines. Two families of block copolymers were synthesised. The parent block copolymers containing PEG methacrylate and PFPA repeating units, had a size exclusion chromatography (SEC) measured M_n of 35,500 and dispersity, Đ, of 1.33, while the PEG acrylates and PFPA precursor block copolymers had a SEC measured M_n of 12,000 and dispersity, *Đ*, of 1.31. Both parent block copolymers were prepared with 2-cyano-2-propyl benzodithioate as the RAFT chain transfer agent and azobisisobutyronitrile (AIBN) as the source of primary radicals in 1,4-dioxane. The thiocarbonylthio end-group in the parent block copolymers was removed *via* radical-mediated desulfurisation employing an excess of AIBN prior to modification of the pentafluorophenyl (PFP) ester side-groups. Complete removal of the thiocarbonylthio end-group was confirmed by UV-vis spectroscopy with minimal effect on the molecular weight distribution of the parent block copolymers based on SEC analysis.

The pendent PFP ester groups were subsequently modified in a sequential manner with 5-aminotetrazole and a range of primary amines of variable hydrophobicity, yielding the corresponding random acrylamido species quantitatively as judged by ^{19}F NMR and FTIR spectroscopies. The tetrazole functional copolymers were subsequently reacted with $Re(CO)_3(phen)Br$ (phen = 1,10-phenanthroline) yielding the corresponding rhenium-polymer hybrids *via* coordination through the pendent tetrazole functional group. Coordination of the tetrazole functional groups to the rhenium precursor was confirmed by FTIR spectroscopy. Detailed photophysical studies in dimethyl sulfoxide (DMSO) were performed. The absorption profiles of all hybrid materials exhibited broad bands centred around ca. 400 nm associated with metal-to-ligand charge transfer (MLCT) transitions; excitation at this wavelength resulted in a broad emission due to emission from the triplet MLCT excited states centred at around 590 nm for all hybrid species. The different compositions in the rhenium-polymer hybrid materials did not affect their photophysical properties, as confirmed by lifetime and quantum yield analysis.

4.2 Introduction

Biocompatibility, low cytotoxicity, and specific targeting in biological systems are of pivotal importance for the design of polymeric materials for biological and pharmaceutical applications. In Chapter 1, we highlighted the outstanding photophysical properties of d^6 transition metal complexes such as long Stokes shifts, high quantum yield and their applicability as luminescent probes for biological imaging. Nevertheless, they suffer from some issues which can limit their use as luminescent sensors for imaging. However, desirable improvements in these complexes, and their subsequent use in imaging, could be obtained by appropriately

tuning their solubility and biocompatibility and preventing the generation of singlet oxygen from excited states of triplet multiplicity. One approach is to incorporate poly(ethylene glycol) (PEG) into the metal probe's structure. This has been done, for example, by employing a general approach referred to as "PEGylation" which consists of the covalent or non-covalent attachment of PEG into another molecule (or macromolecule).

Because PEG is non-toxic, non-immunogenic, non-antigenic, highly soluble in water and is FDA (Food and Drugs Administration) approved, it plays an important role in drug delivery and today forms the basis of a multimillion-dollar industry.[1] The first FDA approved PEGylated drugs commercialised in the 1990s were Oncaspar® (used for the treatment of leukaemia) and Adagen® (employed for the treatment of immunodeficiency diseases) and consisted of PEGylated enzymes.[2] Another example of the use of PEG to enhance drug delivery is the incorporation of PEG chains into cisplatin, increasing its blood circulation time before reaching the target site.[3]

Because of the concomitant decrease in toxicity of molecules attached to PEG and the retention of their biological or therapeutic properties, the interest in attaching PEG chains to transition metal complexes for biological applications is not limited to cisplatin. Lo's group have investigated the use of PEG to functionalise luminescent transition metal complexes. For instance, iridium(III) polypyridine PEG complexes have been reported and were shown to serve as potential photosensitisers for photodynamic therapy and localisation in mitochondria.[4] Moreover, it has been observed that PEG chains, in iridium PEGylated complexes, are able to prevent molecular oxygen from approaching the excited complexes.[5] The same group has also attached PEG to rhenium(I) polypyridine complexes, which exhibited cytoplasmatic localisation and overall attenuation of cytotoxicity.[5]

The copolymerisation of PFP (meth)acrylate and hydrophilic monomers has not been widely studied. The strength of this approach is that it offers the possibility to make a library of copolymers that could be readily modified to yield a plethora of functionalised and biocompatible materials. Boyer *et al*. have synthesised various PEG/PFP random copolymers for potential applications in the delivery of therapeutic agents.[6,7]

In this Chapter, we detail the RAFT synthesis of a small library of seven block copolymers comprised of poly(ethylene glycol) acrylate and methacrylates (PEGA/PEGMA) with pentafluorophenyl acrylate (PFPA). The resulting PEG/PFP functional block copolymers were used as macromolecular ligands for the metal complexation of Re(I) luminescent species.

4.3 Experimental

4.3.1 Materials

All reagents were purchased from the Sigma-Aldrich Chemical Company, or Alfa Aesar, at the highest available purity and used as received unless noted otherwise.

Poly(ethylene glycol) methyl ether methacrylate (molecular weight of 300 g mol^{-1}) and poly(ethylene glycol) methyl ether acrylate (molecular weight of 480 g mol^{-1}) were purchased from Sigma-Aldrich and purified by passage over a column of basic aluminium oxide to remove inhibitor. $Re(CO)_3(phen)Br$ and pentafluorophenyl acrylate (PFPA) were prepared according to previously published procedures.[8,9] 2,2'-Azobis(2-methylpropionitrile) (AIBN) was purchased as a 12 wt% solution in acetone. Acetone was removed on a rotary evaporator and the remaining solid dissolved in methanol from which AIBN recrystallised.

4.3.2 Size exclusion chromatography (SEC)

SEC was performed on a Shimadzu modular system consisting of a 4.0 mm × 3.0 mm Phenomenex Security Guard^{TM} cartridge guard column and two linear phenogel columns (10^3 and 10^4 Å pore size) in dimethylacetamide (DMAc) with 0.03% w/v LiBr operating at a flow rate of 0.7 mL/min. The system was equipped with a RID-20A refractive index and SPD-M20A prominence diode array detector. The system was calibrated with a series of narrow molecular weight distribution polystyrene standards with molecular weights ranging from 0.27 to 66 kg mol^{-1}. Data were analysed with Lab Solutions SEC software.

4.3.3 NMR Measurements

^{1}H (400 MHz) and ^{19}F (376 MHz) NMR spectra were recorded at 298 K on a Bruker Avance 400 spectrometer. Chemical shifts were referenced against residual non-deuterated solvent. Data were processed with Bruker's TopSpin 3.1 software.

4.3.4 FTIR Analysis

Infrared spectra (4000-650 cm^{-1}) were recorded on solid-state samples using attenuated total reflectance on a Perkin Elmer Spectrum Two and Spectrum 100 FT-IR.

4.3.5 Photophysical Measurements

Absorption spectra were recorded at room temperature using a Perkin Elmer Lambda 35 UV/Vis spectrometer. Uncorrected steady-state emission spectra were recorded using an Edinburgh FLSP980-stm spectrometer equipped

with a 450 W xenon arc lamp and emission monochromators, a Peltier cooled Hamamatsu R928P photomultiplier (180-850 nm) and a Hamamatsu R5509-42 photomultiplier for detection of NIR radiation (800-1400 nm). Emission and excitation spectra were corrected for source intensity (amp and grating) and emission spectral response (detector and grating) by a calibration curve supplied with the instrument. Luminescent quantum yields were measured from absorption spectra on a wavelength scale (nm) and compared to the reference emitter by **Equation 4-1**:

$$\Phi_x = \Phi_r \left[\frac{A_r(\lambda_r)}{A_x(\lambda_x)}\right]\left[\frac{I_r(\lambda_r)}{I_x(\lambda_x)}\right]\left[\frac{n_x^2}{n_r^2}\right]\left[\frac{D_x}{D_r}\right] \qquad \textbf{Equation 4-1}$$

where A is the absorbance at the excitation wavelength λ, I is the intensity of the excitation light at the excitation wavelength, n is the refractive index of the solvent, D is the integrated intensity of the luminescence and Φ is the quantum yield. The subscripts r and x refer to the reference and the sample. The quantum yields of complexes were measured against quinine sulphate solution in 0.5 M H_2SO_4.[10] Excited-state decays (τ) were recorded on the same Edinburgh FLSP980-stm spectrometer using pulsed picosecond light emitting diodes (LEDs) (EPLED/EPL 375 nm, FHWM < 800 ps). The goodness of fit was assessed by minimising the reduced χ^2 function and by visual inspection of the weighted residuals. The solvent used (DMSO) in the preparation of the solutions for the photophysical investigations was of spectrometric grade.

4.3.6 Tissue Preparation and Staining

Tissue preparation and tissue staining were performed by David Hartnell. Rodent brain tissue was generated from excess sham operated (10 - 12 weeks old) male Sprague Dawley rats from a previously published traumatic brain injury study.[11] Animal tissue was generated with approval from Monash University Standing Committee on Ethics in Animal Experimentation. Coronal brain tissue sections (10 µm thick) containing cerebellum, were cut on a cryo-microtome (-18 °C) and transferred to glass slides, allowed to air dry and then stored at room temperature.

Tissue sections were then fixed in paraformaldehyde (4% in phosphate buffered saline (PBS)) for 10 minutes. The slides were then washed for 10 minutes with PBS. Slides were then stained with the polymeric probe containing solution (100 µg/mL in DMSO, 200 µL per tissue section) and incubated for 30 minutes at room temperature. The probe containing solution was then washed off the slides with deionised water and then washed in PBS for 10 minutes. Slides were then further rinsed with deionised water and allowed to dry at room temperature and imaged.

4.3.7 Imaging

Imaging was conducted by David Hartnell. Fluorescence microscopy was conducted on a Nikon Ti2-U inverted microscope with a DS-Qi2 camera, pE-300^{white} LED fluorescence lamp and NIS Elements standard software. Images were gathered at an exposure time of 500 ms and an analog gain of 7.6%. Images were processed in ImageJ.

4.4 Synthesis

4.4.1 RAFT polymerisation of poly(ethylene glycol) methacrylate (PEGMA)

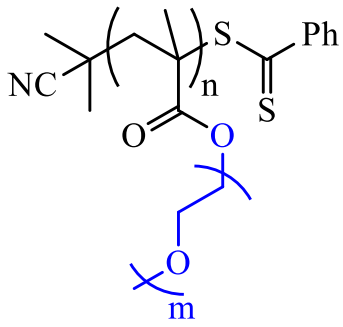

Figure 4-1 Structure of polyPEGMA (**M1**).

Poly(ethylene glycol) methyl ether methacrylate (300 g mol^{-1}) (68.25 g, 0.23 mol), 2-cyano-2-propyl benzodithioate (CPBD, 0.30 g, 1.36 mmol) and AIBN (0.04 g, 0.27 mmol) were added to anhydrous 1,4-dioxane (250.00 mL) in a round-bottomed flask equipped with a magnetic stir bar. The flask was sealed with a rubber septum and the solution was purged with nitrogen for 60 min before being placed in a preheated oil bath set at 65 °C. The homopolymerisation was allowed to proceed for 18 h and was halted by exposure to air and immersion of the reaction vessel in an ice bath. The product homopolymer was purified by three precipitations in *n*-hexane followed by drying under *vacuum*. The product polyPEGMA **M1** was obtained (34.61 g). SEC analysis: M_n = 32,900; M_w = 37,700; $Đ$ = 1.14.

4.4.2 RAFT polymerisation of poly(ethylene glycol) acrylate (PEGA)

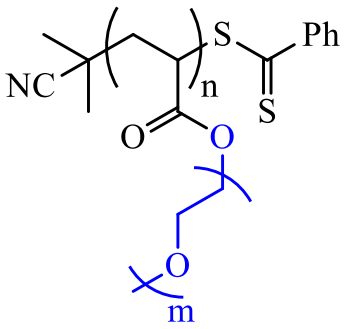

Figure 4-2 Structure of polyPEGA (**A1**).

Poly(ethylene glycol) methyl ether acrylate (480 g mol^{-1}) (21.8 g, 0.045 mol), 2-cyano-2-propyl benzodithioate (CPBD, 0.19 g, 0.86 mmol) and AIBN (0.025 g, 0.15 mmol) were added to acetonitrile (80.0 mL) in a round-bottomed flask equipped with a magnetic stir bar. The flask was sealed with a rubber septum and the solution was purged with nitrogen for 60 min before being placed in a preheated oil bath set at 65 °C. The homopolymerisation was allowed to proceed for 19 h and was halted by exposure to air and immersion of the reaction vessel in an ice bath. The product, polyPEGA (**A1**), was purified by four precipitations in *n*-hexane followed by drying under *vacuum*. The product polyPEGA **A1** was obtained (13.60 g). SEC analysis: M_n = 9,900; M_w = 11,300; $Đ$ = 1.14.

4.4.3 Block copolymerisation of poly(PEGMA-*b*-PFPA) (M2)

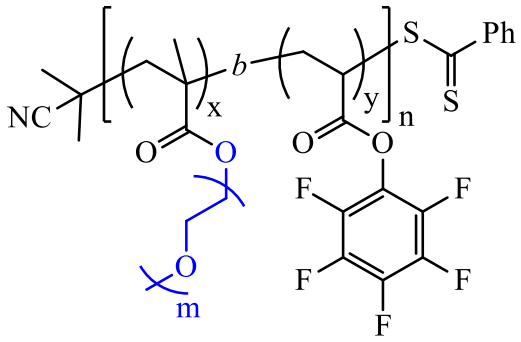

Figure 4-3 General structure of a block copolymer comprised of PEGMA and PFPA (**M2**).

PEGMA homopolymer **M1** (10.00 g), pentafluorophenyl acrylate (PFPA) (7.95 g, 0.03 mol), and traces of AIBN were added to anhydrous 1,4-dioxane (50.0 mL) in a round-bottomed flask equipped with a magnetic stir bar. The flask was sealed with a rubber septum and the solution was purged with nitrogen for 30 min before being placed in a preheated oil bath set at 60 °C. The block copolymerisation was allowed to proceed for 7 h and was halted by exposure to air and immersion of the reaction vessel in an ice bath. The product AB diblock copolymer was purified by three precipitations in cold *n*-hexane followed by drying under *vacuum*. The product **M2** was obtained (6.00 g) as a solid. SEC analysis: M_n = 35,500; M_w = 47,300; $Đ$ = 1.33.

4.4.4 Block copolymerisation of poly(PEGA-*b*-PFPA) (A2)

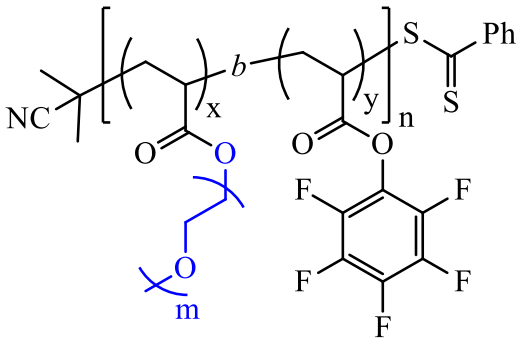

Figure 4-4 General structure of a block copolymer of polyPEGA and PFPA (**A2**).

PEGA homopolymer **A1** (12.22 g), pentafluorophenyl acrylate (PFPA) (6.06 g, 0.02 mol) and traces of AIBN were added to anhydrous acetonitrile (50.0 mL) in a round-bottomed flask equipped with a magnetic stir bar. The flask was sealed with a rubber septum and the solution was purged with nitrogen for 30 min before being placed in a preheated oil bath set at 70 °C. The block copolymerisation was allowed to proceed for 4 h and was halted by exposure to air and immersion of the reaction vessel in an ice bath. The product was purified by three precipitations in cold *n*-hexane followed by drying under *vacuum*. The product **A2** was obtained (11.00 g) as a solid. SEC analysis: M_n = 12,000; M_w = 15,800; $Đ$ = 1.31.

4.4.5 End-group modification of poly(PEGMA-*b*-PFPA) (M3)

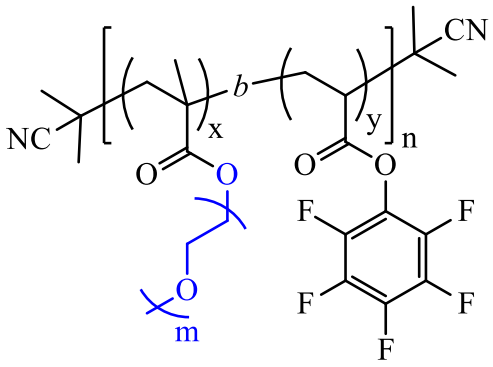

Figure 4-5 General structure of end-group modified block copolymer poly(PEGMA-*b*-PFPA) (**M3**).

Poly(PEGMA-*b*-PFPA) **M2** (1.00 g, 0.03 mmol) and AIBN (0.02 g, 0.12 mmol) were dissolved in anhydrous 1,4-dioxane (8.0 mL) in a round-bottomed flask equipped with a magnetic stir bar. The flask was sealed with a rubber septum and the solution was purged with nitrogen for 30 min before being placed in a preheated oil bath set at 80 °C. After 6 h the clear solution was allowed to cool to room temperature. The product (0.85 g) was isolated by precipitation into cold *n*-pentane. SEC analysis: M_n = 35,600; M_w = 44,300; $Đ$ = 1.45.

4.4.6 End-group modification of poly(PEGA-*b*-PFPA) (A3)

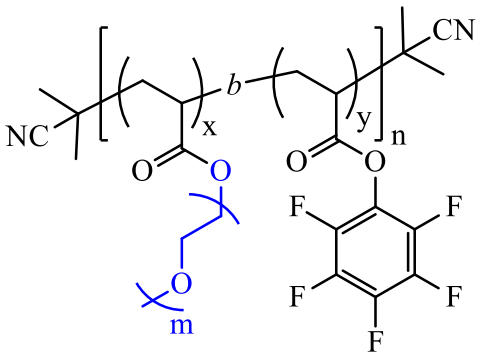

Figure 4-6 General structure of end-group modified block copolymer of poly(PEGA-*b*-PFPA) (**A3**).

Poly(PEGMA-*b*-PFPA) **A2** (1.00 g, 0.08 mmol) and AIBN (0.05 g, 0.30 mmol) were dissolved in anhydrous 1,4-dioxane (8.0 mL) in a round-bottomed flask equipped with a magnetic stir bar. The flask was sealed with a rubber septum and the solution was purged with nitrogen for 30 min before being placed in a preheated oil bath set at 80 °C. After 6 h the clear solution was allowed to cool to room temperature. The product (0.82 g) was isolated by precipitation into cold *n*-pentane. SEC analysis: M_n 12,500; M_w = 16,000; $Đ$ = 1.27.

4.4.7 Procedure for the sequential modification of the poly(PEGMA-*b*-PFPA) block copolymer with primary amines

4.4.7.1 Synthesis of M3-40%tet-60%oct

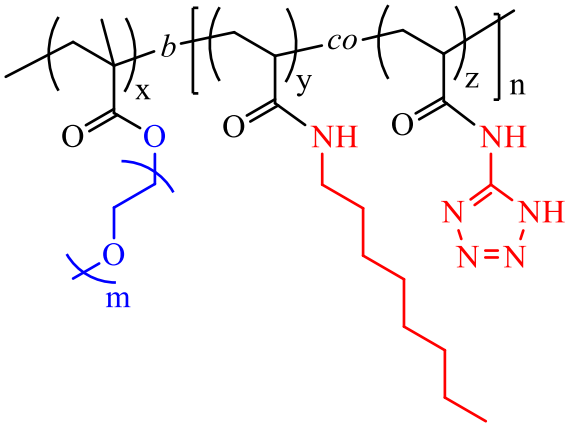

Figure 4-7 Post-functionalised structure of the poly(PEGMA-*b*-PFPA) block copolymer (**M3**) with 5-aminotetrazole and *n*-octylamine (**M3-40%tet-60%oct**).

To a round-bottomed flask equipped with a magnetic stir bar was added **M3** (1.00 g, 0.03 mmol), *n*-octylamine (0.05 g, 0.41 mmol) and dimethylformamide (DMF) (4.0 mL). The reaction mixture was left stirring overnight at room temperature. Subsequently, an excess of 5-aminotetrazole (0.03 g, 0.02 mmol) was added to the reaction mixture and the solution was left stirring overnight at 40 °C. The solution was subsequently dialysed against methanol for 36 h. Methanol from the polymer solution was removed using rotary evaporator and the product was dried *in vacuo* overnight at 50 °C. 0.67 g of the product **M3-40%tet-60%oct** was obtained. SEC analysis: M_n 39,200; M_w = 53,200; $Đ$ = 1.35.

4.4.7.2 Synthesis of M3-10%tet-90%oct

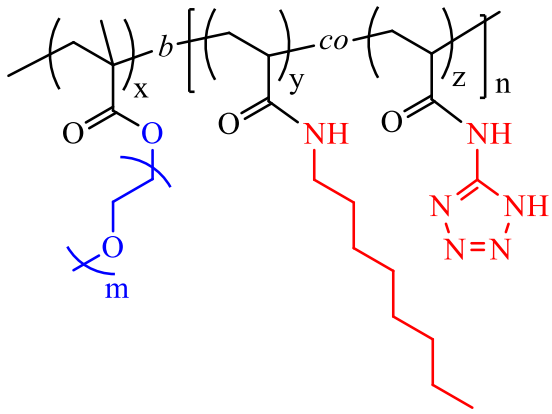

Figure 4-8 Post-functionalised structure of the poly(PEGMA-*b*-PFPA) block copolymer (**M3**) with 5-aminotetrazole and *n*-octylamine (**M3-10%tet-90%oct**).

To a round-bottomed flask equipped with a magnetic stir bar was added **M3** (0.77 g, 0.02 mmol), 5-aminotetrazole (0.003 g, 0.025 mmol) and DMF (4.00 mL). The reaction mixture was left stirring overnight at room temperature. Subsequently, an excess of *n*-octylamine (0.05 g, 0.36 mmol) was added to the reaction mixture and the solution was left stirring overnight at 40 °C. The solution was subsequently dialysed against methanol for 36 h. Methanol from the polymer solution was removed using a rotary evaporator and the product was dried *in vacuo* overnight at 50 °C. 0.63 g of the product **M3-10%tet-90%oct** was obtained. SEC analysis: M_n 35,000; M_w = 44,100; $Đ$ = 1.26.

4.4.7.3 Synthesis of M3-40%tet-60%hexadec

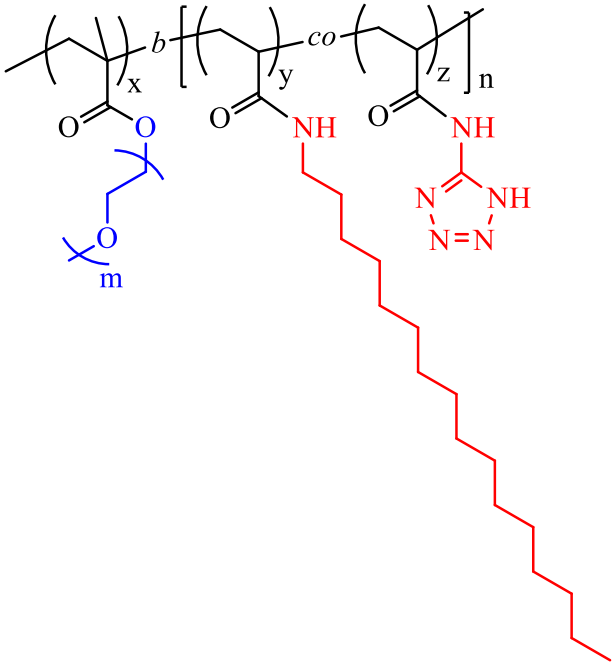

Figure 4-9 Post-functionalised structure of the poly(PEGMA-*b*-PFPA) block copolymer (**M3**) with 5-aminotetrazole and *n*-hexadecylamine (**M3-40%tet-60%hexadec**).

To a round-bottomed flask equipped with a magnetic stir bar was added **M3** (0.70 g, 0.02 mmol), 5-aminotetrazole (0.01 g, 0.12 mmol) and DMF (4.00 mL). The reaction mixture was left stirring overnight at room temperature. Subsequently, an excess of *n*-hexadecylamine (0.05 g, 0.23 mmol) was added to the reaction mixture and the solution was left stirring overnight at 40 °C. The solution was subsequently dialysed against methanol for 36 h. Methanol from the polymer solution was removed using rotary evaporator and the product was dried *in vacuo* overnight at 50 °C. 0.60 g of the product **M3-40%tet-60%hexadec** was obtained. SEC analysis: M_n 40,400; M_w = 50,200 $Đ$ = 1.24.

4.4.8 Procedure for the sequential modification of the poly(PEGA-*b*-PFPA) block copolymer with primary amines

4.4.8.1 Synthesis of A3-65%tet-35%dec

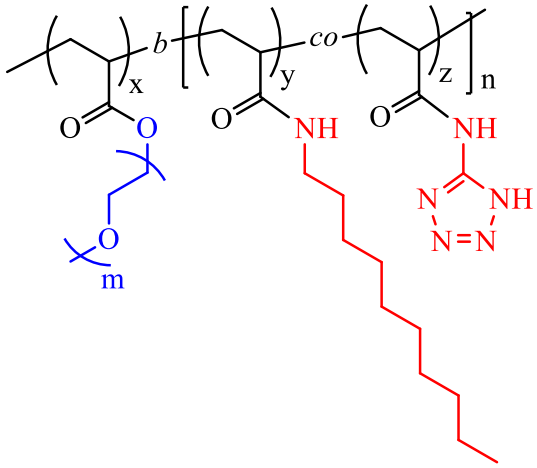

Figure 4-10 Post-functionalised structure of the poly(PEGA-*b*-PFPA) block copolymer (**A3**) with 5-aminotetrazole and *n*-decylamine (**A3-65%tet-35%dec**).

To a round-bottomed flask equipped with a magnetic stir bar was added **A3** (0.82 g, 0.01 mmol), *n*-decylamine (0.02 g, 0.10 mmol) and tetrahydrofuran (THF) (3.00 mL). The reaction mixture was left stirring overnight at room temperature. Subsequently, an excess of 5-aminotetrazole (0.01 g, 0.01 mmol) and traces of triethylamine were added to the reaction mixture and the solution was left stirring overnight at room temperature. The solution was subsequently dialysed against methanol for 36 h. Methanol was removed from the polymer solution using a rotary evaporator and the product was dried *in vacuo* overnight at 50 °C. 0.48 g of **A3-65%tet-35%dec** was obtained. SEC analysis: M_n 14,500; M_w = 18,900; $Đ$ = 1.29.

4.4.8.2 Synthesis of A3-50%tet-50%dec

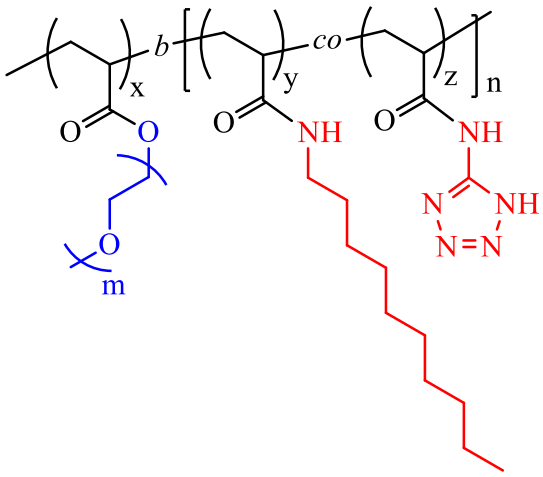

Figure 4-11 Post-functionalised structure of the poly(PEGA-*b*-PFPA) block copolymer (**A3**) with 5-aminotetrazole and *n*-decylamine (**A3-50%tet-50%dec**).

To a round-bottomed flask equipped with a magnetic stir bar was added **A3** (0.80 g, 0.01 mmol), *n*-decylamine (0.02 g, 0.15 mmol) and tetrahydrofuran (THF) (3.00 mL). The reaction mixture was left stirring overnight at room temperature. Subsequently, an excess of 5-aminotetrazole (0.01 g, 0.01 mmol) and traces of triethylamine were added to the reaction mixture and the solution was left stirring overnight at room temperature. The solution was subsequently dialysed against methanol for 36 h. Methanol was removed from the polymer solution using a rotary evaporator and the product was dried *in vacuo* overnight at 50 °C. 0.75 g of **A3-50%tet-50%dec** was obtained. SEC analysis: M_n 14,000; M_w = 18,200; $Đ$ = 1.29.

4.4.8.3 Synthesis of A3-90%tet-10%hexadec

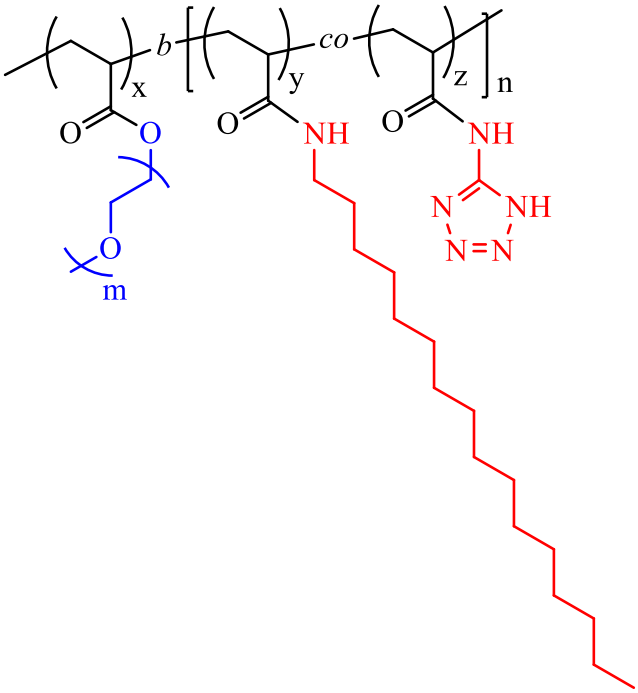

Figure 4-12 Post-functionalised structure of the poly(PEGA-*b*-PFPA) block copolymer (**A3**) with 5-aminotetrazole and *n*-hexadecylamine (**A3-90%tet-10%hexadec**).

To a round-bottomed flask equipped with a magnetic stir bar was added **A3** (0.80 g, 0.01 mmol), *n*-hexadecylamine (0.01 g, 0.03 mmol) and tetrahydrofuran (THF) (3.00 mL). The reaction mixture was left stirring overnight at room temperature. Subsequently, an excess of 5-aminotetrazole (0.02 g, 0.02 mmol) and traces of triethylamine were added to the reaction mixture and the solution was left stirring overnight at room temperature. The solution was subsequently dialysed against methanol for 36 h. Methanol was removed from the polymer solution using a rotary evaporator and the product

was dried *in vacuo* overnight at 50 °C. 0.60 g of **A3-90%tet-10%hexadec** was obtained. SEC analysis: M_n 14,700; M_w = 21,200; $Đ$ = 1.44.

4.4.8.4 Synthesis of A3-75%tet-25%hexadec

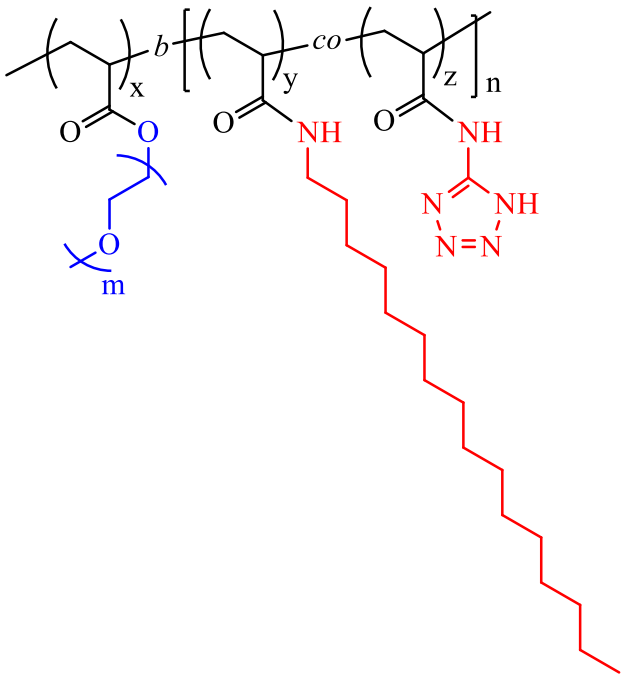

Figure 4-13 Post-functionalised structure of the poly(PEGA-*b*-PFPA) block copolymer (**A3**) with 5-aminotetrazole and *n*-hexadecylamine (**A3-75%tet-25%hexadec**).

To a round-bottomed flask equipped with a magnetic stir bar was added **A3** (0.80 g, 0.01 mmol), *n*-hexadecylamine (0.01 g, 0.02 mmol) and tetrahydrofuran (THF) (3.00 mL). The reaction mixture was left stirring overnight at room temperature. Subsequently, an excess of 5-aminotetrazole (0.01 g, 0.01 mmol) and traces of triethylamine were added to the reaction mixture and the solution left stirring overnight at room temperature. The solution was subsequently dialysed against methanol for 36 h. Methanol was

removed from the polymer solution using a rotary evaporator and the product was dried *in vacuo* overnight at 50 °C. 0.60 g of **A3-75%tet-25%hexadec** was obtained. SEC analysis: M_n 15,600; M_w = 20,900; $Đ$ = 1.34.

4.4.9 Complexation of $Re(CO)_3(phen)Br$ to a PEGMA/PFPA tetrazole functional copolymer (M3-40%tet-60%oct-[Re])

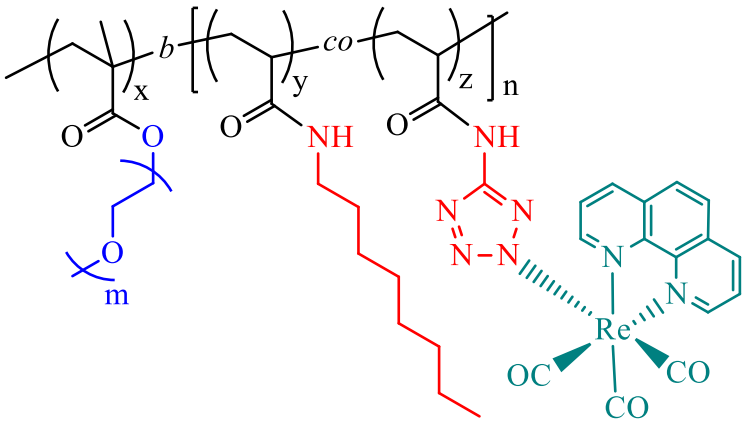

Figure 4-14 Structure of **M3-40%tet-60%oct** after reaction with the rhenium precursor $Re(CO)_3(phen)Br$ to synthesise (**M3-40%tet-60%oct-[Re]**). Attachment to the N2 atom of the tetrazole ring is shown for convenience.

To a round-bottomed flask equipped with a magnetic stir bar was added $Re(CO)_3(phen)Br$ (0.011 g, 0.021 mmol) and **M3-40%tet-60%oct** (0.150 g, 0.004 mmol) in DMSO (4.00 mL). The solution was heated under refluxing conditions for 24 h. The solution was subsequently dialysed against methanol for 36 h. Methanol from the polymer solution was removed using a rotary evaporator and the product **M3-40%tet-60%oct-[Re]** (0.150 g) was dried *in vacuo* overnight at 50 °C.

The remaining rhenium-functionalised copolymers **M3-10%tet-90%oct-[Re]** and **M3-40%tet-60%hexadec-[Re]** were synthesised following the same procedure, but with differing amounts of polymer and Re precursor. In the case of **M3-10%tet-90%oct-[Re]**, $Re(CO)_3(phen)Br$ (0.003 g, 0.006 mmol) and **M3-10%tet-90%oct** (0.150 g, 0.004 mmol) were employed and 0.130 g of product was obtained. In the case of **M3-40%tet-60%hexadec-[Re]**, $Re(CO)_3(phen)Br$ (0.014 g, 0.028 mmol) and **M3-40%tet-60%oct** (0.200 g, 0.005 mmol) were employed and 0.190 g of product was obtained.

4.4.10 Complexation of $Re(CO)_3(phen)Br$ to a PEGA/PFPA tetrazole functional copolymer (A3-65%tet-35%dec-[Re])

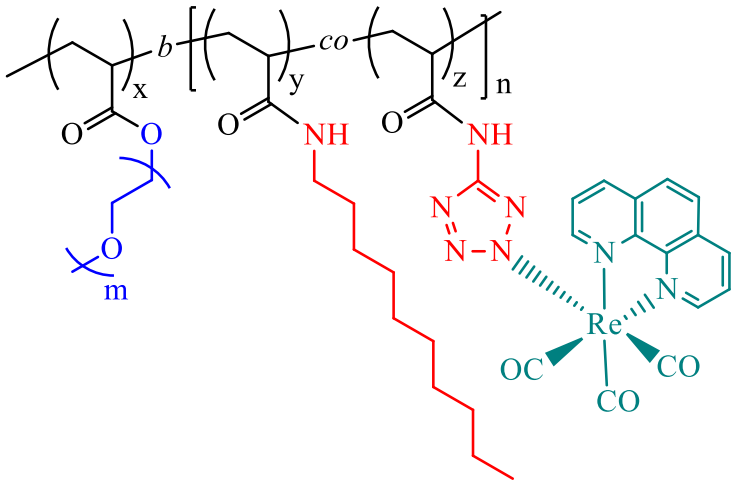

Figure 4-15 Structure of **A3-65%tet-35%dec** after reaction with the rhenium precursor $Re(CO)_3(phen)Br$ to synthesise (**A3-65%tet-35%dec-[Re]**). Attachment to the N2 atom of the tetrazole ring is shown for convenience.

To a round-bottomed flask equipped with a magnetic stir bar was added $Re(CO)_3(phen)Br$ (0.01 g, 0.01 mmol) and **A3-65%tet-35%dec** (0.20 g, 0.01

mmol) in a mixture of ethanol (10.00 mL) and water (3.50 mL). The solution was heated under refluxing conditions for 24 h. The solution was subsequently dialysed against methanol for 36 h. Methanol from the polymer solution was removed using a rotary evaporator and the product **A3-65%tet-35%dec-[Re]** (0.19 g) was obtained after drying *in vacuo* overnight at 50 °C.

The remaining rhenium-functionalised polymers **A3-50%tet-50%dec-[Re]**, **A3-10%tet-90%hexadec-[Re]** and **A3-25%tet-75%hexadec-[Re]** were synthesised following the same procedure, but with differing amounts of polymer and Re precursor. In the case of **A3-50%tet-50%dec-[Re]**, $Re(CO)_3(phen)Br$ (0.01 g, 0.01 mmol) and **A3-50%tet-50%dec** (0.2 g, 0.01 mmol) were employed and 0.42 g of product was obtained. For **A3-10%tet-90%hexadec-[Re]**, $Re(CO)_3(phen)Br$ (0.01 g, 0.02 mmol) and **A3-10%tet-90%hexadec** (0.28 g, 0.02 mmol) and 0.18 g of product was obtained. For **A3-75%tet-25%hexadec-[Re]**, $Re(CO)_3(phen)Br$ (0.01 g, 0.02 mmol) and **A3-75%tet-25%hexadec** (0.28 g, 0.02 mmol) were employed and 0.20 g of product was obtained.

4.5 Results and Discussion

4.5.1 RAFT homopolymerisation of poly(ethylene glycol) methyl ether methacrylate (M1)

With the aim to synthesise block copolymers, we initially synthesised a PEGMA homopolymer (**Scheme 4-1**) which was subsequently employed as a macro chain transfer agent (macro CTA) for the synthesis of the target block copolymer.

The parent PEGMA homopolymer (polyPEGMA, target M_n of 50,000) was prepared by RAFT polymerisation employing 2-cyano-2-propyl

benzodithioate (CPBD) as the RAFT CTA. AIBN was employed as the source of primary radicals in 1,4-dioxane.

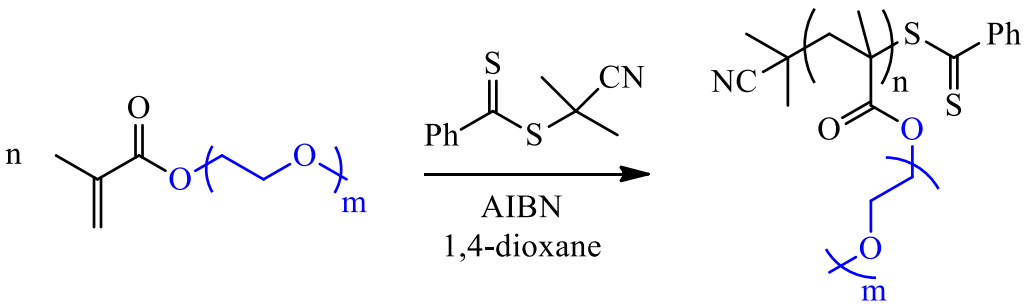

M1

Scheme 4-1 RAFT homopolymerisation of poly(ethylene glycol) methyl ether methacrylate.

After polymerisation for 18 h at 65 °C, polyPEGMA homopolymer **M1** was isolated with ca. 50 % monomer conversion (as determined by ^{1}H NMR spectroscopy). Conversion was calculated by end-group analysis of the ^{1}H NMR, by comparing aromatic signals from the RAFT agent with the signal labelled "f" arising from the polymer **M1** (**Figure 4-16**). It is important to note that NMR is considered the "absolute" method to determine conversion and "absolute" molecular weight of polymers. Nevertheless, for polymers with a high molecular weight like **M1**, the signal to noise ratio interferes with the accuracy of this method. On the other hand, SEC analysis of molecular weights is considered a "relative" method because the hydrodynamic volume of the material analysed is compared to a series of standards, in this case polystyrene standards. For **M1**, SEC measured an M_n of 32,900 and dispersity ($Đ = M_w/M_n$) of 1.14. The degree of polymerisation of the PEGMA homopolymer was calculated from the SEC data acquired in dimethylacetamide (DMAc) and

determined to be = 110. **Figure 4-16** shows the ^{1}H NMR spectrum of **M1**, recorded in deuterated DMSO.

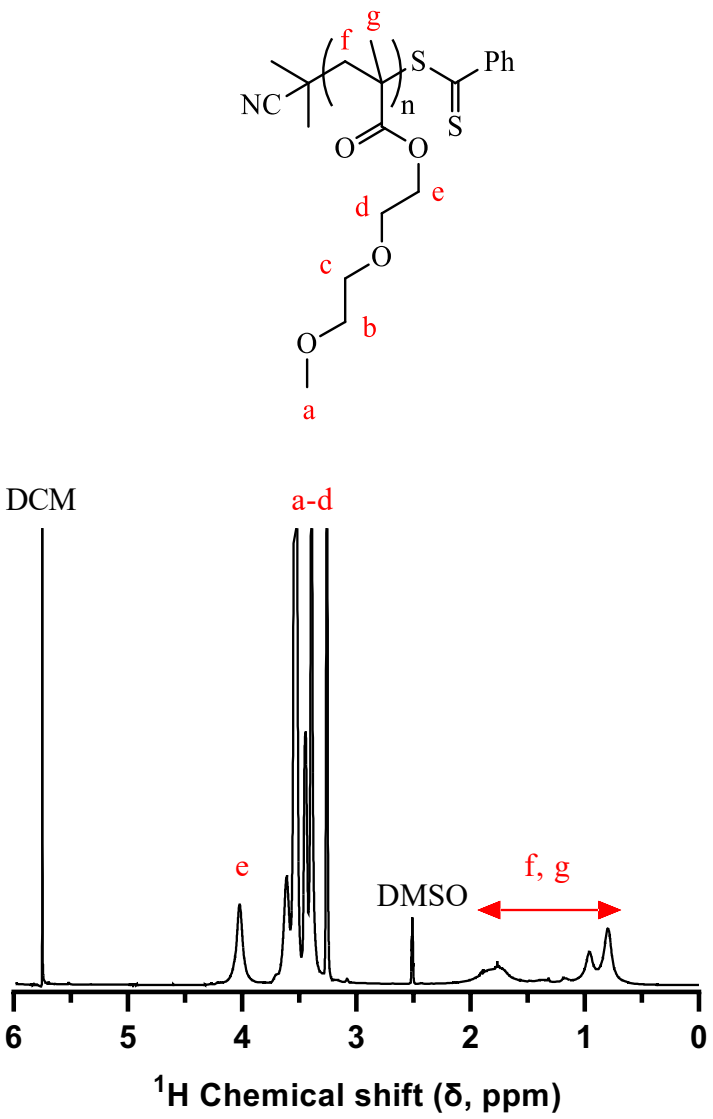

Figure 4-16 ^{1}H NMR spectrum of **M1**, with key peak assignment, recorded in DMSO-*d6*.

4.5.2 RAFT homopolymerisation of poly(ethylene glycol) methyl ether acrylate (A1)

The parent PEGA homopolymer (polyPEGA, target M_n of 25,000) was prepared by RAFT polymerisation employing CPBD as the RAFT CTA. AIBN was employed as the source of primary radicals in 1,4-dioxane.

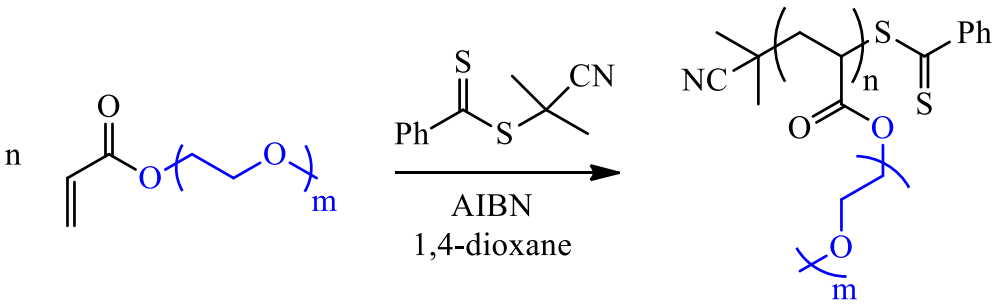

A1

Scheme 4-2 RAFT homopolymerisation of poly(ethylene glycol) methyl ether acrylate.

After polymerisation for 19 h at 65 °C, polyPEGA homopolymer **A1** was isolated with *ca*. 50 % monomer conversion as determined by ^{1}H NMR spectroscopy. Conversion was calculated by end-group analysis *via* ^{1}H NMR spectroscopy, by comparing aromatic signals from the RAFT agent with the signal labelled "f" arising from the polymer **A1** (**Figure 4-17**). SEC measured an M_n of 9,900 and dispersity ($Đ$ = M_w/ M_n) of 1.14. The degree of polymerisation of the PEGA homopolymer was calculated from the SEC data acquired in DMAc and determined to be = 21.

Moreover, the absolute M_n was calculated from ^{1}H NMR by analysing signal f and aromatic signal arising from the CTA at 7.7 ppm (not visible in **Figure 4-17**). M_n = 15,400. Repeating units = 32. **Figure 4-17** shows the ^{1}H NMR spectrum of **A1**.

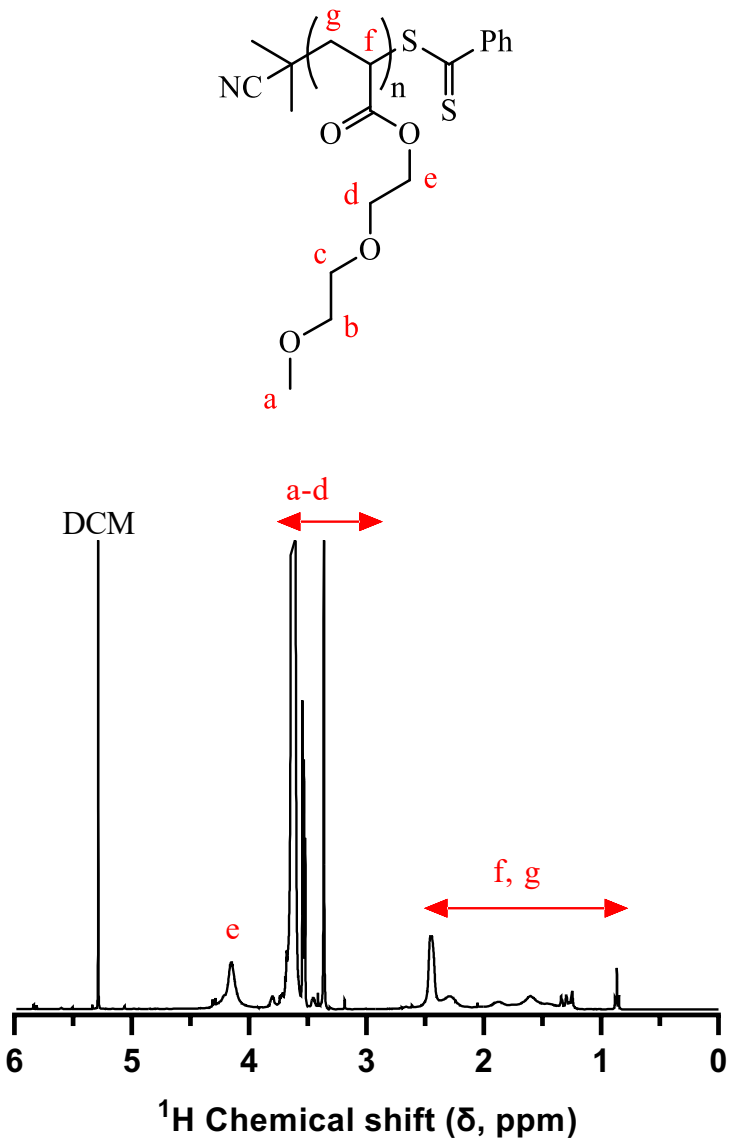

Figure 4-17 ^{1}H NMR spectrum of **A1**, with key peak assignment, recorded in $CDCl_3$.

4.5.3 Block copolymerisation of polyPEGMA with PFPA (M2)

The PEGMA and PEGA homopolymers were subsequently employed as macro CTAs in the block copolymerisation of pentafluorophenyl acrylate. In the case of poly(PEGMA-*b*-PFPA) (**M2**), pentafluorophenyl acrylate was polymerised with polyPEGMA **M1** as macro CTA (**Scheme 4-3**).

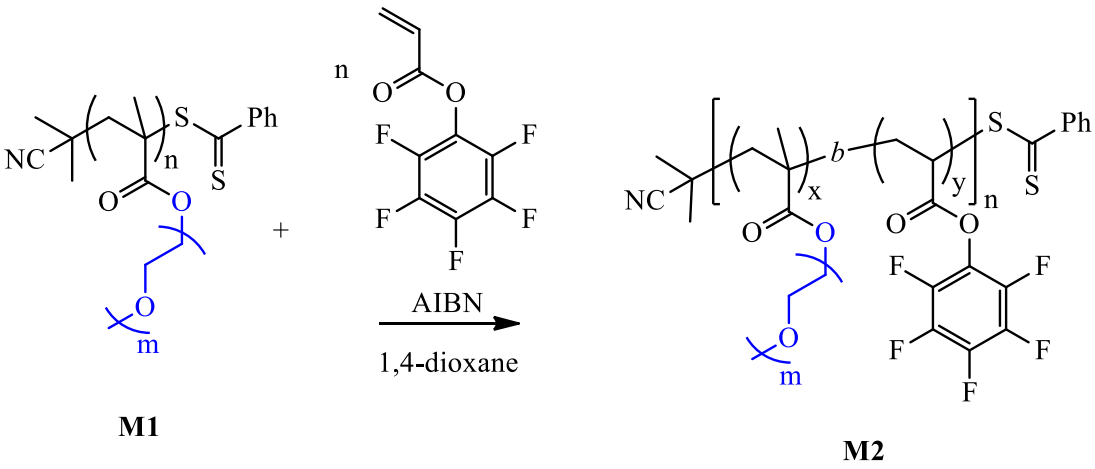

M1 **M2**

Scheme 4-3 Block copolymerisation of polyPEGMA **M1** with pentafluorophenyl acrylate to yield poly(PEGMA-*b*-PFPA) **M2**.

After copolymerisation for 7 h at 60° C, the block copolymer **M2** was isolated by precipitation in *n*-hexane. SEC analysis in DMAc indicated a M_n of 35,500 and $Đ$ of 1.33.

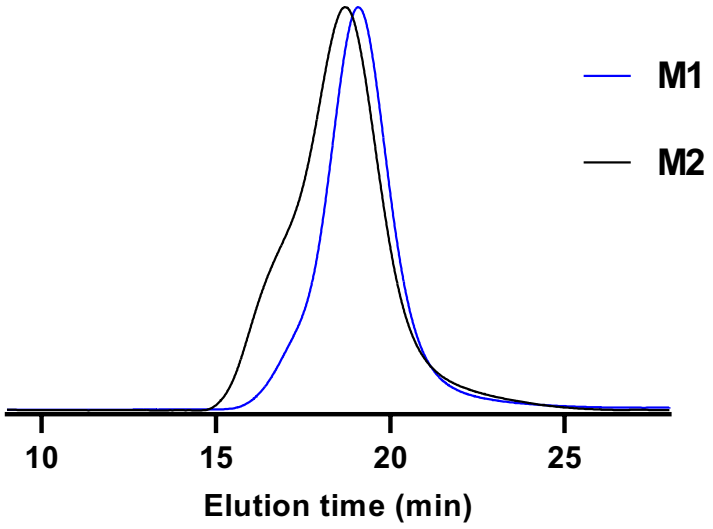

Figure 4-18 SEC traces of **M1** and **M2**. For **M1** M_n = 32,900; M_w = 37,700; $Đ$ = 1.14. For **M2** M_n = 35,500; M_w = 47,300; $Đ$ = 1.33.

The SEC traces in **Figure 4-18** show a lower retention time for **M2**, which confirms an increase in molecular weight and successful block copolymer formation, as expected. Moreover, there is clearly some polymer-polymer coupled products in **M2**, not present in **M1**, as evidenced by the "shoulder" at low elution time on the **M2** traces. Polymer-polymer coupled product is the result of two polymeric chains coupling via S-S bond. S-S formation occurs between two different chains after the thiocarbonylthio end-group have been converted to thiols. This is not an uncommon observation in RAFT block copolymerisations and the presence of coupled material was not anticipated to adversely affect the material itself and the subsequent modification reactions. **Figure 4-19** shows the ^{1}H NMR spectrum of **M2**.

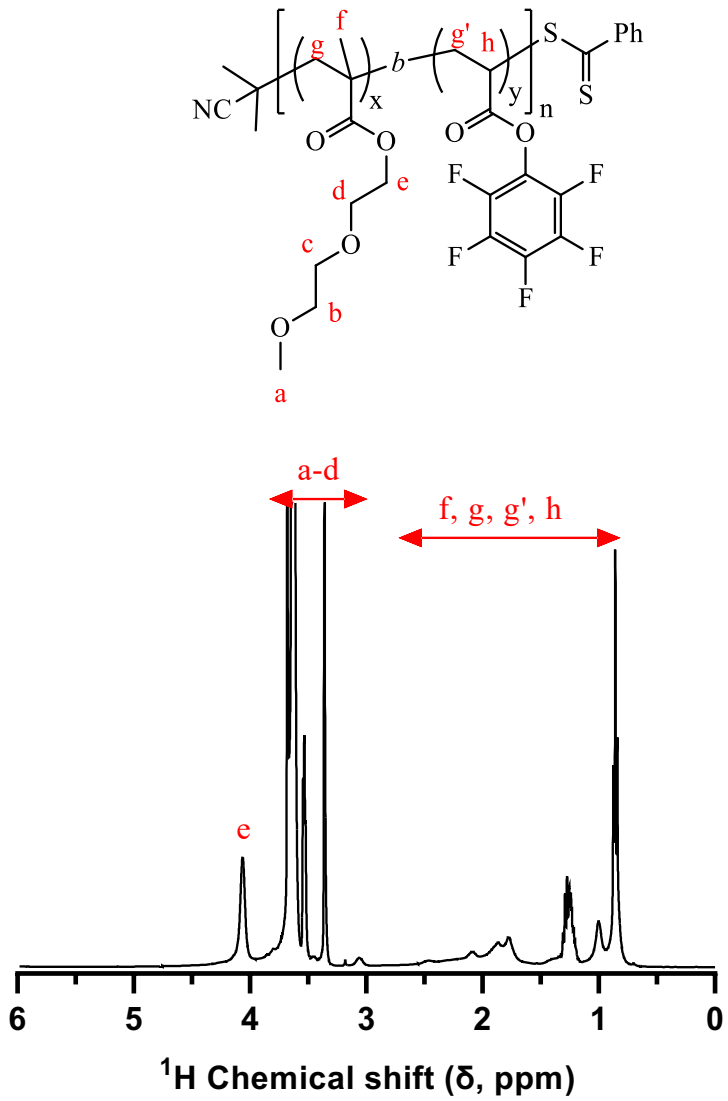

Figure 4-19 ^{1}H NMR spectrum of **M2**, with key peak assignment, recorded in $CDCl_3$.

4.5.4 Block copolymerisation of polyPEGA with PFPA (A2)

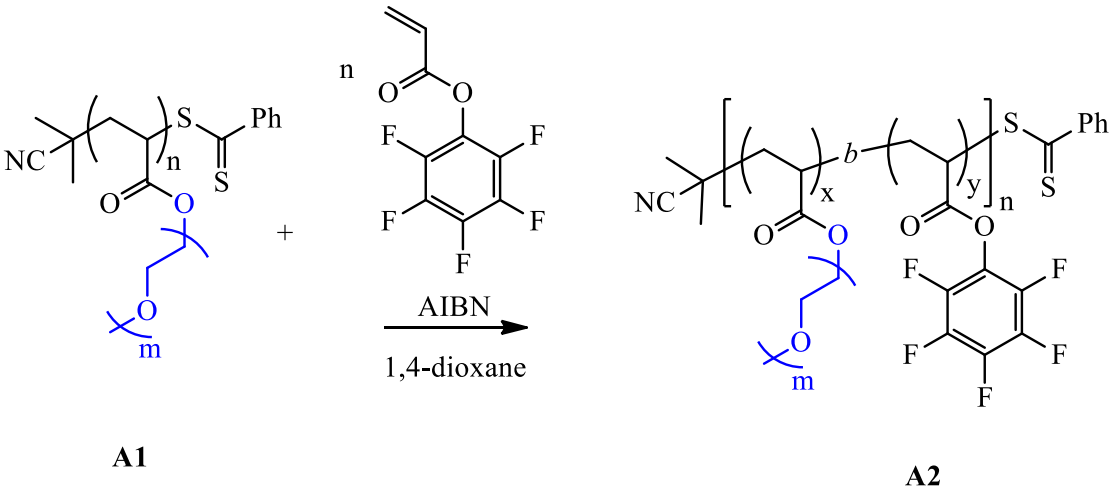

A1 **A2**

Scheme 4-4 Block copolymerisation of polyPEGA **A1** with pentafluorophenyl acrylate to yield poly(PEGA-*b*-PFPA) **A2**.

After copolymerisation for 4 h at 70 °C, the block copolymer **A2** was isolated by precipitation in *n*-hexane. Characterisation of the block copolymer by SEC indicated a M_n of 12,000 and $Đ$ of 1.31, **Figure 4-20**.

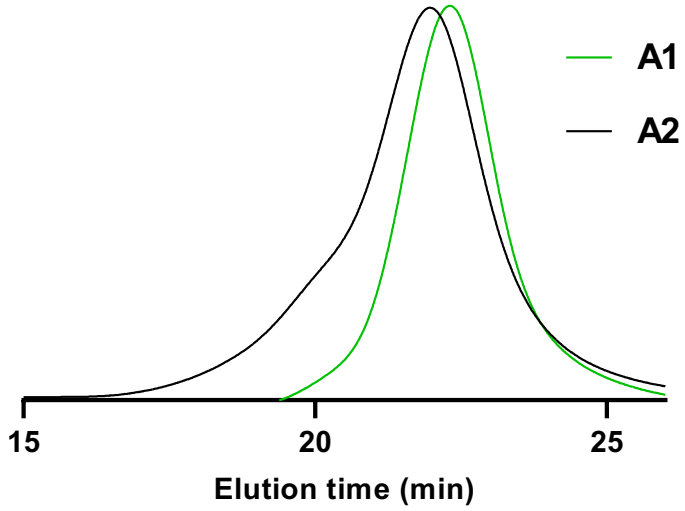

Figure 4-20 SEC traces of **A1** and **A2**. For **A1** M_n = 9,900; M_w = 11,300; $Đ$ = 1.14. For **A2** M_n = 12,000; M_w = 15,800; $Đ$ = 1.31.

The SEC traces in **Figure 4-20** show a lower retention time for **A2**, which confirms an increase in molecular weight, as expected. Moreover, one can see the clear presence of some coupled product in **A2**, not present in **A1**. The formation of undesirable coupled product is more pronounced than in poly(PEGMA-*b*-PFPA) block copolymer, although the measured values are still acceptable. **Figure 4-21** shows the ^{1}H NMR spectrum of **A2**, with relative peak assignments.

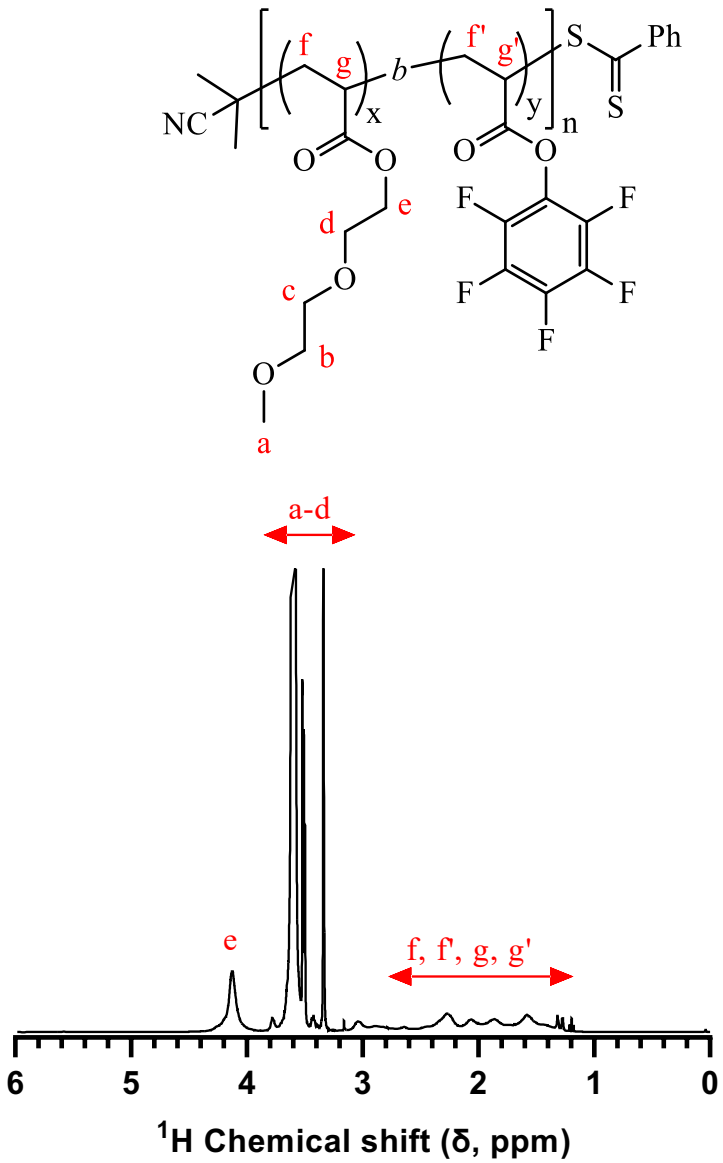

Figure 4-21 ^{1}H NMR spectrum of **A2**, with key peak assignment recorded in $CDCl_3$.

4.5.5 Dithioester end-group removal in the poly(PEGMA-*b*-PFPA) (M3)

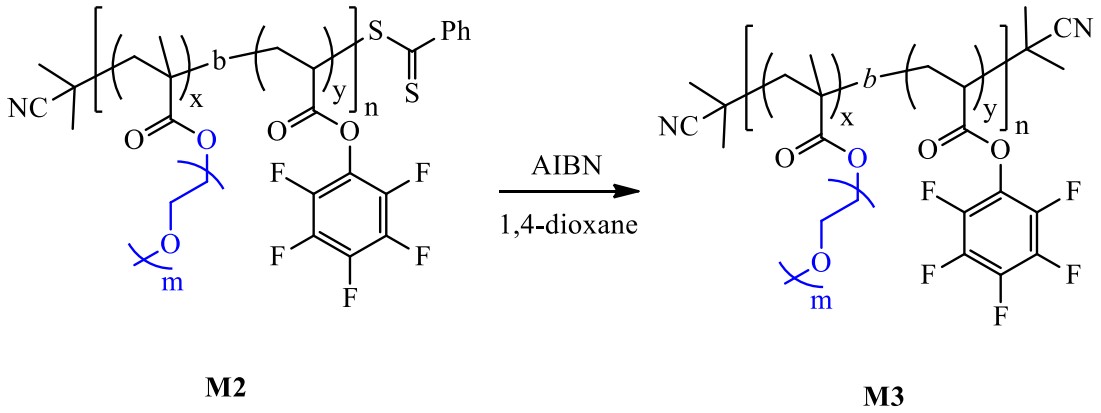

M2 **M3**

Scheme 4-5 End-group cleavage by addition-fragmentation coupling of poly(PEGMA-*b*-PFPA) to achieve complete desulfurisation of the block copolymer **M2** to obtain **M3**.

Before side-group modification of the poly(PEGMA/PEGA-*b*-PFPA) block copolymers, thiocarbonylthio end-group removal was performed to avoid any potential complicating side reactions with RAFT-end groups in the subsequent nucleophilic acyl substitution modification step. Complete end-group desulfurisation was accomplished following the same procedure for both block copolymer. Only the reaction of PEGMA-PFPA **M2** to **M3** is shown for simplicity (**Scheme 4-5**).

The desulfurisation reactions were monitored by UV-Vis spectroscopy. **Figure 4-22** shows the UV absorption spectra of the poly(PEGMA-*b*-PFPA) copolymer before (**M2**) and after (**M3**) treatment with AIBN. The UV absorption spectrum of **M2** is typical of RAFT-prepared (co)polymers with intact end-groups. The key feature is the broad absorption band associated with the π-π* transition of the C=S bond seen covering ca. 280-340 nm.[12]

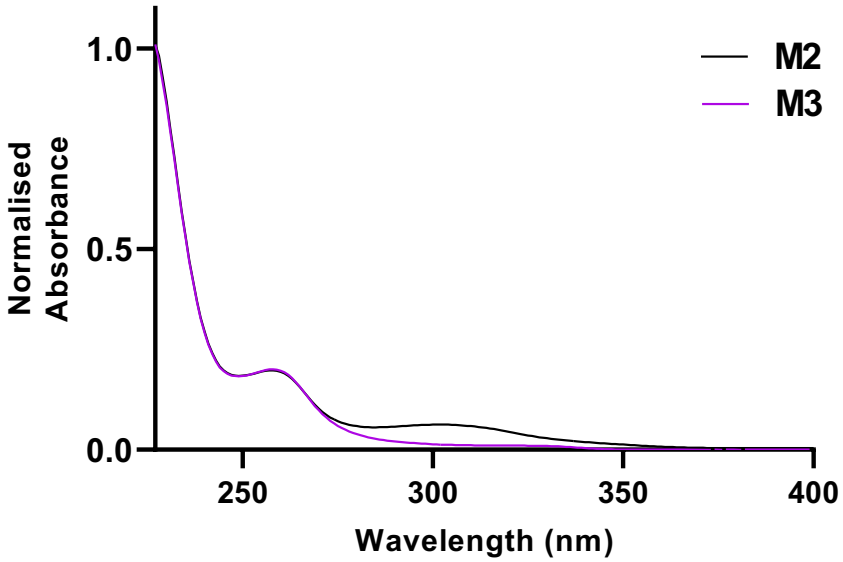

Figure 4-22 UV-Vis spectra of **M2** before end-group modification and the same copolymer, **M3** after reaction with an excess of AIBN.

Following reaction with AIBN this absorption is absent indicating successful end-group modification. A comparison of the SEC traces of both block copolymers **M2** and **M3**, **Figure 4-23**, indicated that the AIBN desulfurisation had no significant impact on the shape of the molecular weight distribution although a small increase in the *Đ* from 1.33 to 1.35 was observed.

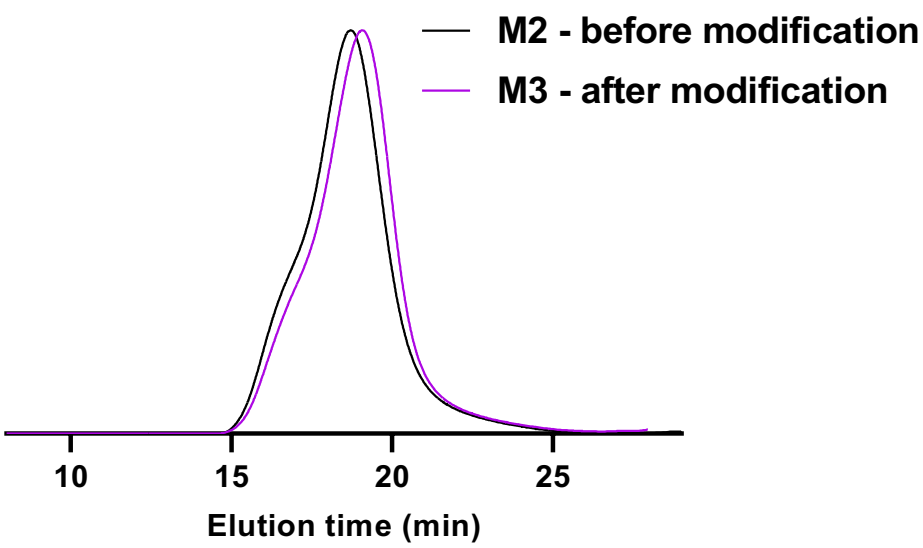

Figure 4-23 SEC traces of **M2** before end-group modification and the same block copolymer, **M3** after reaction with AIBN. For **M3** M_n = 39,200; M_w = 53,200; $Đ$ = 1.35.

The end-group cleavage reaction was performed on the poly(PEGA-*b*-PFPA) block copolymer (**A2**), under the same conditions. The UV absorption spectra of the poly(PEGA-*b*-PFPA) copolymer before (**A2**) and after (**A3**) treatment with AIBN is shown in **Figure 4-24**.

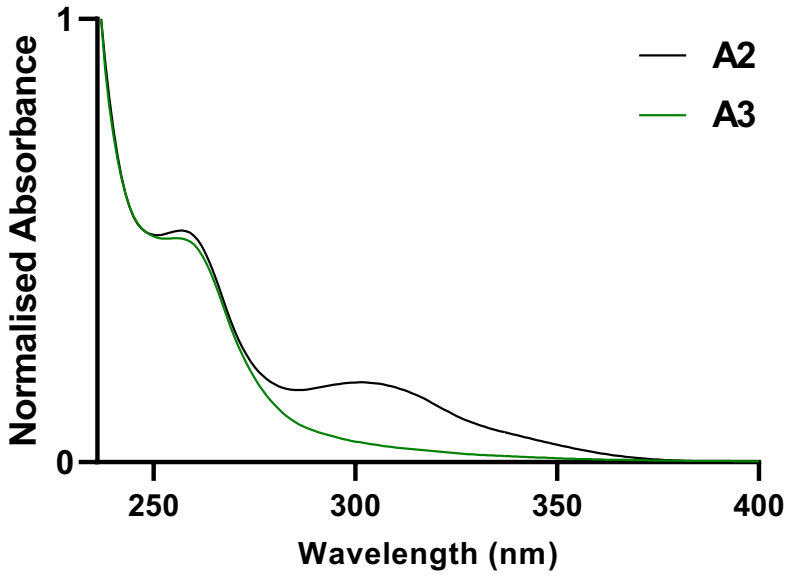

Figure 4-24 UV-Vis spectra of **A2** (black) before end-group modification and the same homopolymer, **A3** after reaction with an excess of AIBN (green).

Following reaction with AIBN the band associated with the π-π* transition of the C=S bond seen covering ca. 280-340 nm absorption is absent, indicating successful end-group modification. SEC traces of both block co-polymers **A2** and **A3** were analysed. Consistent with the poly(PEGMA-*b*-PFPA) end group modification, we observed no significant impact on the molecular weight distribution of the poly(PEGA-*b*-PFPA) copolymer after end-group removal, **Figure 4-25**.

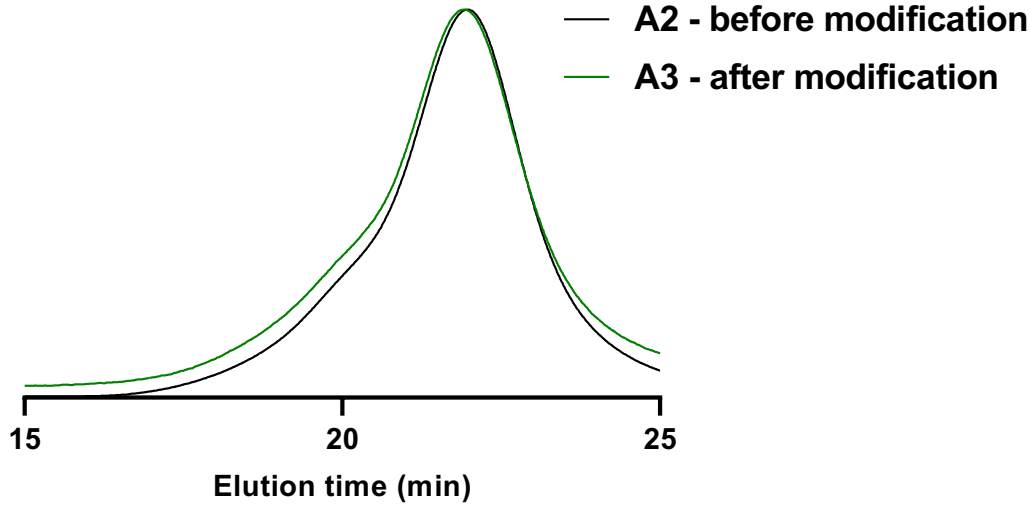

Figure 4-25 SEC traces of **A2** before end-group modification and the same block copolymer, **A3** after reaction with AIBN. For **A3** M_n = 12,500; M_w = 16,000; $Đ$ = 1.27.

4.5.6 Post-functionalisation procedure for the modification of PEGMA/PEGA-PFPA block copolymers with primary amines

Following end-group removal, **M3** and **A3** were modified by the sequential addition of two primary amines (**Scheme 4-6**) and specifically with 5-aminotetrazole ($TetNH_2$) and linear amines with different molecular weights, to synthesise a library of materials with different hydrophilicities.

Specifically, modifications were performed with 5-aminotetrazole ($TetNH_2$) and three primary amines: *n*-octylamine ($OctNH_2$), *n*-decylamine ($DecNH_2$) and *n*-hexadecylamine ($HexadecNH_2$), yielding seven new modified materials containing tetrazole moieties for the complexation of luminescent metal complexes (**Table 4-1**). The amines were introduced in a sequential manner. Typically, the linear amines were introduced first and 5-aminotetrazole second, with the exceptions of **M3-10%tet-90%oct** and the materials

containing *n*-hexadecylamine. In the case of **M3-10%tet-90%oct,** $TetNH_2$ was added first because of the low targeted mol % of 5-aminotetrazole in the target material; in the case of the materials containing *n*-hexadecylamine, $TetNH_2$ was added first because of the steric hindrance of the *n*-hexadecylamine longer chain. The calculated compositions of the materials were found by analysis of ^{19}F NMR signals after the addition of the first amine, as described in Chapter 3.

Table 4-1 Target composition of modified block-copolymers.

Parent copolymer	Linear amine	Target composition [%] $TetNH_2/RNH_2$	Calculated composition [%] $TetNH_2/RNH_2$	Material
M3	*n*-octylamine	40/60	44/66	**M3-40%tet-60%oct**
M3	*n*-octylamine	10/90	10/90	**M3-10%tet-90%oct**
M3	*n*-hexadecylamine	40/60	40/60	**M3-40%tet-60%hexadec**
A3	*n*-decylamine	65/35	63/37	**A3-65%tet-35%dec**
A3	*n*-decylamine	50/50	50/50	**A3-50%tet-50%dec**
A3	*n*-hexadecylamine	90/10	89/11	**A3-90%tet-10%hexdec**
A3	*n*-hexadecylamine	75/25	75/25	**A3-75%tet-25%hexdec**

The acyl substitution reactions were carried out at 40 °C. **Scheme 4-6** shows the general scheme for the acyl substitution of block copolymers **M3** and **A3** with primary amines. All methacrylic copolymers were modified in DMF, while all acrylic copolymers were modified in THF. THF was chosen for convenience, given its lower boiling point. No difference in substitution

efficiency was observed between the two solvents. However, and as expected, the longer amines, such as *n*-hexadecylamine, reacted more slowly due to increasing steric hindrance.

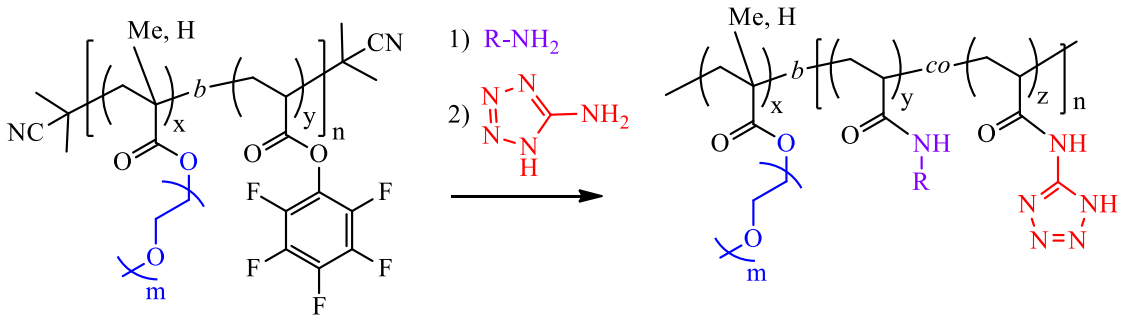

Scheme 4-6 General scheme for the sequential post-functionalisation of block copolymers **M3** and **A3** with primary amines.

As noted previously, the advantage of employing PFPA as a reactive scaffold is that the key nucleophilic acyl substitution reaction between primary amines and the PFP ester groups can be readily monitored by ^{19}F NMR spectroscopy. For example, **Figure 4-26** shows a series of ^{19}F NMR spectra for the modification of **M3** with *n*-octylamine (60 mol % target) and 5-aminotetrazole (40 mol % target) to yield **M3-40%tet-60%oct**. **Figure 4-27** shows a series of ^{19}F NMR spectra for the modification of **A3** with *n*-decylamine (50 mol % target) and 5-aminotetrazole (50 mol % target) to yield **A3-50%tet-50%dec**. Small traces of impurities are present after modification reaction of **A3** with Tet-NH_2 (red spectrum, **Figure 4-27**) due to the presence of triethylamine. The small peaks present in **Figure 4-27**, red trace, are arising from small molecule impurities that we assigned to a mixture of pentafluorophenol and phenolate molecules. Significantly, after dialysis, the small signals disappear, confirming the purification of the materials.

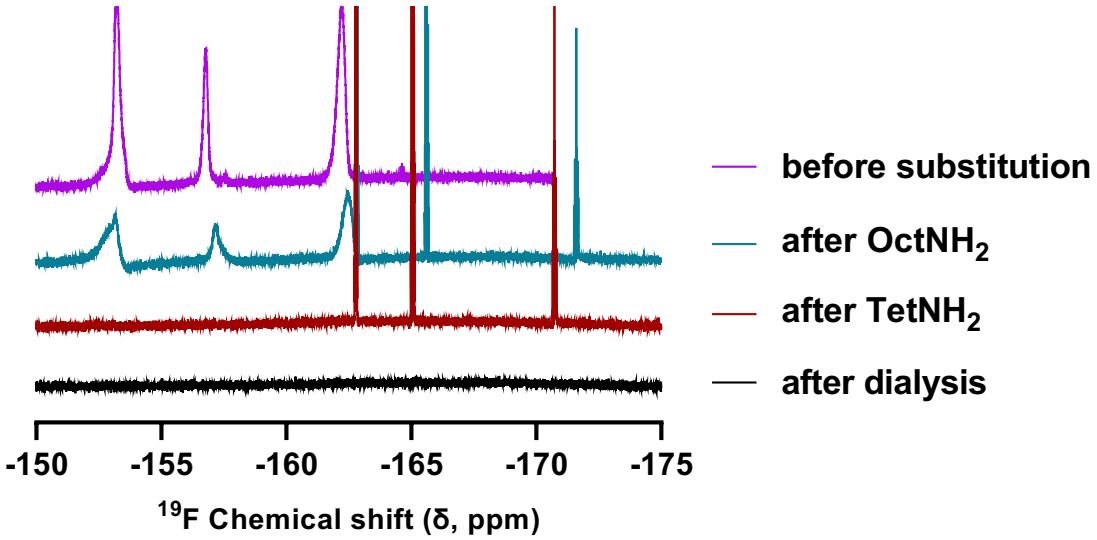

Figure 4-26 ^{19}F NMR spectra, recorded in $CDCl_3$, for the sequential, post-polymerisation modification of **M3** to **M3-40%tet-60%oct** *via* reaction with *n*-octylamine and 5-aminotetrazole.

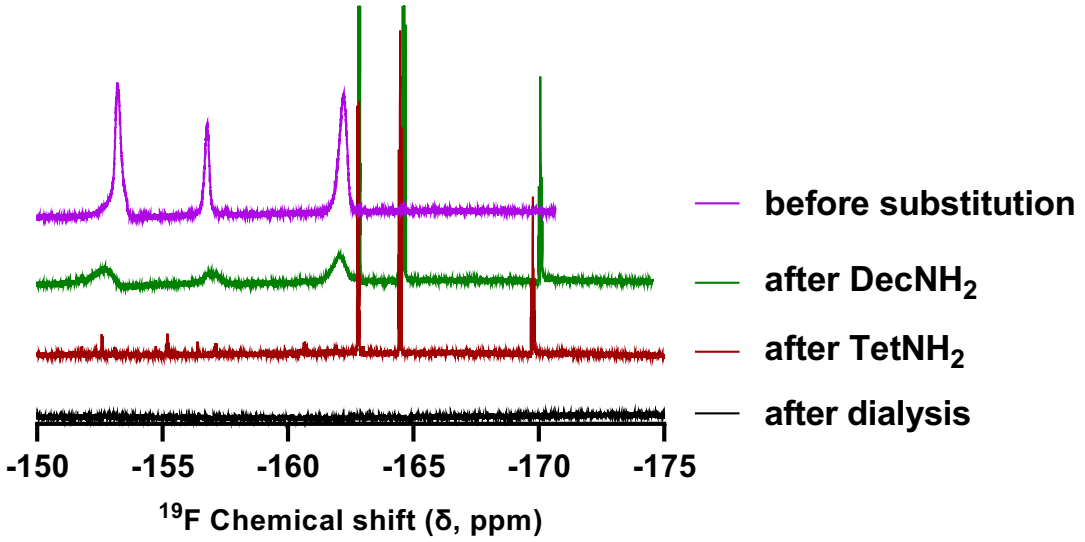

Figure 4-27 ^{19}F NMR spectra, recorded in $CDCl_3$, for the sequential, post-polymerisation modification of **A3** to **A3-50%tet-50%dec** *via* reaction with *n*-decylamine and 5-aminotetrazole.

Prior to chemical modification, **M3** (pink spectrum, **Figure 4-26**) shows the three characteristic signals at δ (ppm) = -152.7 (2 F, *ortho*), -158.1 (1 F, *para*) and -162.5 (2 F, *meta*) consistent with previously reported ^{19}F chemical shifts for polyPFPA.[8] Following reaction with $OctNH_2$ (green spectrum, **Figure 4-26**) these signals decrease in intensity with the concomitant appearance of three sharp resonances associated with pentafluorophenol - small molecule by-product. After subsequent reaction with $TetNH_2$ (red spectrum, **Figure 4-26**), we observed the total disappearance of the signals attributed to polymer-associated pendent PFP functional groups with only those of pentafluorophenol being detected; this confirms successful and quantitative conversion of the pendent PFP groups to the corresponding amide species. Finally, after purification by dialysis (black spectrum, **Figure 4-26**), we observed no detectable signals indicating successful removal of pentafluorophenol from the modified polymer.

Successful modification of the block copolymers **M3** and **A3** was also qualitatively confirmed by FTIR spectroscopy. For example, **Figure 4-28** shows the FTIR spectra of the homopolymer polyPEGA precursor **A1** (top), the block copolymer poly(PEGA-*b*-PFPA) **A2** (middle) and the modified polymer containing 35 mol% decyl acrylamide and 65 mol% *N*-(1*H*-tetrazol-5-yl)acrylamide repeat units **A3-65%tet-45%dec**.

The FTIR results are consistent for all the materials with different compositions. The spectrum of the parent PEG homopolymer **A1** shows the characteristic C=O stretch associated with PEG chains at 1725 cm^{-1} (red dotted line). After copolymerisation with PFPA monomer (**A2**), we can observe the appearance of the characteristic C=O stretch associated with an activated ester at 1785 cm^{-1} (blue dotted line), and the appearance of a band at 1500 cm^{-1} (green

dotted line) associated with C-O ester stretching, both confirming the presence of the PFP moieties in the parent homopolymer. Following sequential modification with $DecNH_2$ and $TetNH_2$ (**A3-65%tet-35%dec**) both the distinguishing ester band associated with PFP moieties, and the band associated with C-O stretching completely disappears, confirming successful, and quantitative, side-chain modification.

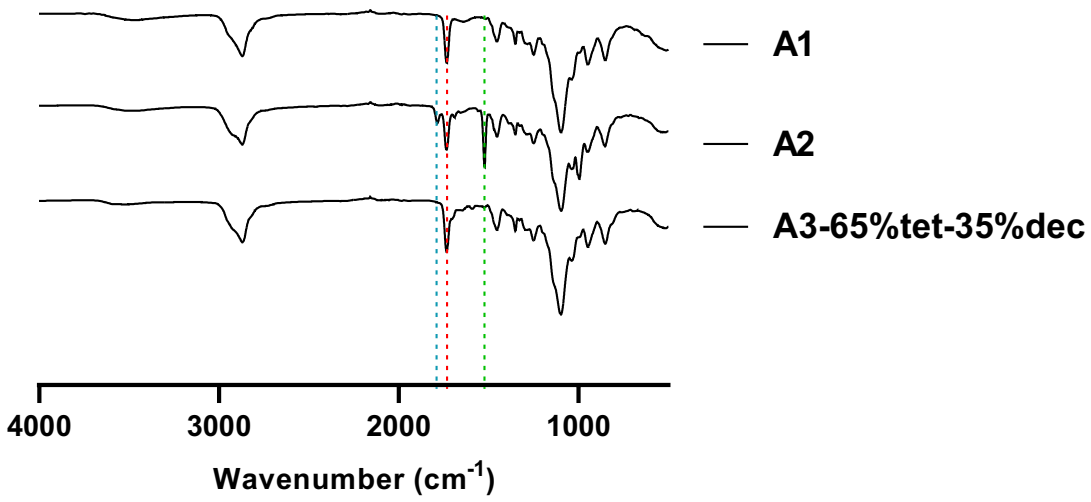

Figure 4-28 FTIR spectra of the homopolymer polyPEGA precursor **A1** (top), the block copolymer poly(PEGA-*b*-PFPA), **A2** (middle), the modified polymer **A3-65%tet-35%dec**, containing 35 mol% decyl acrylamide and 65 mol% *N*-(1*H*-tetrazol-5-yl) acrylamide repeat units.

4.5.7 Synthesis of hybrid polymeric-rhenium(I) luminescent materials

Following successful modification of the parent PEGMA/PEGA-PFPA block copolymers **M3** and **A3** to give a series of seven amide-based block copolymers containing tetrazole and different length functional side groups, each copolymer was further modified by reaction with $Re(CO)_3(phen)Br$; such reactions yielded the target polymer-Re(I) hybrids *via* coordination through the

tetrazole functional groups. The complexation reaction was conducted in DMSO for the methacrylate derivatives and in ethanol/water 3:1 (v/v) for the acrylate copolymers. The solvent was changed for simplicity and no difference in solubility of the materials or reaction rate was observed. After heating at reflux overnight, the desired polymer-metal hybrid materials were obtained by dialysis in methanol for 36 hours, yielding the final rhenium modified materials.

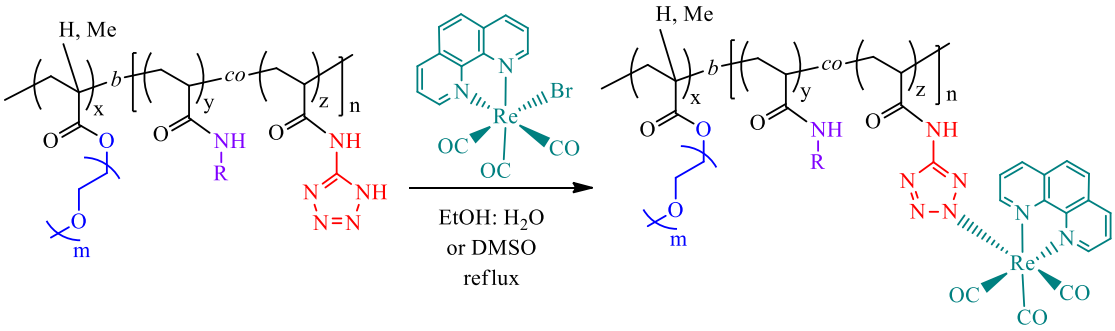

Scheme 4-7 Complexation reaction of **M3** and **A3** modified copolymers with rhenium precursor $Re(CO)_3(phen)Br$ to yield **M3/A3-x%-[Re]**.

In **Scheme 4-7**, the coordination of the Re(I) metal centre to nitrogen atom N2 on the tetrazole is shown for convenience. Successful coordination was confirmed by FTIR spectroscopy, **Figure 4-29** and **Figure 4-30**. For all modified materials **A3/M3-x%-[Re]** we observed the appearance of two new bands at around 2025 and 1915 cm^{-1} associated with the stretch of the carbonyl ligands on the coordinated Re complex (light blue area). Compared to the $Re(CO)_3(phen)Br$ precursor (**Figure 3-16,** Chapter 3) these bands are shifted as a result of the decrease in the electron density at the Re(I) metal centre upon exchange between the bromo and tetrazolato ligand.[13] This observation further

confirms successful coordination of the luminescent Re species to the polymeric scaffold.

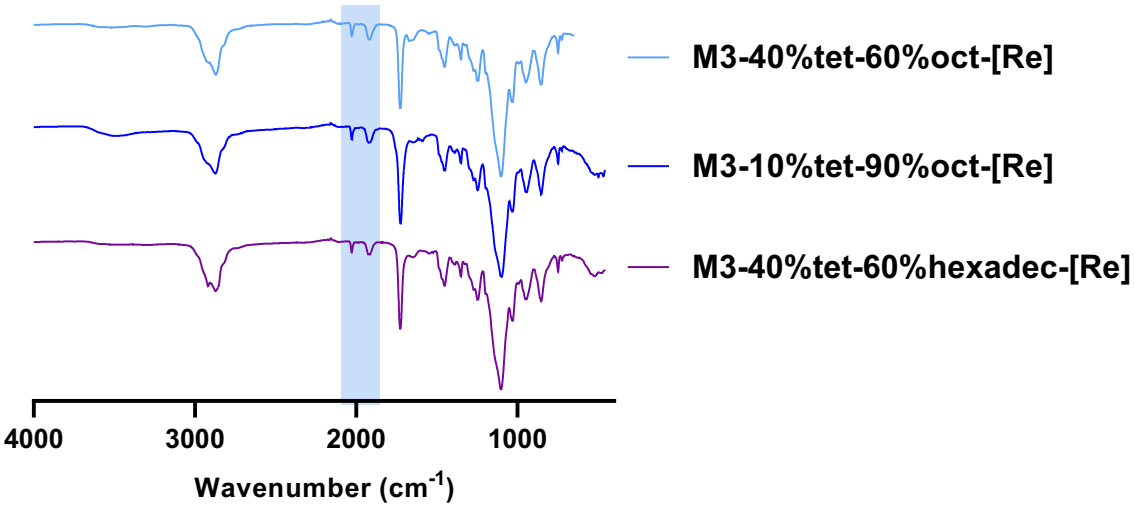

Figure 4-29 FTIR spectra of methacrylate polymeric-Re(I) species. Highlighted in light blue are bands at around 2025 and 1915 cm^{-1} associated with the stretch of the carbonyl ligands on the coordinated Re complex.

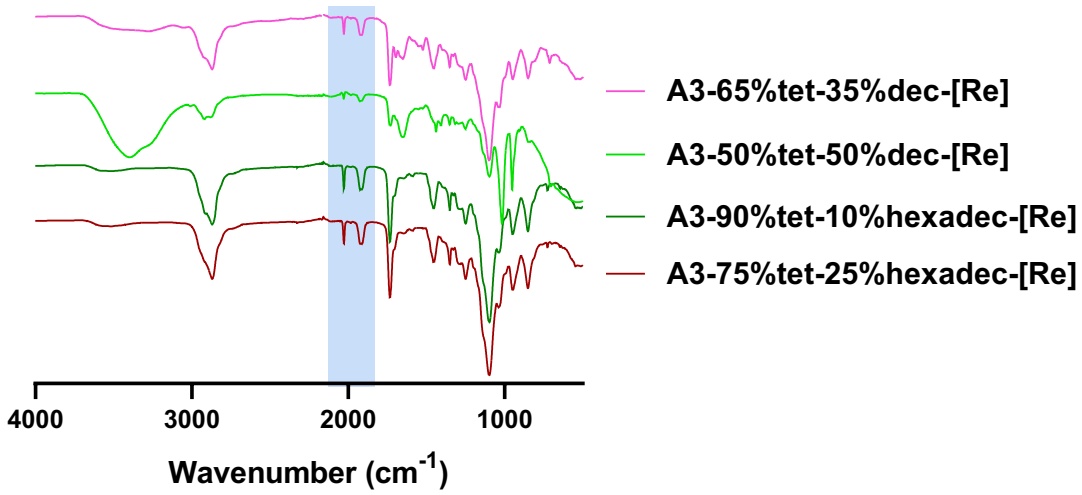

Figure 4-30 FTIR spectra of acrylate polymeric-Re(I) species. Highlighted in light blue are bands at around 2025 and 1915 cm^{-1} associated with the stretch of the carbonyl ligands on the coordinated Re complex.

4.5.8 Photophysical studies of PEG/PFPA copolymer containing luminescent rhenium complexes

Having synthesised the target Re(I) block copolymer hybrid materials, we subsequently performed detailed photophysical studies, **Table 4-2**. The samples for photophysical studies were prepared by dissolving 1 mg of polymeric-rhenium material in 10 mL of spectroscopic grade DMSO.

Table 4-2 Summary of photophysical data for polymer-rhenium materials, **M3/A3-x%-[Re]** in dilute DMSO.

Material	Absorption	Emission						
	λ_{abs}[nm]	λ_{em} [nm]	τ^a [ns]	τ^b [ns]	Φ^a	Φ^b	k_r^b [10^6 s^{-1}]	k_{nr}^b [10^6 s^{-1}]
M3-40%tet-60%oct-[Re]	375, 285	595	172.54	319.36	1.56	2.42	0.076	3.05
M3-10%tet-90%oct-[Re]	375, 285	595	211.49	340.20	0.86	1.15	0.034	2.90
M3-40%tet-60%hexadec-[Re]	375, 285	580	272.16	398.17	1.23	1.62	0.054	3.30
A3-65%tet-35%dec-[Re]	375, 278	592	243.00	360.00	1.26	1.58	0.044	2.73
A3-50%tet-50%dec-[Re]	375, 278	592	304.26	472.34	1.53	2.28	0.048	2.07
A3-90%tet-10%hexdec-[Re]	375, 278	592	297.96	456.96	1.41	2.03	0.044	2.14
A3-75%tet-25%hexdec-[Re]	375, 278	592	285.18	441.24	1.45	2.23	0.050	2.21

[a] Measured from an air-equilibrated solution. [b] Measured from a degassed solution. All solutions contain approximately 1.0 mg of Re(I)-polymers into 10 mL of DMSO. Excitation wavelength = 400 nm for emission measurements. Excitation wavelength = 375 for lifetime measurements.

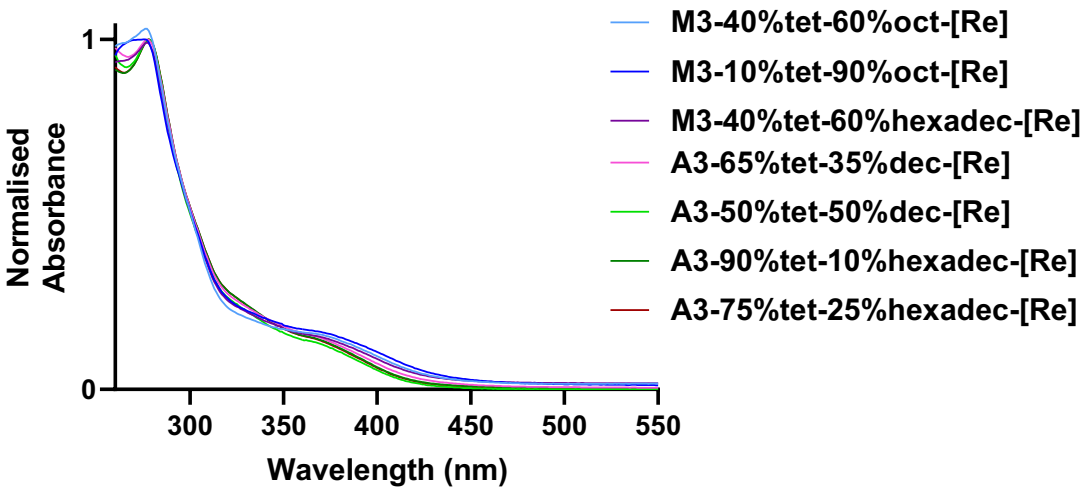

Figure 4-31 Normalised absorption profiles of the **M3/A3-x%-[Re]** copolymers measured in DMSO by dissolving 1 mg of Re-hybrid material in 10 ml of the solvent.

The absorption profiles of all seven Re(I)-polymer hybrid materials were essentially identical, exhibiting a UV region dominated by intense broad bands at $\lambda_{abs} < 300$ nm arising from π–π^* ligand-centred (LC) transitions of the phenanthroline ligands bound to the Re metal centres, **Figure 4-31**. The UV region at wavelengths longer than 350 nm is dominated by broad bands of lower intensity attributed to metal-to-ligand charge transfer transitions typical of Re diimine tetrazolato complexes.

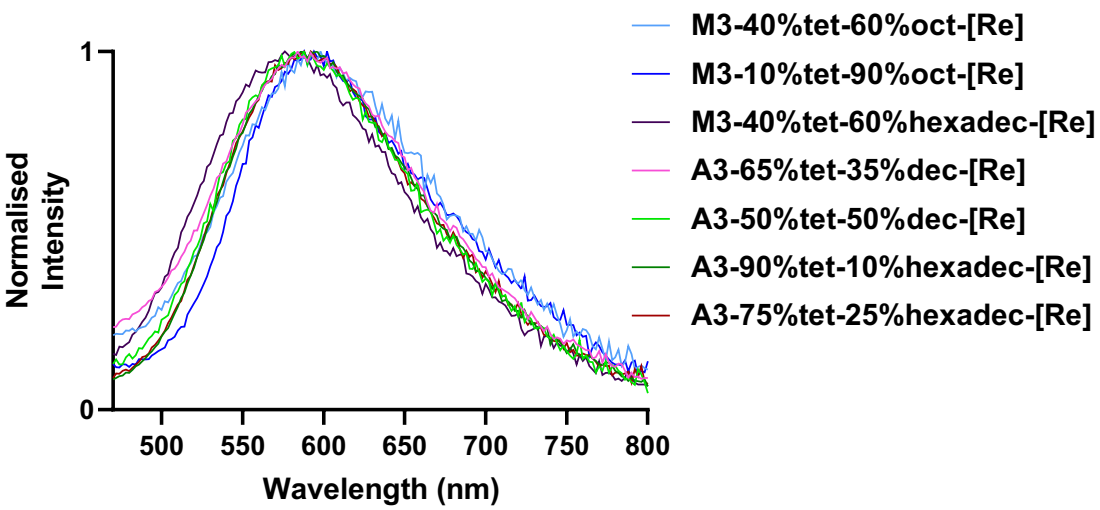

Figure 4-32 Normalised emission profiles of the **M3/A3-x%-[Re]** copolymers measured in DMSO, air-equilibrated samples.

Upon excitation at 400 nm, similar broad emission bands centred between 580 and 595 nm are observed for all hybrid materials, **Figure 4-32**. These bands arise from emission from ^{3}MLCT excited states and are consistent with previously reported tetrazolato-Re(I) complexes.[13]

The triplet spin multiplicity is in agreement with the relatively long excited-state lifetime decays measured to be within the range 172 - 304 ns. In general, we observed shorter lifetimes for methacrylate polymers. For example the lifetime values for **M3-40%tet-60%oct-[Re]** are 172.54 ns and 319.36 ns for air-equilibrated and degassed samples respectively, while the same values for **A3-50%tet-50%dec-[Re]** are 304.26 ns and 472.34 ns.

For all seven Re(I)-hybrid materials the excited state lifetime (τ) and quantum yield (Φ) increase from air-equilibrated to degassed solutions. This behaviour is due to the phosphorescent nature of the emission from the ^{3}MLCT state and its sensitivity to quenching due to the presence of $^3O_2$.[14]

The values of Φ are within the range typical of this kind of neutral Re complexes. The radiative [$k_r = \Phi \cdot \tau^{-1}$] and non-radiative [$k_{nr} = (1-\Phi) \cdot \tau^{-1}$] decay constants, measured in degassed solutions, are reported in **Table 4-2**. In general, we observed slightly longer non-radiative constants for methacrylate hybrid materials. Nevertheless, the values of k_r and k_{nr} can be considered similar for all samples. Significantly, the consistency of k_r and k_{nr}, combined with the similar emission profiles of all seven species, suggested that the distribution and quantity of coordinated Re(I) species has no major effect on the photophysical properties of the polymer-bound luminescent metal species.

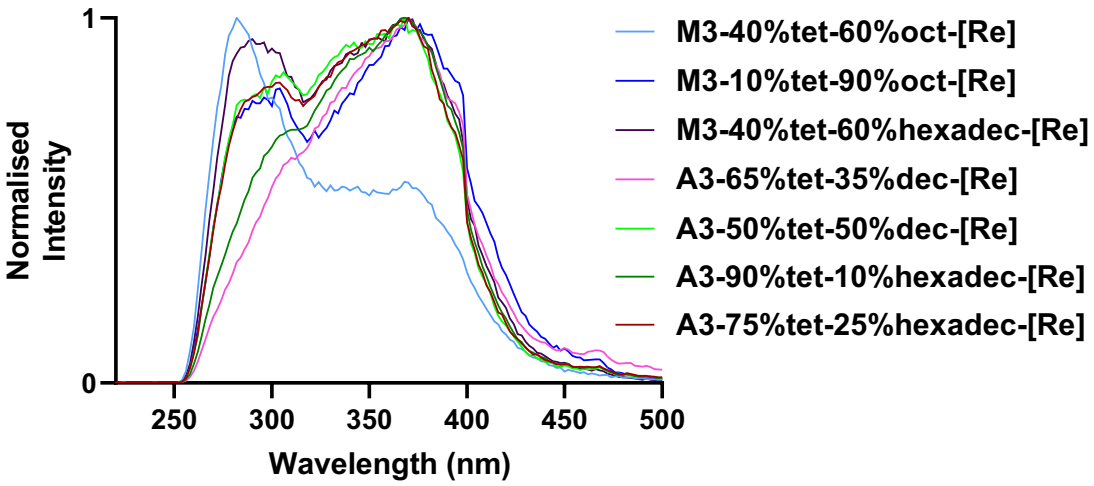

Figure 4-33 Normalised excitation profiles of the **M3/A3-x%-[Re]** copolymers measured in DMSO, air-equilibrated samples.

From the excitation spectra (**Figure 4-33**) we observed that the range of excitation profiles matches the absorption profiles, as expected.

4.5.9 Rodent brain tissues staining

The four acrylate Re-hybrid materials derived from the poly(PEGA-*b*-PFPA) parent copolymer, were examined as probes for the staining of rodent brain tissues (**Figure 4-34** and **Figure 4-35**). The images suggested uptake of the probes into brain tissues and non-specific binding of the Re(I) polymeric luminescent probes in the staining of the tissues was observed.

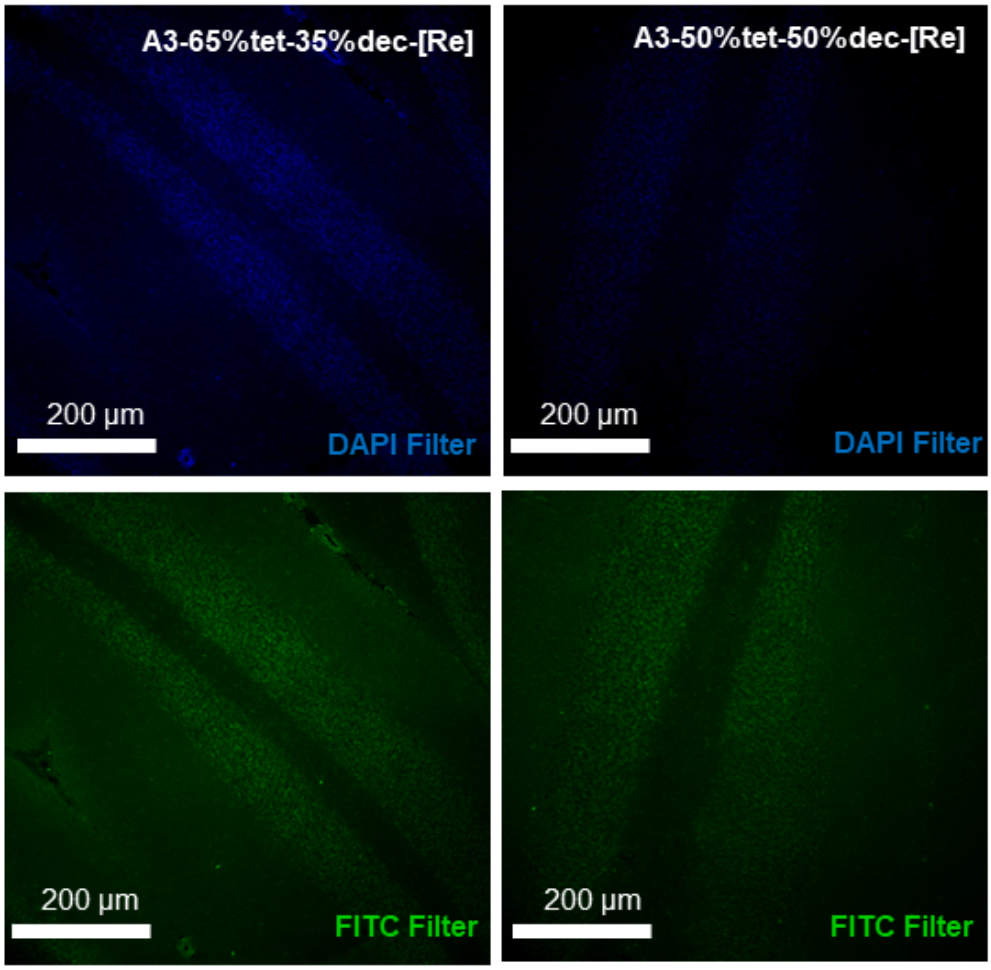

Figure 4-34 Images of rodent brain tissues by employing the materials **A3-65%tet-35%dec-[Re]** and **A3-50%tet-50%dec-[Re]** as luminescent probes.

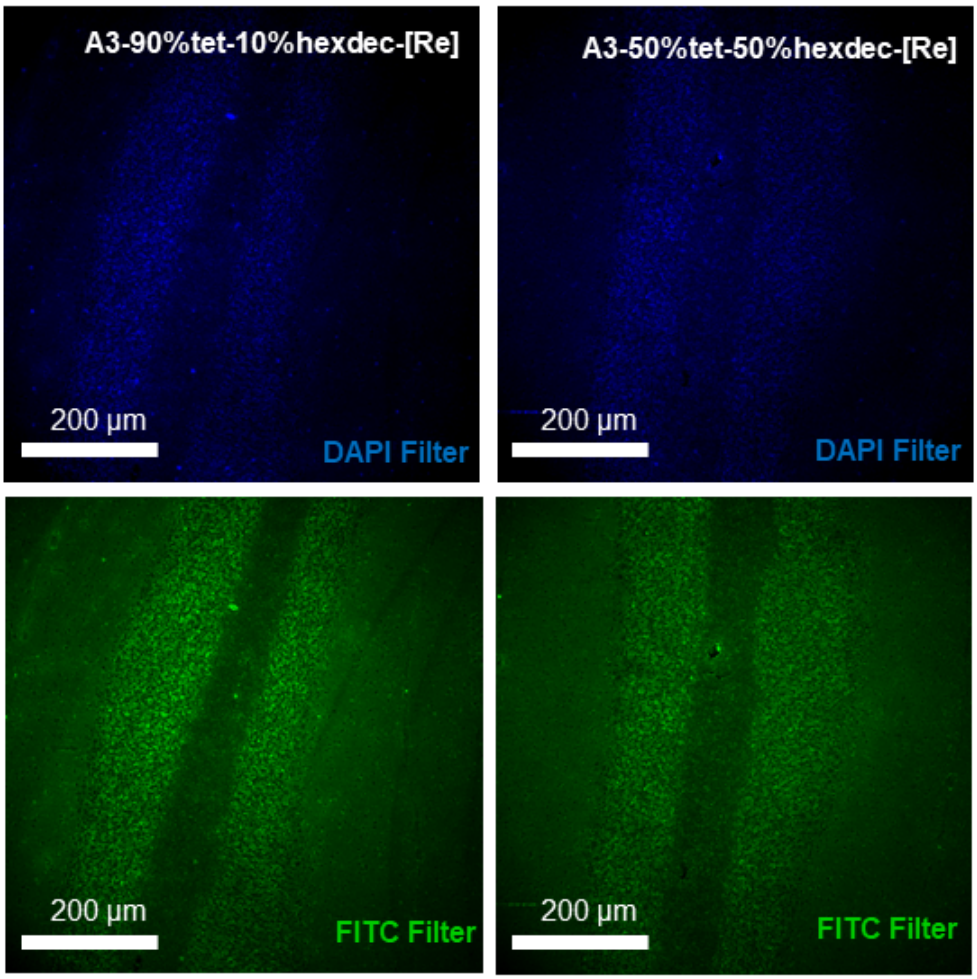

Figure 4-35 Images of rodent brain tissues by employing the materials **A3-90%tet-10%hexadec-[Re]** and **A3-50%tet-50%hexadec-[Re]** as luminescent probes.

4.6 Conclusions

In this Chapter, the RAFT synthesis of well-defined, block copolymers based on PEG/PFP structural motifs containing tetrazolato functional groups was detailed. A total of seven new materials bearing tetrazole functionalities were prepared. The new materials were synthesised by RAFT homopolymerisation of poly(ethylene glycol) methyl ether acrylate or poly(ethylene glycol) methyl ether methacrylate. The

two parent homopolymers were subsequently employed as macro chain transfer agents (CTA) for the block copolymerisation of pentafluorophenyl acrylate. Following block copolymer end-group desulfurisation, the pentafluorophenyl esters in the copolymer backbones were subsequently reacted with 5-aminotetrazole and *n*-octylamine, *n*-decylamine or *n*-hexadecylamine, yielding amide functionalised block copolymers. The synthetic approach to such materials, exploiting the facile reaction between pentafluorophenyl esters and primary amines, was monitored by a combination of ^{19}F NMR and FTIR spectroscopies. The incorporation of poly(ethylene glycol) functionalities yielded materials that are soluble in water, making them excellent candidates for biological application (such as their use as probes for staining of tissues).

Coordination of the seven materials with a luminescent rhenium(I) species was successfully accomplished by the reaction of the tetrazole-functional copolymers with $Re(CO)_3(phen)Br$, and confirmed by FTIR spectroscopy. The absorption and emission profiles of the rhenium-polymer hybrid materials supported successful metal coordination and the luminescent properties of the rhenium species were not affected by direct coordination to a polymeric scaffold. The acrylate Re-hybrid materials have been employed as probes for the staining of rodent brain tissues. The results suggest non-specific binding of the polymeric probes in the staining of tissues.

4.7 References

1. F. M. Veronese and G. Pasut, *Drug Discovery Today*, 2005, **10**, 1451-1458.
2. M. Swierczewska, K. C. Lee and S. Lee, *Expert Opinion on Emerging Drugs*, 2015, **20**, 531-536.
3. S. Dhar, F. X. Gu, R. Langer, O. C. Farokhzad and S. J. Lippard, *Proceedings of the National Academy of Sciences*, 2008, **105**, 17356-17361.
4. S. P.-Y. Li, C. T.-S. Lau, M.-W. Louie, Y.-W. Lam, S. H. Cheng and K. K.-W. Lo, *Biomaterials*, 2013, **34**, 7519-7532.
5. A. M.-H. Yip and K. K.-W. Lo, *Coordination Chemistry Reviews*, 2018, **361**, 138-163.
6. M. Beija, Y. Li, A. B. Lowe, T. P. Davis and C. Boyer, *European Polymer Journal*, 2013, **49**, 3060-3071.
7. H. T. T. Duong, C. P. Marquis, M. Whittaker, T. P. Davis and C. Boyer, *Macromolecules*, 2011, **44**, 8008-8019.
8. P. A. Woodfield, Y. Zhu, Y. Pei and P. J. Roth, *Macromolecules*, 2014, **47**, 750-762.
9. Z. Si, X. Li, X. Li and H. Zhang, *Journal of Organometallic Chemistry*, 2009, **694**, 3742-3748.
10. G. A. Crosby and J. N. Demas, *Journal of Physical Chemistry*, 1971, **75**, 991-1024.
11. D. Hartnell, K. Gillespie-Jones, C. Ciornei, A. Hollings, A. Thomas, E. Harrild, J. Reinhardt, D. J. Paterson, D. Alwis, R. Rajan and M. J. Hackett, *ACS Chemical Neuroscience*, 2020, **11**, 248-257.
12. T. G. McKenzie, L. P. d. M. Costa, Q. Fu, D. E. Dunstan and G. G. Qiao, *Polymer Chemistry*, 2016, **7**, 4246-4253.

13. M. V. Werrett, D. Chartrand, J. D. Gale, G. S. Hanan, J. G. MacLellan, M. Massi, S. Muzzioli, P. Raiteri, B. W. Skelton, M. Silberstein and S. Stagni, *Inorganic Chemistry*, 2011, **50**, 1229-1241.

14. L. A. Casson, S. Muzzioli, P. Raiteri, B. W. Skelton, S. Stagni, M. Massi and D. H. Brown, *Dalton Transactions*, 2011, **40**, 11960-11967.

Chapter 5

Functional copolymers containing iridium and/or rhenium luminescent pendent species: synthesis, properties and application in bioimaging

5.1 Abstract

The well-defined poly(*n*-butyl acrylamide-*co*-*N*-(1*H*-tetrazol-5-yl) acrylamide) copolymers containing tetrazole functionalities described in Chapter 3 were reacted with 12.5 mol% $[Ir_2(ppy)_4(\mu\text{-}Cl)_2]$, where ppy = 2-phenylpyridine, based on tetrazole residues. This resulted in the introduction of the luminescent $[Ir(ppy)_2]^+$ fragment *via* coordination to two polymer-bound pendent tetrazole functional groups. Two additional samples containing 50 mol% Ir species were also prepared, for a total of three Ir functionalised materials with different compositions. Successful coordination of the $[Ir(ppy)_2]^+$ fragment to the polymeric backbone was quantitatively assessed from a calibration curve established from the small molecule analogue $[Ir(ppy)_2(PhTz)_2][NEt_4]$ (where PhTz = 5-phenyltetrazolate). The photophysical properties of the Ir-functionalised materials were investigated, confirming the attachment of the iridium fragments to the materials and the formation of a negatively charged, polymer-bound iridium luminescent species. Finally, the functionalised polymer with 12.5 mol% Ir species was further modified with a second luminescent metal species, $Re(CO)_3(phen)Br$, to yield hybrid metal Ir/Re copolymers with 6.25, 12.5 and 25 mol% Re fragments for a fixed Ir content.

The photophysical properties of the luminescent functionalised materials containing both iridium and rhenium were investigated and confirmed the attachment of both metal fragments. Interestingly, the photophysical results of the materials containing Ir and Re species indicated energy transfer phenomena occurring from Ir to Re metal centres.

5.2 Introduction

Octahedral d^6 metal complexes, such as cyclometalated Ir(III) derivatives and Re(I) tricarbonyl diimine complexes, have been studied extensively due to their outstanding photophysical properties in a wide variety of applications in the fields of material and life sciences.[1-3] The luminescent properties of these metal complexes arise from triplet metal-to-ligand charge transfer (^{3}MLCT). The phosphorescent nature of this type of emission confers exceptional properties to this class of metal complexes compared to organic fluorophores, such as large Stokes shifts and longer excited state lifetimes (τ). Fine-tuning of the chemical and photophysical properties is achievable upon variation of coordinated ligands. In particular, Massi's group has studied Re(I) tricarbonyl diimine complexes with different tetrazolate ligands which have shown promising results for applications in biology given their affinity for lipid droplets, in the targeting of metal cations, in the luminescent staining of proteins and for studies of interaction with bovine serum albumin (BSA).[4-7]

Cyclometalated Ir(III) complexes containing tetrazolate ligands have shown their ability for localisation towards specific organelles by functionalisation of the coordinated ligands. For instance, cationic Ir(III) tetrazolato complexes have been reported to localise in mitochondria and the endoplasmatic reticulum.[8] More recently,

examples of cationic and neutral Ir(III) tetrazolato complexes have found application as antimicrobial agents and in the luminescent bio-imaging of living bacteria.[9, 10]

Expanding on our previous work on tetrazole-functional polymers containing luminescent Re fragments described in Chapters 2, 3 and 4, we extended our investigation to the synthesis and photophysical properties of acrylamido-based tetrazole (co)polymers containing luminescent Ir(III) metal species and hybrid (co)polymers containing both Re(I) and Ir(III).

5.3 Experimental

5.3.1 Materials

All reagents were purchased from the Sigma-Aldrich Chemical Company, or Alfa Aesar, at the highest available purity and used as received unless noted otherwise. $Re(CO)_3(phen)Br$ and $[Ir_2(ppy)_4(\mu\text{-}Cl)_2]$ were prepared according to previously published procedures.[11,12]

5.3.2 FTIR Analysis

Infrared spectra (4000-650 cm^{-1}) were recorded on solid-state samples using attenuated total reflectance on a Perkin Elmer Spectrum Two and Spectrum 100 FT-IR.

5.3.3 Photophysical Measurements

Absorption spectra were recorded at room temperature using a Perkin Elmer Lambda 35 UV/Vis spectrometer. Uncorrected steady-state emission spectra were recorded using an Edinburgh FLSP980-stm spectrometer equipped with a 450 W xenon arc lamp and emission monochromators, a Peltier cooled Hamamatsu R928P photomultiplier (180-850 nm) and a Hamamatsu R5509-42

photomultiplier for detection of NIR radiation (800-1400 nm). Emission and excitation spectra were corrected for source intensity (amp and grating) and emission spectral response (detector and grating) by a calibration curve supplied with the instrument. Luminescent quantum yields were measured from absorption spectra on a wavelength scale (nm) and compared to the reference emitter by **Equation 5-1**:

$$\Phi_x = \Phi_r \left[\frac{A_r(\lambda_r)}{A_x(\lambda_x)}\right]\left[\frac{I_r(\lambda_r)}{I_x(\lambda_x)}\right]\left[\frac{n_x^2}{n_r^2}\right]\left[\frac{D_x}{D_r}\right] \qquad \textbf{Equation 5-1}$$

where A is the absorbance at the excitation wavelength λ, I is the intensity of the excitation light at the excitation wavelength, n is the refractive index of the solvent, D is the integrated intensity of the luminescence and Φ is the quantum yield. The subscripts r and x refer to the reference and the sample. The quantum yields of complexes were measured against quinine sulphate solution in 0.5 M H_2SO_4.[13] Excited-state decays (τ) were recorded on the same Edinburgh FLSP980-stm spectrometer using pulsed picosecond light emitting diodes (LEDs) (EPLED/EPL 375 nm, FHWM < 800 ps). The goodness of fit was assessed by minimising the reduced χ^2 function and by visual inspection of the weighted residuals. The solvent used (DMSO) in the preparation of the solutions for the photophysical investigations was of spectrometric grade.

5.3.4 Tissue Preparation and Staining

Rodent brain tissue was generated from excess sham operated (10 - 12 weeks old) male Sprague Dawley rats from a previously published traumatic brain injury study.[14] Animal tissue was generated with approval from Monash University Standing Committee on Ethics in Animal Experimentation. Coronal brain tissue sections (10 μm thick) containing cerebellum, were cut on a cryo-microtome (-18 °C) and transferred to glass slides, allowed to air dry and then stored at room temperature.

Tissue sections were then fixed in paraformaldehyde (4% in phosphate buffered saline (PBS)) for 10 minutes. The slides were then washed for 10 minutes with PBS. Slides were then stained with the polymeric probe containing solution (100 μg/mL in DMSO, 200 μL per tissue section) and incubated for 30 minutes at room temperature. The probe containing solution was then washed from the slides with deionised water and then washed in PBS for 10 minutes. Slides were then further rinsed with deionised water and allowed to dry at room temperature and imaged.

5.3.5 Imaging

Fluorescence microscopy was conducted on a Nikon Ti2-U inverted microscope with a DS-Qi2 camera, pE-300^{white} LED fluorescence lamp and NIS Elements standard software. Images were gathered at an exposure time of 500 ms and an analog gain of 7.6%. Images were processed in ImageJ.

5.4 Synthesis

$[Ir(ppy)_2(PhTz)_2][NEt_4]$ (where PhTz = 5-phenyltetrazolate) was synthesised by following a published procedure.[12] The targeted anionic Ir(III) polymeric materials have been synthesised by adapting the same procedure.

5.4.1 Complexation of $[Ir_2(ppy)_4(\mu\text{-}Cl)_2]$ to a tetrazole functional copolymer

5.4.1.1 Synthesis of P2-45%-Ir12%

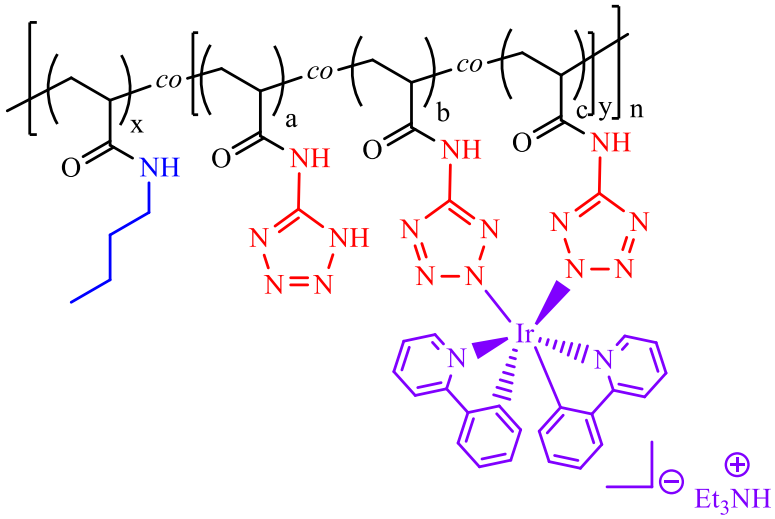

Figure 5-1 Structure of iridium functionalised **P2-45%-Ir12%**.

To a round-bottomed flask equipped with a magnetic stir bar was added copolymer containing 55 mol% *n*-butyl acrylamide and 45 % *N*-(1*H*-tetrazol-5-yl)acrylamide (**P2-45%**) repeat units (0.050 g) to a solution containing 6.00 mL of dichloromethane and 2.0 mL of ethanol. Dichlorobridged iridium dimer $[Ir_2(ppy)_4(\mu\text{-}Cl)_2]$, (0.005 g) and 2 equivalents of triethylamine, with respect to the % of tetrazole functionalities present on the polymer (0.01 mL) were then added to the solution. The resulting mixture was stirred at reflux for 24 hours. Subsequently, the solvents were

removed on a rotary evaporator and the resulting solids were re-dissolved in dichloromethane. The modified copolymer was obtained by precipitation in cold *n*-pentane. The product was collected as a bright yellow solid by Buchner filtration (0.04 g).

The iridium-functionalised polymers **P2-45%-Ir50%** and **P2-24%-Ir50%** were synthesised following the same procedure, but with differing amounts of polymeric materials and Ir precursor. In the case of **P2-45%-Ir50%**, polymeric material containing 55 mol% *n*-butyl acrylamide and 45 % *N*-(1*H*-tetrazol-5-yl)acrylamide (**P2-45%**) repeat units (0.016 g) dichlorobridged iridium dimer $[Ir_2(ppy)_4(\mu\text{-}Cl)_2]$ (0.006 g) were employed and 0.018 g of **P2-24%-Ir50%** was obtained. For the synthesis of **P2-24%-Ir50%**, polymeric material containing 76 mol% *n*-butyl acrylamide and 24 % *N*-(1*H*-tetrazol-5-yl)acrylamide (**P2-24%**) repeat units (0.032 g) and dichlorobridged iridium dimer $[Ir_2(ppy)_4(\mu\text{-}Cl)_2]$ (0.006 g) were employed and 0.025 g of **P2-24%-Ir50%** was obtained.

5.4.2 Complexation of $Re(CO)_3(phen)Br$ to a tetrazole functional copolymer containing Ir(III)

5.4.2.1 Synthesis of P2-45%-Ir12%-Re12%.

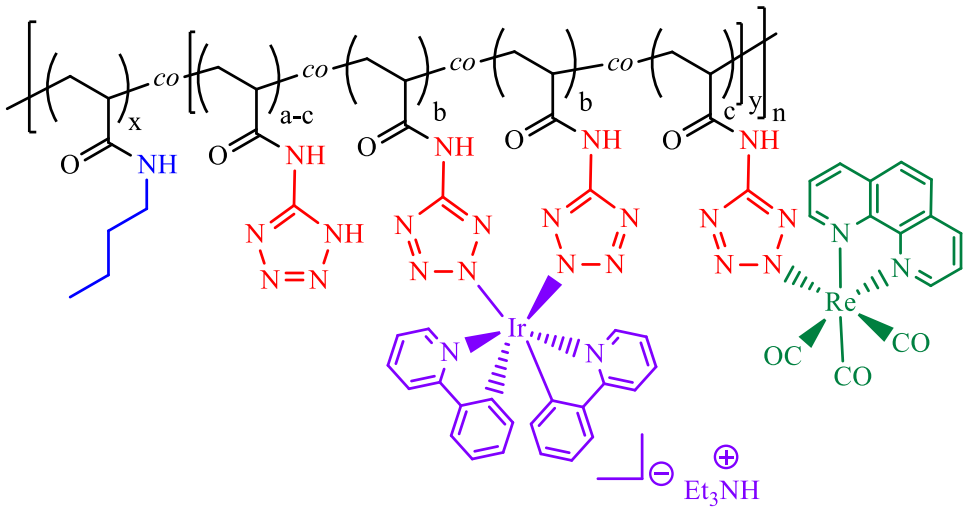

Figure 5-2 Structure of iridium and rhenium functionalised **P2-45%-Ir12%-Re12%**.

P2-45%-Ir12% (0.030 g) was added to a solution containing 6.00 mL of dichloromethane and 2.00 mL of ethanol. $Re(CO)_3(phen)Br$ (0.006 g) and 2 equivalents of triethylamine, with respect to the % of tetrazole functionalities present on the polymer (0.01 mL), were then added to the solution. The resulting mixture was stirred at reflux for 24 hours. The solvents were subsequently removed by rotary evaporation and the solids were re-dissolved in dichloromethane. The targeted material was obtained by precipitation in cold *n*-pentane. The product **P2-45%-Ir12%-Re12%** was collected as a bright yellow solid by Buchner filtration (0.021 g).

The iridium- and rhenium-functionalised polymers **P2-45%-Ir12%-Re25%** and **P2-45%-Ir12%-Re6%** were synthesised following the same procedure, but with different amounts of Ir-containing polymer and Re precursor. In the case of **P2-45%-Ir12%-Re25%, P2-45%-Ir12%** (0.025 g) was reacted with $Re(CO)_3(phen)Br$ (0.010 g) and 0.019 g of **P2-45%-Ir12%-Re25%** was obtained. In the case of **P2-45%-Ir12%-Re6%, P2-45%-Ir12%** (0.025 g) was reacted with $Re(CO)_3(phen)Br$ (0.002 g) and 0.012 g of **P2-45%-Ir12%-Re6%** was obtained.

5.5 Results and Discussion

5.5.1 Complexation of $[Ir_2(ppy)_4(\mu\text{-}Cl)_2]$ to a tetrazole functional copolymer

The synthesis of the polymeric materials was detailed in Chapter 3. Two tetrazole-functionalised copolymers described in Chapter 3 were employed as macromolecular ligands for the complexation with an iridium species. Specifically, polymeric material containing 76 mol% *n*-butyl acrylamide and 24% *N*-(1*H*-tetrazol-5-yl)acrylamide (**P2-24%**) repeat units and copolymer containing 55 mol% *n*-butyl acrylamide and 45% *N*-(1*H*-tetrazol-5-yl)acrylamide (**P2-45%**) repeat units were employed for complexation with the dichlorobridged iridium dimer $[Ir_2(ppy)_4(\mu\text{-}Cl)_2]$.

The tetrazole functional copolymers were used as macromolecular bidentate ligands capable of binding complex fragments of iridium, resulting in the synthesis of negatively charged polymer-Ir hybrid materials. Unlike the Re modified copolymers described in Chapters 2-4, the Ir fragment is attached by complexation to two polymer-bond tetrazole groups. The complexation reaction (**Scheme 5-1**) was conducted in ethanol/DCM 1:3 (v/v) with Et_3N. After heating at reflux overnight, the desired polymer-metal hybrid materials were obtained by precipitation in cold *n*-pentane. Three hybrid materials with different tetrazole compositions and iridium content were synthesised. **P2-45%** was used

for the complexation of two materials targeting 50 mol% and 12.5 mol% $[Ir_2(ppy)_4(\mu\text{-}Cl)_2]$, yielding **P2-45%-Ir50%** and **P2-45%-Ir12%**. **P2-24%** was employed for the complexation of two materials targeting 50 mol% $[Ir_2(ppy)_4(\mu\text{-}Cl)_2]$, yielding **P2-24%-Ir50%**.

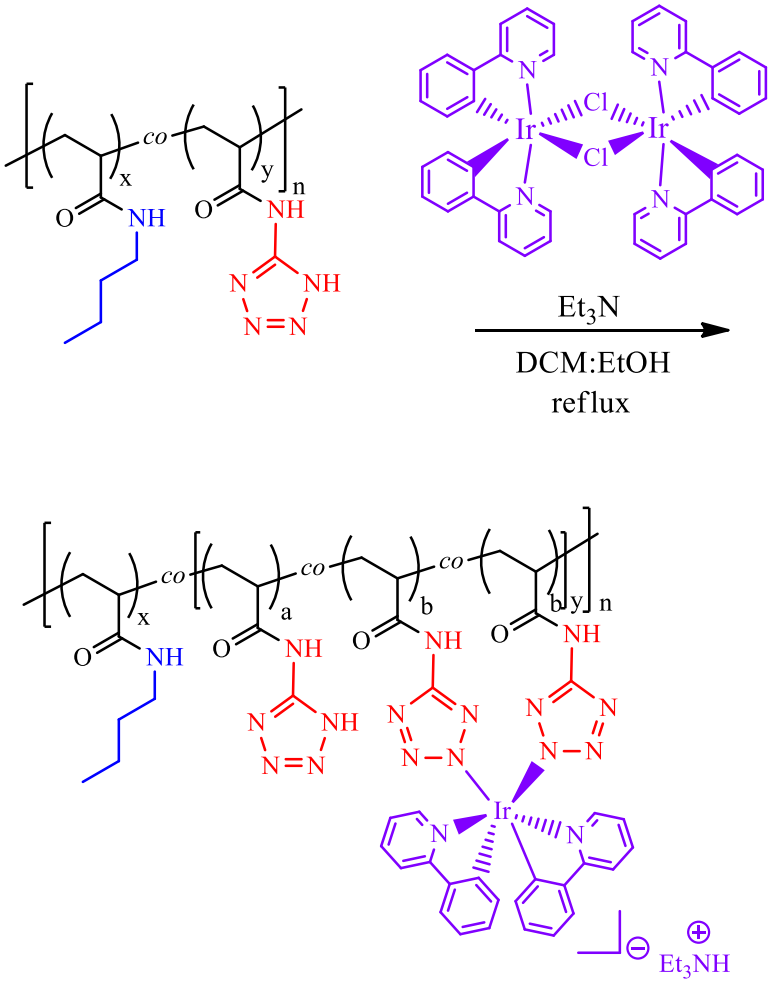

Scheme 5-1 Complexation reaction of **P2-*x*%** with the iridium dichlorobridged precursor $[Ir_2(ppy)_4(\mu\text{-}Cl)_2]$ yielding **P2-*x*%-Ir*x*%**. Coordination to the N2 nitrogen atom on the tetrazole ring is shown for convenience.

The amount of attached iridium was assessed with a calibration curve obtained by preparing five samples of known concentration of the small molecule

$[Ir(ppy)_2(PhTz)_2][NEt_4]$ and measuring their absorbance at 400 nm (**Figure 5-3**). Samples of the hybrid copolymers containing the iridium fragments were prepared by dissolving 1 mg of copolymer in DMSO and the absorbance measured at 400 nm. From the calibration curve, we found the concentration of iridium in the materials. The values are reported in **Table 5-1**. The resulting concentration contents of iridium in the polymeric materials were consistent with the targeted amount.

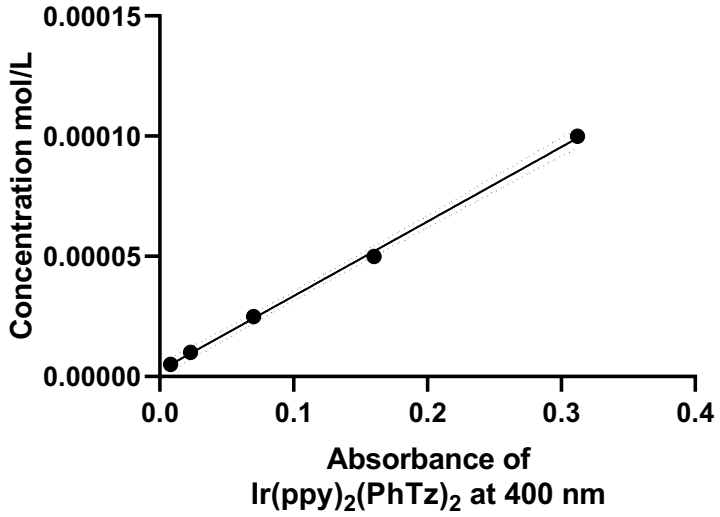

Figure 5-3 Calibration curve of concentration of $[Ir(ppy)_2(PhTz)_2][NEt_4]$ vs absorbance measured at 400 nm.

Table 5-1. Concentration values of the iridium containing materials, as determined by the above calibration curve.

Polymer	Concentration (10^{-5} M)
P2-45%-Ir50%	3.2
P2-24%-Ir50%	2.6
P2-45%-Ir12%	1.4

Successful coordination of the iridium fragments to the tetrazole functional groups of the copolymeric materials was assessed from the emission profile of the luminescent hybrid materials. Detailed photophysical studies of the materials will be described in **Section 5.5.3**. While the iridium dimer precursor is not luminescent, we observed emission arising from the copolymers containing iridium species (**Figure 5-4**). Using the emission profile of the small molecule $[Ir(ppy)_2(PhTz)_2][NEt_4]$ as a reference, we observed nearly identical emission profiles from the hybrid copolymers, with maxima at 495 and 522 nm for all three iridium-containing materials as well as the reference compound.

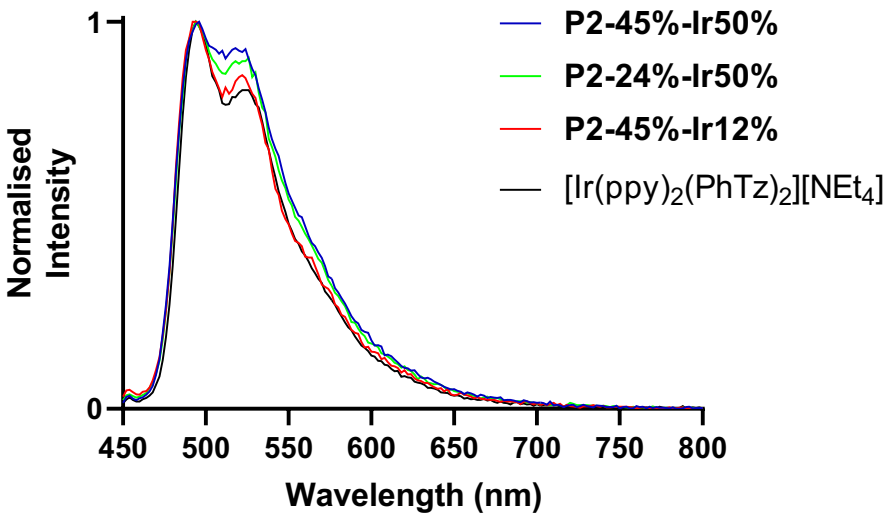

Figure 5-4 Normalised emission profiles of the iridium-containing copolymers **P2-45%-Ir50%**, **P2-24%-Ir50%**, **P2-45%-Ir12%** and the small molecule reference compound $[Ir(ppy)_2(PhTz)_2][NEt_4]$ in air-equilibrated, dilute DMSO. The emission spectra were recorded upon excitation at 400 nm.

The emission profiles of the Ir-modified copolymers are entirely consistent with the literature value for the emission profile of $[Ir(ppy)_2(PhTz)_2][NEt_4]$, confirming the coordination of iridium fragments into the tetrazole functionalised polymers, where the iridium complex appears to be negatively charged, as expected.[12] The emission band appears to be structured, with two emission maxima associated with the two types of emissive excited states. The structured nature of the emission is representative for the interplay ^{3}LC/^{3}MLCT type emissive excited state which has been previously observed for this type of Ir(III) complexes.[12]

5.5.2 Complexation of $Re(CO)_3(phen)Br$ to a tetrazole functional copolymer containing Ir(III)

The functionalised polymer **P2-45%-Ir12%** with 12.5 mol% Ir species was further modified with a second luminescent metal species, $Re(CO)_3(phen)Br$, to yield three new hybrid Ir/Re copolymers with 6.25, 12.5 and 25 mol% Re fragments for a fixed Ir content.

The complexation reaction (**Scheme 5-2**) was conducted in ethanol/DCM 1:3 (v/v) in the presence of Et_3N. After heating at reflux overnight, the desired polymer-metal hybrid materials were obtained by precipitation in cold *n*-pentane.

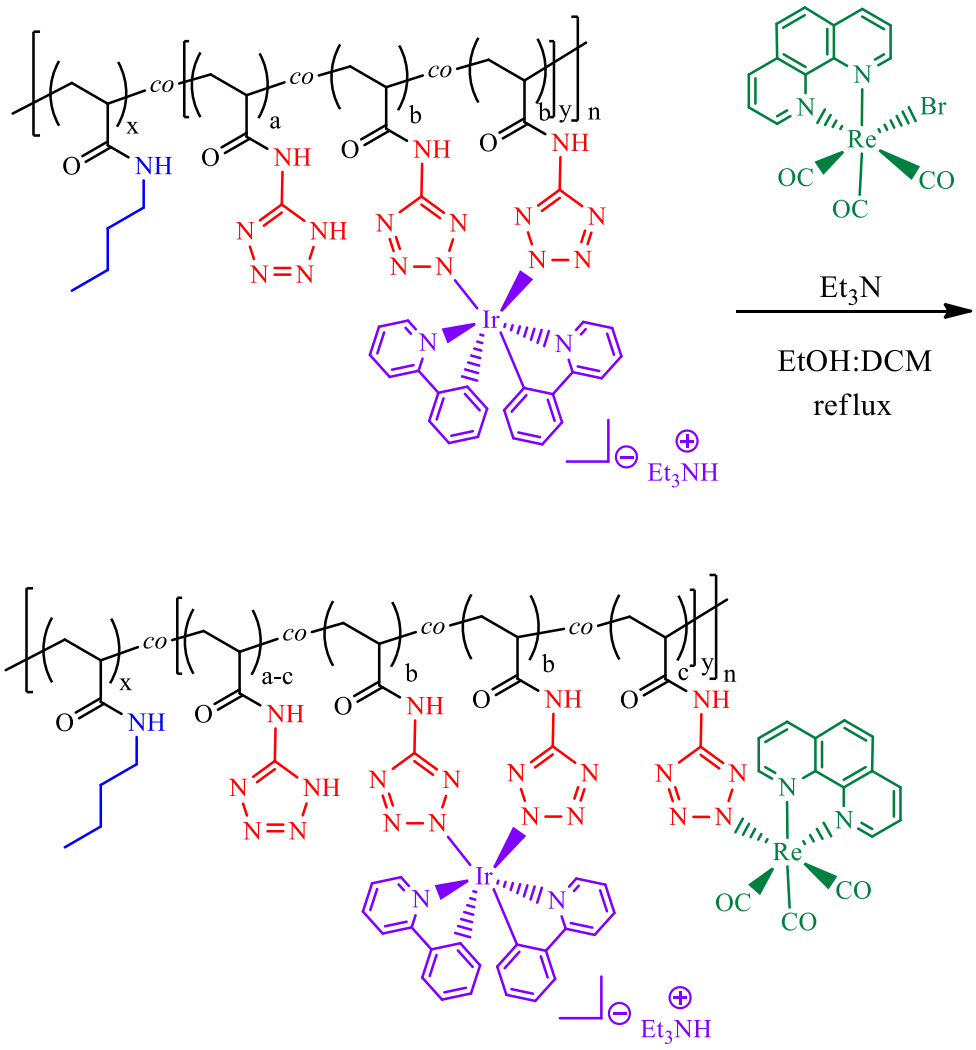

Scheme 5-2 Complexation reaction of **P2-45%-Ir12%** with rhenium precursor $Re(CO)_3(phen)Br$ to give **P2-45%-Ir12%-Re*x*%**. Coordination to the N2 nitrogen atom on the tetrazole ring is shown for convenience.

Qualitative confirmation of successful metal attachment can be seen visually by irradiating the polymer hybrids with long wavelength UV light. For example, **Figure 5-5** shows digital pictures of three polymer samples under irradiation at 365 nm. On the right is a poly(*n*-butyl acrylamide-*co*-*N*-(1*H*-tetrazol-5-yl) acrylamide) copolymer **P2-45%-Ir50%** containing 45 mol% tetrazole repeat units with a targeted 50 mol% of coordinated $[Ir(ppy)_2]^+$ fragment, and appears bright green.

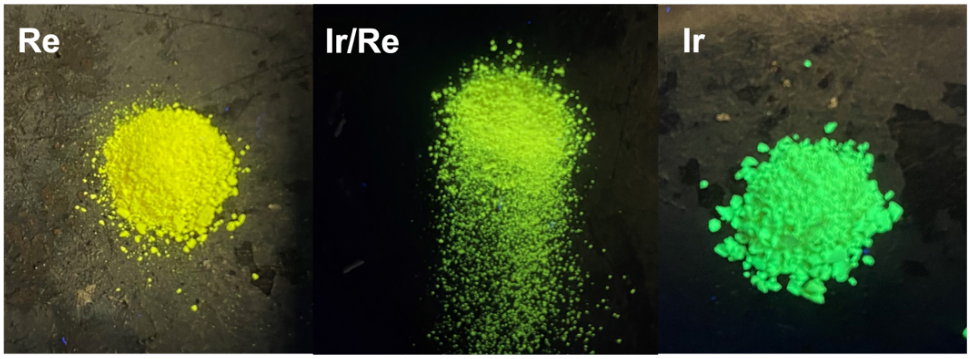

Figure 5-5 Digital images of materials containing Re, Ir and Re/Ir metals. From left to right: **P2-45%-[Re]**, **P2-45%-Ir12%-Re12%** and **P2-45%-Ir50%**.

The middle picture is **P2-45%-Ir12%-Re12%**, containing both metal species. For comparative purposes, we have included a picture of the poly(*n*-butyl acrylamide-*co*-*N*-(1*H*-tetrazol-5-yl) acrylamide) copolymer **P2-45%-[Re]**, containing 45 mol% tetrazole repeat units coordinated to $Re(CO)_3(phen)^+$ (left), to highlight its distinctive yellow colour under irradiation.

Due to the overlap of the absorbance of the rhenium fragments with the absorbance of the iridium fragments, it was not possible to evaluate the rhenium content attached to the materials as we did for the materials containing iridium only. Nevertheless, we could assess the presence of luminescent rhenium metal complex on the polymers by the appearance of a broad band in the emission profile of the hybrid materials containing both metals (discussed in **Section 5.5.4**).

5.5.3 Photophysical studies of copolymers containing iridium

In all syntheses, the cationic fragment $[Ir(ppy)_2]^+$ was introduced onto the polymeric scaffold prior to the attachment of the $Re(CO)_3(phen)^+$ species. To confirm that chelation to the polymeric scaffold did not impact the photophysical properties of the metal species, we first examined the

photophysics of the copolymers containing only the bound $[Ir(ppy)_2]^+$ fragment and compared them to the model small molecule complex $[Ir(ppy)_2(PhTz)_2][NEt_4]$.The photophysical data for the materials containing iridium complexes **P2-45%-Ir50%**, **P2-24%-Ir50%**, **P2-45%-Ir12%**, are listed in **Table 5-2**. All solutions for photophysical measurements were prepared by dissolving 1 mg of material in 10 mL of DMSO.

At room temperature, the anionic Ir(III)-hybrid polymeric materials exhibit similar absorption profiles (**Figure 5-6**), with intense ligand centre (LC) transitions up to 300 nm and bands arising from metal-to-ligand charge transfer (MLCT) above 350 nm.

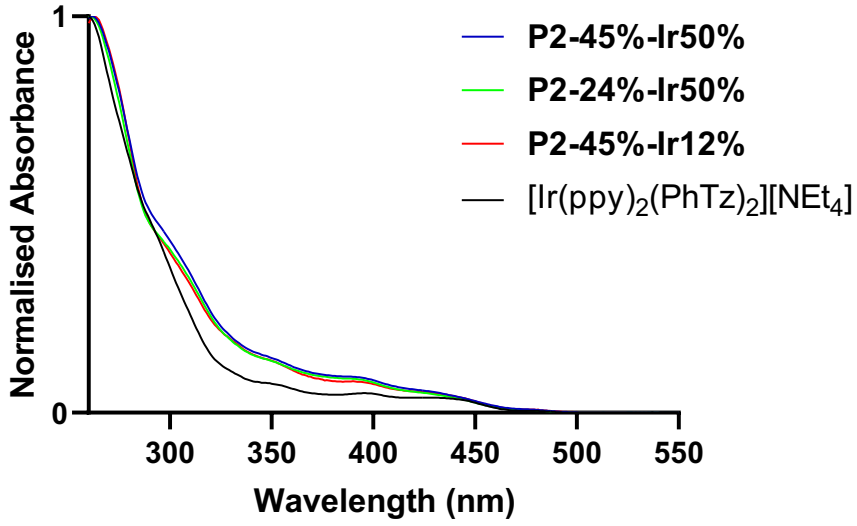

Figure 5-6 Normalised absorption profiles of iridium-containing materials **P2-45%-Ir50%**, **P2-24%-Ir50%**, **P2-45%-Ir12%** and $[Ir(ppy)_2(PhTz)_2][NEt_4]$ in air-equilibrated, dilute DMSO. The emission spectra were recorded upon excitation at 400 nm.

Comparison with the small molecule complex $[Ir(ppy)_2(PhTz)_2][NEt_4]$ indicates that the hybrid copolymers have similar absorption profiles. Upon excitation at 400 nm, the anionic Ir(III)-hybrid materials gave rise to strongly structured blue emission profiles with maxima at 495 and 522 nm, and are ascribed to an admixture of ^{3}LC/^{3}MLCT emissive excited states (**Figure 5-4**). Comparison of emission profile between the three iridium-hybrid materials **P2-45%-Ir50%**, **P2-24%-Ir50%**, **P2-45%-Ir12%** and the small molecule analogue $[Ir(ppy)_2(PhTz)_2][NEt_4]$ suggests coordination of the materials to two tetrazole moieties on the polymeric chain, giving rise to a new class of luminescent anionic iridium materials.[12,15]

Table 5-2. Summary of the photophysical data for hybrid polymer-iridium materials.

Polymer	λ_{abs} [nm]	λ_{em} [nm]	τ^a [ns]	τ^b [ns]	Φ^a [%]	Φ^b [%]	k_r^b [10^6 s^{-1}]	k_{nr}^b [10^6 s^{-1}]
P2-45%-Ir50%	265, 302, 394	495, 522	223.10	802.83	4.30	9.37	0.12	1.13
P2-24%-Ir50%	265, 302, 394	495, 522	234.03	1198.30	4.85	15.60	0.13	0.70
P2-45%-Ir12%	265, 302, 394	495, 522	283.10	1552.20	6.03	26.89	0.17	0.47

[a] Measured from air-equilibrated solutions.
[b] Measured from degassed solutions.

The triplet character of the measured emission was supported by the relatively long excited-state lifetime decays which were measured between 223 and 283 ns and by the oxygen sensitivity of both quantum yield (Φ) and lifetime (τ) values (**Table 5-2**), which increase from air-equilibrated to degassed solutions. It is interesting to note that an inversely proportional trend between photophysical properties and the amount of Ir(III) in the materials is observed, where the material with the lower content of iridium **P2-45%-Ir12%**, showing the higher quantum yield and lifetime values in both air-equilibrated and degassed samples. This could be due to a phenomenon called "concentration quenching".[16]

5.5.4 Photophysical studies of hybrid materials containing iridium and rhenium luminescent metal species

Photophysical studies were subsequently conducted for copolymers containing both iridium and rhenium metal complexes. The photophysical data for complexes **P2-45%-Ir12%-Re6%**, **P2-45%-Ir12%-Re12%** and **P2-45%-Ir12%-Re24%** are listed in **Table 5-3**.

Table 5-3 Summary of experimentally determined photophysical data for copolymers containing both iridium and rhenium metal species.

Polymer	λ_{abs} [nm]	λ_{em}[nm]	τ^a [ns]	Φ^a [%]	k_{ET} [10^6 s^{-1}]
P2-45%-Ir12%-Re6%	265, 380	494, 524	189.65	1.79	1.74
P2-45%-Ir12%-Re12%	265, 380	494, 524, 600	173.06	2.05	2.16
P2-45%-Ir12%-Re25%	265, 380	494, 524, 600	182.06	1.68	1.96

[a] Measured from air-equilibrated solutions.

The materials containing both iridium and rhenium metal fragments exhibit similar absorption profiles (**Figure 5-7**), with intense ligand centre (LC) transitions up to 300 nm and bands arising from metal-to-ligand charge transfer (MLCT) above 350 nm, arising from both Re(I) and Ir(III).

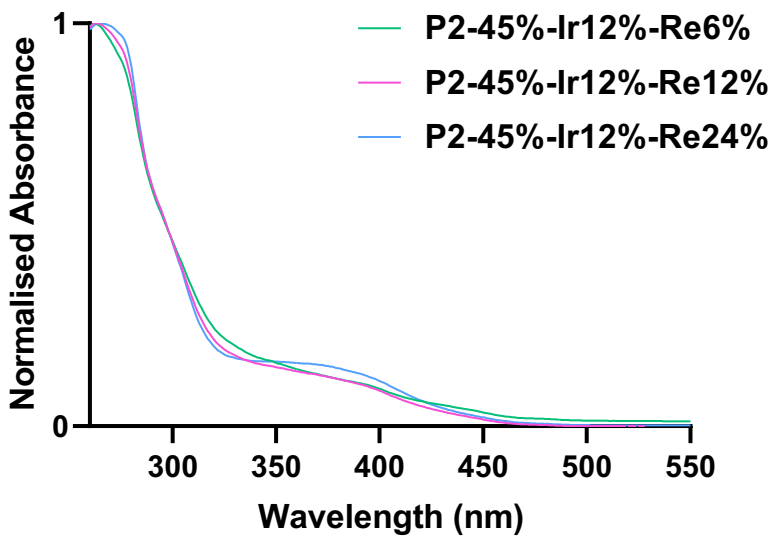

Figure 5-7 Normalised absorption of materials containing both iridium and rhenium **P2-45%-Ir12%-Re6%**, **P2-45%-Ir12%-Re12%** and **P2-45%-Ir12%-Re24%** in air-equilibrated, dilute DMSO. The emission spectra were recorded upon excitation at 400 nm.

Upon excitation at 400 nm, the emission profiles of **P2-45%-Ir12%-Re6%**, **P2-45%-Ir12%-Re12%** and **P2-45%-Ir12%-Re24%** show the presence of the iridium emission with maxima at 495 nm and 505 nm and the appearance of the emission profiles arising from the rhenium complexes at 600 nm, with the intensity increasing with increasing Re(I) content (**Figure 5-8**). The broad emission band at 600

nm arises from the ^{3}MLCT excited state of Re(I) species and is consistent with previously reported Re(I) diimine tetrazolato complexes including the polymer-Re hybrid materials described in this thesis.[17]

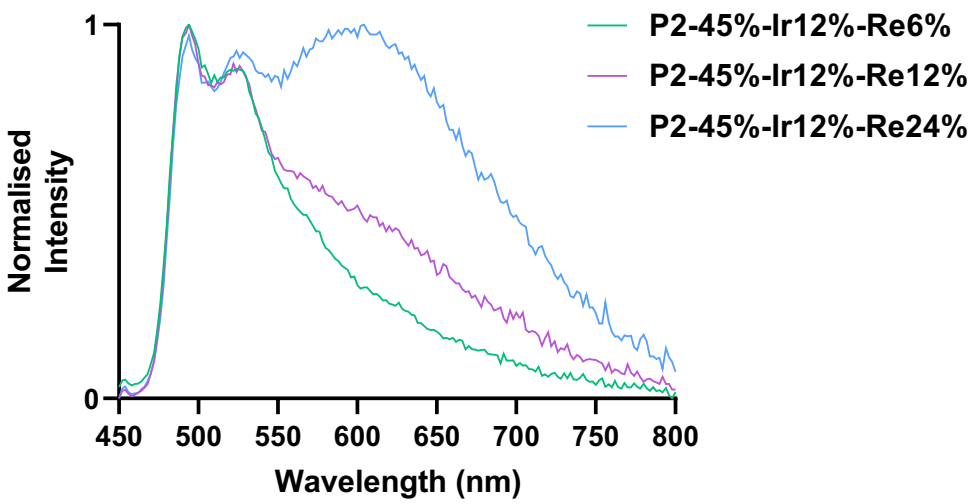

Figure 5-8 Normalised emission of materials containing both iridium and rhenium **P2-45%-Ir12%-Re6%**, **P2-45%-Ir12%-Re12%** and **P2-45%-Ir12%-Re24%** in air-equilibrated, dilute DMSO. The emission spectra were recorded upon excitation at 400 nm.

Emission lifetime values for materials **P2-45%-Ir12%-Re6%**, **P2-45%-Ir12%-Re12%** and **P2-45%-Ir12%-Re24%** reported in **Table 5-3** for air-equilibrated solutions ranged between 173 and 189 ns, while quantum yield values were determined to be between 1.74 % and 2.16 %. It is important to note that quantum yield values for air-equilibrated samples decrease from 6.03 % for material **P2-45%-12%Ir** containing 12 mol % iridium metal to values between 1.74 % and 2.16 % for the materials containing both iridium and rhenium metals. Moreover, the same trend is observed for lifetime values, with a decrease from 283 ns for air-equilibrated hybrid-

material **P2-45%-12%Ir** containing iridium only, to a range between 173 ns and 189 ns for materials **P2-45%-12%Ir-6%Re**, **P2-45%-12%Ir-12%Re** and **P2-45%-12%Ir-24%Re**. The decrease in lifetime of the Ir(III) metal complex in the hybrid copolymers containing both iridium and rhenium metal fragments, suggests that energy transfer (ET) is occurring from the iridium metal centres to the rhenium metal species on the polymeric backbone.

The rate constant for the energy-transfer process k_{ET} can be obtained by the following equation:

$$k_{ET} = \tau_i^{-1} - \tau_0^{-1} \qquad \textbf{Equation 5-2}$$

where $\tau_i = \tau$ value of Ir complex in the presence of Re(III) complex as acceptor (**P2-45%-Ir12%-Re6%**, **P2-45%-Ir12%-Re12%** and **P2-45%-Ir12%-Re24%**); $\tau_0 = \tau$ value of Ir(III) complex not in the presence of Re(III) complex as acceptor (**P2-45%-12%**).

The calculated rates for the energy-transfer processes are reported in **Table 5-3**, with the calculated rates being similar for the three Ir/Re hybrid materials.

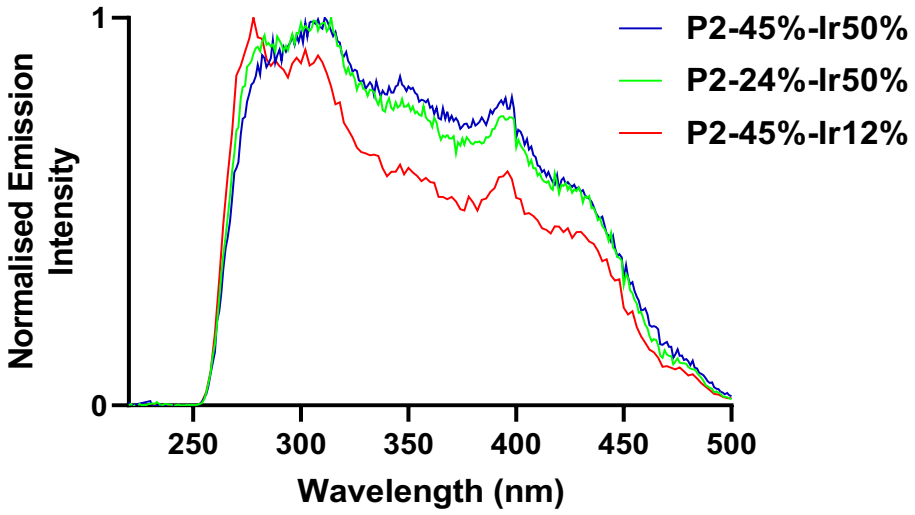

Figure 5-9 Normalised excitation profiles of **P2-45%-Ir50%**, **P2-24%-Ir50%**, **P2-45%-Ir12%**, in dilute DMSO, air-equilibrated samples.

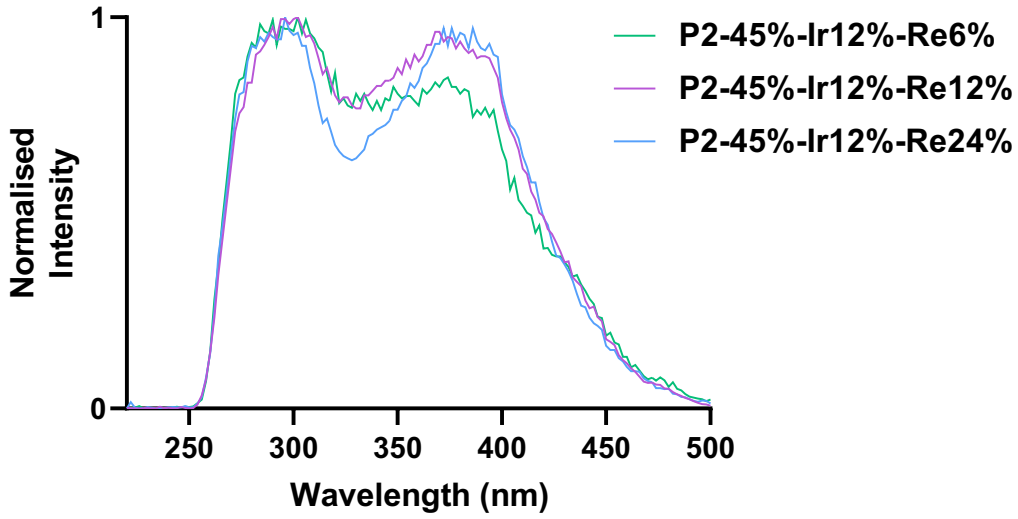

Figure 5-10 Normalised excitation profiles of **P2-45%-Ir12%-Re6%**, **P2-45%-Ir12%-Re12%** and **P2-45%-Ir12%-Re24%** in dilute DMSO, air-equilibrated samples.

From the excitation spectra (**Figure 5-9** and **Figure 5-10**) we observed that the range of excitation profiles matches the absorption profiles, as expected.

5.6 Rodent brain tissues staining

Finally, the six luminescent materials were evaluated as luminescent probes for the staining of rodent brain tissues (**Figure 5-11** and **Figure 5-12**).

Among the three materials containing iridium (**P2-45%-Ir12%**, **P2-24%-Ir50%** and **P2-45%-Ir12%**), **P2-24%-50%Ir** appeared to possess the best binding to the lipidic rich regions in the brain white matter. This may be due to changes in the increased hydrophobicity, where a higher content of *n*-butylamine could lead to changes in the overall affinity of the probe to brain tissues.

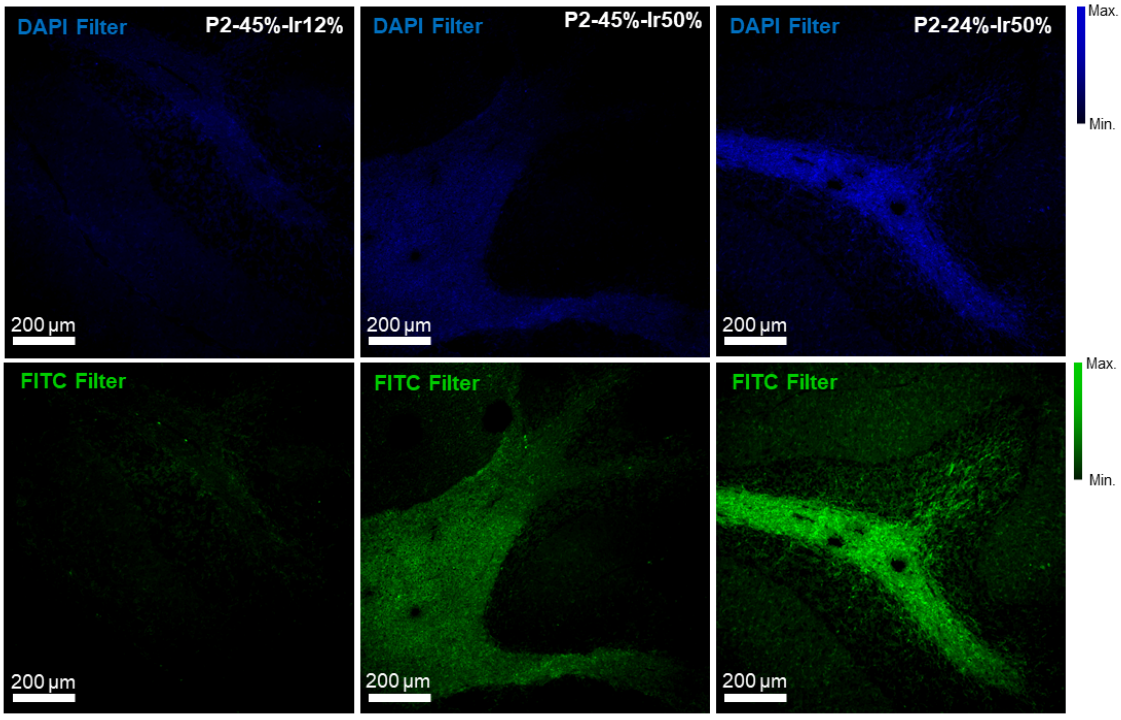

Figure 5-11 Images of rodent brain tissues by employing the materials containing Ir as probes for the tissues.

The fluorescence images of the materials containing both iridium and rhenium are shown in **Figure 5-12**. **P2-45%-Ir12%-Re6%** appears to have the best binding to the lipidic rich regions in the brain white matter. Moreover, fluorescent intensity appears to have an inverse relationship with the content of rhenium in the polymeric materials, this could be related to the Ir/Re ET. Nevertheless, the preliminary studies of the polymeric materials as luminescent probes for the imaging of tissues are still under investigation.

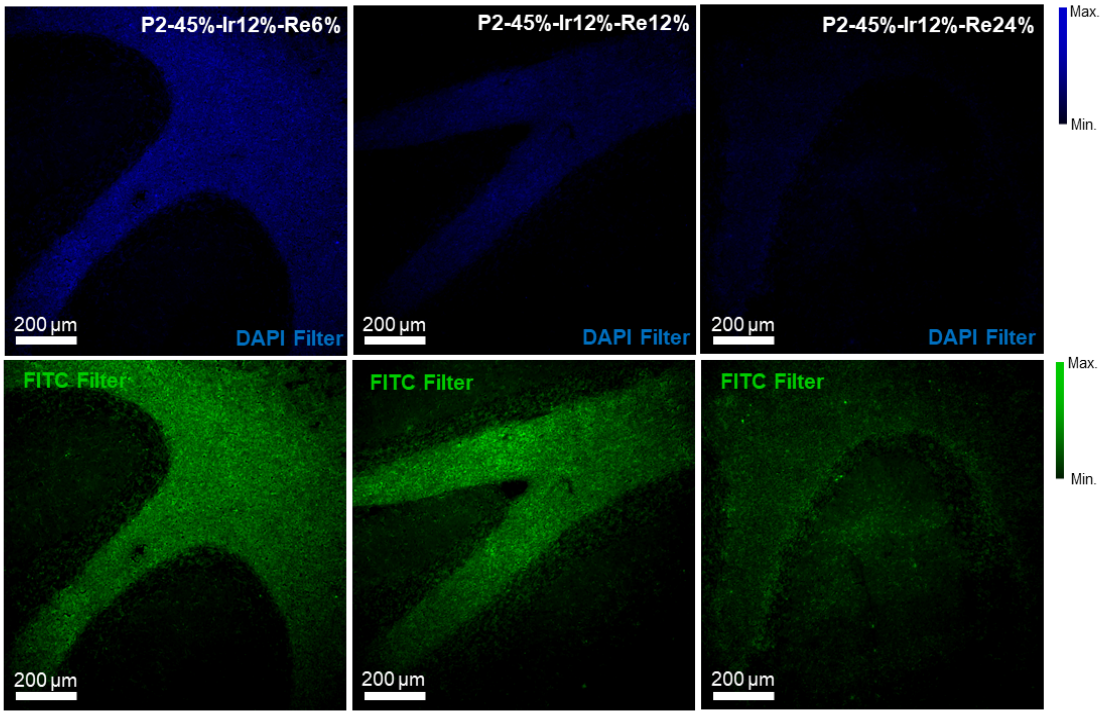

Figure 5-12 Images of rodent brain tissues by employing the materials containing both Ir and Re as probe for the tissues.

5.7 Conclusions

In conclusion, in this Chapter we have detailed the modification of acrylamide-based copolymers containing tetrazolato functionalities, poly(*n*-butyl acrylamide-*co*-

N-(1*H*-tetrazol-5-yl) acrylamide) with $[Ir_2(ppy)_4(\mu\text{-}Cl)_2]$ yielding new iridium functionalised luminescent copolymers *via* the direct coordination of the Ir species to the polymer, giving access to negatively charged luminescent iridium functionalised materials. A series of three new materials with different iridium contents were prepared. Successful attachment of the metal fragments was assessed by UV-Vis spectroscopy and photophysical investigation of the resulting materials. The absorption and emission profiles of the iridium-polymer hybrid materials supported successful metal coordination and indicated that the metal attachment to the tetrazole functionalised polymers did not fundamentally impact the photophysical properties of the iridium species.

Furthermore, the functionalised polymer with 12.5 mol% Ir species was modified with a second luminescent metal species, $Re(CO)_3(phen)Br$, to yield hybrid metal Ir/Re copolymers with 6.25, 12.5 and 25 mol% Re fragments for a fixed Ir content. Full photophysical investigation of the luminescent functionalised materials containing both iridium and rhenium was conducted, confirming the attachment of rhenium fragments. Interestingly, lifetime and quantum yield analysis of materials containing both metal fragments suggest energy transfer (ET) phenomena occurring from the iridium to the rhenium metal centre on the polymeric backbone. Moreover, the materials have been employed for the staining of rodent brain tissues. From preliminary results, it can be observed that between the three materials containing iridium, the one with the higher content of *n*-butylamine on the polymeric chains, **P2-24%-50%Ir**, appears to show the best binding to the lipidic rich regions in the brain white matter. Among the materials with both iridium and rhenium, the one with the lower content of Re(I) luminescent complex shows the best binding to the lipidic rich regions in rodent brain tissues.

5.8 References

1. T.-Y. Li, J. Wu, Z.-G. Wu, Y.-X. Zheng, J.-L. Zuo and Y. Pan, *Coordination Chemistry Reviews*, 2018, **374**, 55-92.
2. C. Caporale and M. Massi, *Coordination Chemistry Reviews*, 2018, **363**, 71-91.
3. C. A. Bader, A. Sorvina, P. V. Simpson, P. J. Wright, S. Stagni, S. E. Plush, M. Massi and D. A. Brooks, *FEBS Letters*, 2016, **590**, 3051-3060.
4. C. A. Bader, R. D. Brooks, Y. S. Ng, A. Sorvina, M. V. Werrett, P. J. Wright, A. G. Anwer, D. A. Brooks, S. Stagni, S. Muzzioli, M. Silberstein, B. W. Skelton, E. M. Goldys, S. E. Plush, T. Shandala and M. Massi, *RSC Advances*, 2014, **4**, 16345-16351.
5. V. Fiorini, A. M. Ranieri, S. Muzzioli, K. D. M. Magee, S. Zacchini, N. Akabar, A. Stefan, M. I. Ogden, M. Massi and S. Stagni, *Dalton Transactions*, 2015, **44**, 20597-20608.
6. V. Fiorini, L. Bergamini, N. Monti, S. Zacchini, S. E. Plush, M. Massi, A. Hochkoeppler, A. Stefan and S. Stagni, *Dalton Transactions*, 2018, **47**, 9400-9410.
7. N. Monti, V. Longo, S. Zacchini, G. Vigarani, L. Giorgini, E. Bonora, M. Massi, V. Fiorini and S. Stagni, *Inorganica Chimica Acta*, 2021, **518**, 120244.
8. C. Caporale, C. A. Bader, A. Sorvina, K. D. M. MaGee, B. W. Skelton, T. A. Gillam, P. J. Wright, P. Raiteri, S. Stagni, J. L. Morrison, S. E. Plush, D. A. Brooks and M. Massi, *Chemistry – A European Journal*, 2017, **23**, 15666-15679.

9. V. Fiorini, I. Zanoni, S. Zacchini, A. L. Costa, A. Hochkoeppler, V. Zanotti, A. M. Ranieri, M. Massi, A. Stefan and S. Stagni, *Dalton Transactions*, 2017, **46**, 12328-12338.

10. A. M. Ranieri, C. Caporale, V. Fiorini, A. Hubbard, P. Rigby, S. Stagni, E. Watkin, M. I. Ogden, M. J. Hackett and M. Massi, *Chemistry – A European Journal*, 2019, **25**, 10566-10570.

11. Z. Si, X. Li, X. Li and H. Zhang, *Journal of Organometallic Chemistry*, 2009, **694**, 3742-3748.

12. V. Fiorini, A. D'Ignazio, K. D. M. Magee, M. I. Ogden, M. Massi and S. Stagni, *Dalton Transactions*, 2016, **45**, 3256-3259.

13. G. A. Crosby and J. N. Demas, *Journal of Physical Chemistry*, 1971, **75**, 991-1024.

14. D. Hartnell, K. Gillespie-Jones, C. Ciornei, A. Hollings, A. Thomas, E. Harrild, J. Reinhardt, D. J. Paterson, D. Alwis, R. Rajan and M. J. Hackett, *ACS Chemical Neuroscience*, 2020, **11**, 248-257.

15. V. Fiorini, S. Zacchini, P. Raiteri, R. Mazzoni, V. Zanotti, M. Massi and S. Stagni, *Dalton Transactions*, 2016, **45**, 12884-12896.

16. M. A. Baldo, S. Lamansky, P.E. Burrows, M. E. Thompson and S. R. Forrest, *Applied Physics Letters*, 1999, **75**, 4-6.

17. M. V. Werrett, D. Chartrand, J. D. Gale, G. S. Hanan, J. G. MacLellan, M. Massi, S. Muzzioli, P. Raiteri, B. W. Skelton, M. Silberstein and S. Stagni, *Inorganic Chemistry*, 2011, **50**, 1229-1241.

Every reasonable effort has been made to acknowledge the owner of copyright material. I would be pleased to hear from any copyright owner who has been omitted or incorrectly acknowledged.

Chapter 6

Conclusions and future work

The work presented in this thesis investigated the design and synthesis of new, well-defined copolymers prepared by reversible addition-fragmentation chain transfer (RAFT) containing tetrazole functional groups. We synthesised three new families of copolymers with pendent tetrazole functionalities: the first series was based on modified polystyrenic copolymers, the second on acrylamido-based copolymers containing tetrazole functional groups obtained from modified polyPFPA (poly pentafluorophenyl acrylate), and the last series was based on block copolymers made of PEG (polyethylene glycol) and modified PFPA (pentafluorophenyl acrylate). We demonstrated that such materials as capable of serving as macromolecular ligands for the coordination of luminescent metal species based on Re(I) and Ir(III) *via* the direct coordination of the polymer-bound tetrazolato groups species, yielding new luminescent materials which can be employed as probes for imaging of biological tissues.

The work detailed in this thesis was motivated by the dearth of literature reports detailing the incorporation of tetrazole functionality in well-defined polymers and specifically with the aim of such functional polymers being able to serve as macromolecular ligands for transition metal species. We developed a research program focused on the synthesis and evaluation of the photophysical properties of new metal tetrazolato functionalised copolymers and on the evaluation of the luminescent materials as potential probes for tissue staining imaging.

In Chapter 2, we reported the first examples of well-defined, styrenic-based copolymers containing pendent tetrazole functional groups and demonstrated the ability of such materials to serve as macromolecular ligands capable of complexing a Re(I) tricarbonyl diimine precursor *via* tetrazole coordination to the metal centre.

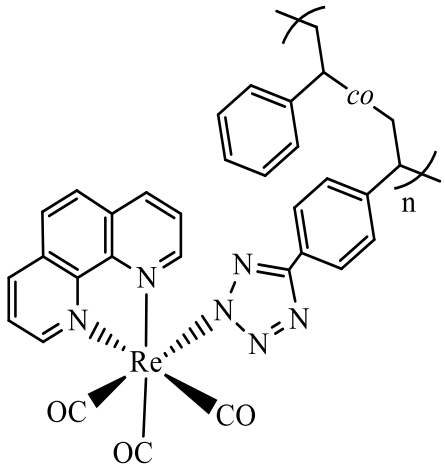

Figure 6-1 Structure of model targeted rhenium-tetrazolato functional material based on polystyrenic copolymers.

A series of four new copolymers, two statistical and two block copolymers, were synthesised by RAFT random copolymerisation of styrene and 4-cyanostyrene. The resulting random copolymers were then reacted with NaN_3, yielding materials containing various molar content of tetrazole moieties. The new tetrazole functionalised copolymers were subsequently reacted with a Re(I) tricarbonyl diimine precursor, to yield four new polymeric luminescent materials (**Figure 6-1**). The photophysical properties of the new hybrid polymeric-inorganic materials were investigated, demonstrating that the polymeric scaffold does not impact the luminescent properties of the final hybrid materials. Absorption and emission measurements were employed to confirm coordination between tetrazole appended

groups and the Re(I) complex. Significantly, these studies opened the route to the development of a new class of transition metal tetrazolato functional luminescent polymers.

In Chapter 3, the RAFT synthesis of well-defined, acrylamido-based copolymers containing tetrazole functional groups was described and it was demonstrated that such copolymers can serve as macromolecular ligands for rhenium(I) tricarbonyl diimine luminescent complexes *via* direct coordination to the tetrazolato species (**Figure 6-2**). To synthesise the polymers containing tetrazole species, we adopted a different approach compared to the one described in Chapter 2. In Chapter 3 we prepared homopolymers of polyPFPA, followed by modification at room temperature with 5-aminotetrazole and *n*-butylamine, yielding four materials with different compositions. The advantages of using PFPA over the synthesis of the styrenic-based copolymers, are the lower cost of PFPA monomers over 4-cyanostyrene monomers and the comparatively milder conditions required for the insertion of tetrazole functionalities into the polymers.

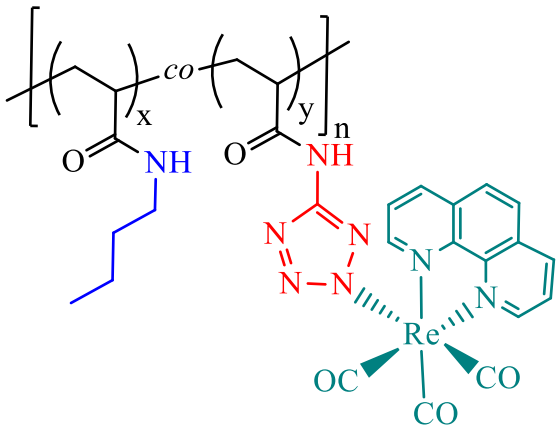

Figure 6-2 Structure of model targeted rhenium-tetrazolato functional hybrid species based on acrylamide copolymers.

The synthetic approach to obtain such materials, exploiting the facile reaction between pentafluorophenyl esters and primary amines, was significantly more facile than the conventional approach for introducing tetrazole functionality involving the reaction between nitrile functional groups and an azide source, as detailed and utilised in Chapter 2. Coordination of the four materials with $Re(CO)_3(phen)^+$ was successfully accomplished by the reaction of the tetrazole-functional copolymers with $Re(CO)_3(phen)Br$ (**Figure 6-2**) and confirmed by FTIR spectroscopy. The absorption and emission profiles of the rhenium-polymer hybrid materials supported successful metal coordination and the luminescent properties of the rhenium species were not affected by direct coordination to a copolymeric scaffold. The final Re-hybrid materials were employed as probes for the staining of rodent brain tissues. The imaging results suggested probe uptake in the tissues with non-specific binding of the Re(I) polymeric luminescent in rodent brain tissues.

In Chapter 4, we described the RAFT synthesis of well-defined, block copolymers based on PEG/PFP structural motifs containing tetrazolato functional groups. A total of seven new materials bearing tetrazole functionalities were prepared. The first step in the synthesis of the new materials was the RAFT homopolymerisation of poly(ethylene glycol) methyl ether acrylate (PEGA) or poly(ethylene glycol) methyl ether methacrylate (PEGMA). The two parent homopolymers were then used as macro chain transfer agents (CTA) for the block copolymerisation of pentafluorophenyl acrylate. The pentafluorophenyl esters in the copolymer backbones were subsequently reacted with 5-aminotetrazole and either *n*-octylamine, *n*-decylamine or *n*-hexadecylamine, yielding amide functionalised block copolymers of varying composition and amphiphilicity. The synthetic approach to such materials, exploiting the facile reaction between pentafluorophenyl esters and primary amines, was

monitored by a combination of ^{19}F NMR and FTIR spectroscopies. The incorporation of poly(ethylene glycol) functionalities yielded materials that were completely soluble in water (**Figure 6-3**), making them excellent candidates in bio-related applications.

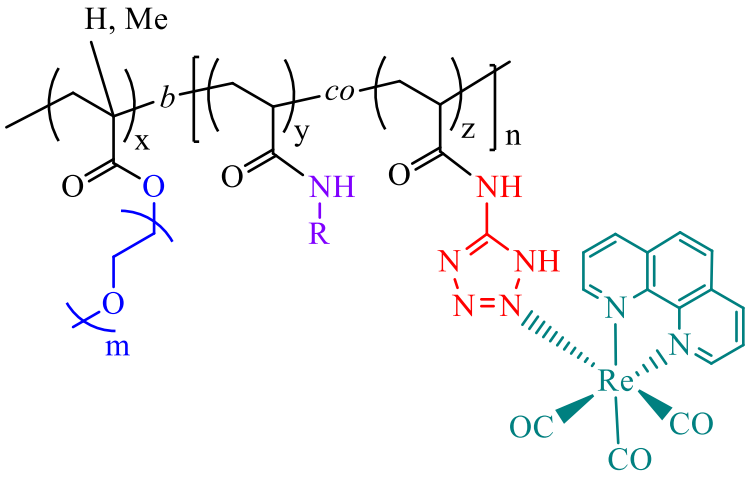

Figure 6-3 Structure of model targeted rhenium-tetrazolato functional material based on PEG/PFPA block copolymers.

Attachment of a luminescent rhenium(I) species to the PEG-based copolymers, was successfully accomplished by the reaction of the tetrazole-functional copolymers with $Re(CO)_3(phen)Br$ with complexation confirmed by FTIR spectroscopy. The absorption and emission profiles of the rhenium-polymer hybrid materials supported successful metal coordination and the luminescent properties of the rhenium species were not affected by direct coordination to a polymeric scaffold. The final Re-hybrid materials based on PEG acrylate copolymers were employed as probes for the staining of rodent brain tissues, showing the ability of the materials to act as probes for non-specific binding of biological tissues.

In Chapter 5, two of the acrylamido based random copolymers described in Chapter 3, containing butyl and tetrazole functional side groups**,** were reacted with

$[Ir_2(ppy)_4(\mu\text{-}Cl)_2]$ (where ppy = phenylpyridine) yielding iridium functionalised luminescent copolymers *via* direct coordination of the Ir species on the tetrazole ligands, giving access to new negatively charged polymer-Ir hybrid materials.

Iridium fragments were attached into the polymeric scaffold to exploit the enhanced photophysical properties of iridium(III) luminescent complexes compared to rhenium(I) fragments for application of the materials as probes for the staining of biological tissues.

A small series of three new materials with different iridium compositions were prepared. Confirmation of attachment of the metal fragments was assessed by UV-Vis spectroscopy and *via* the photophysical investigation of the resulting luminescent materials. The absorption and emission profiles of the iridium-polymer hybrid materials supported successful metal coordination and indicated that the photophysical properties of the iridium species were not adversely impacted by metal attachment to the tetrazole functionalised polymers.

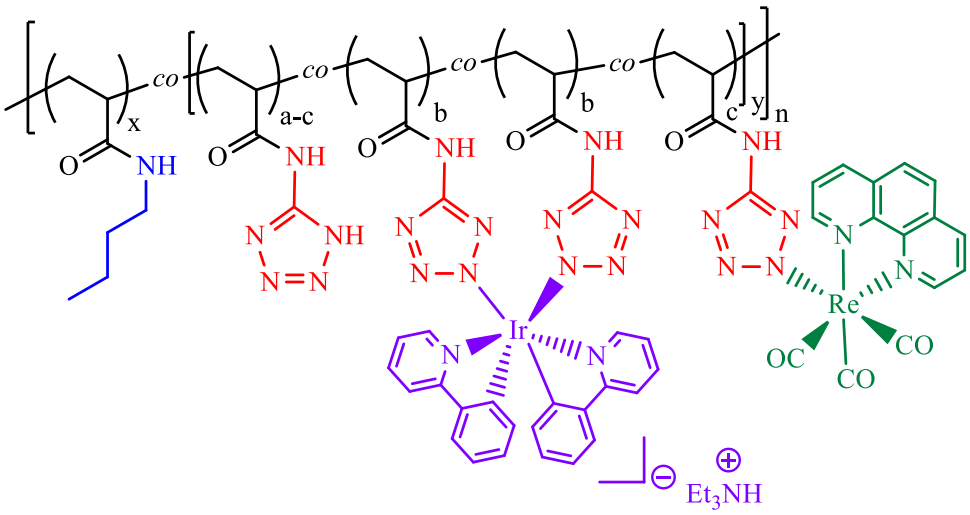

Figure 6-4 Structure of model targeted tetrazolato functional material containing both iridium and rhenium.

Furthermore, one of the iridium-functionalised copolymers was further modified with a second luminescent metal species, $Re(CO)_3(phen)Br$, to yield three hybrid metal Ir/Re copolymers containing different amounts of Re fragments for a fixed Ir content. Full photophysical investigation of the luminescent functionalised materials containing both iridium and rhenium confirmed attachment of the rhenium fragments. Interestingly, lifetime and quantum yield analysis of the materials containing both metal fragments suggested energy transfer (ET) phenomena occurring from the iridium to the rhenium metal centre. The final hybrid materials have been employed as luminescent probes for the biological imaging of rodent brain tissues, showing affinity for the lipidic rich regions in the brain white matter of brain tissues. Interestingly, the probe containing both metal centres with a low quantity of rhenium appeared to have a higher affinity for white matter in brain tissues.

In summary, this thesis details the synthesis and application of new, well-defined styrenic and acrylamide copolymers containing tetrazole functional groups.

The materials have been successfully employed as macromolecular ligands for the complexation of rhenium(I) tricarbonyl diimine and iridium(III) phenylpyridine metal complexes, yielding new luminescent materials. Importantly, we showed that the polymeric backbones do not impact the photophysical properties of the final materials. Preliminary investigation into the use of the materials as probes for the imaging of biological tissues has demonstrated the potential of such materials, with the iridium-hybrid material showing to be the most effective probes in the imaging of biological tissues.

Finally, further studies to assess whether the architecture of the polymers has an impact on the photophysical properties could be conducted. For instance, the synthesis of copolymers with different architectures such as graft, star or branched structures, containing tetrazole functionalities able to serve as macromolecular ligands, could be evaluated. Other ligand fragments (such as pyridine derivatives or triazole derivatives) could also be investigated as potential chelating species and incorporated into the polymeric structures and examined as macromolecular ligands for the complexation of luminescent metal fragments.

Moreover, it would be interesting to synthesise monomers containing tetrazolato metal complexes to facilitate the direct RAFT synthesis of different (co)polymers, of varying architecture and topology. Monomer-containing metal complexes could enable access to block copolymeric structures as opposed to a random distribution achieved for the PFPA-based materials described in this thesis. In fact, with the controlled sequence of different monomers containing luminescent tetrazolato complexes, it would be possible to obtain polymeric materials containing blocks with different metals and defined compositions. The role of the polymeric chain in the energy transfer process described in Chapter 5 could be investigated by, for

example, synthesising block copolymers where the first block is made of rhenium and the second block based on iridium.

Lastly, the staining ability of the materials could be further developed by performing the tissue staining in aqueous media or in biological buffers in the future, to gain a better understanding of the interaction of the materials in biological media. The materials could be optimised with the focus of implementing the study of the luminescent materials to be employed as effective probes for the imaging of biological tissues.

Appendix

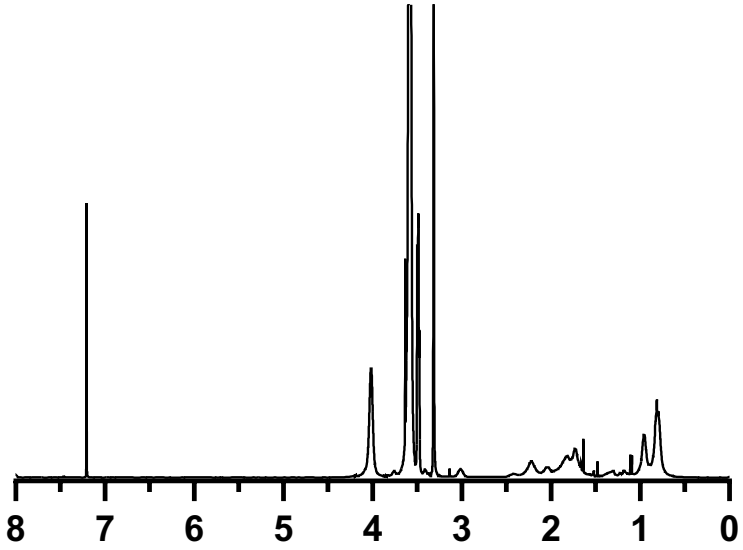

Figure A-1 ^{1}H NMR spectrum of **M3**, recorded in $CDCl_3$.

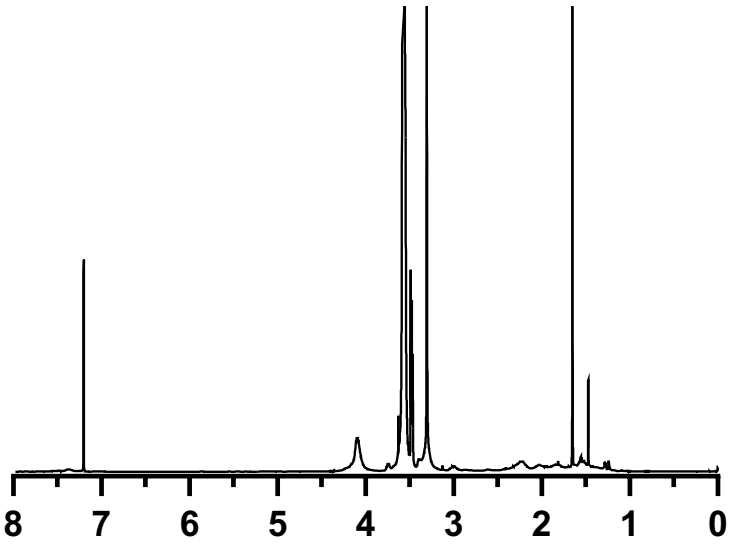

Figure A-2 ^{1}H NMR spectrum of **A3**, recorded in $CDCl_3$.

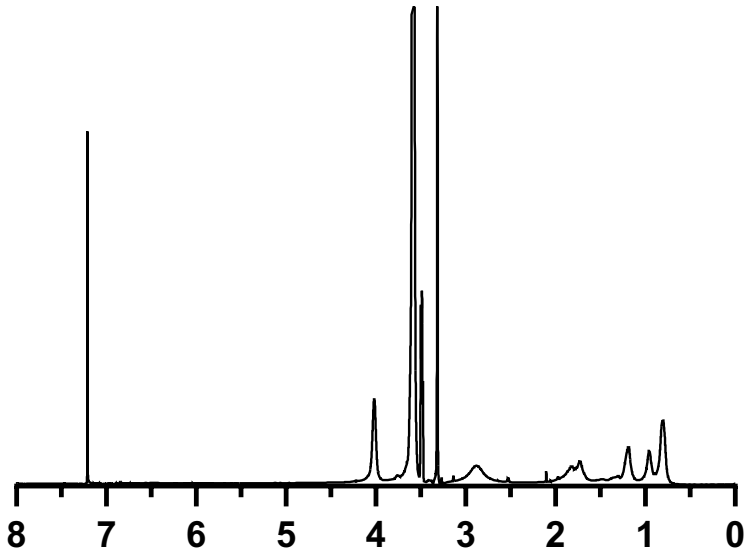

Figure A-3 ^{1}H NMR spectrum of **M3-40%tet-60%oct**, recorded in $CDCl_3$.

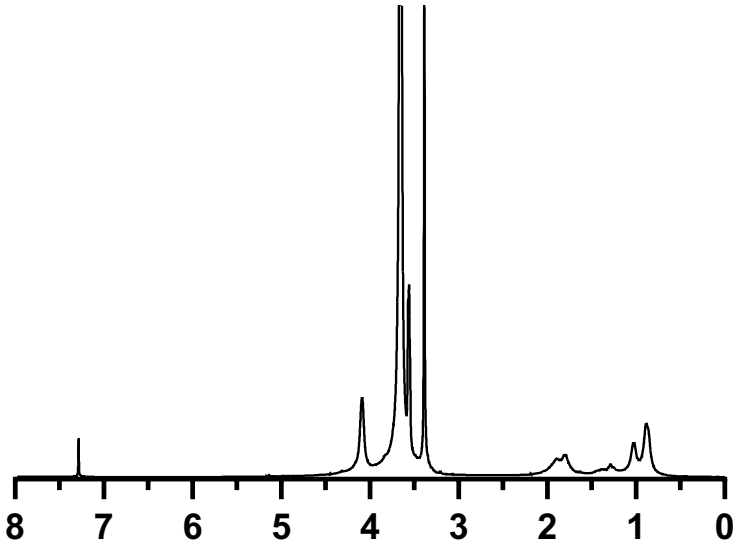

Figure A-4 ^{1}H NMR spectrum of **M3-10%tet-90%oct**, recorded in $CDCl_3$.

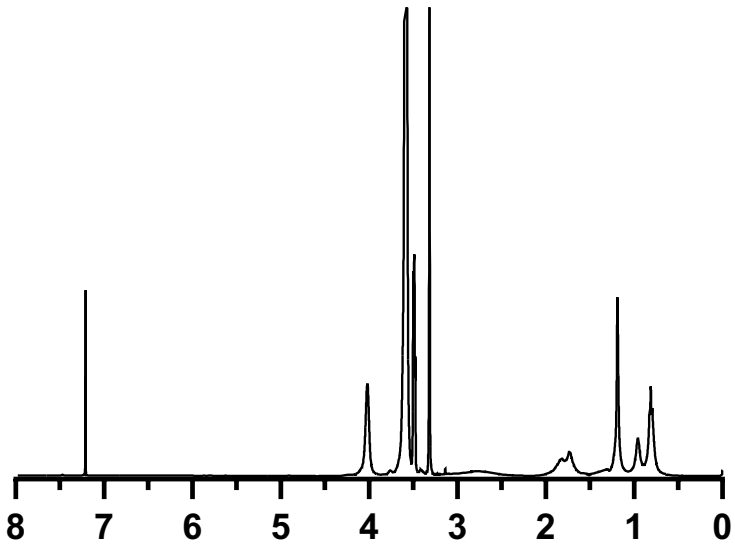

Figure A-5 ^{1}H NMR spectrum of **M3-40%tet-60%hexadec**, recorded in $CDCl_3$.

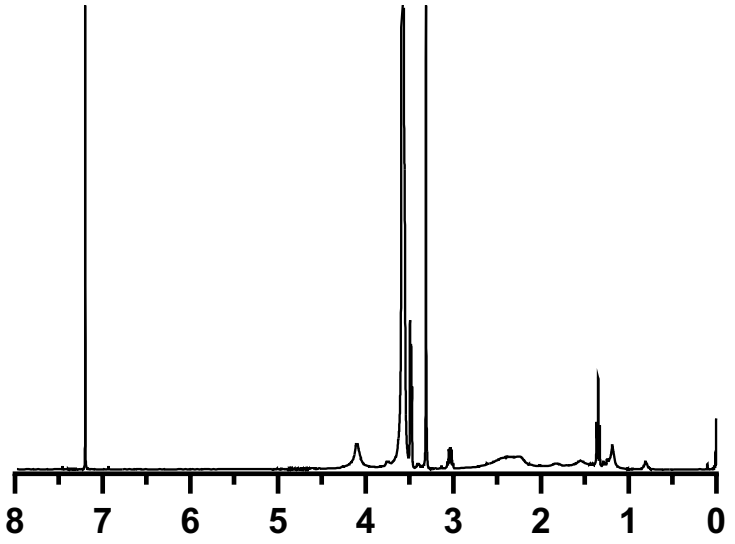

Figure A-6 ^{1}H NMR spectrum of **A3-65%tet-35%dec**, recorded in $CDCl_3$.

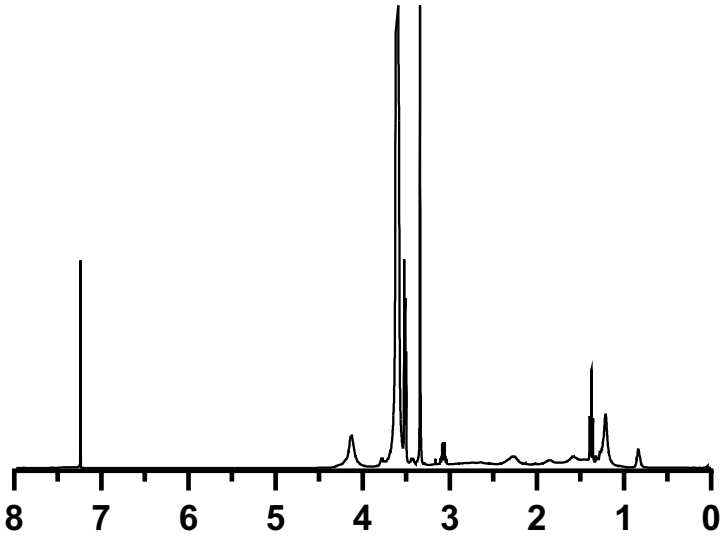

Figure A-7 ^{1}H NMR spectrum of **A3-50%tet-50%dec**, recorded in $CDCl_3$.

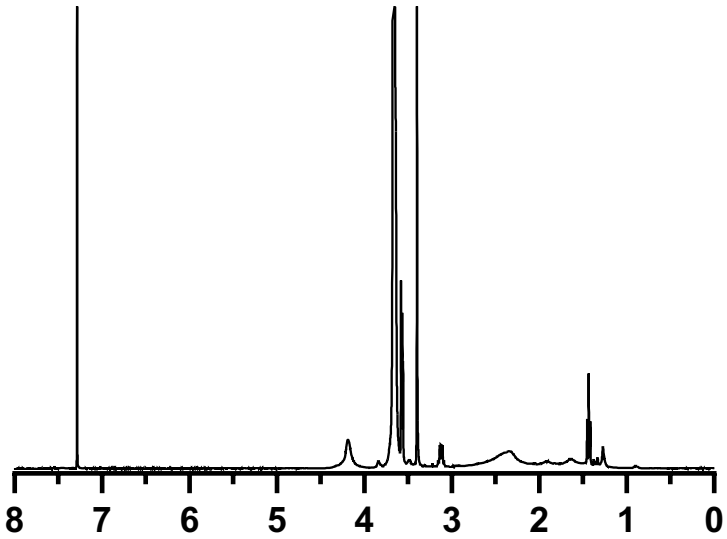

Figure A-8 ^{1}H NMR spectrum of **A3-90%tet-10%hexdec**, recorded in $CDCl_3$.

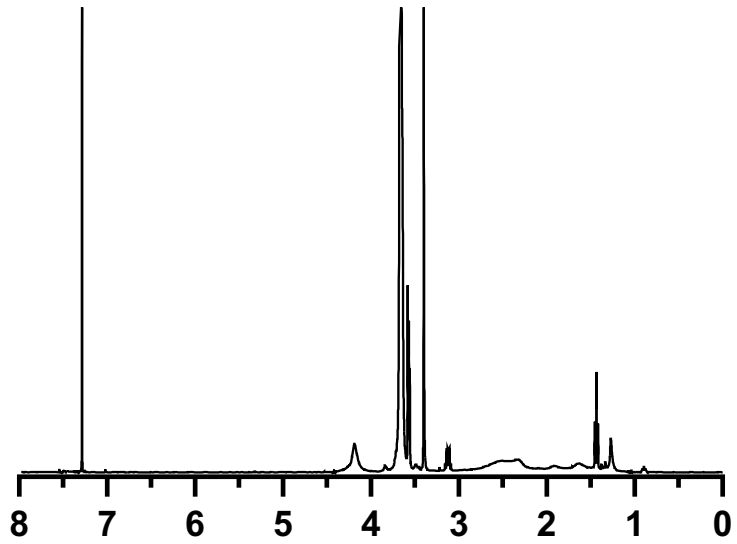

Figure A-9 ^{1}H NMR spectrum of **A3-75%tet-25%hexdec**, recorded in $CDCl_3$.

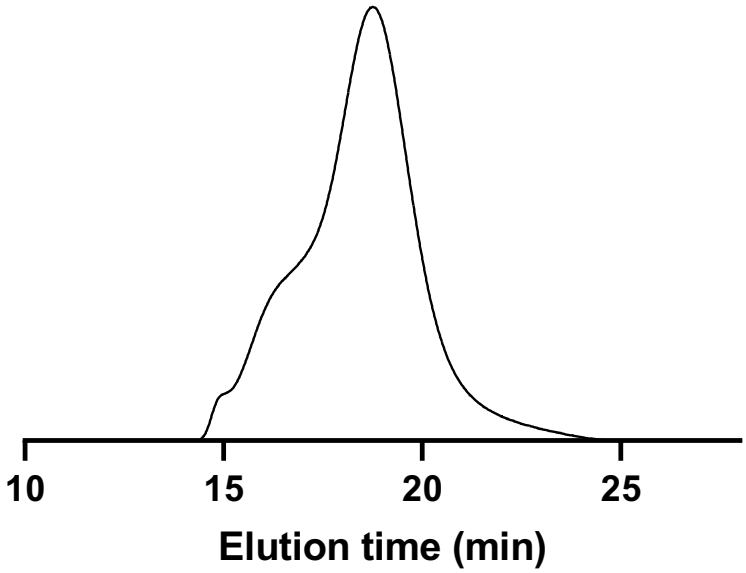

Figure A-10 SEC traces of **M3-40%tet-60%oct**. M_n = 39,200; M_w = 53,100.

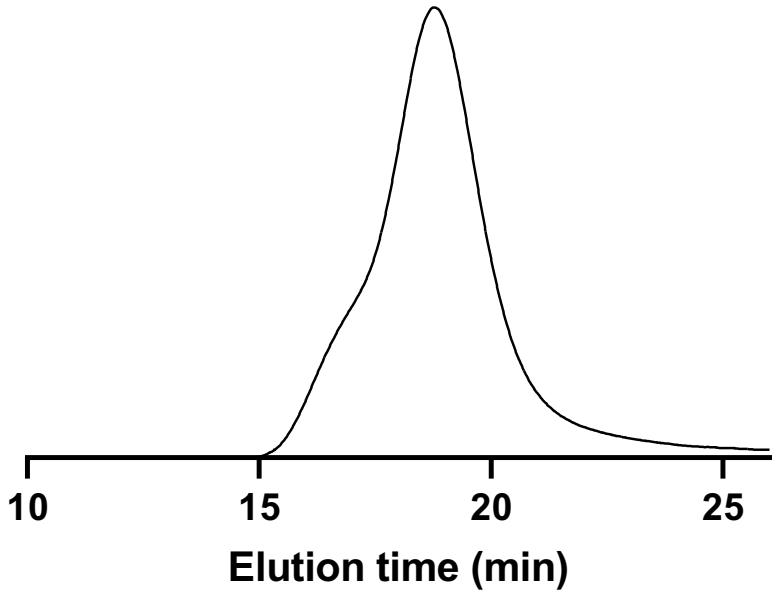

Figure A-11 SEC traces of **M3-10%tet-90%oct**. M_n = 35,100; M_w = 44,100.

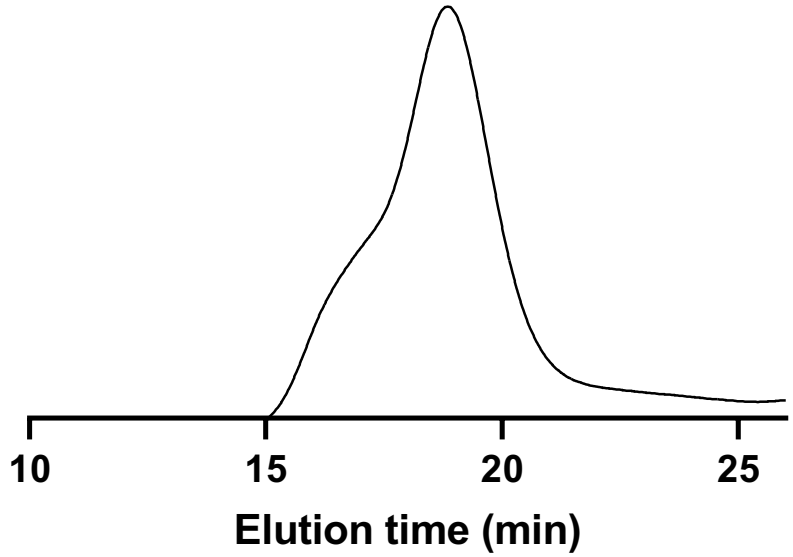

Figure A-12 SEC traces of **M3-40%tet-60%hexadec**. M_n = 40,400; M_w = 50,200.

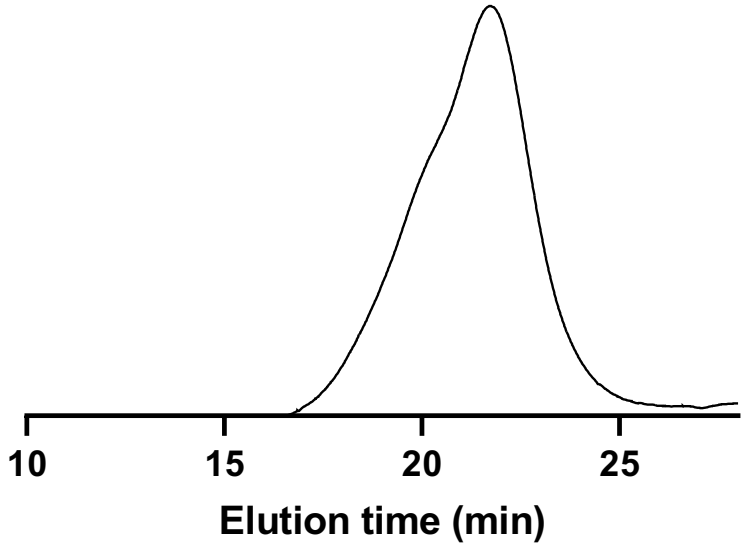

Figure A-13 SEC traces of **A3-65%tet-35%dec**. M_n = 14,500; M_w = 18,900.

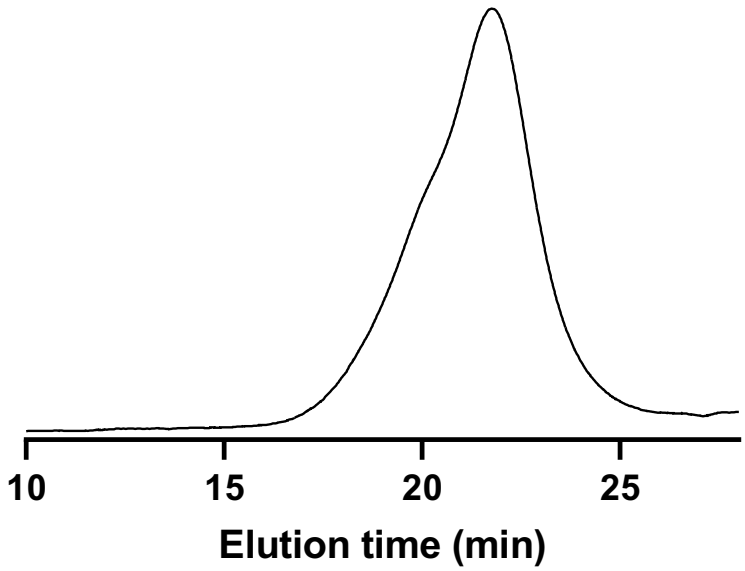

Figure A-14 SEC traces of **A3-50%tet-50%dec**. M_n = 14,000; M_w = 18,200.

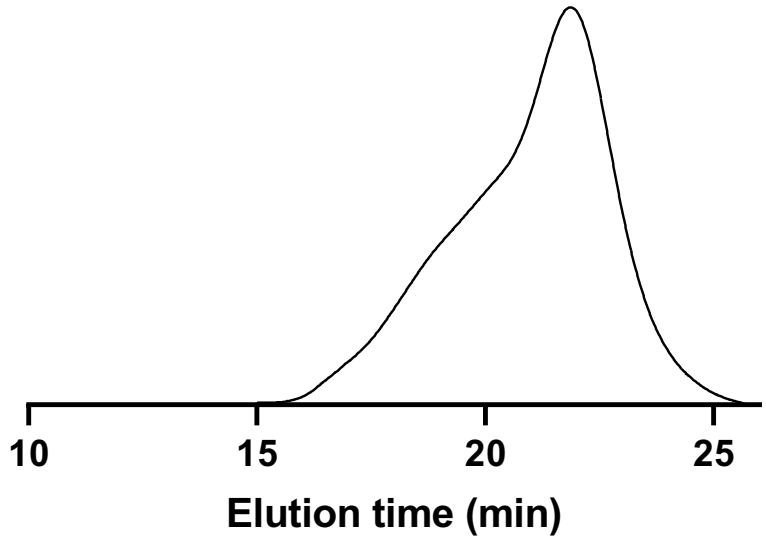

Figure A-15 SEC traces of **A3-90%tet-10%hexadec**. M_n = 14,700; M_w = 21,200.

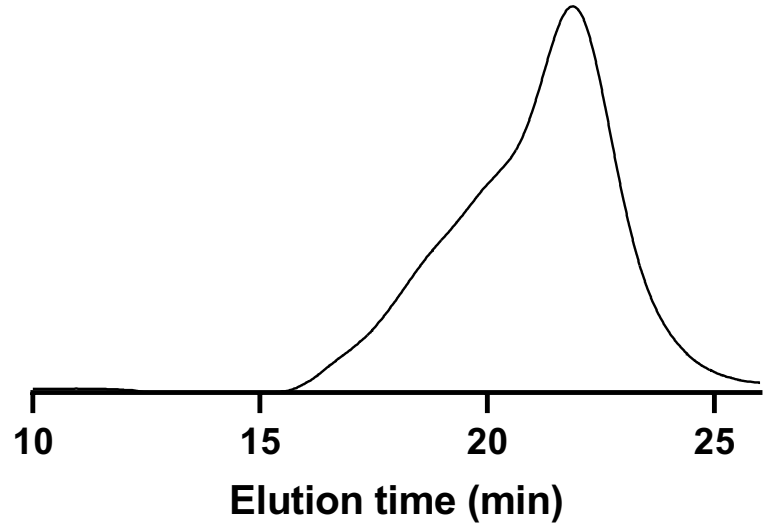

Figure A-16 SEC traces of **A3-75%tet-25%hexadec**. M_n = 15,600; M_w = 21,000.

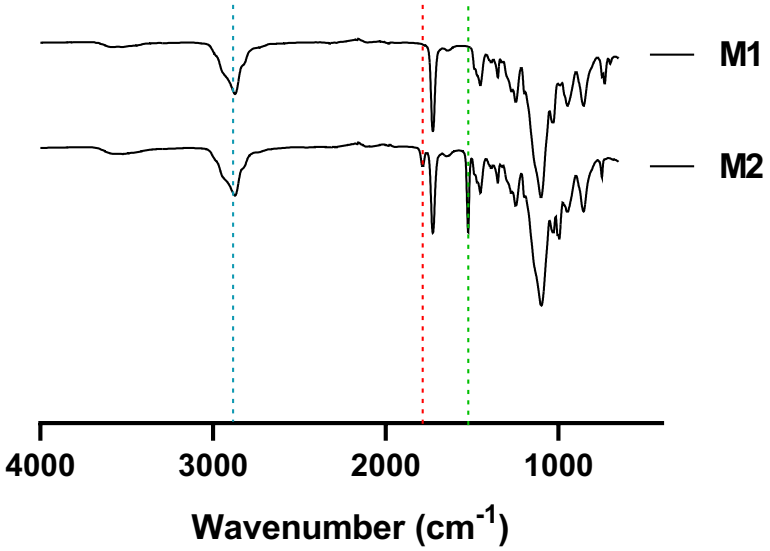

Figure A-17 FTIR spectra of the homopolymer polyPEGMA precursor **M1** (top), the block copolymer poly(PEGMA-*b*-PFPA), **M2** (bottom).

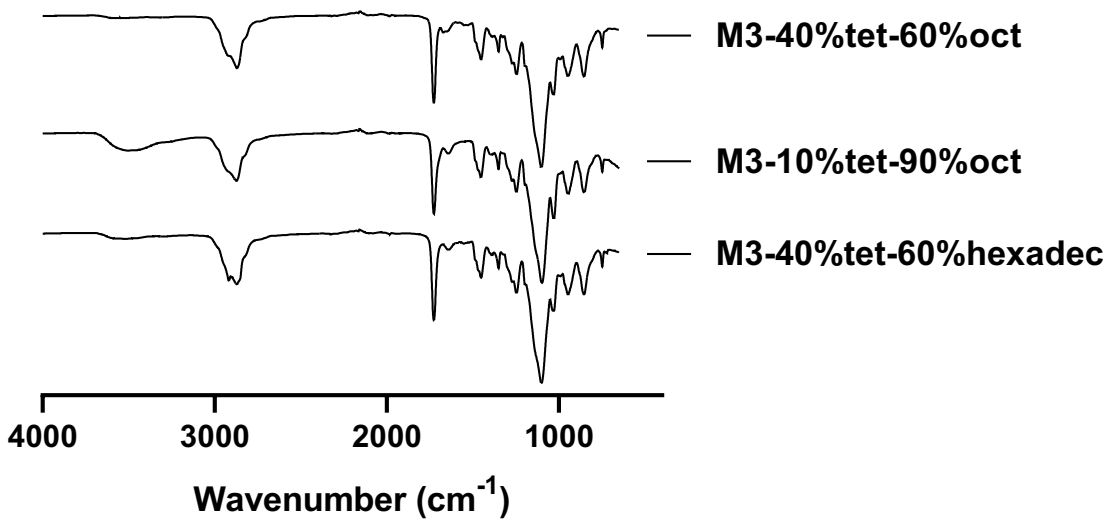

Figure A-18 FTIR spectra of the modified methacrylate species.

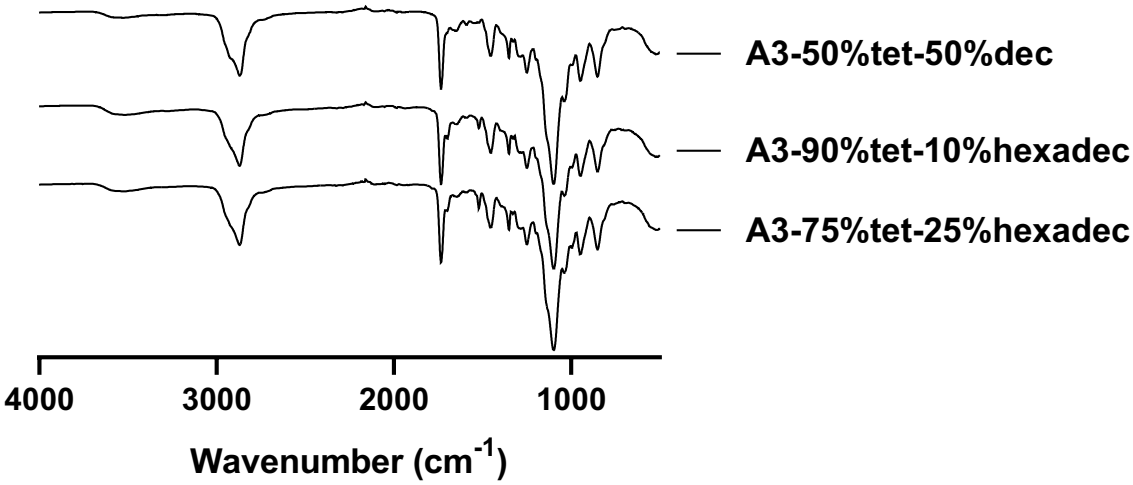

Figure A-19 FTIR spectra of the modified acrylate species.

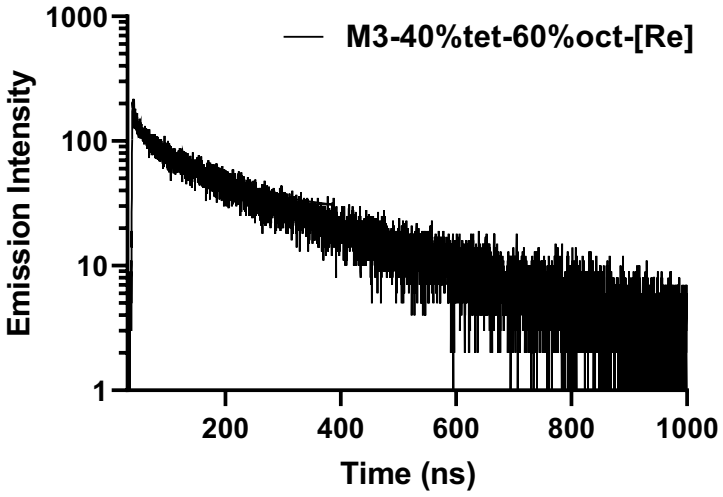

Figure A-20 TCSPS decay of ^{3}MLCT emission of air equilibrated solutions of **M3-40%tet-60%oct-[Re]** in dilute DMSO, air-equilibrated solutions, under excitation at 375 nm.

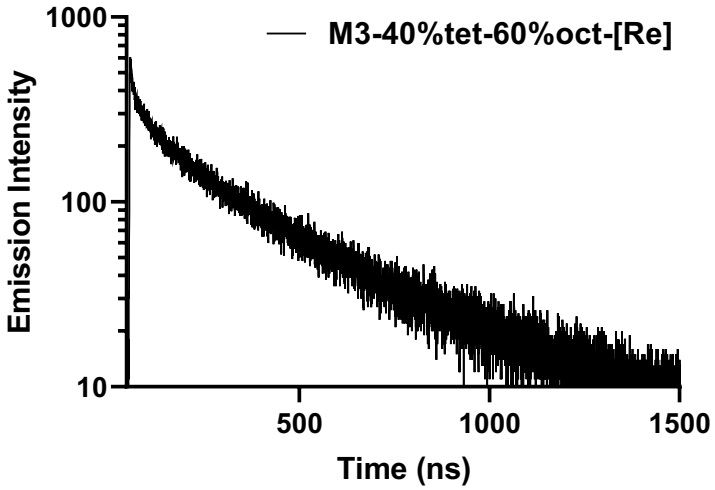

Figure A-21 TCSPS decay of ^{3}MLCT emission of air equilibrated solutions of **M3-40%tet-60%oct-[Re]** in dilute DMSO, degassed solutions, under excitation at 375 nm.

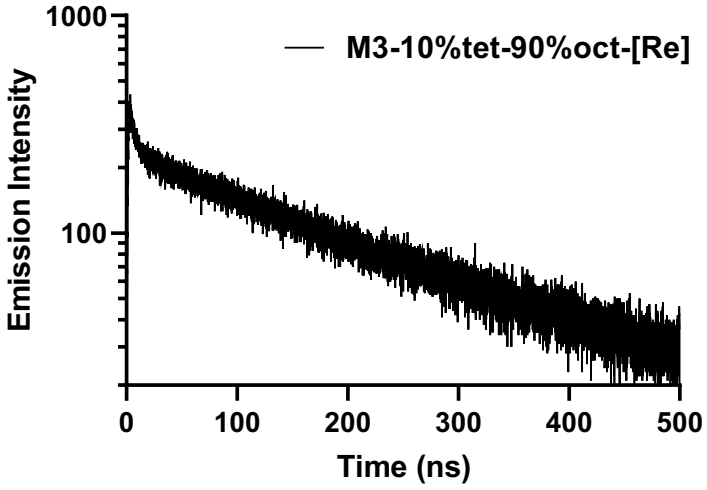

Figure A-22 TCSPS decay of ^{3}MLCT emission of air equilibrated solutions of **M3-10%tet-90%oct-[Re]** in dilute DMSO, air-equilibrated solutions, under excitation at 375 nm.

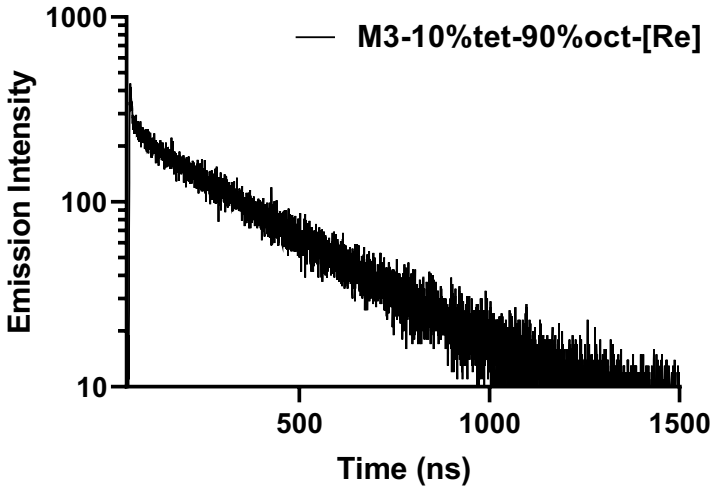

Figure A-23 TCSPS decay of ^{3}MLCT emission of air equilibrated solutions of **M3-10%tet-90%oct-[Re]** in dilute DMSO, degassed solutions, under excitation at 375 nm.

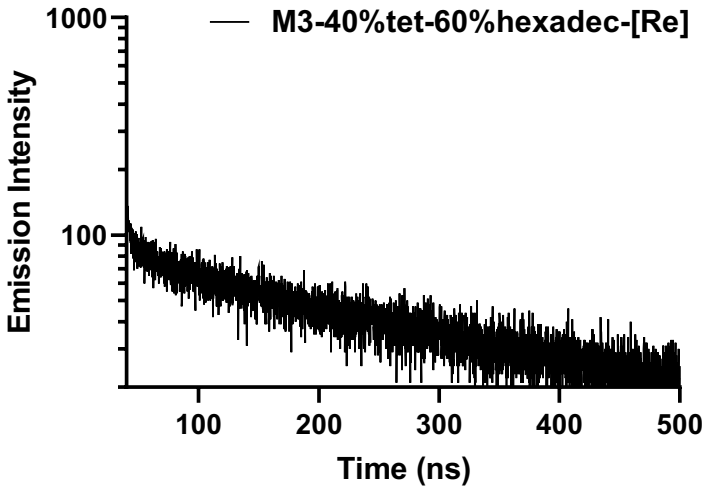

Figure A-24 TCSPS decay of ^{3}MLCT emission of air equilibrated solutions of **M3-40%tet-60%hexadec-[Re]** in dilute DMSO, air-equilibrated solutions, under excitation at 375 nm.

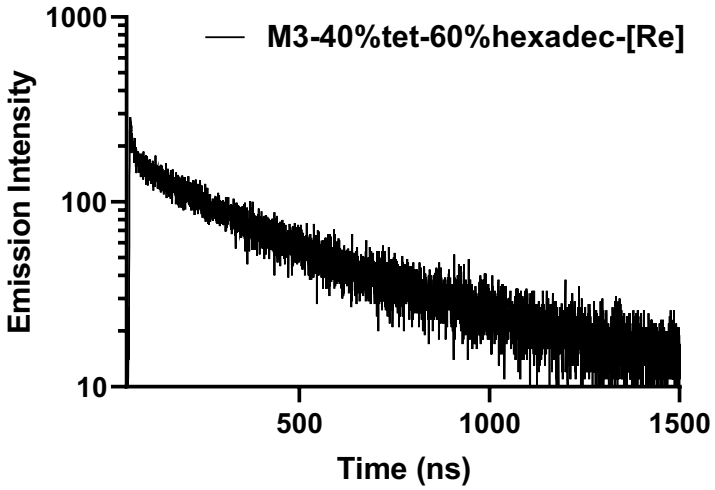

Figure A-25 TCSPS decay of ^{3}MLCT emission of air equilibrated solutions of **M3-40%tet-60%hexadec-[Re]** in dilute DMSO, degassed solutions, under excitation at 375 nm.

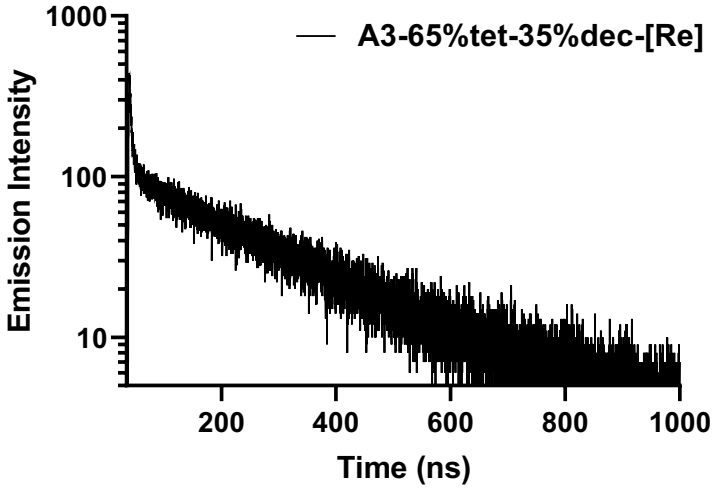

Figure A-26 TCSPS decay of ^{3}MLCT emission of air equilibrated solutions of **A3-65%tet-35%dec-[Re]** in dilute DMSO, air-equilibrated solutions, under excitation at 375 nm.

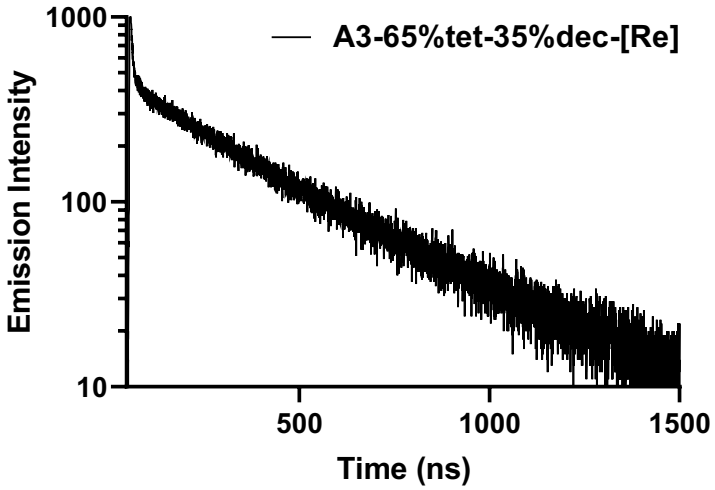

Figure A-27 TCSPS decay of ^{3}MLCT emission of air equilibrated solutions of **A3-65%tet-35%dec-[Re]** in dilute DMSO, degassed solutions, under excitation at 375 nm.

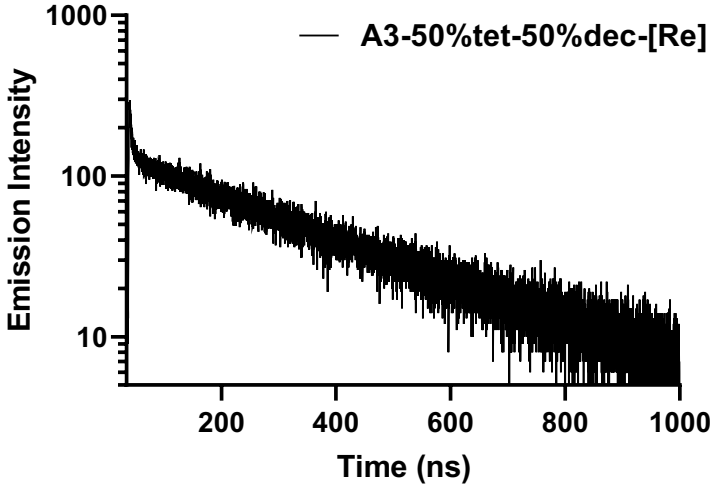

Figure A-28 TCSPS decay of ^{3}MLCT emission of air equilibrated solutions of **A3-50%tet-50%dec-[Re]** in dilute DMSO, air-equilibrated solutions, under excitation at 375 nm.

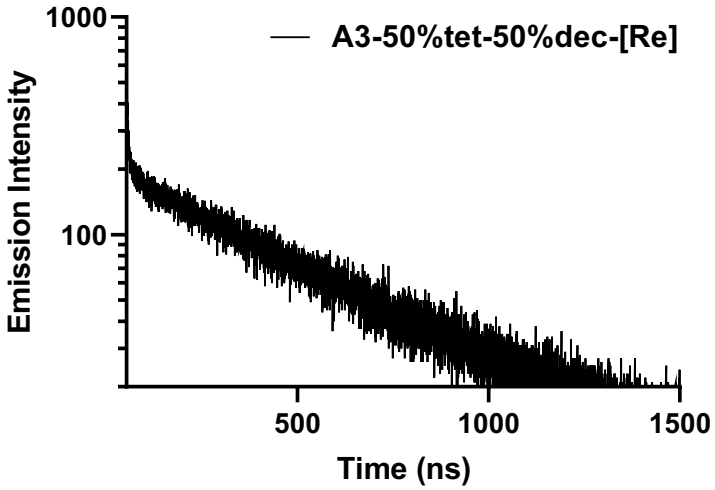

Figure A-29 TCSPS decay of ^{3}MLCT emission of air equilibrated solutions of **A3-50%tet-50%dec-[Re]** in dilute DMSO, degassed solutions, under excitation at 375 nm.

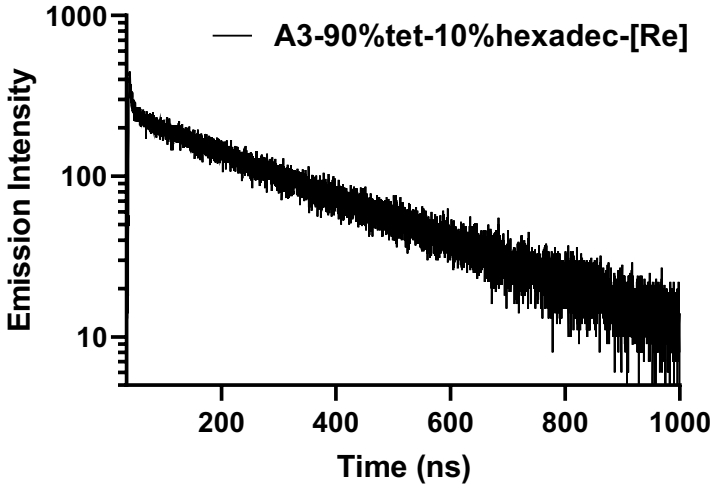

Figure A-30 TCSPS decay of ^{3}MLCT emission of air equilibrated solutions of **A3-90%tet-10%hexadec-[Re]** in dilute DMSO, air-equilibrated solutions, under excitation at 375 nm.

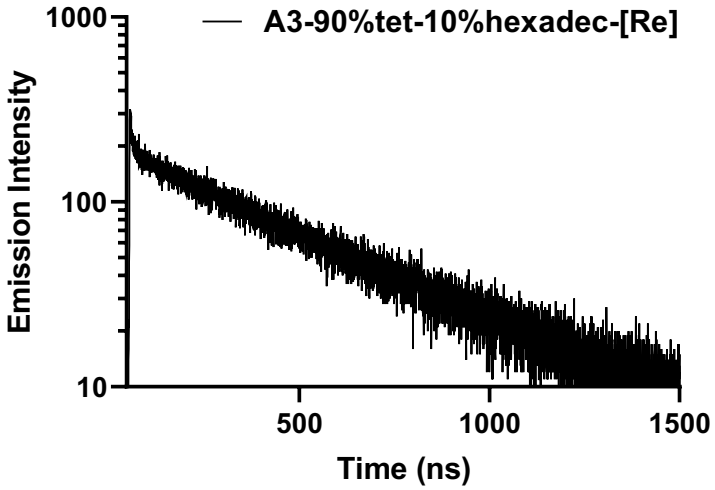

Figure A-31 TCSPS decay of ^{3}MLCT emission of air equilibrated solutions of **A3-90%tet-10%hexadec-[Re]** in dilute DMSO, degassed solutions, under excitation at 375 nm.

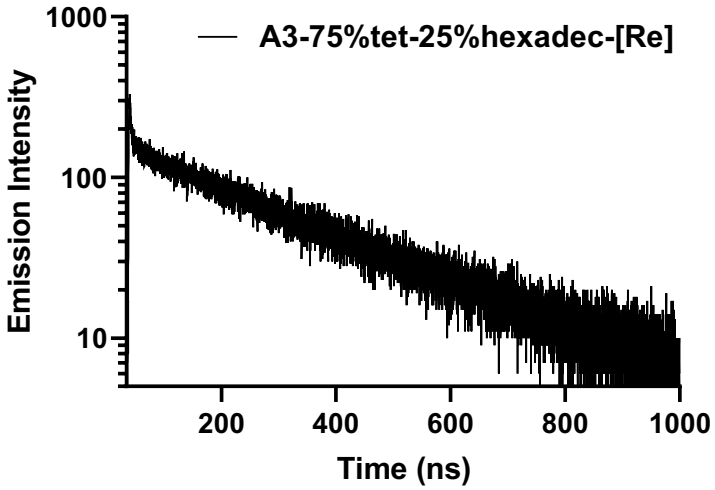

Figure A-32 TCSPS decay of ^{3}MLCT emission of air equilibrated solutions of **A3-75%tet-25%hexadec-[Re]** in dilute DMSO, air-equilibrated solutions, under excitation at 375 nm.

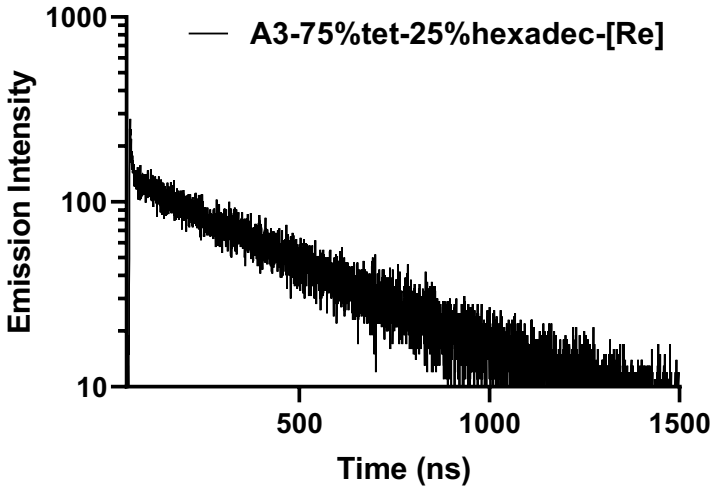

Figure A-33 TCSPS decay of ^{3}MLCT emission of air equilibrated solutions of **A3-75%tet-25%hexadec-[Re]** in dilute DMSO, degassed solutions, under excitation at 375 nm.

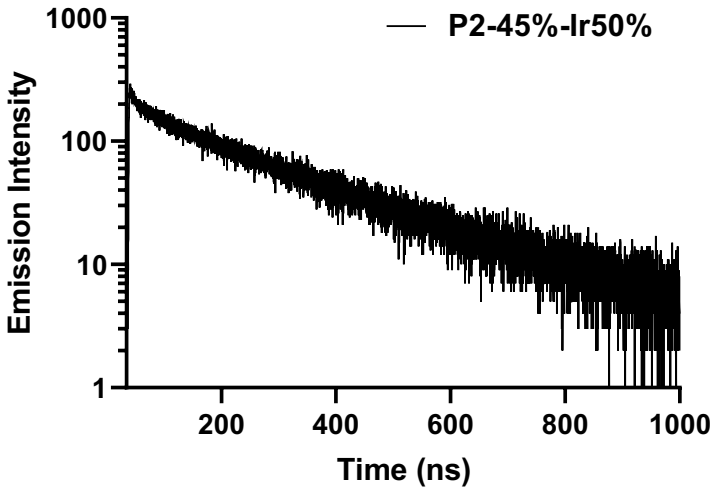

Figure A-34 TCSPS decay of ^{3}MLCT emission of air equilibrated solutions of **P2-45%-Ir50%** in dilute DMSO, air-equilibrated solutions, under excitation at 375 nm.

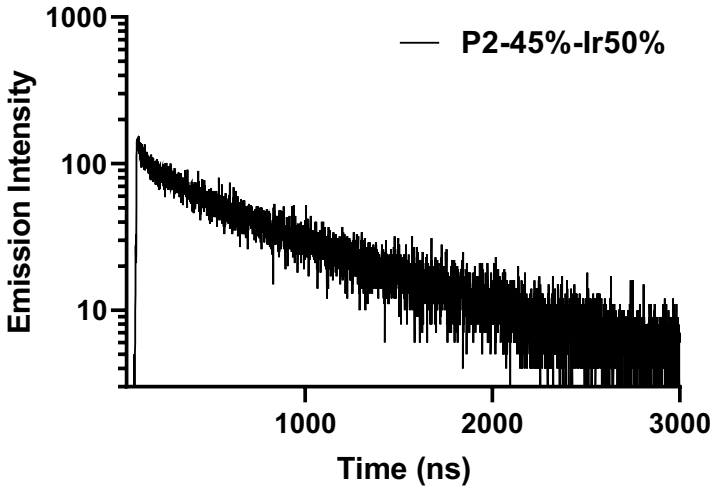

Figure A-35 TCSPS decay of ^{3}MLCT emission of air equilibrated solutions of **P2-45%-Ir50%** in dilute DMSO, degassed solutions, under excitation at 375 nm.

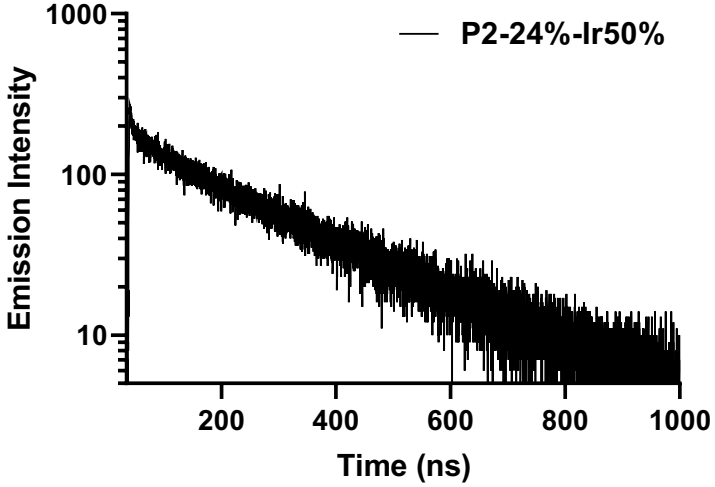

Figure A-36 TCSPS decay of ^{3}MLCT emission of air equilibrated solutions of **P2-24%-Ir50%** in dilute DMSO, air-equilibrated solutions, under excitation at 375 nm.

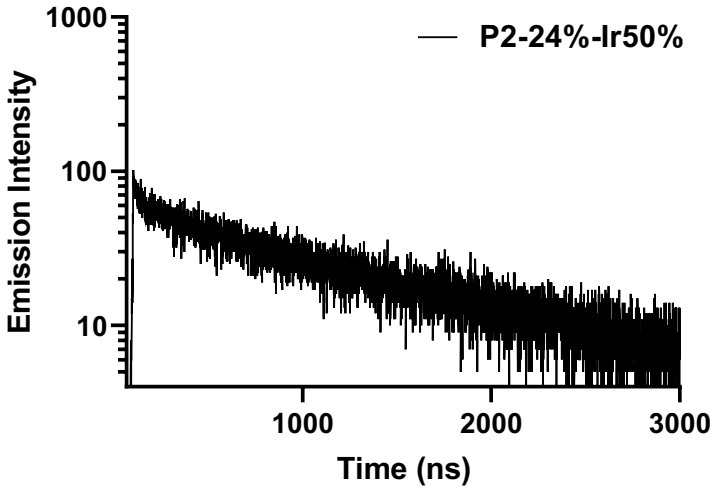

Figure A-37 TCSPS decay of ^{3}MLCT emission of air equilibrated solutions of **P2-24%-Ir50%** in dilute DMSO, degassed solutions, under excitation at 375 nm.

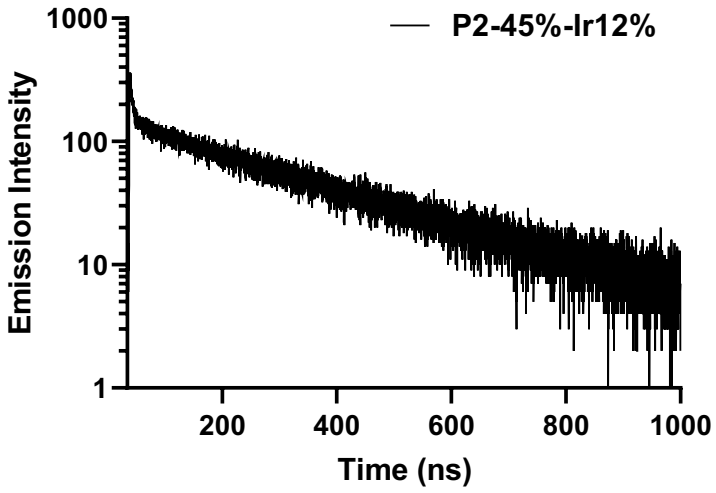

Figure A-38 TCSPS decay of ^{3}MLCT emission of air equilibrated solutions of **P2-45%-Ir12%** in dilute DMSO, air-equilibrated solutions, under excitation at 375 nm.

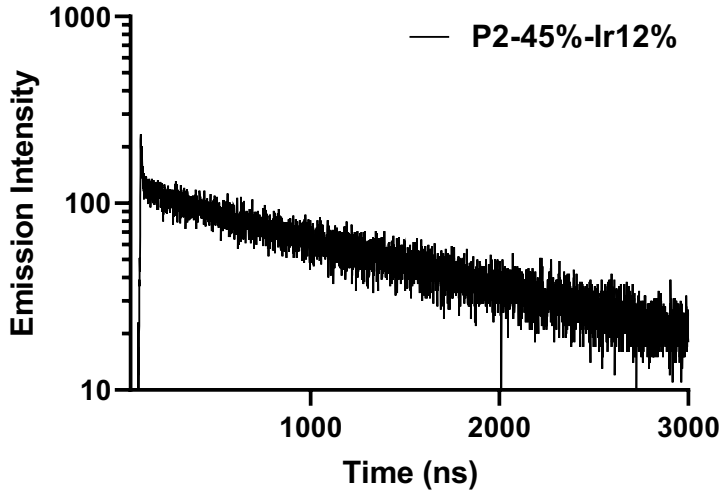

Figure A-39 TCSPS decay of ^{3}MLCT emission of air equilibrated solutions of **P2-45%-Ir12%** in dilute DMSO, degassed solutions, under excitation at 375 nm.

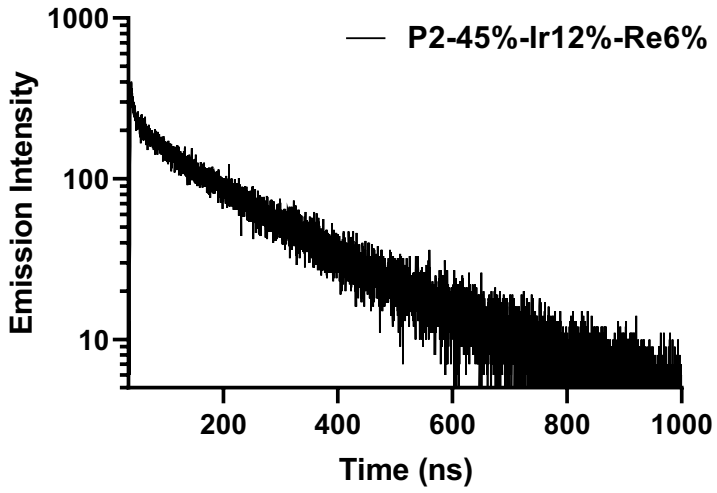

Figure A-40 TCSPS decay of ^{3}MLCT emission of air equilibrated solutions of **P2-45%-Ir12%-Re6%** in dilute DMSO, air-equilibrated solutions, under excitation at 375 nm.

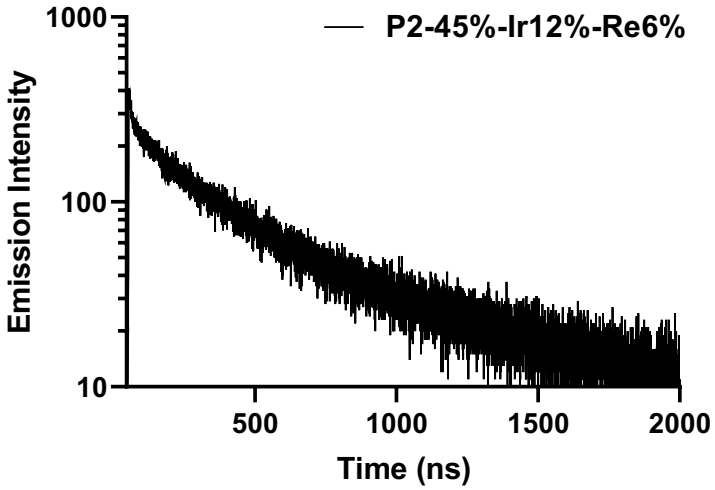

Figure A-41 TCSPS decay of ^{3}MLCT emission of air equilibrated solutions of **P2-45%-Ir12%-Re6%** in dilute DMSO, degassed solutions, under excitation at 375 nm.

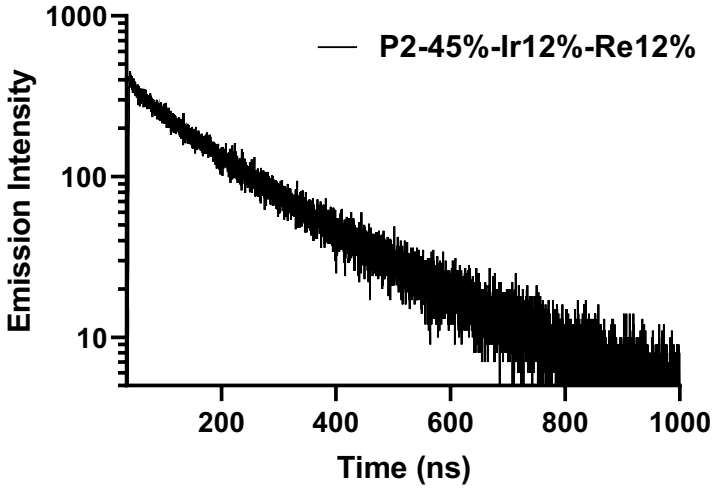

Figure A-42 TCSPS decay of ^{3}MLCT emission of air equilibrated solutions of **P2-45%-Ir12%-Re12%** in dilute DMSO, air-equilibrated solutions, under excitation at 375 nm.

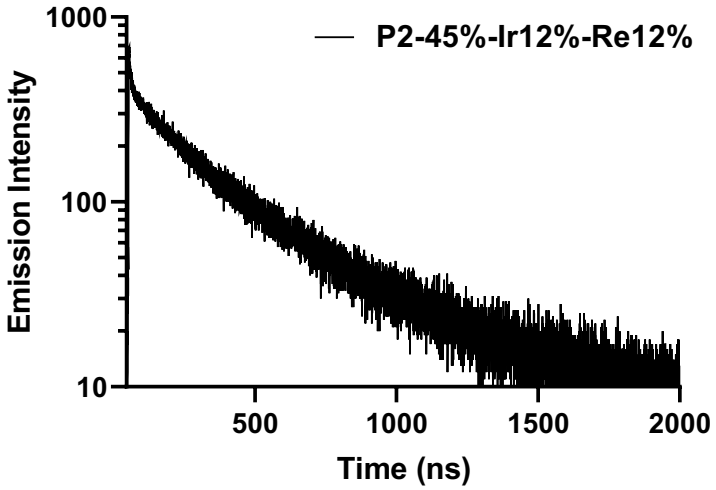

Figure A-43 TCSPS decay of ^{3}MLCT emission of air equilibrated solutions of **P2-45%-Ir12%-Re12%** in dilute DMSO, degassed solutions, under excitation at 375 nm.

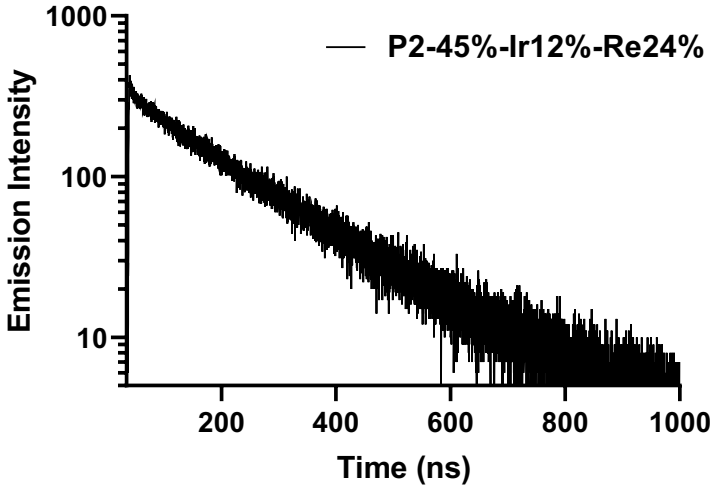

Figure A-44 TCSPS decay of ^{3}MLCT emission of air equilibrated solutions of **P2-45%-Ir12%-Re24%** in dilute DMSO, air-equilibrated solutions, under excitation at 375 nm.

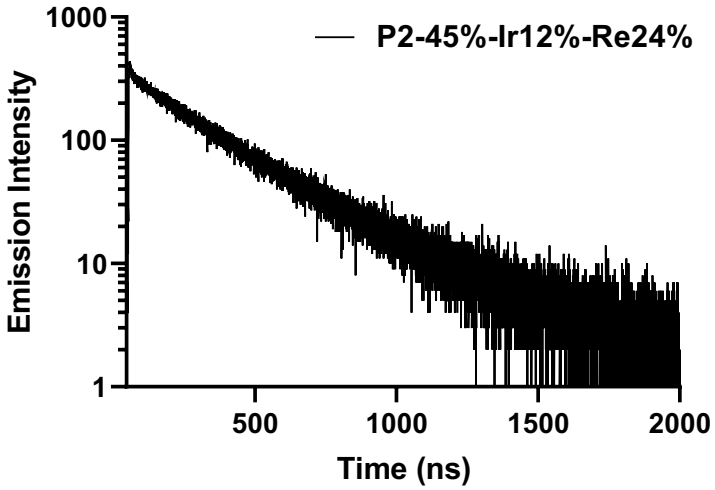

Figure A-45 TCSPS decay of ^{3}MLCT emission of air equilibrated solutions of **P2-45%-Ir12%-Re24%** in dilute DMSO, degassed solutions, under excitation at 375 nm.